pH Responsive Chiral Europium Complexes

JACK DAVID FRADGLEY

pH Responsive Chiral Europium Complexes

Jack David Fradgley

A thesis submitted for the degree of Doctor of Philosophy

2021

Declaration

The work described herein was undertaken at the Department of Chemistry, Durham University between October 2017 and March 2021. All of the work is my own, except where specifically stated otherwise. No part has previously been submitted for a degree at this or any other university.

Statement of Copyright

For Mum & Dad

Abstract

A series of novel emissive europium(III) complexes, varying in their number of antennae, has been synthesised and their photophysical properties studied. These complexes incorporate highly conjugated arylalkynylpyridyl antennae onto the macrocycle 1,4,7-triazacyclononane, and display highly pH responsive luminescence behaviour, with a significant switching-on of the total emission, emission lifetime, and circularly polarised luminescence with lowering pH.

The potential of such complexes as models for *in cellulo* probes of pH was demonstrated through the successful monitoring of cellular uptake with time (living NIH-3T3 cells) of the brightest complex using confocal microscopy. Additionally, the use of time-gated measurements and optimisation of the acquisition window was shown to allow for enhanced switching on of luminescence.

A further five pH-responsive europium(III) complexes have been thoughtfully designed, with the optimisation of the properties of the model parent complex and introduction of appropriate functionality for bioconjugation. These pH probes were synthesised and the photophysical behaviour analysed in detail.

In a proof-of-concept study, two probe candidates were converted to their benzyl guanine derivatives and the successful labelling of a SNAP-tag functionalised glucagon-like peptide-1 receptor, a targeted receptor for anti-diabetic drugs, was demonstrated.

Further studies were performed on the C_3-symmetric parent europium(III) complex, examining the solvent dependence of the absorption and emission behaviour and the kinetics of enantiomeric interconversion, demonstrating that the spectral form, absorption maximum, and half life for racemisation are strongly influenced by local solvent.

Acknowledgements

I would like to express my deep gratitude to the following people:

Firstly, I would like to thank my supervisor Prof. David Parker who first gave me this opportunity to explore lanthanide chemistry. Thank you for always making time for questions and discussions, your continuous encouragement over my studies, both subtle and obvious when needed, and for consistently going far beyond the call of duty. I will remember knocking on your office door out of the blue as a Masters student to enquire about this PhD and enjoying a long chat about chemistry with you. I am incredibly grateful for your guidance over the past three and a half years, both professional and personal, and the opportunity to learn under you.

I would like to thank my co-supervisor Dr. Robert Pal. Thank you for everything, from the hours tirelessly spent in the cell lab studying my complexes and hauling a replacement UV/Vis around the department at the drop of a hat, to always making delicious food for our Christmas meal and caring to check in on me. I'm grateful for always being made to feel like a member of the Pal group.

Special thanks must be given to Dr. Laurent Lamarque and Dr. Jurriaan Zwier at Cisbio for their insightful suggestions and discussions, and passion for this project. I have enjoyed our meetings immensely, both in Codolet and in Durham (although I'll admit French cuisine and wine are far better!). Thanks must also be given to Dr. Emmanuel Bourrier for the preparation of the BG derivatives, and Dr. Elodie Dupuis and Dr. Michel Laget for the cell receptor internalisation studies.

Within the Durham Chemistry Department, I would like to thank: Dr. Juan Aguilar, Catherine Heffernan, Dr. Eric Hughes, and Dr. Alan Kenwright for the running of the NMR Spectroscopy service; Pete Stokes, Dr. Dave Parker, and Dr. Jackie Mosely for the running of the Mass Spectrometry service and custom experiments; Dr. Aileen Congreve for being so accommodating and assisting with HPLC (with good chat as well); Prof. Gareth Williams for kindly helping me with low temperature photophysical measurements; and finally Annette Passmoor, Gary Southern, and Claire for the friendly chats whenever we happened to meet.

Thanks to my fellow members of the Parker group, both past and present. In particular, I must thank: Matthieu, for taking me under his wing, teaching me so much in the lab,

and reciprocating my enthusiasm two-fold; Kanthi, for sharing a few of her column trade secrets and the fun at staff badminton; Kevin, for introducing me to the scrambled egg breakfast roll; and finally, Alice and Laura, for the laughter in the lab and putting up with me. Thank you all for your friendship and for making me feel welcome and right at home in CG027 from the moment I arrived.

Davide, Helen, and Luca (in order of appearance): When we first met, I didn't realise the months would feel like years and we'd end up as the good friends we are. Thank you for your friendship, kindness, the fun, banter, good food, cocktails, and great craic. You're all CEOs in my book. Thank you for everything.

Clare: Thanks for always being so friendly, kind, and keen to join the fun. I will be forever grateful for the combination of two of my favourite things: Tangfastics and vodka.

Hopefully we will all play a game of Durham Chemistry Monopoly soon.

I want to also thank: Matt for our runs which almost certainly kept me sane, and for always offering a listening ear; the original Durham crew for the past eight years of friendship; and my friends at St. Hild and St. Bede Badminton club (club of the year).

Aisha: Thank you for our brunches on the weekend and helping me (begin to) work through my hatred of buses. Thank you for unknowingly pushing me to strive and work as hard as you. 3, 6, 9, 11.

Finally, and most importantly, I must thank my Mum and Dad. I would not be where I am, as I am, without them. Thank you for your steadfast belief and unyielding support every step of the way, and enabling me to do what I love. I am blessed to have you. A special mention must be made for my Grandma and Grandad for their encouragement and enthusiasm for what I do.

List of Abbreviations

α_1-AGP	alpha-1-acid glycoprotein
ABS	activity based sensing
Ac	acetyl
AC	alternating current
BET	back energy transfer
BG	benzylguanine
BMS	bulk magnetic susceptibility
BODIPY	boron-dipyrromethene
Boc	*tert*-butyloxycarbonyl
br	broad (NMR)
BS	beam splitter
BSA	bovine serum albumin
Bu	butyl
calcd	calculated
CCD	charge coupled device
CD	circular dichroism
CFAP	chemiluminescent formaldehyde probe
CPL	circularly polarised luminescence
CNF	carboxynaphthofluorescein
CT	charge transfer
cyclen	1,4,7,10-tetraazacyclododecane
Cy5	cyanine-5
d, dd, ddd	doublet, doublet of doublets (NMR)
DC	direct current
DCM	dichloromethane
DFT	density functional theory
DIEA	diisopropylethylamine
DMF	*N,N*-dimethyl formamide
DMSO	dimethyl sulfoxide

DOTA	1,4,7,10-tetraazacyclododecane-tetraacetic acid
DTPA	diethylenetriamine-pentaacetic acid
dppf	1,1'-bis(diphenylphosphino)ferrocene
EDTA	ethylenediamine-tetraacetic acid
ee	enantiomeric excess
ESI	electrospray ionisation
eT	electron transfer
Et	ethyl
ET	energy transfer
ER	endoplasmic reticulum
eq.	equivalents
FAP	fluorogen-activating peptide
FRET	Förster resonance energy transfer
GLP-1R	glucagon-like peptide-1 receptor
GPCR	G-protein coupled receptor
HEPES	4-(2-hydroxyethyl)-1-piperazine-ethanesulfonic acid
HOMO	highest occupied molecular orbital
HPLC	high performance liquid chromatography
HRMS	high resolution mass spectrometry
HSA	human serum albumin
IC	internal conversion
ICP-MS	inductively coupled plasma mass spectrometry
ICT	internal charge transfer
IPA	isopropanol
IR	infrared
ISC	intersystem crossing
LC/MS	liquid chromatography mass spectrometry
LED	light emitting diode
Ln	lanthanide
LP	linear polariser

LPF	long pass filter
LRMS	low resolution mass spectrometry
LSD	lysosomal storage disease
LTG	LysoTracker Green
NIR	near-infrared
m	multiplet (NMR)
MCF-7	human breast cancer cell line
*m*CPBA	*meta*-chloroperoxybenzoic acid
MES	2-(*N*-morpholino)ethanesulfonic acid
MRI	magnetic resonance imaging
MLCT	metal-to-ligand charge transfer
Ms	methanesulfonyl
Nap	1,8-naphthalimide
NIH-3T3	mouse skin fibroblast cell line
NMR	nuclear magnetic resonance
OA	oxidative addition
PCA	principal component analysis
PCTA	3,6,9,15-tetraazabicylco[9.3.1]pentadeca-1-(15),11,13-triene-3,6,9-triacetic acid
PEG	polyethylene glycol
PEM	photoelastic modulator
PeT	photoinduced electron transfer
PD	photodiode
Ph	phenyl
PMT	photomultipler tube
ppm	parts per million
pyclen	3,6,9,15-tetraazabicylco[9.3.1]pentadeca-1-(15),11,13-triene
Q	quencher
QWP	quarter wave plate
RE	reductive elimination

RP-HPLC	reverse phase high performance liquid chromatography
S	singlet (energy level)
s	singlet (NMR)
SM	scanning monochromator
SPF	short pass filter
ST	SNAP-tag
T	triplet (energy level)
t	triplet (NMR)
TACN	1,4,7-triazacyclononane
TEAAc	triethylammonium acetate
TFA	trifluoroacetic acid
TFAA	trifluoroacetic anhydride
TFE	2,2,2-trifluoroethanol
THF	tetrahydrofuran
TLC	thin layer chromatography
TM	transmetallation
TMS	trimethylsilyl
TO	thiazole orange
tpy	terpyridine
tta	2-thenoyltrifluoroacetone
UV	ultra violet
Vis	visible
VT	variable temperature

Table of Contents

If I have seen further, it is by standing on the shoulders of Giants

~ Sir Isaac Newton

CHAPTER ONE

Introduction

Chapter One: Introduction

1.1. Luminescence of Lanthanides

1.1.1. Theory of Luminescence

From its earliest observation in ancient times to the present day, the phenomenon of luminescence has intrigued humanity. Ancient records and literature are abundant with observations of light: unbeknown to the people of the time, many were forms of luminescence. Early examples include the “intermittent glowing” of fireflies and the “fitful light” of glow-worms, documented within Chinese poetry (*Shih Ching*, 1500 – 1000 B.C.), and the luminescence of the sea observed by the Roman historian Titus Livius (59 B.C – A.D. 17) who described the “sea aflame” and the “shores with fires”, (Figure 1.1).[1]

Figure 1.1. Early accounts of natural luminescence include fireflies *(left)*, glow-worms *(middle)* and certain organisms at the surface of the sea *(right)*.

Much later, in 1852, examination of the light emitted from a mineral form of calcium fluoride (CaF_2, fluorspar) discovered in County Durham, UK, led George G. Stokes to propose the term fluorescence, as an alternative to dispersive reflection.[2] Over 80 years later, further study of this particular fluorite under UV excitation led to the attributing of the blue fluorescence to the presence of traces of bivalent europium doped within the fluorite structure, (Figure 1.2).[3]

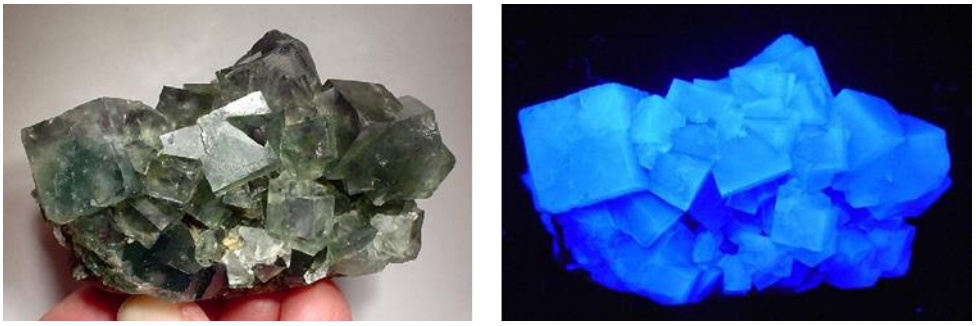

Figure 1.2. Europium(II) doped CaF_2 (fluorspar) under white light and UV excitation.

The term luminescence (“luminescenz”) was subsequently coined in 1888 by Eilhardt Wiedemann to distinguish from incandescence “all those phenomena of light which are not solely conditioned by the rise in temperature”.[1] With modern understanding, luminescence is now comprehensively defined as the spontaneous emission of radiation from an electronically excited species or from a vibrationally excited species, not in thermal equilibrium with its environment.[4]

Several examples of luminescence have been mentioned and it is clear different forms exist, differing in the origin of the excited species. These forms include: photoluminescence, where absorption of a photon leads to excitation; chemiluminescence, where a chemical reaction leads to excitation (bioluminescence if within an organism); triboluminescence, where mechanical stress leads to excitation, and electroluminescence, where the passage of electric current leads to excitation. The following work concerns only photoluminescence.

The numerous processes involved in photoluminescence are commonly depicted with a Jabłoński diagram, (Figure 1.3).

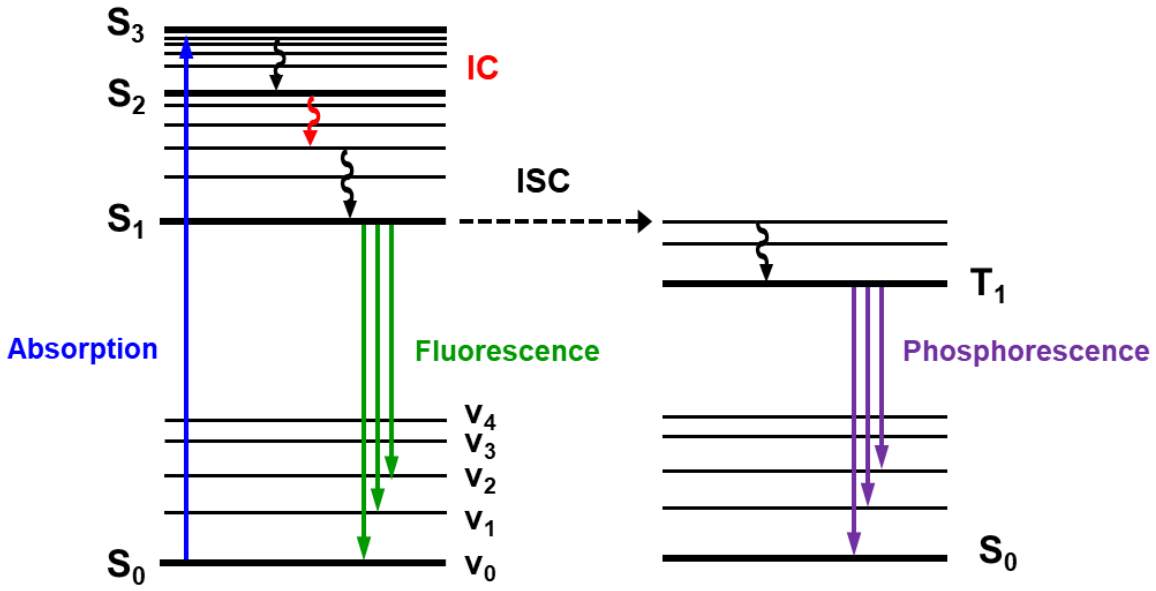

Figure 1.3. A representative Jabłoński diagram showing the major processes involved in photoluminescence.

Absorption of a photon results in electronic excitation of the species from the ground singlet state (S_0) to an excited vibrational level of a higher singlet state, the exact identity being dependent on the photon energy (S_2 is shown as an example). As a process, absorption occurs on a very fast timescale (10^{-15} seconds). Typically, non-radiative vibrational relaxation (10^{-14} – 10^{-11} seconds) immediately follows absorption and energy is dissipated through molecular vibration and rotation. The transition from a vibrational level of a higher electronic state to a vibrational level of a lower electronic state is then possible via internal conversion (IC). This is more probable at higher excited states where there is overlap between the vibrational and electronic energy states. IC occurs on a similar timescale to non-radiative vibrational relaxation. Through these two processes, the lowest excited singlet state (S_1) is reached from which there are three potential outcomes. The S_1 state can return to the S_0 state by either non-radiative decay or the emission of a photon (fluorescence, 10^{-9} – 10^{-7} seconds). Alternatively, the excited species can undergo intersystem crossing (ISC) from the S_1 state to the lowest excited triplet state (T_1) through the change in spin of an electron. ISC is formally forbidden by electronic selection rules and this is reflected in its slow timescale (10^{-8} – 10^{-3} seconds). Similarly to the S_1 state, decay from the T_1 state may occur radiatively (phosphorescence, 10^{-4} – 10^{-1} seconds) or non-radiatively. It is noted that Kasha's rule states that luminescence occurs only from the lowest excited state of a given multiplicity.[5]

The rare earth metals as their trivalent cations (Ln^{3+}) demonstrate intriguing photophysical properties as a consequence of their unique electronic configurations ([Xe]4f^n where n = 0 – 14). The arrangement of the electrons within these partially filled 4*f* orbitals may be described using the Russell-Saunders coupling scheme to define term symbols, $^{2S+1}L_J$, where *S* and *L* are the spin and total orbital angular momentum quantum numbers respectively for the lanthanide. The total angular momentum quantum number, *J*, is determined by the vector addition of *S* and *L*.

A diverse range of electronic levels arises from the electronic configurations of the lanthanides, (Figure 1.4). Luminescence is observable from most of the lanthanides, excluding La^{3+} and Lu^{3+}, emission ranging from the NIR to the UV. The emission bands corresponding to the *f-f* transitions are sharp, in contrast to organic molecules. This is a direct consequence of the lack of involvement of the 4*f* orbitals in lanthanide binding. Promotion of the 4*f* electron, yielding the excited state, causes minimal rearrangement and perturbation of the structure, giving a sharp emission band. In summary, emission is exhibited in the NIR by Pr^{3+}, Nd^{3+}, Ho^{3+}, Er^{3+} and Yb^{3+}; in the visible by Pr^{3+}, Sm^{3+}, Eu^{3+}, Tb^{3+}, Dy^{3+} and Tm^{3+}; and in the UV by Gd^{3+}.

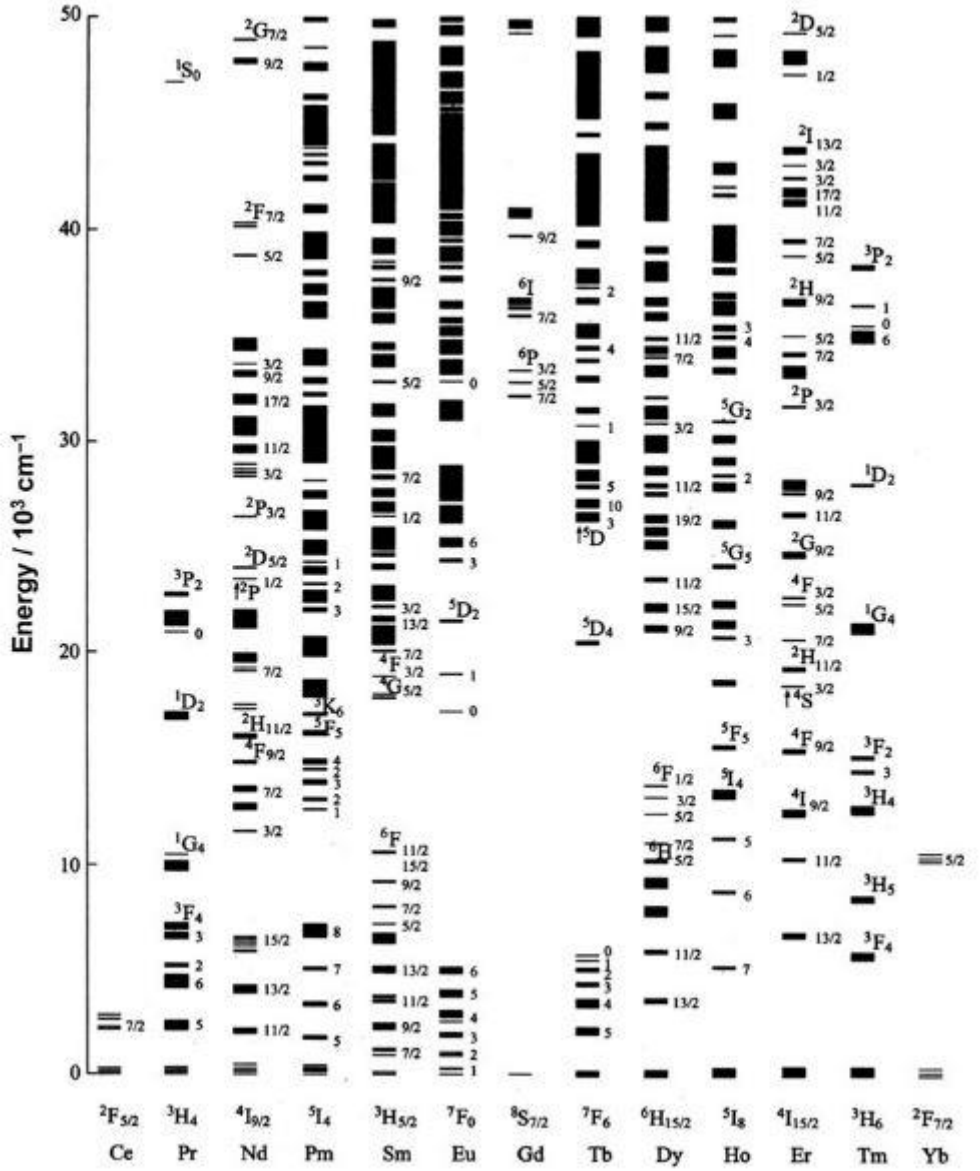

Figure 1.4. A partial energy level diagram for Ln^{3+} ions in a low symmetry crystal. Figure taken from reference [6].

The lanthanide europium(III) has the electronic configuration [Xe]4*f*^{6} and is the principal focus of this work. The six electrons may be distributed in 3003 degenerate electronic arrangements, or microstates, within the seven 4*f* orbitals. The degeneracy of these microstates may be partly removed by the perturbation of the Eu^{3+} ion by various factors. In brief, these factors are: electrostatic repulsion between the 4*f* electrons; spin-orbit coupling between the electron spin magnetic moment and the magnetic field produced by the mobile electron; interactions between the 4*f* electrons and ligand electrons (crystal field splitting); and an external magnetic field (the Zeeman effect).[7]

Europium(III) emission is often intense, commonly arising from the $^5D_0 \rightarrow {}^7F_J$ transitions where $J = 0 – 6$. Most of these are induced electric dipole transitions. This observation contradicts the Laporte selection rule which prohibits intraconfigurational electric dipole transitions. However, the selection rule may be relaxed as the environment is rarely strictly centrosymmetric and factors such as vibronic coupling and mixing of wavefunctions must be also considered.

1.1.2. Sensitised Lanthanide Emission

Lanthanides inherently possess low molar extinction coefficients (ε values are typically of the order 0.5 – 3 M^{-1} cm^{-1}), the $^5D_0 \rightarrow {}^7F_J$ transitions absorbing very weakly. This property is a manifestation of lanthanide luminescence involving *f-f* transitions, formally forbidden by the Laporte selection rule, as mentioned previously.

This relationship between absorbance, A, and molar extinction coefficient, ε, may be summarised by the Beer-Lambert law, where c is the concentration of the species concerned and l is the path length travelled by the light through the sample (typically 1 cm). Both the absorbance and molar extinction coefficient have wavelength dependence.

$$( ) = \quad ( )$$

Whilst excitation of the lanthanides may be achieved directly, it is often highly inefficient. This issue of efficient excitation may be overcome using laser excitation or circumvented entirely via the antenna effect, the latter of which will be discussed, (Figure 1.5).

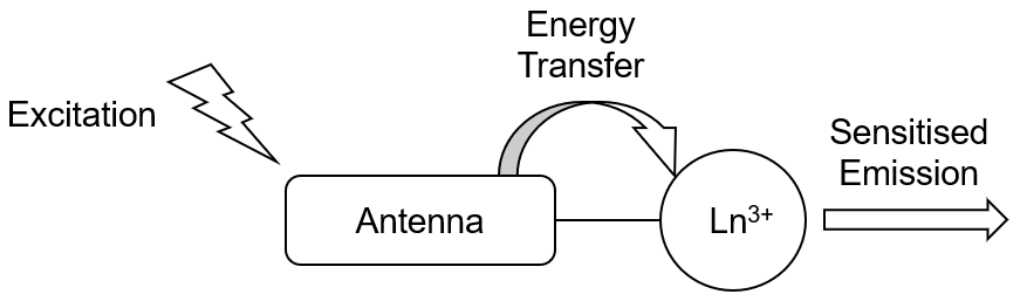

Figure 1.5. A representation of the antenna effect.

The antenna effect involves the incorporation of a chromophore, or antenna, into the system structure, typically covalently linked to a chelating moiety which binds the lanthanide ion. A key criterion for a suitable antenna is a high molar extinction coefficient at an appropriate wavelength allowing efficient absorption. Absorption of incident light by the antenna precedes intramolecular energy transfer to the lanthanide ion. Sensitised lanthanide emission is then possible. The intramolecular energy transfer described is commonly described using either the Förster or Dexter mechanisms. The Förster mechanism involves non-radiative energy transfer from a donor in an excited electronic state to an acceptor through a long range dipole-dipole interaction. This mechanism is highly distance dependent with an r^{-6} dependence. Conversely, the Dexter mechanism involves a short-range electron transfer from a donor to an acceptor.

Considering the antenna effect, it is necessary to expand the earlier Jabłoński diagram to provide a more accurate representation of the processes involved, (Figure 1.6).

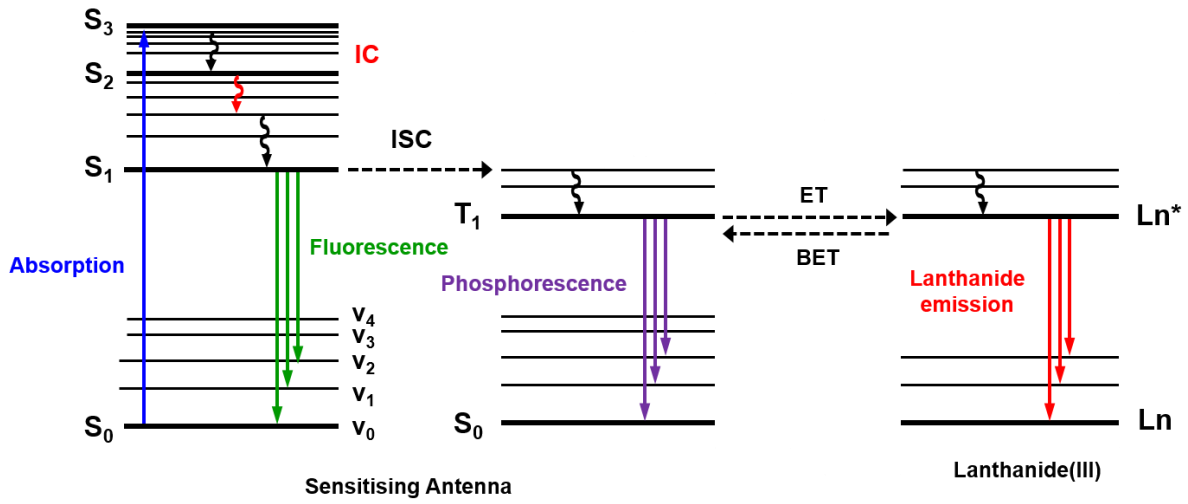

Figure 1.6. An expanded Jabłoński diagram showing the major processes involved in sensitised lanthanide emission.

In addition to a high molar extinction coefficient, several other criteria must be satisfied for efficient excitation using an antenna. The energy gap between the S_1 and T_1 states of the antenna should be small, allowing for efficient ISC. If these energy levels are heavily mismatched then processes such as antenna fluorescence and non-radiative decay will outcompete ISC to the excited triplet state. In addition, it is necessary for the antenna T_1 state to have appropriate energy relative to the accepting excited

lanthanide energy level. The energy of the T_1 state must be at least 1700 cm^{-1} above the relevant lanthanide energy level to minimise back energy transfer (BET) and antenna phosphorescence. However, the T_1 – Ln* energy gap must not be too large; otherwise, the efficiency of the energy transfer step is reduced.

In some instances, an alternative sensitisation mechanism is more appropriate, involving an internal charge transfer (ICT) excited state. Charge transfer (CT) excited states are typically observed in systems where separated electron-donating and electron-accepting moieties are connected electronically through p conjugation.[8] Characteristic absorption spectra are often indicative of a CT excited state with broad, structureless bands. When considering ICT sensitisation, energy transfer to the europium(III) ion is possible directly from the CT excited state without participation of excited triplet state, (Figure 1.6). It is difficult to assign the mechanism of sensitisation unambiguously and in some instances it is likely achieved partially through both ICT and triplet mediated processes.[8]

1.1.3. Emission Lifetime

A consequence of the forbidden nature of the *f-f* transitions involved in lanthanide luminescence is that the resulting emission decays with a long lifetime, typically on the order of milliseconds. This time scale is significantly longer than those of emissive transition metal complexes (microseconds) and organic compounds (nanoseconds).

The decay of the lanthanide luminescence signal from a single species can be expected to adhere to a first order rate profile, where I_t and I_0 are the emission intensities at times t and zero respectively and is the lifetime of emission.

$$_t = \ _0e^{--}$$

As the emission lifetime is the inverse of the observed rate constant for decay of the emissive state, k, t can be obtained experimentally by measuring emission intensity at several time points after excitation. The emission lifetime may be extracted from a plot of $\ln(I_t)$ against t which has a gradient equivalent to $-1/t$.

The relative longevity of lanthanide emission to that of emissive organic compounds allows for the unique opportunity for time-gated detection, (Figure 1.7). By delaying

the detection of emission on the order of microseconds, the autofluorescence observed from organic species or as a consequence of light scattering decays to zero before the detection of lanthanide emission. This technique returns cleaner spectra with improved signal-to-noise ratios. This is a valuable tool for biological applications.

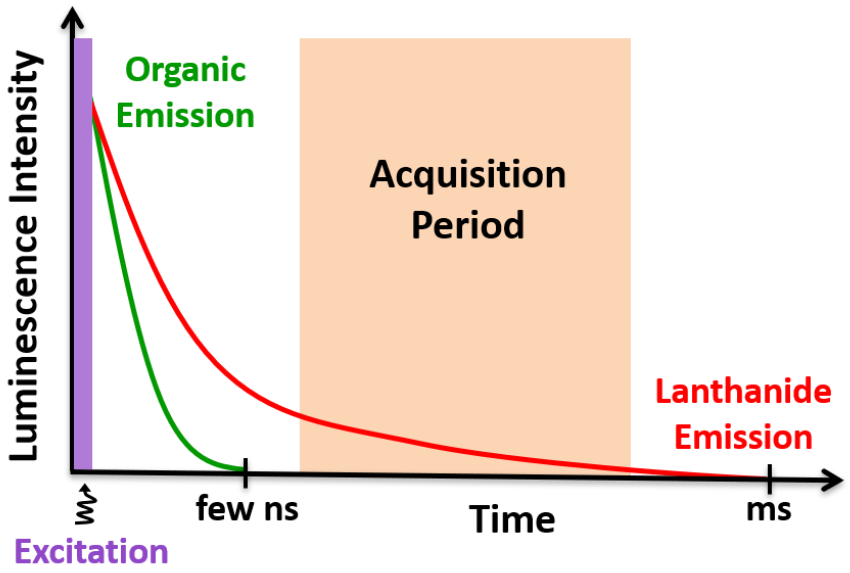

Figure 1.7. Time-gated detection involves a short delay following an excitation pulse (*purple*), allowing for fluorescence (*green*) to decay, before the detection of lanthanide emission (*red*).

1.1.4. Quantum Yields and Quenching

An important parameter in characterising the luminescence of a species is the photoluminescence quantum yield, Φ. This is generally defined as the ratio between the number of emitted and absorbed photons:

$$= \frac{\text{number of emitted photons}}{\text{number of absorbed photons}}$$

In the instance of sensitised lanthanide emission, the quantum yield can alternatively be expressed as:

$$= {}_{ISC}\ {}_{ET}\ {}^{Ln}$$

Here, η_{ISC} is the efficiency of the intersystem crossing process from the chromophore excited singlet state to the excited triplet state and η_{ET} is the efficiency of the energy transfer process from the chromophore excited triplet state to the excited lanthanide

energy levels. The superscript Ln is used to differentiate Φ^{Ln} as the intrinsic quantum yield, *i.e.* the quantum yield of the metal-centred luminescence from the 4*f* levels following direct excitation.

The intrinsic quantum yield can also be considered as the ratio of the radiative rate constant, k_{rad}, to the summation of rate constants for all deactivating pathways:

$$\Phi^{Ln} = \frac{\text{obs}}{\text{rad}} = \frac{\text{rad}}{\text{rad} + \sum \text{nonrad}}$$

In practice, quantum yields are typically measured either against a literature reference with a known quantum yield or, in more recent times, using an integrating sphere. One such reference used within this work is $[Ru(bipy)_3]Cl_2$ in water.[9] The quantum yield of the emissive sample, Φ, against that of the reference, Φ_{ref}, may be determined using:

$$\frac{}{\text{ref}} = \frac{^2}{^2_{\text{ref}}} \times \frac{}{\text{ref}} \times \frac{\text{ref}}{} \times \frac{\text{lamp}}{\text{lamp}_{\text{ref}}}$$

Where, *n* is the refractive index of the solvent being used, *S* is the integral of the emission spectrum between appropriate limits, *A* is the absorbance of the species at the chosen wavelength and *I* is the intensity of the lamp at the wavelength of excitation.

Both the photoluminescence quantum yield, Φ, and the molar extinction coefficient, ε, of an emissive species may be used to describe the brightness, *B*:

$$( ) = ( )$$

The brightness parameter encompasses the molar extinction coefficient and quantum yield; both of which typically must be large for the overall brightness value to be sizeable.

There are numerous pathways through which the quantum yield may be reduced. These routes may reduce the overall efficiency of the energy transfer process or lead to quenching of the observed lanthanide emission, (Figure 1.8).

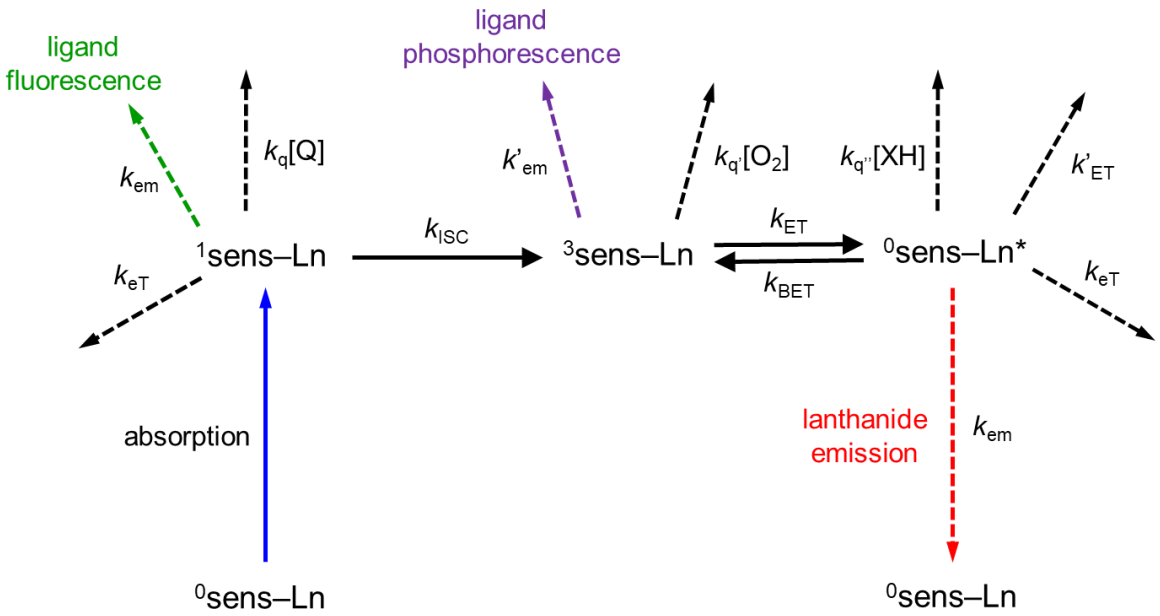

Figure 1.8. The various ligand and metal based excited state reaction pathways in conventional sensitised lanthanide emission. Adapted from reference [10].

Following the absorption of a photon by the sensitising antenna, the excited singlet can be quenched by electron transfer (eT) or through collision with a quencher, Q. There is also the possibility for triplet quenching of the antenna excited triplet by molecular oxygen, which possesses a triplet ground state. After energy transfer to the lanthanide, numerous quenching pathways exist. These include electron transfer (eT), energy transfer (ET) to a second species, back energy transfer (BET) to the antenna triplet state or involve energy transfer to X-H vibrational oscillators in close proximity (X = C, N, O). The NH and OH oscillators are most efficient at deactivating the europium $^5D_0$ excited state as they possess higher vibrational levels of appropriate energy.

1.1.5. Ligands for Lanthanide Chelation

It is important to consider the ligand used to bind to the metal in a lanthanide complex. Variation of the ligand allows for modulation of several properties. These include kinetic and thermodynamic stability, general photophysical properties and response to external stimuli, *e.g.* sensors and probes.

Lanthanide ions in solution have a preferred coordination number of 8 or 9, and this must be considered when designing a ligand for a given purpose. It should be noted

that ligand-lanthanide bonding is predominantly electrostatic in nature. This is a consequence of the contraction of the 4*f* orbitals due to a lack of effective shielding from the nucleus by the penetrating 5*s* and 5*p* subshells. For the majority of applications, stability of the complex towards dissociation of the lanthanide ion is essential, as will be exampled shortly.

1.1.5.1. Lanthanide Ligands for Magnetic Resonance Imaging

The use of a sensitising antenna is not always necessary, *e.g.* non-luminescent applications where efficient electronic excitation of the lanthanide is not required. One such application involves the use of Gd(III) in Magnetic Resonance Imaging (MRI) contrast agents, two examples of which are shown, (Figure 1.9).

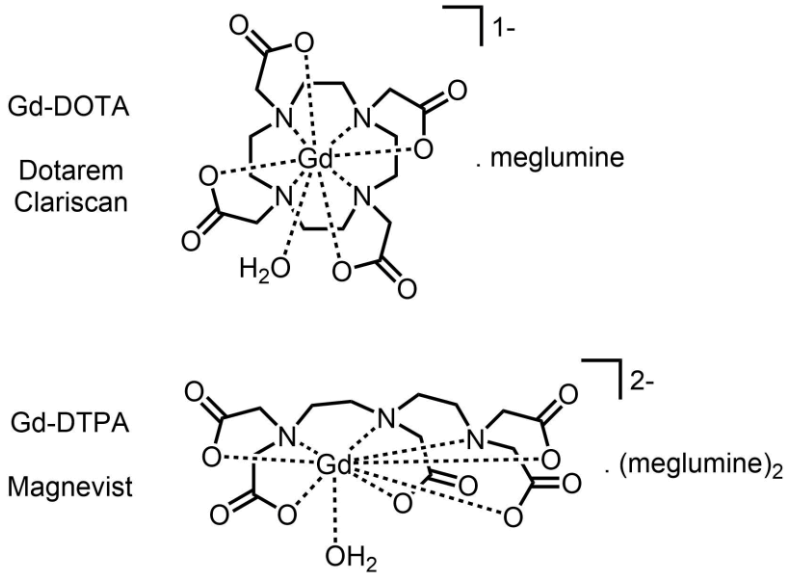

Figure 1.9. Typical structures of Gd(III) MRI contrast agents. DOTA = 1,4,7,10-tetraazacyclododecanetetraacetic acid. DTPA = diethylenetriaminepentaacetic acid.

The current agents approved for clinical usage comprise of an octadentate polyaminocarboxylate ligand chelating a 9-coordinate Gd(III) ion; the coordination sphere fully satisfied with a water co-ligand.[11] The water co-ligand is vital and allows for the modulation of the water proton T_1 and T_2 relaxation times through interaction with the paramagnetic Gd(III) ion.[12]

The ligands used to chelate Gd(III) may be categorised as either “open” linear chelates, such as Gd-DTPA, or “macrocyclic” chelates, such as Gd-DOTA. These

ligands demonstrate high stability with Gd(III) towards lanthanide dissociation: log(*K*) = 17.7 vs. 19.3 for Gd-DTPA and Gd-DOTA respectively (determined at physiological pH 7.4).[13] High kinetic stability *in vivo* is also required as premature metal ion dissociation is highly undesirable. It is well accepted that the toxicity of such Gd(III) chelates are often much lower than the free ligand and Gd(III) ion, which are considerably higher: LD_{50} ~10 – 20 mmol kg^{-1} for $[Gd(DTPA)(H_2O)]^{2-}$ compared with LD_{50} ~ 0.5 mmol kg^{-1} for $GdCl_3$.[14]

1.1.5.2. Lanthanide Ligands for Luminescence

Sensitising antennas are required, however, for luminescence to facilitate the efficient excitation of the lanthanide. As discussed earlier, the antenna must be carefully selected as the lowest excited state varies with the lanthanide, for example: $^4F_{9/2}$ for Dy(III) (21,100 cm^{-1}); $^5D_4$ for Tb(III) (20,500 cm^{-1}); $^5D_1$ and $^5D_0$ for Eu(III) (19,000 and 17,400 cm^{-1}, respectively), and $^4G_{5/2}$ for Sm(III) (17,800 cm^{-1}).[15] Hence, some antennas are more suited for the sensitisation of particular lanthanides because of this varying energy gap.

Luminescent complexes with europium(III) have been reported with numerous antennae. Some select examples of ligands are shown with antennae based on phenanthroline[16], 8-benzyloxyquinoline[17], azaxanthone[18] and azathioxanthone[18] moieties, (Figure 1.10).

In order to satisfy the coordination requirement of the europium(III) and exclude water from the inner coordination sphere, it is common for the antenna to participate in the lanthanide binding through appropriate donor groups. Such coordination is observed through the nitrogen adjacent to the methylene group in each of these examples, except for the 8-benzyloxyquinoline chromophore with the amide linker, where coordination occurs through the carbonyl oxygen atom. This direct coordination of the chromophore to the metal centre may be confirmed through an absorbance shift on complexation or using IR spectroscopy to monitor the frequency of aromatic ring or carbonyl vibrations.

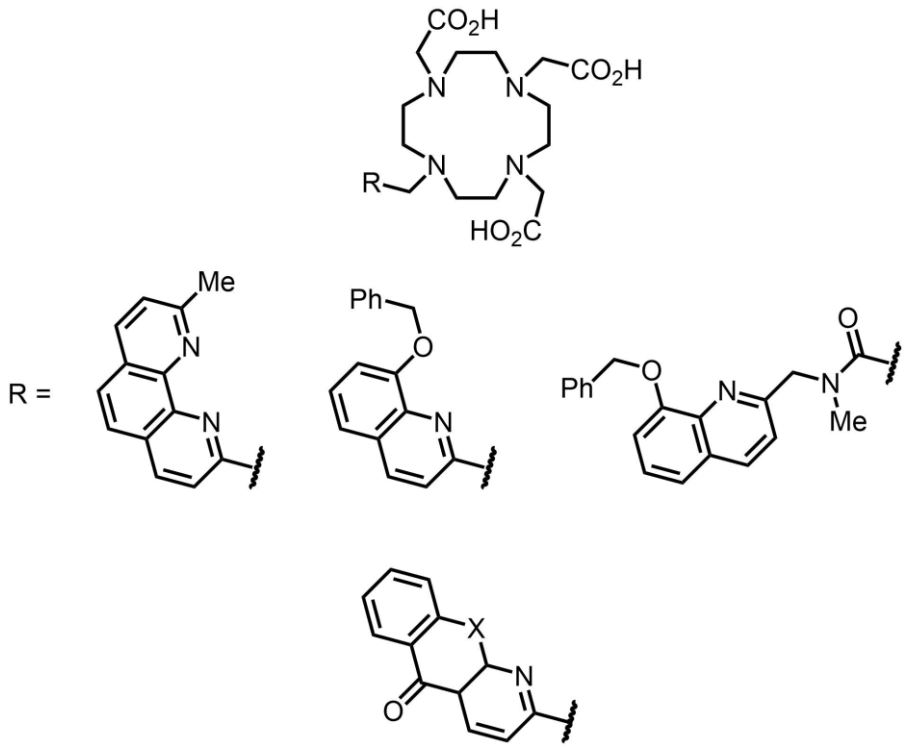

Figure 1.10. Examples of ligands with phenanthroline *(centre left)*, 8-benzyloxyquinoline (*centre and centre right*), azaxanthone and azathioxanthone (*bottom*, X = O and S respectively) based antennae for the sensitisation of europium(III).

The triple energy of 1,10-phenanthroline is reported to be ~22,100 cm^{-1}, ~4,500 cm^{-1} above the Eu(III) $^5D_0$ state. Relative to the homonuclear equivalent phenanthrene, significantly lower lifetime and quantum yield values for the fluorescence of phenanthroline are observed, suggesting a significantly greater likelihood of ISC.[16] Correspondingly, metal centred luminescence is observed from the europium(III) complex (Φ = 21%, t_{H2O} = 1.24 ms). However, the absorption maximum is at 278 nm and, despite an absorption tail protruding to higher wavelength, this is not ideal for most applications. A similar issue is encountered with the 8-benzyloxyquinoline derived antenna: an intense band is reported with a maximum at 245 and 252 nm, with and without the amide linker respectively, although there is also a broad weak absorbance in the 290–350 nm range.

The effective sensitisation of europium(III) by 8-benzyloxyquinoline derivatives has been known for some time[19] and sensitisation is possible by exciting into either absorption band. From measurements made at 77 K with the corresponding non-luminescent Gd(III) complex, the triplet energy of 8-benzyloxyquinoline is found to be ~17,700 cm^{-1}, above that of the Eu(III) $^5D_0$ but below $^5D_1$.[17] The presence of the amide

linker was found to govern the proximity of the antenna to the lanthanide and whether the quinaldine nitrogen coordinates. With the amide linker, one water molecule was found to coordinate to europium(III), in contrast to the case without the linker where coordination of the antenna causes the benzyloxy group to occupy the space of the ninth coordinating group. Although the deactivation of the metal excited state by water is inhibited here, it was found that alternative deactivating pathways from the metal excited state, *e.g.* high energy vibrations of the aromatic system, were enabled through the proximity of the antenna to the metal.

The chromophore 1-azaxanthone shows an absorption maximum at 335 nm as well as a high efficiency for the ISC process. This wavelength is advantageous, suitable for biological use when using pulsed excitation for example. In fact, systems featuring azaxanthone and azathioxanthone derivatives have been visualised *in cellulo* and systems have been developed that were responsive to bicarbonate and citrate.[20] Azaxanthone derivatives have been found to have triplet energies in the range ~21,200 – 25,400 cm^{-1}, depending on the nature of the substituents. The nature of the substituents determines the position of the absorption maximum (~330 – 370 nm). The sulphur analogue of azaxanthone, azathioxanthone, displayed a red-shifted absorption maximum at ~375 nm. However, competitive fluorescence is always observed with these complexes.[18]

These examples utilise either $n \rightarrow p^*$ or $p \rightarrow p^*$ transitions in order to sensitise europium(III) emission. However, sensitisation of europium(III) through other excited state transitions is also possible, *e.g.* ICT transitions. Such behaviour is observed with systems consisting of pyridine moieties *para*-substituted with arylalkynyl groups, (Figure 1.11).[21] These complexes display broad intense absorption bands, typical of an ICT transition. The charge separation arises due to the separation of the electron rich aryl moiety from the electron accepting pyridine group by the alkyne linker, and is enhanced by the coordination of the pyridine N to a lanthanide ion, that serves as a charge sink.

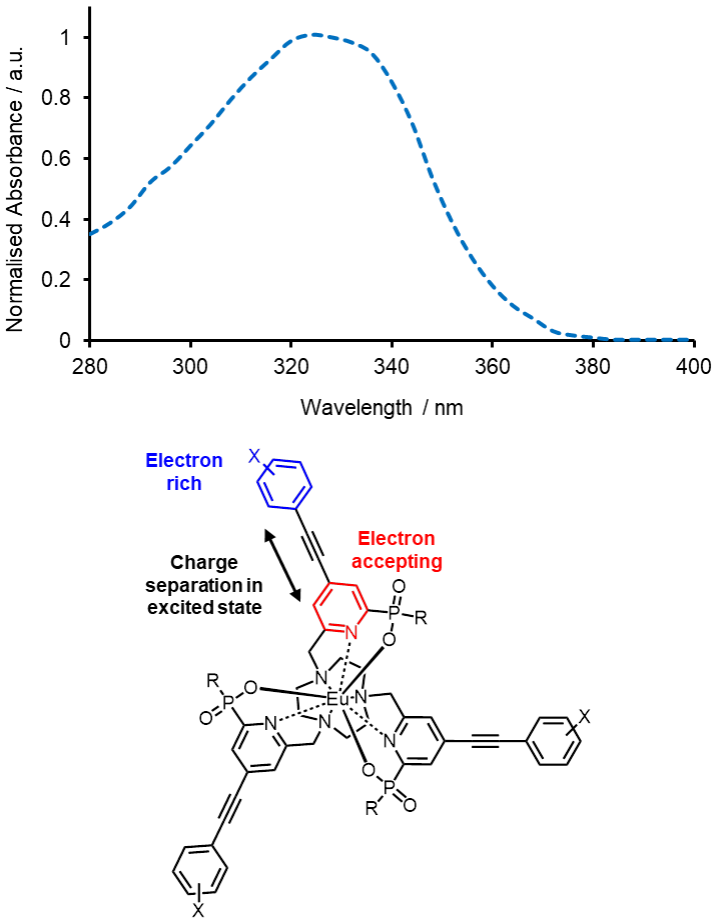

Figure 1.11. *(Top)* An example of a broad absorption spectrum due to an internal charge transfer transition. *(Bottom)* A generalised europium(III) complex structure with arylalkynylpyridine sensitisers. R = Me or Ph, X = electron donating groups.[22]

These structures are highly conjugated and are strongly absorbing. Impressive molar extinction coefficients are reported (ε ~40,000 – 60,000 M^{-1} cm^{-1}) at excitation wavelengths in the range 310 – 360 nm. A degree of tunability of the absorption maximum has been demonstrated by modulating the nature and number of electron donating groups (X) functionalising the aryl moiety. As the aryl ring becomes increasingly electron rich, the absorption maximum shifts to longer wavelength.[22] A nonadentate ligand suitable for satisfying the coordination requirements of Eu(III) is reached by incorporating donors in the *ortho* position of the pyridine and grafting the sensitisers onto a 1,4,7-triazacyclononane macrocycle. Complexes have been prepared where the *ortho* donors are either carboxylate or phosphinate groups. In the case of the phosphinate donor, further functionalisation is possible with the identity of R (Me or Ph).[21-22] Efficient energy transfer from the sensitiser to the europium(III) is

observed with the excitation spectra typically mirroring the absorption spectra, indicating the participation of the extended chromophore in the sensitisation process.

X-ray diffraction studies show that such nonadentate ligands bind the europium(III) ion with an arrangement similar to that of a tricapped trigonal prism, with no water molecules in the inner coordination sphere. This aspect is confirmed in solution by lifetimes measurements in H_2O and D_2O.[21] Correspondingly, quantum yields are often high (~50%) resulting in very bright complexes that are easily visualised in cellular optical imaging, *e.g.* with these EuroTracker® dyes.[23-24]

The synthesis of these highly conjugated sensitisers is versatile and has been reported, with the carboxylate donor, grafted onto cyclen[25], pyclen[26] and bis(bipyridine)[27] azamacrocyles.

Whilst some of the systems mentioned have also been shown to sensitise terbium(III), they generally do so inefficiently as the ICT excited state is not sufficiently high in energy. There has been some work on designing terbium(III) specific sensitisers, *e.g.* bi-aryl systems, (Figure 1.12).[15] Similarly to the arylalkynlpyridine sensitisers, these systems display intra-ligand charge-transfer transitions. Here, the successive addition of *ortho* methyl groups force the antenna into an increasingly twisted conformation about the aryl-aryl bond.

The quantum yield and emission lifetime were observed to markedly increase with addition of the first methyl group, (Table 1.1). Non-radiative relaxation through the free rotation about the aryl-aryl bond is prominent in the absence of any methyl groups. This is reduced substantially, however, with the steric effect of the methyl group. Despite disruption of the conjugation, and an associated decrease in the ε value, a sizeable increase in overall brightness was recorded with one methyl group due to the significant quantum yield. The brightness value was approximately half that of the common benchmark Tb-Lumi4[28] at 330 nm (8,900 vs. ~15,800 M^{-1} cm^{-1}).

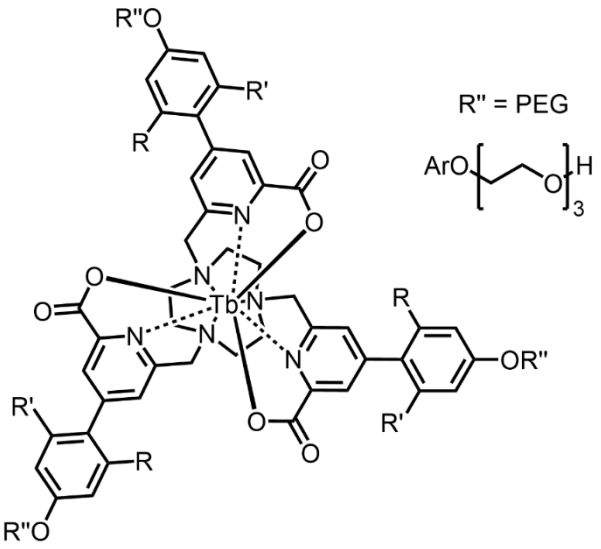

Figure 1.12. An example of a complex with a biaryl antenna sensitising terbium(III) emission (PEG = polyethylene glycol).

Table 1.1. Select photophysical properties[a] of the biaryl complexes shown in Figure 1.12.					
	λ_{max} / nm	ε / M^{-1} cm^{-1}	Φ / %	B(λ_{max})	t / ms
R = R' = H	308	47,000	30	14,100	0.45
R = Me, R' = H	302	30,400	74	23,000	1.36
R = R' = Me	300	11,800	66	7,800	1.46
[a] All values recorded in water. Data from reference [15].					

Addition of a second *ortho* methyl group twists the aryl groups to where they are almost perpendicular with one another. This further loss of conjugation is reflected in the values displayed in Table 1.1. Effective sensitisation of the terbium(III) is achieved with all three complexes, demonstrated by the absence of residual ligand-centred emission.

The sensitisation of NIR-emitting lanthanides, such as Yb(III), Nd(III) and Er(III), is worthy of brief mention. There has been particular interest partly due to the relative transparency of human tissue to light in the NIR, offering a potential new avenue for bio-probe development. Examples with Yb(III), Nd(III) and Er(III) have been reported utilising ligands with 8-hydroxyquinolinate-based sensitisers.[29-30] Because of the much lower energy of the emissive metal based excited state, a much wider range of

sensitisers can be pursued. Systems featuring transition metals, bound either by a sensitiser[31] or through self-assembly of the ligand,[32] have also been reported, (Figure 1.13). Here, the lanthanide is sensitised through a d→f transition.

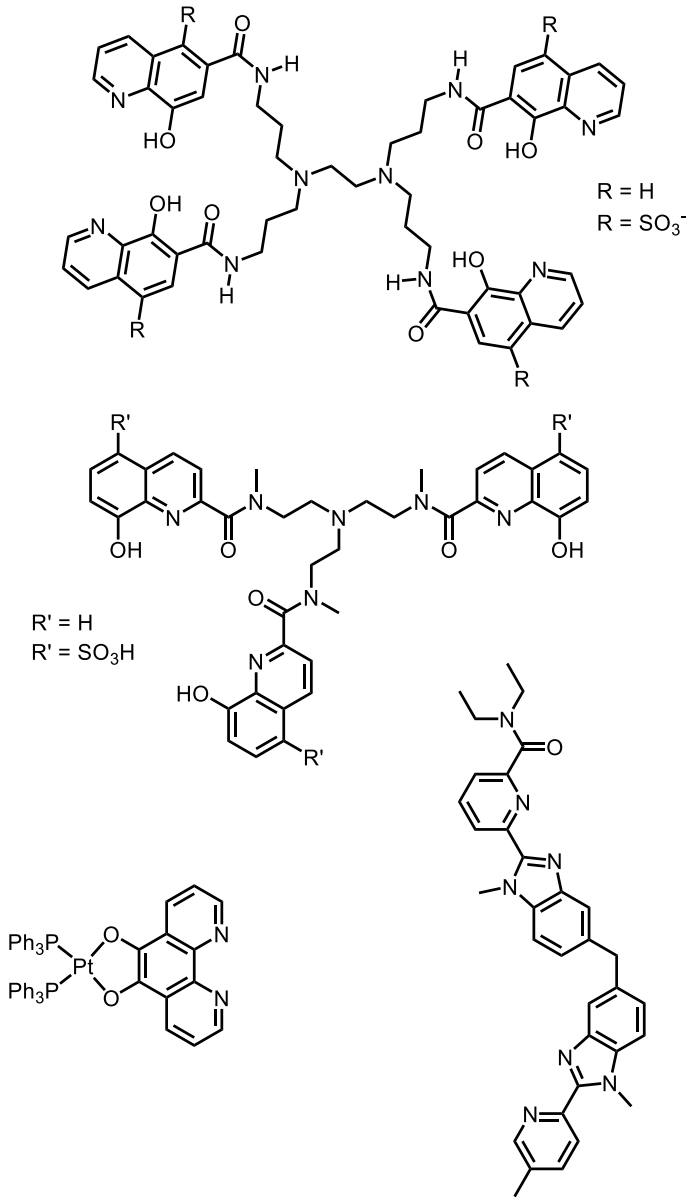

Figure 1.13. Examples of ligands used for Yb(III), Nd(III) and/or Er(III) reported in the literature: *(Top & Centre)* Ligand with 8-hydroxyquinolinate-based chelating arms/sensitisers (4 & 3 arms respectively); *(Bottom left)* 5,6-dihydroxyphenanthroline-based ligand with bound Pt(II) *(Bottom right)* Ligand self-assembles into a triple-stranded helicate able to bind both Ln(III) and Cr(III).

1.2. Circularly Polarised Luminescence (CPL)

1.2.1. Theory of CPL

Circularly polarised luminescence (CPL) is a phenomenon wherein a chiral emissive species emits left and right circularly polarised light with differing relative intensity. First observed from a sodium uranyl acetate crystal by Samoilov[33] in 1948, the measurement of CPL (CPL spectroscopy) is frequently regarded as the emission counterpart of and a complementary technique to circular dichroism (CD) spectroscopy, which concerns the differential *absorption* of left and right circularly polarised light.

When initially discussing circularly polarised light, it is useful to first consider polarised light which is classically described as a propagating wave comprising of an electric and a magnetic vector component. These vector components are perpendicular with respect to one another, as well as to the direction of propagation. The electric field vector can be further subdivided into two perpendicular components; the amplitude and phase of which must be examined. In the case of linearly polarised light, the electric field vector components are in phase but differ in amplitude. In contrast, circularly polarised light arises where the electric field vector components are identical in amplitude but are phase-shifted, specifically by a quarter of a wavelength, (Figure 1.14). The direct result of this phase difference is that one component becomes equal to zero when the other takes a maximum or minimum value. In this scenario, the light is circularly polarised and propagates with a defined helicity.

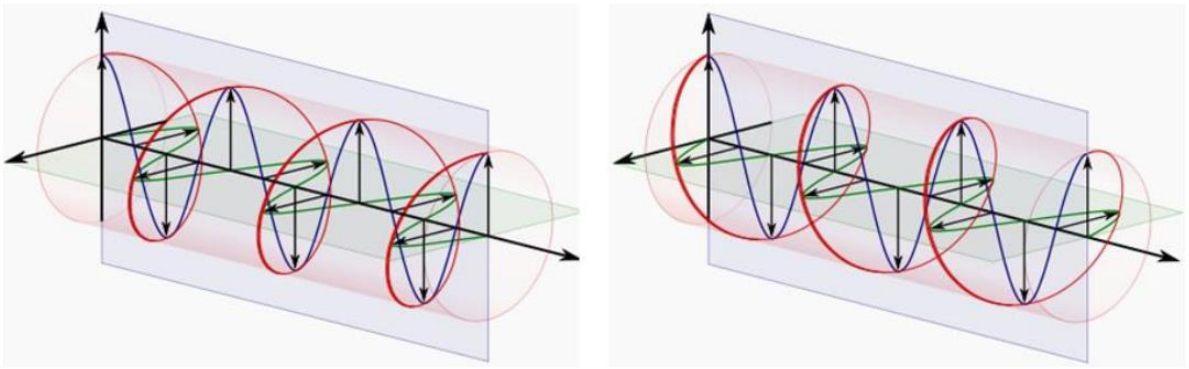

Figure 1.14. Representations of left and right circularly polarised light. The components of the electric field vector are in blue and green; the overall electric field vector is in red.

1.2.2. Observables and Parameters in CPL Spectroscopy

CPL Spectroscopy concerns the emission of left and right circularly polarised light from a luminescent system. In practice, it is the emission circular intensity differential, Δ ( ), and the total luminescence intensity, ( ), that are measured by the instrument, where Δ ( ) and ( ) are equal to the difference and sum of the intensities of left and right circularly polarised light respectively. It is typical for the degree of CPL to be quantified, at a given emission wavelength, by the emission dissymmetry factor, $_{m}( )$. It is noted that the emission dissymmetry factor is also frequently denoted as $_{lum}$. The emission dissymmetry factor can take a minimum value of zero, corresponding to an emission circular intensity differential of zero, *i.e.* in the event where either $_{L}( ) = _{R}( )$ or there is no circular polarisation. In contrast, the theoretical maximum value of $_{em}( )$ is ±2, corresponding to a luminescent system which emits either only left or right circularly polarised light, *i.e.* $_{L}( )$ or $_{R}( )$ equals zero.

$$\Delta ( ) = _{L}( ) - _{R}( ) \qquad ( ) = _{L}( ) + _{R}( )$$

$$_{em}( ) = \frac{2\Delta ( )}{ ( )}$$

The emission dissymmetry factor can be expressed in terms of the rotational strength, R_{ji}, and the dipole strength, D_{ji}, for a transition between states i and j, where R_{ji} relates to the magnitude of CPL of the transition and D_{ji} relates to the total luminescence intensity. The rotational and dipole strengths may be further defined in terms of the transition's electric and magnetic dipole vectors, **ε** and **m** respectively.[34]

$$_{em}( ) = \frac{4 _{ji}}{ _{ji}}$$

$$_{ji} = \mathrm{Im} \cdot \qquad = | |^2 + |m|^2$$

It follows that, as the magnetic dipole transition moment is usually significantly smaller in magnitude than the electric counterpart, the expression for $_{em}(\ )$ may be simplified further, where the angle between the magnetic and electric moments for the transition is denoted by .

$$_{em}(\ ) = \frac{4|\ \ |}{|\ \ |}\cos(\ )$$

It is therefore expected that larger $_{em}$ values will be observed for transitions which are magnetic dipole allowed but electric dipole forbidden. In general for enantiopure chiral europium and terbium complexes $_{em}$ values typically fall in the range ±0.1 – 0.5.[35] More sizeable $_{em}$ values than this have been reported however, *e.g.* +1.38 and +1.32 for the Δ*J* = 1 band of caesium tetrakis(3-heptafluoro-butylryl-(+)-camphorato) europium(III) complex in ethanol and chloroform respectively.[36]

1.2.3. CPL Instrumentation

Whilst commercial CPL spectrometers exist, they are expensive (>£100,000 at time of writing) and have only recently become available. As a result, it is commonplace for most CPL studies present in the literature to be performed using CPL spectrometers which are custom-built. These “home-built” spectrometers typically possess several common features in their set-up. An example set-up, used at Durham University, is shown, (Figure 1.15).

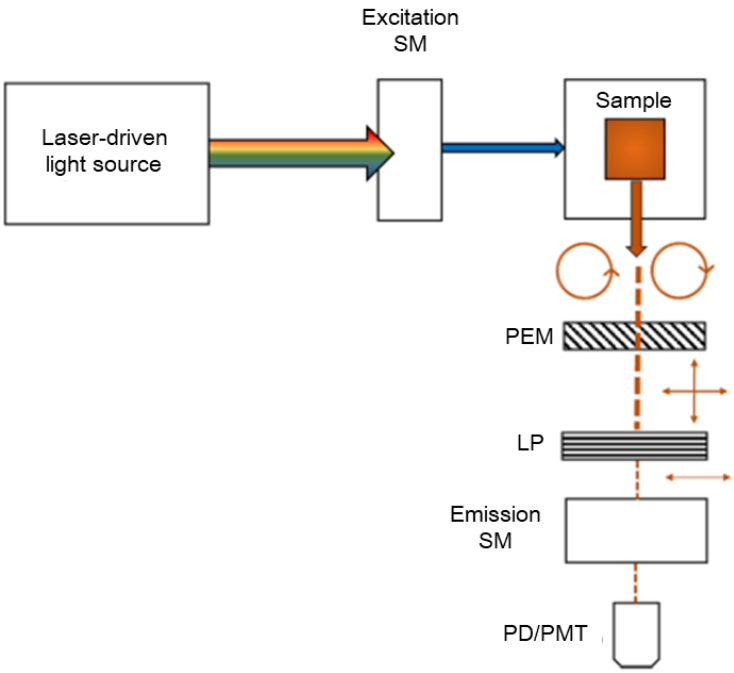

Figure 1.15. An example set-up of a home-built CPL spectrometer used at Durham University. SM = scanning monochromator, PEM = photoelastic modulator, LP = linear polariser, PD = photodiode, PMT = photomultipler tube. Circles with arrows represent circularly polarised light; vertical and horizontal arrows represent linearly polarised light. Adapted from reference [37].

During a typical experiment using this set-up, the sample is excited at an angle of 90^{o} relative to the direction of emission detection. The incident light is either linearly polarised or unpolarised and is usually passed through a scanning monochromator (SM), allowing the selection of the absorption maximum of the luminescent complex under investigation. The subsequent emitted light then passes through a circular analyser which consists of a photo-elastic modulator (PEM) and a linear polariser (LP). The PEM contains a clear isotropic material, such as quartz, which becomes anisotropic when periodic physical stress is applied. When driven by an AC signal, the PEM functions as an oscillating quarter-wave plate. During the application of this AC signal, the left and right components of the emitted circularly polarised light are alternatively converted into linearly polarised light which is subsequently selected by the linear polariser. An emission scanning monochromator is then used to select the wavelength before the photomultiplier tube (PMT) enhances the signal prior to detection. A lock-in amplifier then detects the difference signal (AC) and total signal (DC) and converts them to the CPL and total luminescence respectively. It is typically necessary to apply a red correction as at higher wavelengths, and lower photon energies, there is a lower probability of producing an electric current in the detector.

Although systems such as these are more affordable than those found commercially, the cost of constructing such instrumentation is still high (~£50,000 at time of writing). The time required to produce an adequate CPL emission spectrum for a sample is also fairly long, *e.g.* tens of minutes required to acquire a single CPL scan and approximately 45 minutes for a typical scan protocol for a chiral lanthanide system. Such a protocol typically involves 5 accumulated scans over a 150 nm range with 0.5 nm integration steps and a 500 μs integration time.

Recent work by Pal *et al*. has seen the development of a new CPL emission spectrometer, tackling these discussed drawbacks, (Figure 1.16).[37]

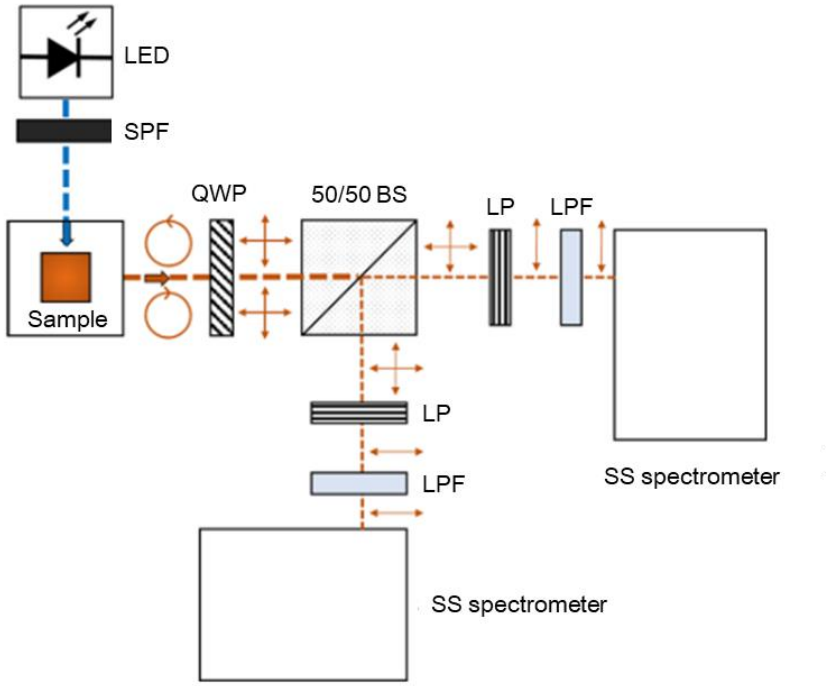

Figure 1.16. A new CPL spectrometer set-up designed at Durham University. LED = light emitting diode, SPF = short pass filter (<400 nm), QWP = quarter wave plate, 50/50 BS = 50/50 non-polarising beam splitter, LP = linear polariser, LPF = long pass filter (>450 nm), SS spectrometer = solid state CCD spectrometer. Circles with arrows represent circularly polarised light; vertical and horizontal arrows represent linearly polarised light. Adapted from reference [37].

Here, the sample is excited with light produced from an LED source, passed through a short pass filter (SPF, <400 nm) prior to excitation. The emitted left- and right-hand circularly polarised light is converted to orthogonal linearly polarised light by a static achromatic quarter wave plate (QWP). A 50/50 non-polarising beam splitter (50/50 BS) is then used to split the linearly polarised light into two distinct detection channels;

each channel capable of independently analysing both left- and right-hand circularly polarised light through the automated rotation of a linear polariser (LP) following the beam splitter. A long pass filter (LPF, >450 nm) precedes a solid state CCD spectrometer (SS spectrometer) in both channels (CCD = charge coupled device). The simultaneous operation of both spectrometers allows for the real-time acquisition of CPL spectra.

The use of the SS CCD spectrometer and dual-channel layout results in scan times of 10 milliseconds. Furthermore, the required components to set up this system are estimated to cost approximately £12,000 (at time of writing), a fraction of the cost of the earlier system.

This advancement in instrumentation is a significant step forwards in the field of CPL spectroscopy.

1.3. Responsive Luminescent Probes

As our understanding of the importance and roles of various analytes in human life grows, the number of responsive sensors reported is correspondingly increasing. Whilst these responsive systems are reported across numerous fields of chemistry, the general method of action is the same.

The sensor interacts with the analyte, often through a chemical reaction or a reversible binding event. This interaction perturbs the sensor and causes a change in a property unique to the sensor or the wider system. The modulation of the property serves as the ‘signal’ and may be interpreted to deduce information about the analyte. There is considerable variety in the nature of the properties modulated, reported in the literature. For luminescent systems, it is usually either the modulation of the emission intensity or the emission lifetime that serves as the signal. Commonly, these systems are often termed OFF-ON & ON-OFF luminescent switches, although very few actually show such digital behaviour.

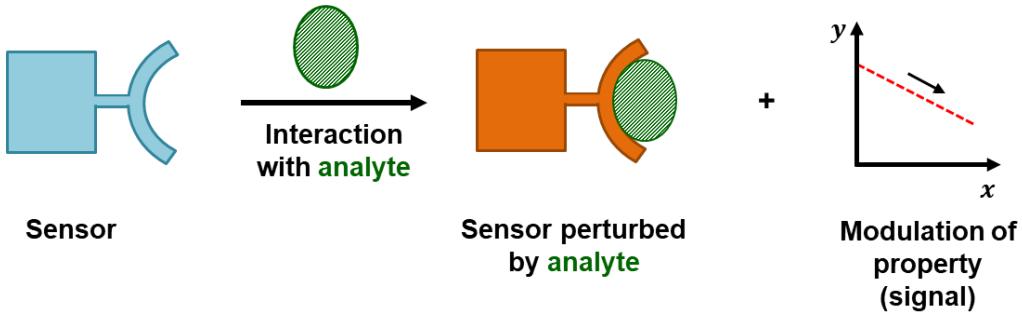

Figure 1.17. General representation of a sensor interacting with an analyte resulting in modulation of a property (the signal).

The nature of the interaction between the sensor and analyte can be either irreversible or reversible.

Irreversible binding occurs often in the form of a permanent chemical transformation. It is also possible, however, for the sensor to simply be unable to release the analyte after binding on the timescale of the experiment due to the high strength of interaction. The probe is often 'consumed' in order to generate the signal and cannot be reused, unless first recycled which is not usually possible.

In recent years, the concept of 'Activity Based Sensing' (ABS) has been proposed and discussed.[38] Here, an emphasis is placed on the inherent reactivity of the chosen analyte and how this can be manipulated with intelligent sensor design to achieve high selectivity and sensitivity. Examples of these are the Chemiluminescent Formaldehyde Probes (CFAPs) 540 and 700 by the group of Chang, (Figure 1.18).[39]

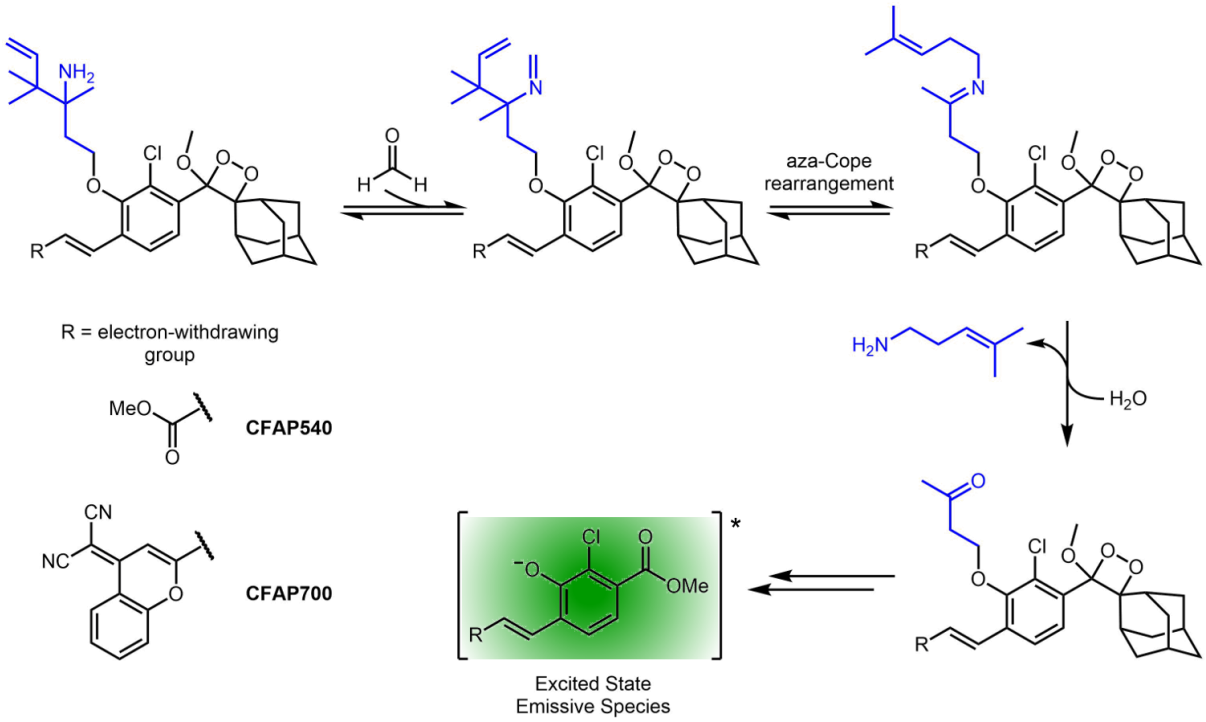

Figure 1.18. The reaction sequence by which CFAP540 and CFAP700 interact with formaldehyde selectively to form an excited emissive species.[39]

The excited emissive species is released through a specific reaction sequence. Whilst reversible imine formation at the amine group is not specific to only formaldehyde, *e.g.* other aldehydes such as acetylaldehyde, the subsequent 2-aza-Cope rearrangement is only chemically possible when formaldehyde is captured. The design of these sensors with a 2-aza-Cope reactive trigger sensitive to formaldehyde affords high specificity. This is demonstrated over selected reactive carbon species and biological analytes.

It is highly challenging to design a good sensor and the desired properties are heavily situation dependent. Often the optimisation of one property can have a detrimental effect on others. Both the CFAP540 and CFAP700 showed impressive and reasonable increases in emission intensity in turn (500- and 33-fold respectively). Whilst CFAP700 possesses an emission profile in the NIR, making it potentially suitable for *in vivo* applications, it has a significantly reduced switch-on emission intensity ratio, attributed to additional deactivation pathways that are not present for CFAP540.

The irreversible consumption of the probe is slow and occurred over several hours, likely due to the lengthy reaction sequence required to produce the emissive species. Although this elongated emission may be advantageous and desirable for *in vivo*

applications, this slow speed of response results in a detection process that is time-consuming.

A disadvantage of irreversible probes is the inability to probe the concentration of an analyte and monitor it at equilibrium in real time. This can be possible, however, in the case of reversible binding, where the perturbation of the system generating the signal is not permanent. It is important to note that signal calibration is essential in these circumstances for any meaningful interpretation of data.

A recent example of a reversible sensor system from the Lin group consists of a polysiloxane-based fluorescent probe to follow oxidation by ClO^- and subsequent recovery by glutathione (GSH) within cells and zebrafish, (Figure 1.19).[40]

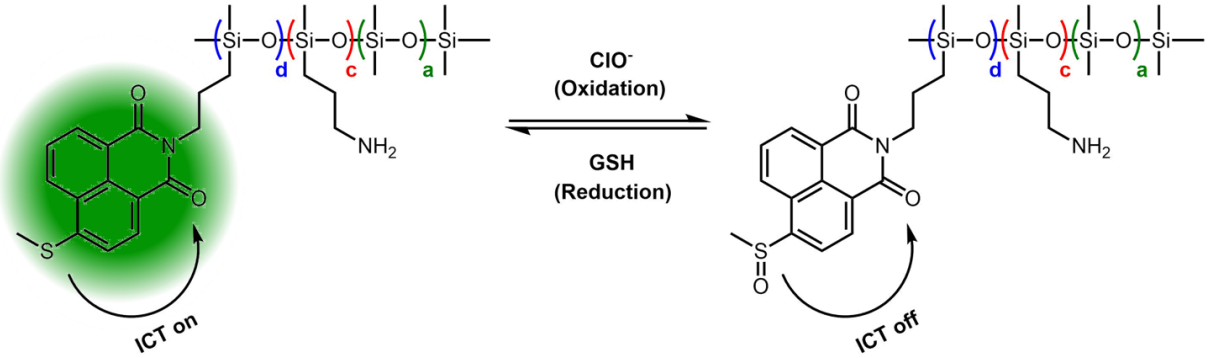

Figure 1.19. The suggested sensing mechanism for switching off fluorescence in this reversible sensor system. GSH = glutathione.

Fluorescence intensity was observed to decrease on oxidation of the thioether to the sulfoxide, with a corresponding disappearance of the UV band at 390 nm and appearance of a new band at 330 nm. This fluorescence can be recovered through the reduction of the sulfoxide with GSH. Both the oxidation and reduction processes were shown to be specific to ClO^- and GSH over other select reactive oxygen species and thiols respectively. The reversibility of this system has been validated with five repeated redox cycles, showing adequate recovery of the fluorescence. When compared to the earlier irreversible example, the response speed of the system to the analyte is significantly faster (~200 seconds for almost complete fluorescence intensity loss).

Despite successful validation of the proof-of-concept of the system in both living cells and zebrafish, there has been no further study beyond merely demonstrating the

fluorescence response to the ClO^-/GSH redox pair, *e.g.* the possibility of calibration and monitoring of concentration *in cellulo*. Further studies such as this will likely be complicated by the lack of a ratiometric signal, meaning that any signal change observed is a function of both the internalised sensor as well as the analyte concentration.

These discussed examples all feature sensors specific to one particular analyte of interest. An alternative approach worthy of mention is the use of a fluorescence sensing array. Here, the use of several less selective fluorescent receptors in parallel produces a fingerprint pattern of emission in response to an analyte. Multiple analytes can be screened against the fluorescent sensing array, allowing them to be distinguished, (Figure 1.20).[41] The amount of data obtained from this approach can be significant, drastically increasing with the number of fluorescent receptors and analytes involved. Data analysis is therefore often performed using statistical techniques, *e.g.* such as principal component analysis (PCA) to simplify the data whilst retaining the important information contained within the variation of receptor response towards the analytes.

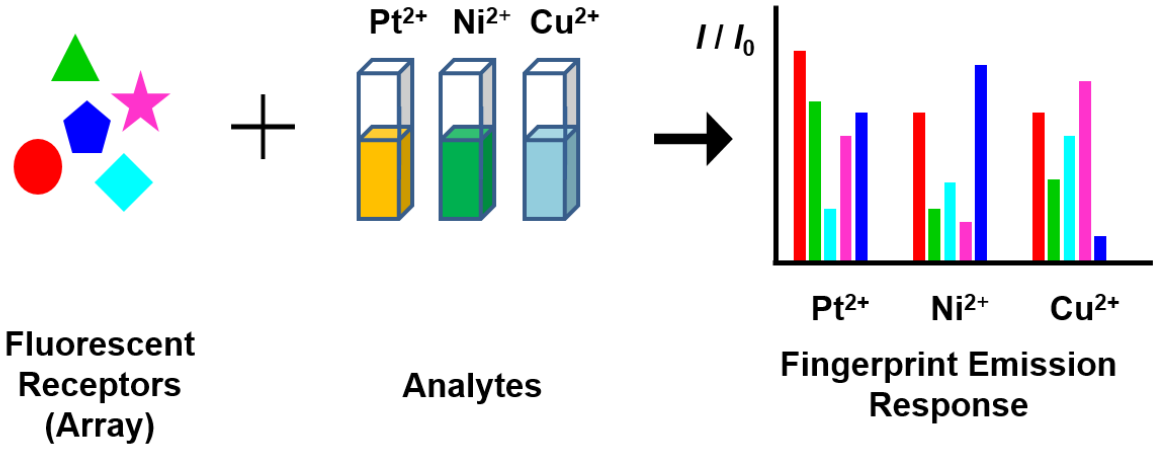

Figure 1.20. A fluorescent sensing array uses multiple non-specific fluorescent receptors to elicit a fingerprint emission response from the different analytes.

Recently, an interesting thiocoumarin example has been reported where, rather than using an array of different receptors, a fluorescent sensing array is achieved with one receptor species. The required diversity in response arises from the double dependence of the emission intensity to both the identity of the heavy metal ion and the solvent, (Figure 1.21).[42] The fluorescence response from the thiocoumarin derivative arises from the conversion of the non-fluorescent thiocarbonyl to the highly

fluorescent carbonyl, facilitated by the heavy metal analyte. Desulfurisation such as this is well-documented in the literature.[43]

Pattern recognition methods, such as PCA, were used to analyse the interactions of the thiocoumarin derivative with eight different metal ions in both pure water and lake water samples. Adequate differentiation was achieved between the analytes. This example is akin to an irreversible sensor: the desulfurisation of the receptor required for the fluorescence response renders the sensor suitable for single use only.

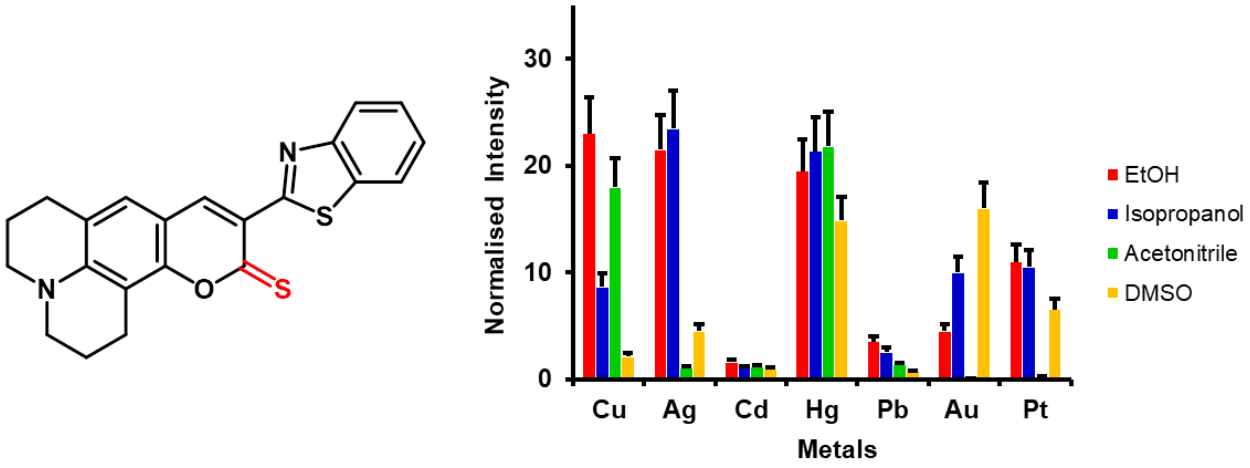

Figure 1.21. The thiocoumarin with the thiocarbonyl susceptible to desulfurization in red *(left)* and a graphical representation of the diverse solvent-dependent response of emission intensity to heavy metal ion *(right)*.[42]

1.3.1. Design Criteria for a Luminescent Sensor

A recurring theme in many, if not all, of the discussed examples is the great challenge associated with designing a good luminescent sensor. Whilst all of the reported responsive systems demonstrate success to varying degree, very few, if any, truly satisfy the demanding requirements of a successful responsive luminescent system.

The format in which a luminescent sensor will be used is an important element to consider and inevitably influences design. For example, the necessary criteria will vary significantly for a sensor proposed for use in a cuvette only, when compared to one intended for biological systems, *i.e. in cellulo* or *in vitro*, or for use in a high throughput assay.

For biological applications the sensor must first be able to enter the system itself. Studies *in cellulo* require the sensor to pass through the cell membrane independently or be attached to a mobile vector capable of dragging it inside, often to a specific cellular compartment. Many chemical moieties have been found to hinder or be entirely incompatible with passage through the cell membrane and this aspect must be considered to ensure the sensor is biocompatible. Following internalisation, the sensor must exhibit a change in luminescence in response to the analyte. If this is achieved through photon excitation, then this must be possible at a practicable wavelength. It is widely recognised that wavelengths above 330 nm are desirable to avoid photo-bleaching and damage to the biological system.[44] It is often advantageous to use an excitation wavelength that coincides with the emission of common lasers and LEDs (*e.g.* 355, 365, 405 or 488 nm) to avoid the need for expensive quartz optics (<340 nm).

The sensor must therefore be fit for purpose according to the context in which it will be used. If monitoring of a stimulus in real-time is desired, then the sensor must have the capability of responding rapidly on the required timescale.

Signal transduction for a luminescent sensor involves either the modulation of the emission intensity at a given wavelength, changes in the ratio of two emission intensities at different wavelengths or variation of the lifetime or polarisation of emission. Interaction of the sensor with the analyte must be clearly signalled and it is desirable to have as significant a modulation of the signal as possible. Such systems are often rather loosely described as ‘switch on’ sensors. It is beneficial if this luminescence change is exclusively due to the intended analyte (specificity), rather than being a function of a secondary stimulus, such as a competing analyte or a process like undesired excited state quenching. The observation of a time-gated signal is also a desirable option, in order to remove light scattering or the autofluorescence of any biological chromophores from consideration.

Calibration of the sensor’s output signal is essential and is highly medium-specific. It is highly advantageous for a sensor to generate a ratiometric response, allowing for elimination of the signal dependence on concentration, reducing sensitivity to other external factors and serving as an ‘internal’ self-calibration process.

Several criteria are universal. The need for high solubility in the medium, often aqueous to be relevant for most applications, is self-evident. For a luminescent lanthanide system, there must be high inherent kinetic stability towards dissociation of the lanthanide ion. This is particularly pertinent for biology where, as demonstrated with Gd(III) in the context of MRI contrast agents, toxicity concerns must be thoroughly eliminated. Finally, in the case of lanthanide systems, it is desirable to maximise the molar extinction coefficient, ε, in addition to the quantum yield, in order for the sensor system to be as bright as possible.

Table 1.2. Summary of criteria for a responsive luminescent sensor intended for *in cellulo* use.

Property	*Essential*	*Highly Desirable*	*Beneficial*
High medium solubility	■		
Low toxicity	■		
Efficient and rapid cell-uptake of sensor		■	
High brightness ($B = \varepsilon\Phi$)		■	
Appropriate excitation wavelength (>330 nm)		■	
Significant modulation of signal		■	
Specific signal response	■		
Capability for time-gated reading		■	
Ratiometric reading			■
Signal calibration in medium	■		
Capability for monitoring in real-time		■	
Fast response to analyte			■

1.3.2. Importance of pH in biology

pH is a critical determinant in biology and is tightly controlled, with the efficient operation of most processes being reliant on the pH being maintained within a specific range.[45] This is evidenced by how pH is naturally regulated by various buffered systems within the body, *e.g.* phosphate and bicarbonate buffers are responsible for

a significant proportion of the buffering within intra- and extra-cellular fluid, urine and blood plasma.[46-49]

There is a natural variation of pH across the various regions and compartments of a cell, (Figure 1.22). Throughout the body, key enzymes only function optimally inside a particular pH range. A significant deviation from this optimum pH range perturbs the protonation equilibrium of an enzyme, subsequently reducing its activity.[50] If the pH deviation is significant enough that the enzymes are unable to efficiently operate then this can ultimately compromise the functioning of the cell.

In many cases, the mismanagement of pH inside a particular compartment and ensuing cell malfunction has been linked to several diseases, *e.g.* lysosomal storage diseases (LSDs).[51] LSDs are a group of metabolic disorders, most involving neuronal dysfunction and neurodegeneration, *e.g.* Fabry and Gaucher type II disease. Concisely, the mutation of proteins critical for the function of the lysosome compromises the capability of the cell to regulate the digestion of species within the lysosome. The uncontrolled accumulation of undigested molecules impacts other cellular processes, including the regulation of lysosomal pH.[52]

In contexts such as these, it is evident that the ability to probe pH variations with spatial and temporal control in a biological setting becomes highly relevant. Other biological processes may also be monitored, *e.g.* processes of internalisation and endosomal uptake. For example, a common feature of the ageing process of endosomes and phagosomes is that their pH tends to fall with time over the cell cycle period, and endosomes may finally evolve into lysosomes. Thus, whilst cytosolic pH is around 7.2, endosomal pH ranges from 6.5 to 5.5 and the lowest pH is to be found in mature lysosomes, and is typically around 4.5. If the species being internalised (either a receptor or substrate) is labelled with an appropriate luminescent pH sensitive probe, the process can be followed with time.[53]

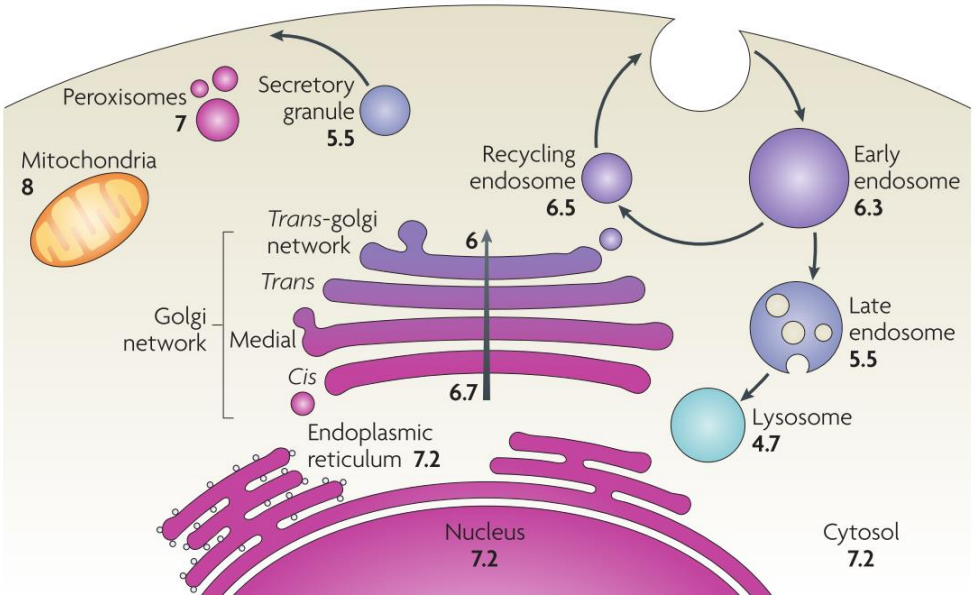

Figure 1.22. A pictorial representation of the cellular compartments within a cell. Typical pH values are given in bold.[45]

1.3.3. Fluorescent pH Sensitive Dyes

For biological applications, much work with pH has been reported using adaptations of the molecular structures of common fluorophores, *e.g.* BODIPY, rhodamine and various cyanine dyes, (Figure 1.23). It is important that the pK_a of the pH sensitive moiety is appropriately matched to the expected pH range of the system, *i.e.* the probe is fit for purpose. The pK_a can be tuned carefully through judicious structural modification that influences the position of the protonation equilibrium.

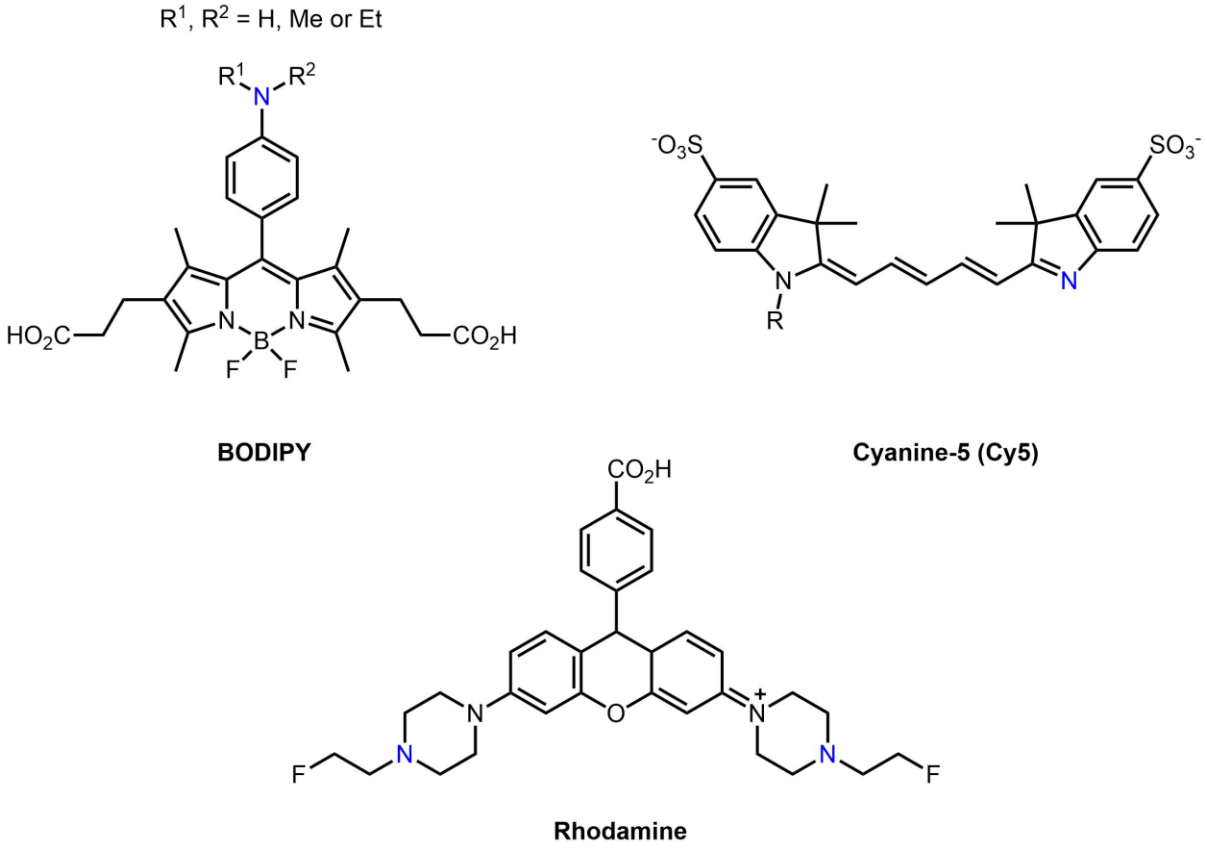

Figure 1.23. Structures of derivatives of common pH sensitive fluorescent dyes. The protonation site from which pH sensitivity arises is indicated in blue.

Work by Nagano and co-workers has used a 2,6-dicarboxyethyl-1,3,5,7-tetramethyl boron-dipyrromethene (BODIPY) fluorophore coupled with a substituted aniline in the C8 position (Figure 1.23, *top left*) to prepare a pH activatible fluorescent probe.[54] Whilst emission from BODIPY is usually pH independent and 'always on', a pH response arises from the quenching of the fluorophore emission by photoinduced electron transfer (PeT) from the highest occupied molecular orbital (HOMO) of the aniline, (Figure 1.24). The HOMO of the disubstituted aniline is sufficiently high in energy for the BODIPY fluorophore to act as an acceptor.[55] This PeT mechanism is supported by the observation that the strong fluorescence observed with the benzyl derivative is insensitive to pH.

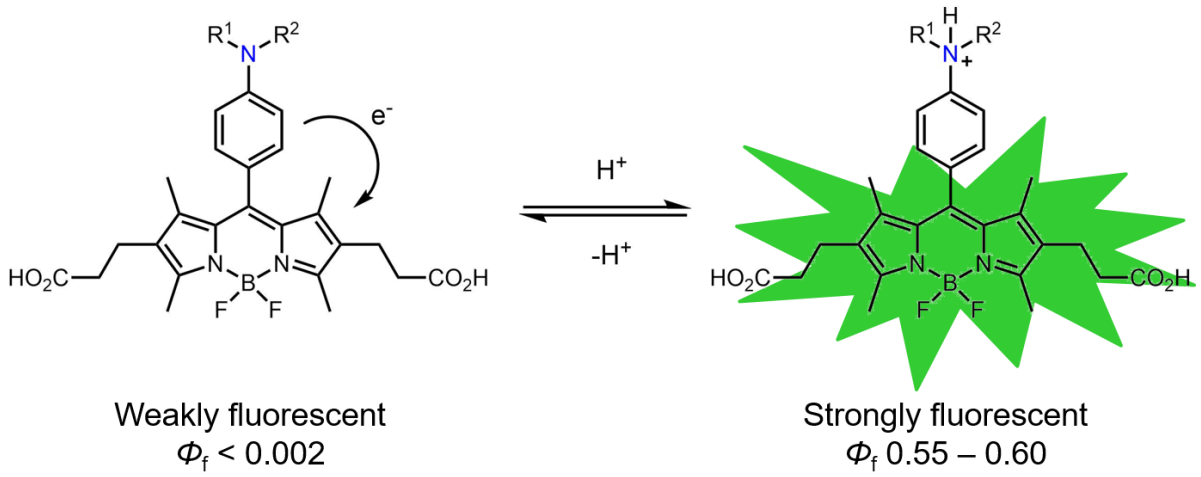

Figure 1.24. Fluorescence is quenched by PeT where the aniline is not protonated. On protonation, emission intensity increases by ~300-fold (Φ_f = fluorescence quantum yield).

The pK_a of the system is easily tuned by variation of the aniline substituents R^1 and R^2: the pK_a increases from 3.8 to 6.0 in the sequence H<Me<Et, as lone pair conjugation is increasingly disfavoured and the conjugate acid is less strongly stabilised by solvation. Regardless of the identity of the aniline substituents, general fluorescence is observed to increase ~300-fold between the pH limits of 8 and 4 (switching factor). A switching factor of this magnitude is highly desirable.

Such systems were used to examine breast cancer tissue samples and permitted the internalisation of the HER-2 antibody receptor in mice to be followed by microscopy, by labelling the immunotherapeutic agent Herceptin (Trastuzumab) through amide coupling between the antibody lysine residue and the activated NHS ester derivative of the fluorescent probe. These conjugated derivatives possessed pK_a values similar to the free probes (pK_a 4.4, 4.9 and 5.8 for the dimethyl, methylethyl, and diethyl analogues, respectively). As a consequence of the pK_a, *in cellulo* fluorescence was observed only after endosomal uptake of the dye, with increasing intensity as the dye localised in the acidic lysosome.[54]

Rhodamine fluorescence derivatives have been investigated for the purpose of visualising the dynamics of vesicular exocytosis. The trifluoroethyl derivative RhP-EF was chosen as the most suitable candidate for distinguishing intra-vesicular pH values (4 – 6) from physiological pH (7.4) with a pK_a of 5.1, (Figure 1.23, *bottom*).[56] These particular derivatives feature a piperazine pH switch which operates similarly to the

BODIPY example, via a PeT mechanism. Rhodamine derivatives are well recognised as being photostable dyes with high quantum yields[57] and accordingly RhP-EF is resistant to photolytic damage and possesses a high quantum yield under acidic conditions (Φ_f ~0.6). An *in vivo* switching factor of 95 (pH 5/pH 7.4) was determined when the dye is functionalised with an *N,N*-dimethylamino group to promote vesicle localisation, significantly lower than the switching factor of the BODIPY dye. Related studies used the methyl rhodamine derivative, RhP-M, in an assay to successfully track the internalisation of HER-2 antibodies within a human ovarian cancer cell line.[58] The HER-2 antibody was fused with engineered haloalkane dehalogenase and labelled with the pH-sensitive dye, RhP-M, which was separately functionalised with a reactive terminal haloalkane linker (Halotag protein labelling technology[59]).

Grover has reported a tandem dye system where variation in the efficiency of Förster resonance energy transfer (FRET) from a thiazole orange derivative (TO1) donor to a cyanine-5 (Cy5) analogue accepter gives rise to a pH dependent intensity ratio of green to red emission.[60] This ratiometric modulation arises from a bathchromic shift of the Cy5 absorption spectrum on protonation, increasing the spectral overlap and efficiency of the FRET process, (Figure 1.25).

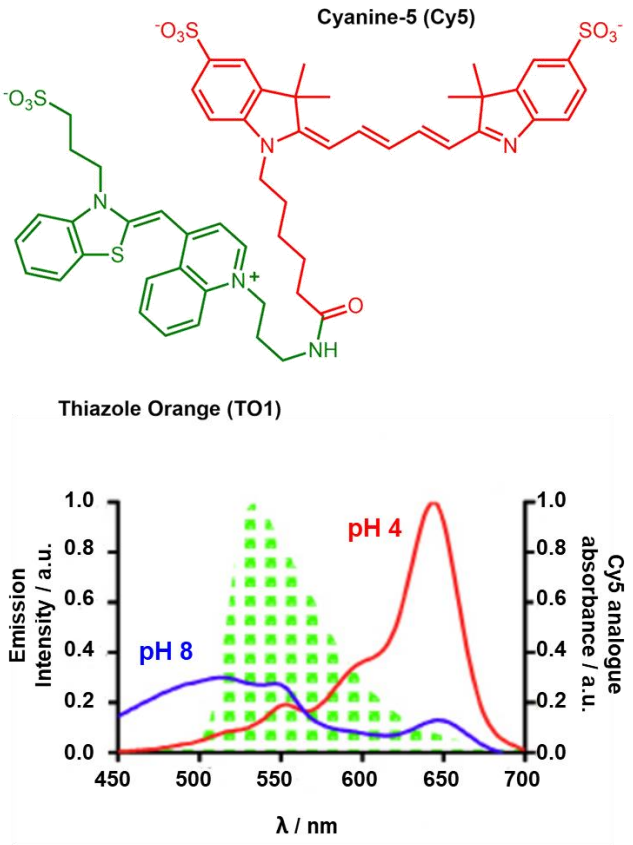

Figure 1.25. *(Top)* Structure of a pH probe where the pH independent thiazole orange derivative (TO1, green) is linked to the pH dependent cyanine-5 analogue (Cy5, red). *(Bottom)* The pH dependent spectral overlap between the TO1 emission (green, shaded) and the Cy5 absorption spectra (blue and red for pH 8 and 4 respectively) is shown.[60]

Exposure of a fluorogen-activating peptide (FAP) to the tandem dye afforded a FAP/tandem dye complex (pK_a 6.4) which demonstrated modest intensity enhancements of a factor of 5, between pH 5 and 8. The complex is chemically capable of discriminating between surface proteins at the plasma membrane over others, *e.g.* endosomal proteins. This methodology has been previously demonstrated for the selective labelling of other cell surface proteins.[61] This pH-sensitive system has been used for the selective monitoring of the β_2-adrenergic receptor, a G-protein coupled receptor (GPCR) which is a common therapeutic target for asthma and cardiovascular diseases.[62-63]

Despite demonstrating some beneficial properties and switching factors of modest to appreciable value, these fluorescent dye systems offer no significant emission lifetime modulation and suffer from the inherent issues associated with autofluorescence. A ratiometric reading is a useful property and responses from such dye systems are rare, *e.g.* the pHlourins,[64] and are not produced by either the BODIPY or rhodamine

examples. Furthermore, in some instances, photo-stability issues become prevalent, *e.g.* the 50% decrease in fluorescence intensity of the diethyl BODIPY analogue DiEtNBDP (R^1=R^2=Et) following significant light irradiation (10 J cm^{-2}) when compared to RhP-EF and two commercial dyes, pHrodo™ and CypHer5E, (Figure 1.26).[56]

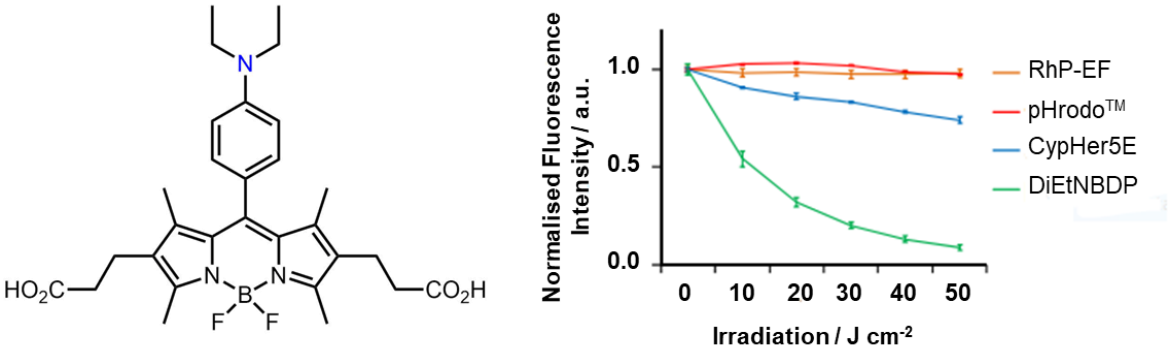

Figure 1.26. *(Left)* The diethyl BODIPY analogue DiEtNBDP. *(Right)* The photo-stability of a selection of pH responsive fluorescent probes was evaluated following irradiation (pH 5, 1 μM probe in 200 mM sodium phosphate buffer).[56]

1.3.4. pH Sensitive Lanthanide Systems

The functions of luminescence which can serve as a signal for a responsive luminescent sensor have been discussed. There are various methods for modulating these luminescent signals in response to pH for a lanthanide system and these will be examined in turn.

1.3.4.1. Reversible pH Dependent Ligation

One common method of signal modulation is reversible donor ligation. This typically involves the incorporation of a suitable arm on the chelating backbone which features a functional group with pH-dependent coordination to the lanthanide centre. The emission spectral form of europium(III) is strongly influenced by and is representative of its coordination environment.[7]

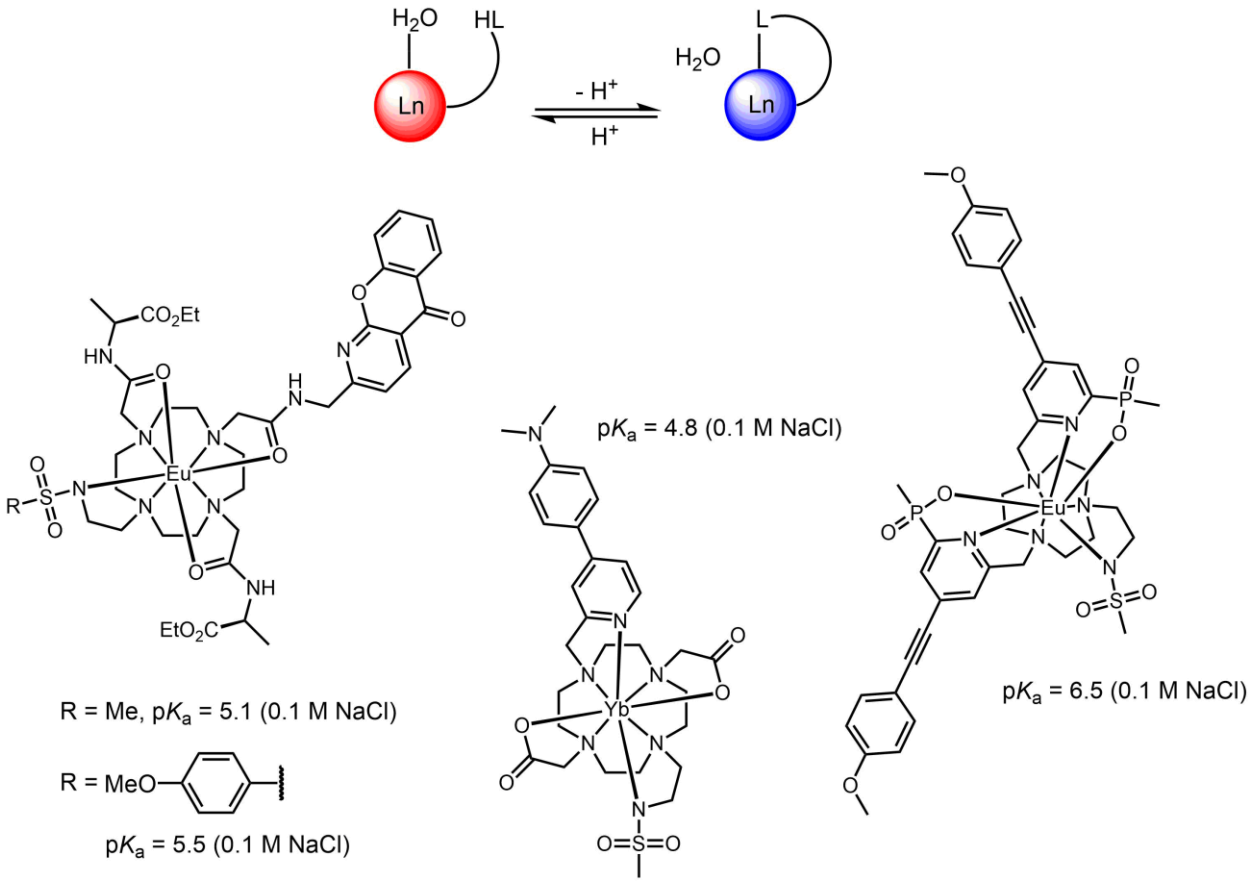

Figure 1.27. *(Top)* Schematic of reversible ligation to a lanthanide centre. *(Bottom)* Selected examples of lanthanide systems with a reversibly bound sulphonamide N atom, featuring azaxanthone *(bottom left)*, biaryl *(bottom centre)* and extended arylalkynylpyridyl *(bottom right)* sensitisers.

Several examples have been reported of the reversible coordination of a sulphonamide nitrogen atom, (Figure 1.27, *bottom*). A cyclen-based complex with an azaxanthone sensitising chromophore is one such example, (Figure 1.27, *bottom left*).[65] With decreasing pH, the sulphonamide nitrogen atom is protonated and is replaced in the europium(III) coordination sphere by a water molecule, altering the emission spectral form as a function of pH. The pK_a value was found to be dependent on the nature of the sulphonamide substituent and values of 5.1 and 5.5 were determined for the methyl and *para*-methoxyphenyl substituted sulphonamides respectively, in 0.1 M salt solution. An increase in overall emission intensity from the complex was observed on acidification, despite coordination of a water molecule capable of emission quenching by vibrational energy transfer. This behaviour was attributed to ICT quenching of the sensitiser excited state by the *p*-MeOPh group, which is only possible in the bound form at high pH.[65] A switching factor of 10 (pH

3.5/pH 9) was reported, somewhat lower compared to earlier examples. The choice of chromophore permitted excitation at 355 nm, appropriate for *in cellulo* studies where localisation to the lysosome has been suggested to be pre-determined by the nature of the aromatic sensitiser.[20] Lysosomal localisation of the complex was rapid after a one hour incubation and lysosomal pH change was assessed in real-time by confocal microscopy by monitoring the green/red Tb/Eu emission intensity ratio. The pK_a was observed to vary with the nature of the background medium, at most by half a pK_a unit in the presence of the bicarbonate anion. Such behaviour suggests that the system needs careful calibration before use.

Interestingly, the pH dependence of the sulphonamide ligation was also signalled by a modulation in the europium CPL, (Figure 1.28). The increase in the g_{em} value under basic conditions was attributed to the more rigidified structure when the sulphonamide nitrogen atom is coordinated.

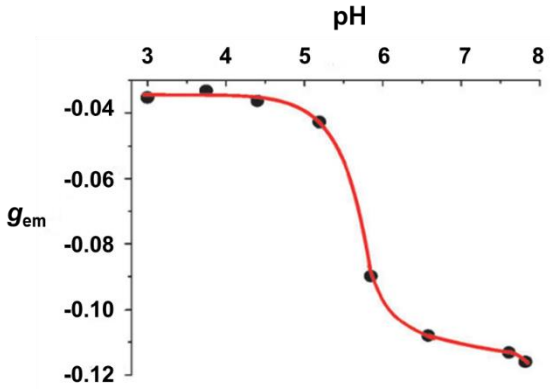

Figure 1.28. Variation of the emission dissymmetry factor, g_{em} (λ_{em} 632 nm) with pH in 0.1 M NaCl solution.[65]

A similar cyclen-based europium complex with an azathiaxanthone sensitising chromophore has also been reported, demonstrating a similar switching factor with increasing pH and a longer wavelength of excitation (370 – 405 nm).[66] Rather than using a europium/terbium emission intensity ratio, a ratiometric response was achieved using a ratio of the intensity of the $\Delta J = 1$ and $\Delta J = 4$ emission bands. This complex localised in the protein rich region of the nucleolus.

Whilst successfully meeting some of the key design criteria, these examples suffer from low molar extinction coefficients (ε = 5,700 and 6,500 M^{-1} cm^{-1} for typical azaxanthone and azathiaxanthone groups respectively), modest quantum yields (Φ <

6%) and have limited overall brightness. A related triazacyclononane europium complex with two extended arylalkynylpyridyl sensitisers and a sulphonamide arm demonstrated a higher quantum yield of 38% at high pH. The extinction coefficients (*e* values) of these sensitisers have previously been shown to be around 20,000 M^{-1} cm^{-1} for each conjugated chromophore (Figure 1.27, *bottom right*).[67] A pK_a value of 6.5 was determined for this system in 0.1 M NaCl solution, which shifted to 7.1 in a simulated extracellular medium, where competitive binding to protein and bicarbonate occurs. This pK_a value is well-matched to the pH of the cytosol and the endoplasmic reticulum (ER) (see Figure 1.22) where the complex was predominantly observed to localise in living NIH 3T3 cells. A ratiometric response was obtained (80% change from pH 4 to pH 9), monitoring the D*J* = 2/(D*J* = 0 + D*J* = 1) emission intensity ratio and the response to induced pH changes in the ER was also followed in living cells using confocal microscopy.

More recent, preliminary work from the same group reported a ratiometric NIR emitting ytterbium complex with a biaryl sensitiser and a reversibly binding sulphonamide arm, (Figure 1.27, *bottom centre*).[68] The pK_a value was observed to vary radically from 4.8 in 0.1 M NaCl to 7.1 and 7.5 in the presence of HSA and BSA proteins respectively, indicative of a strong complex-protein interaction.

Reversible ligation has also been demonstrated by Lowe *et al.*, with cyclen-based complexes functionalised with a diphenylphosphinamide arm, (Figure 1.29).[69] Coordination of the phosphinamide oxygen atom was proposed, consistent with the favourable formation of a 7-membered chelate ring, *c.f.* 5-membered ring with nitrogen coordination, and the oxophilicity of the lanthanides. Switching enhancements of 70 to 250% were demonstrated, (Figure 1.29, *bottom*). Modulation of the relaxivity of the gadolinium(III) analogues with pH was also observed. Without an appropriate sensitiser, excitation had to be performed at 270 nm, which is too short a wavelength to be compatible with biological systems.

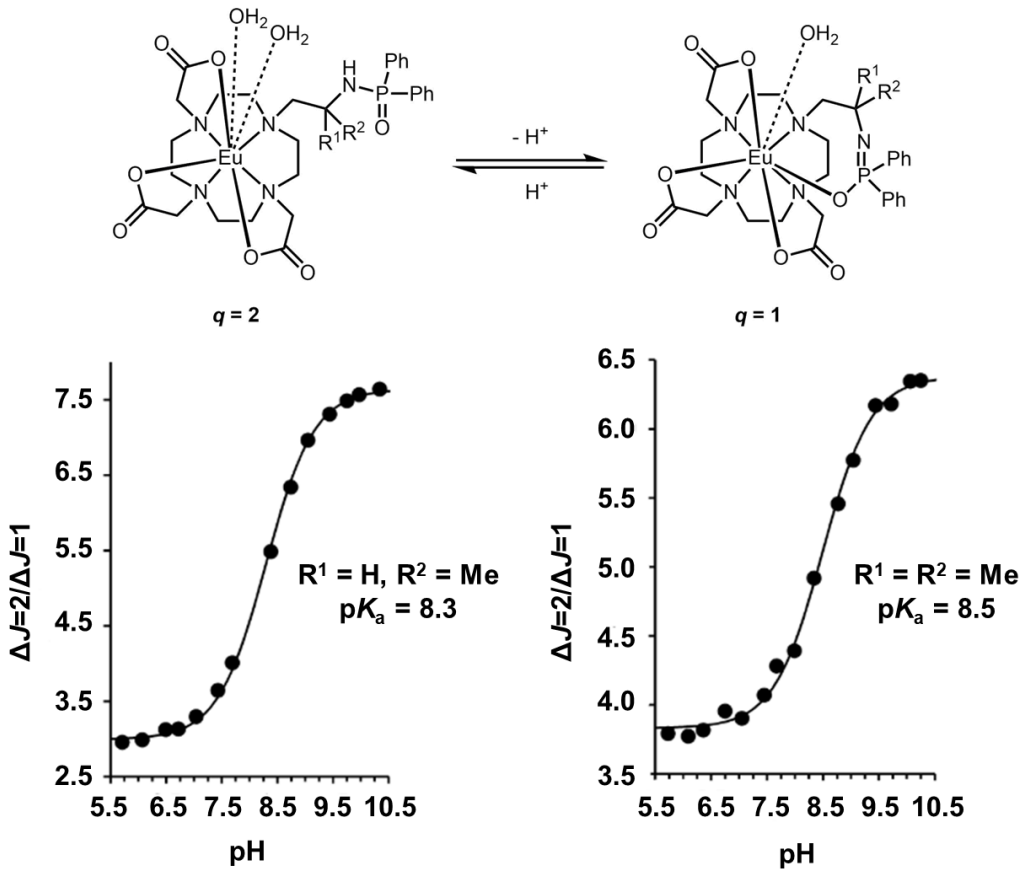

Figure 1.29. *(Top)* Suggested nature by which the diphenylphosphonamide arm reversibly binds to the lanthanide centre. *(Bottom)* Variation of the $\Delta J = 2/\Delta J = 1$ europium(III) emission intensity ratio with pH for the discussed complexes (0.1 M NaCl, λ_{exc} 270 nm). Adapted from reference [69].

With these examples, the number of water molecules in the lanthanide inner coordination sphere varied with pH. Introduction of quenching oscillators other than those of coordinated water is also possible. One such example is a dimetallic system reported by Allen, where an isopropoxy linker joins a pair of cyclen macrocycles cooperatively binding two europium ions, (Figure 1.30, *top*).[70] Protonation of the isopropoxy linker with decreasing pH introduces a hydroxyl oscillator in close proximity to the emissive europium centres through which vibrational deactivation may occur. A linear modulation in luminescence decay rate with pH was observed, independent of concentration. Selectivity of the luminescence response to pH is proposed with the coordination of other cationic species to the isopropoxy group unable to produce deactivating oscillators of appropriate energy relative to the europium centres. This assertion was hypothesised but not demonstrated.

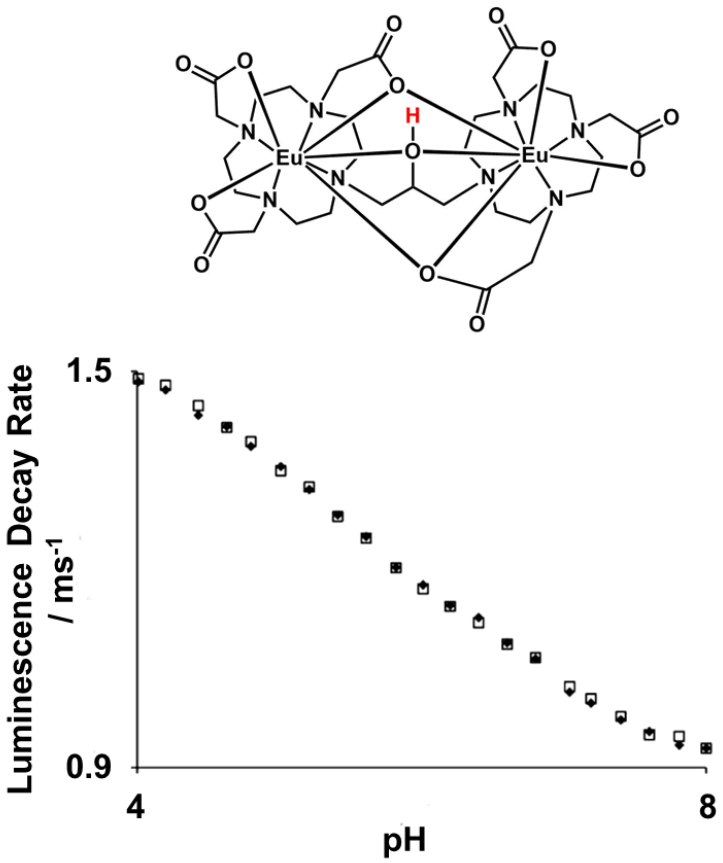

Figure 1.30. *(Top)* A pH-responsive dimetallic europium(III) system. Protonation of the isopropoxy linker is shown in red. *(Bottom)* Linear variation of the luminescence decay rate with pH (50 mM citrate and phosphate buffers, λ_{exc} 395 nm, λ_{em} 595 nm). Black diamonds and white squares correspond to 0.5 mM and 1 mM complex, respectively. Adapted from reference [70].

The reversible binding to the europium centre does not have to be intramolecular. Recent work from Patra reports a reversible pH response from a europium(III) complex bound by 1,8-naphthalimide appended terpyridine (Naptpy) and 2-thenoyltrifluoroacetone (tta) ligands, (Figure 1.31, *top*).[71] The mechanism of pH response was attributed to the dissociation of tta with either increasing or decreasing pH and subsequent replacement with coordinating water molecules, capable of quenching the europium(III) emission through vibrational energy transfer. Although an impressive ε value is reported at a suitable wavelength (ε = 64,000 M^{-1} cm^{-1} at 349 nm), efficient sensitisation of the europium centre was not achieved, evident from the broad emission band at ~450 nm characteristic of ligand luminescence. The S_1 and T_1 energy levels for tta are 25,164 and 18,954 cm^{-1} in energy respectively,[72] whilst DFT calculations estimated the energy of the S_1 and T_1 levels to be 28,025 and 22,987 cm^{-1} respectively for Naptpy.[71] The inefficiency of europium sensitisation can therefore

be ascribed to either the sizeable ligand S_1-T_1 energy gaps (~5,000 and 6,000 cm^{-1} for Naptpy and tta respectively), promoting ligand fluorescence over ISC, or the large energy gap between the Naptpy T_1 and the excited europium $^5D_0$ (~6,000 cm^{-1}), promoting Naptpy phosphorescence and BET over energy transfer to the lanthanide.

A minimal pH change is observed over the physiological pH range, (Figure 1.31, *bottom inset*). An emission response was reported in the presence of citrate, fluoride, acetate, tartaric acid, bicarbonate and ascorbate anions via the displacement of the tta ligands. It is clear that this system demonstrates little selectivity, with the response mechanism appearing to arise from a lack of complex stability; such a system has no practicable use in a complex medium.

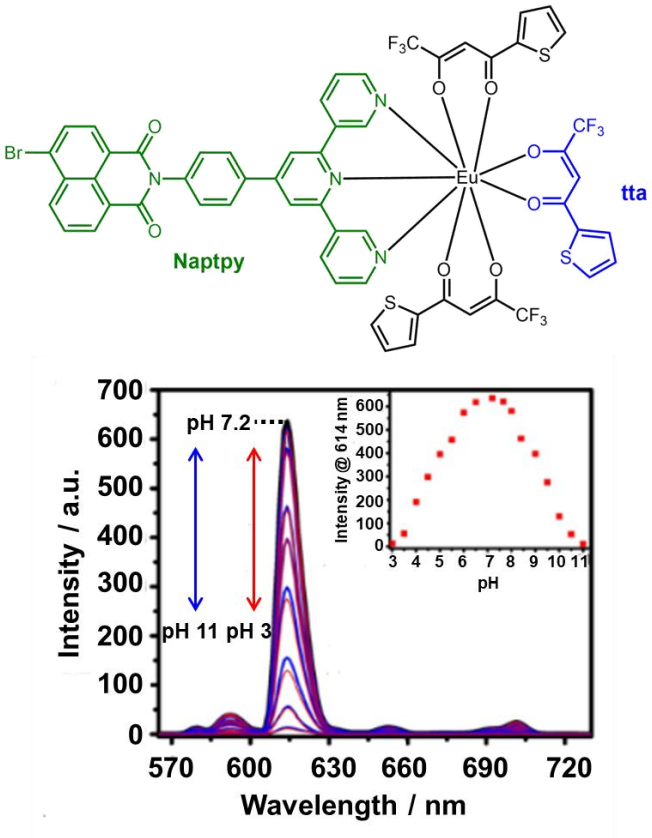

Figure 1.31. *(Top)* Structure of the discussed europium(III) complex, [Eu(Naptpy)(tta)$_3$]. *(Bottom)* Variation of the europium(III) emission intensity with pH (5 mM Tris-buffer, λ_{exc} 349 nm). The emission intensity at 614 nm (ΔJ = 2 manifold) with pH is given in the inset. Adapted from reference [71].

1.3.4.2. Modulating Transfer Processes

Signal modulation may also be achieved through mechanisms other than pH-dependent ligation, *e.g.* involving processes such as ICT or PeT. Here, the coordination environment around the lanthanide remains constant.

A europium(III) complex based on a terpyridine poly-acid derivative from Yuan shows reversible pH-dependent luminescence, with a pK_a of 5.8.[73] At higher pH, deprotonation of a phenolic OH group enables a metal-to-ligand charge transfer (MLCT) state to quench europium(III) emission. The degree of quenching reflects the position of the equilibrium between the protonated and unprotonated species. In contrast, the analogous terbium(III) complex lacks this MLCT state and is insensitive to pH, allowing a green/red ratiometric probe to be created. A ratiometric absorbance variation was also found, characterised by an isosbestic point. This ratiometric system demonstrates a small switching factor of around 6 (pH 4/pH 8.5) and involved fairly long luminescence lifetimes (1.38 and 2.11 ms for the europium(III) and terbium(III) complexes, respectively). In support of the nature of the proposed response mechanism and consistent with the lack of a change in the europium coordination environment, the emission response was shown to be selective for pH in the presence of a range of biologically relevant cations and molecules, *c.f.* [Eu(Naptpy)(tta)$_3$].

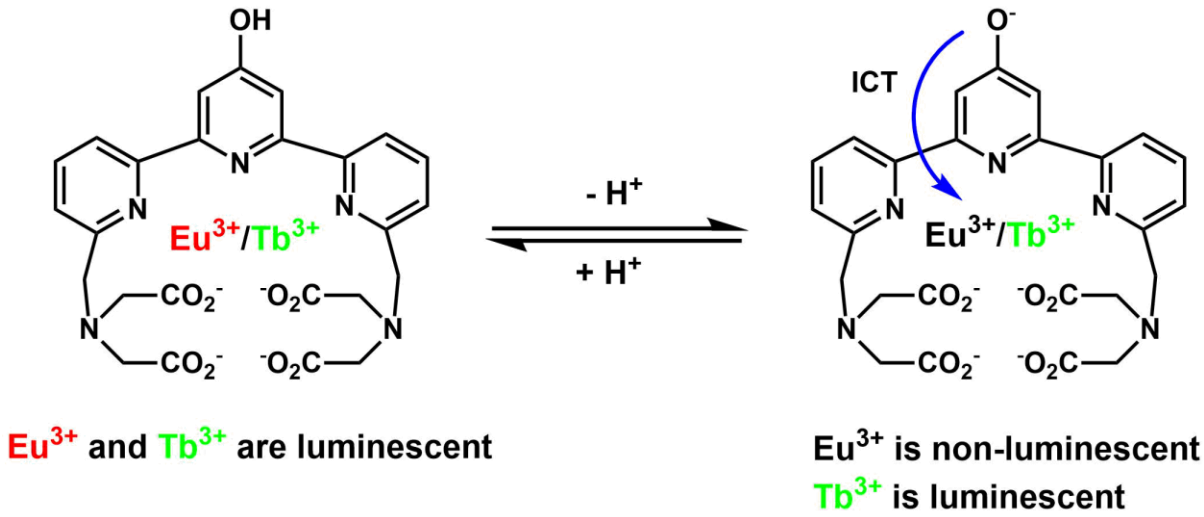

Figure 1.32. Emission from the europium(III) complex is quenched by internal charge transfer (ICT) following phenol deprotonation under basic conditions, whereas emission from the terbium(III) complex is independent of pH. Adapted from reference [73].

Another example from Patra features a conjugated diethylenetriaminepentaacetic acid (DTPA) derivative with sensitising napthalimides appended with morpholine groups,

(Figure 1.33, *left*).[74] An emission pH response was reported and attributed to pH dependent PeT quenching of the sensitising naphthalimide excited state by the morpholine nitrogen lone pair. This hypothesis was supported by the lack of pH response from an analogous complex without morpholine units. The switching factors reported were very low, across all emission manifolds (<2.5, pH 2/pH 10), suggesting, in this instance, that the degree to which europium(III) emission is quenched by PeT is not significant. Consistent with this rationalisation was the observation of emission at pH 10, where the equilibrium is strongly in favour of the unprotonated complex and PeT quenching ought to be most prominent. A straightforward rationale for this behaviour is that the morpholine group is relatively distant from the naphthalimide moiety and is not conjugated to the sensitiser.

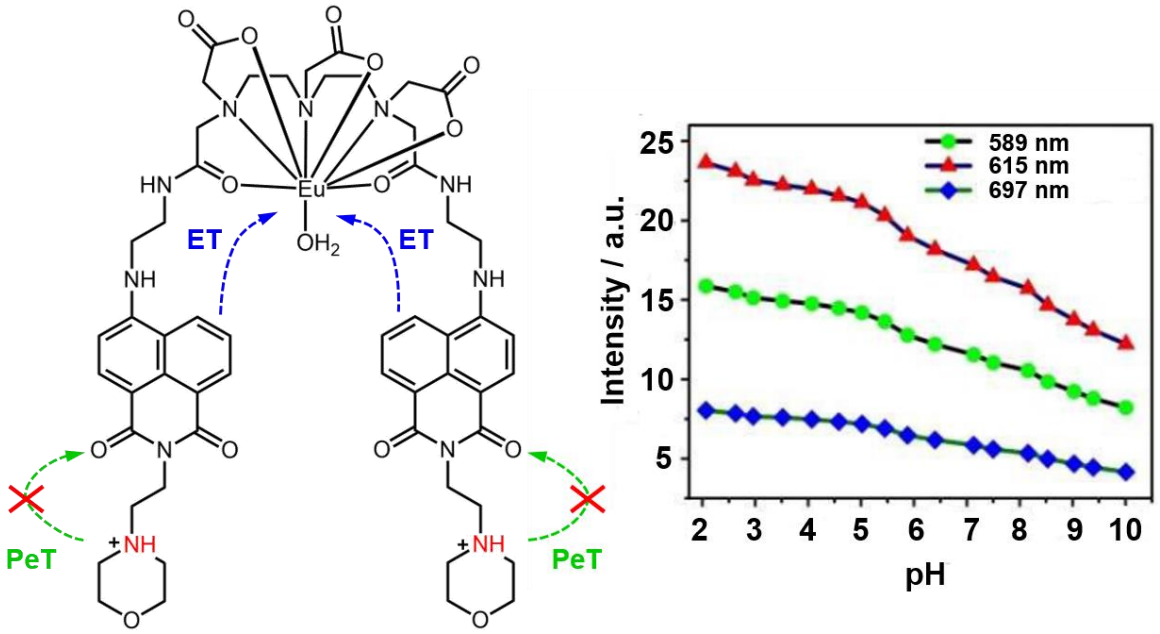

Figure 1.33. *(Left)* Structure of a pH responsive europium(III) system, where PeT in the unprotonated complex quenches the sensitiser excited state. *(Right)* Variation of emission intensity at 589 nm (green, Δ*J* = 1 manifold), 615 nm (red, Δ*J* = 2 manifold) and 697 nm (blue, Δ*J* = 4 manifold) with pH (30 μM complex, λ_{exc} 445 nm, 0.1 ms delay time, 10 mM phosphate buffer). Adapted from reference [74].

Morpholine units were chosen primarily to induce internalisation and localisation to the lysosome. Although the pK_a of the system was not reported, pK_a values of morpholine moieties substituted with various alkyl groups are known to lie in the range 7 – 8.[75] Whilst functionalisation will modify the pK_a, it is reasonable to assume the complex's pK_a will be somewhat similar. Given that the system is designed for the acidic lysosome (pH<5), the choice of a morpholine unit is not good and is not suitable for

probing pH in this environment, where pH changes in the range 4 – 5 will have little or no impact on the protonation equilibrium, as is evident from the small signal changes observed in the range 4 – 5, (Figure 1.33, *right*).

Although excitation at a beneficial wavelength (λ_{exc} 445 nm), aqueous solubility and time-gated measurements are demonstrated, competition studies have not been performed. In this instance, the emission signal may not be a simple function of pH, given the emission is partially quenched by vibrational energy transfer to a coordinating water molecule.

Other luminescent systems have been designed to probe pH based on a FRET mechanism. One such example from Meier combined a europium chelate donor and a pH sensitive carboxynaphthofluorescein (CNF) acceptor separated by a dodecyl spacer to assess pH changes in urine as an example biological fluid.[76] The pH indicator CNF possesses a broad absorption band in the range 550 – 650 nm which decreases in intensity as the pH decreases. This creates a pH emission response as the efficiency of FRET from the excited europium donor to the CNF acceptor is reduced with the decreasing degree of overlap between the CNF absorption and europium emission bands. The system was shown to cover a broad pH range (3 – 9). The pH response of CNF is dependent upon ionic strength and must be considered when calibrating the system.

1.4. Project Specification

The aim of this project is to design, synthesise, and characterise a highly pH responsive luminescent europium(III) complex for the purpose of monitoring the internalisation of a selected G-protein coupled receptor (GPCR) in living cells. If a suitable candidate is identified, the viability of the complex for this purpose will be evaluated using appropriate cell internalisation experiments.

After reviewing the numerous pH responsive systems earlier within this chapter, none of these responsive species meets the desired full specifications. The general design criteria for a successful luminescent sensor and the need for thoughtful design considering the purpose of the probe have already been discussed (section 1.3.1).

In brief, we set the following criteria for a luminescent europium(III) complex for this purpose:

i. **Appropriate pH responsive luminescent behaviour** – Luminescence from the system must be pH responsive and reversible, independent of the concentration of other endogenous species. An ideal complex will be non-luminescent around pH 7/7.5, and strongly luminescent at pH 4, with a significant ‘switch-on’ of both emission intensity and lifetime.
ii. **Long luminescence lifetime** – On acidification, a luminescence lifetime of at least 1 ms is desirable for time-gated measurements.
iii. **Suitable absorption wavelength** – In the context of a lanthanide system, the antenna must absorb light strongly above 320 nm, to avoid excitation of competing fluorophores and be compatible with common excitation sources (337, 355 and 365 nm).
iv. **High brightness** – Both the molar extinction coefficient and quantum yield must be maximised to achieve a high brightness permitting the use of the complex in low concentrations in bioassays.
v. **Defined speciation** – The speciation of the complex in the medium must be understood for any meaningful interpretation of data to be drawn. Ideally, the number of species should be minimised.
vi. **Low toxicity** – Minimal toxicity is essential for the probe to be biocompatible.
vii. **High complex stability** – The central europium(III) ion must be kinetically and thermodynamically stable with respect to lanthanide dissociation in biological media. The coordination environment of the europium(III) should be fully satisfied to avoid modulation of the luminescent signal by coordination of undesired species to the europium(III) centre.
viii. **High aqueous solubility** – The complex should be soluble in aqueous media over a broad pH range (4 – 8), appropriate for use in the cellular environment.
ix. **Suitable linker for conjugation** – The complex should contain an appropriate chemical functionality to allow for coupling of the complex to a suitable targeting vector, or for further derivatisation.
x. **Negligible non-specific binding** – The functionalisation of the complex should be appropriate such that undesirable binding of the complex in the cellular

environment (*e.g.* to proteins or the cell membrane) is minimised and preferably eliminated during internalisation experiments.

The following chapters detail the pursuit of europium(III) complexes possessing the properties described above. In chapter two, a series of core europium(III) complexes is designed, evaluated, and the nature of the mechanism for the responsive luminescence signal investigated. Chapter three focuses on the further development of these core complexes and the synthesis of these new targets. The photophysical properties of these probe candidates are then evaluated in chapter four; two of the candidates being tested in GPCR internalisation experiments. Finally, chapter five summarises parallel studies exploring the CPL, racemisation kinetics and solvatochromism behaviour of these emissive europium(III) complexes.

1.5. References

[1] E. N. Harvey, A History of Luminescence: From the Earliest Times Until 1900, Philadelphia, American Philosophical Society, 1957.

[2] G. G. Stokes, *Phil. Trans. R. Soc.,* 1852*,* **142**, 463–562.

[3] K. Przibram, *Nature,* 1935, **135**, 100.

[4] S. E. Braslavsky, *Pure Appl. Chem*., 2007, **79**, 293–465.

[5] M. Kasha, *Discuss. Faraday Soc.*, 1950, **9**, 14–19.

[6] J.-C. G. Bünzli and S. V. Eliseeva, Lanthanide Luminescence: Photophysical, Analytical and Biological Aspects, Springer, Berlin, Heidelberg, 2010.

[7] K. Binnemans, *Coord. Chem. Rev.*, 2015, **295**, 1–45.

[8] A. D'Aléo, F. Pointillart, L. Ouahab, C. Andraud and O. Maury, *Coord. Chem. Rev*., 2012, **256**, 1604–1620.

[9] K. Nakamaru, *Bull. Chem. Soc. Jpn.,* 1982, **55**, 2697–2705.

[10] D. Parker, *Chem. Soc. Rev.*, 2004, **33**, 156–165.

[11] J. Wahsner, E. M. Gale, A. Rodríguez-Rodríguez and P. Caravan, *Chem. Rev*., 2019, **119**, 957−1057.

[12] Y.-D. Xiao, R. Paudel, J. Liu, C. Ma, Z.-S. Zhang and S.-K. Zhou, *Int. J. Mol. Med.*, 2016, **38**, 1319–1326.

[13] J.-M. Idée, M. Port, C. Robic, C. Medina, M. Sabatou and C. Corot, *J. Magn. Reson. Imaging*, 2009, **30**, 1249–1258.

[14] R. B. Lauffer, *Chem. Rev*., 1987, **87**, 901–927.

[15] A. T. Bui, A. Roux, A. Grichine, A. Duperray, C. Andraud and O. Maury, *Chem. Eur. J.,* 2018, **24**, 3408–3412.

[16] S. Quici, G. Marzanni, M. Cavazzini, P. L. Anelli, M. Botta, E. Gianolio, G. Accorsi, N. Armarol and F. Barigelletti, *Inorg. Chem.,* 2002, **41**, 2777–2784.

[17] D. Maffeo and J. A. G. Williams, *Inorganica Chim. Acta,* 2003, **355**, 127–136.

[18] P. Atkinson, K. S. Findlay, F. Kielar, R. Pal, D. Parker, R. A. Poole, H. Puschmann, S. L. Richardson, P. A. Stenson, A. L. Thompson and J. Yu, *Org. Biomol. Chem.,* 2006, **4**, 1707–1722.

[19] E. P. Diamandis, *Analyst*, 1992, **117**, 1879–1884.

[20] B. S. Murray, E. J. New, R. Pal and D. Parker, *Org. Biomol. Chem*., 2008, **6**, 2085–2094.

[21] J. W. Walton, A. Bourdolle, S. J. Butler, M. Soulié, M. Delbianco, B. K. McMahon, R. Pal, H. Puschmann, J. M. Zwier, L. Lamarque, O. Maury, C. Andraud and D. Parker, *Chem. Commun*., 2013, **49**, 1600–1602.

[22] M. Soulié, F. Latzko, E. Bourrier, V. Placide, S. J. Butler, R. Pal, J. W. Walton, P. L. Baldeck, B. Le Guennic, C. Andraud, J. M. Zwier, L. Lamarque, D. Parker and O. Maury, *Chem. Eur. J.*, 2014, **20**, 8636–8646.

[23] S. J. Butler, L. Lamarque, R. Pal and D. Parker, *Chem. Sci*., 2014, **5**, 1750–1756.

[24] S. J. Butler, M. Delbianco, L. Lamarque, B. K. McMahon, E. R. Neil, R. Pal, D. Parker, J. W. Walton and J. M. Zwier, *Dalton Trans*., 2015, **44**, 4791–4803.

[25] A. T. Bui, M. Beyler, Y.-Y. Liao, A. Grichine, A. Duperray, J.-C. Mulatier, B. Le Guennic, C. Andraud, O. Maury and R. Tripier, *Inorg. Chem.,* 2016, **55**, 7020–7025.

[26] N. Hamon, M. Galland, M. Le Fur, A. Roux, A. Duperray, A. Grichine, C. Andraud, B. Le Guennic, M. Beyler, O. Maury and R. Tripier, *Chem. Comm.,* 2018, **54**, 6173–6176.

[27] A. Bourdolle, M. Allali, J.-C. Mulatier, B. Le Guennic, J. M. Zwier, P. L. Baldeck, J.-C. G. Bünzli, C. Andraud, L. Lamarque and O. Maury, *Inorg. Chem.*, 2011, **50**, 4987–4999.

[28] J. Xu, T. M. Corneillie, E. G. Moore, G.-L. Law, N. G. Butlin and K. N. Raymond, *J. Am. Chem. Soc.*, 2011, **133**, 19900–19910.

[29] D. Imbert, S. Comby, A.-S. Chauvin and J.-C. G. Bünzli, *Chem. Commun.*, 2005, **11**, 1432–1434.

[30] S. Comby, D. Imbert, C. Vandevyver and J.-C. G. Bünzli*, Chem. Eur. J.,* 2007, **13**, 936–944.

[31] N. M. Shavaleev, L. P. Moorcraft, S. J. A. Pope, Z. R. Bell, S. Faulkner and M. D. Ward, *Chem. Eur. J*., 2003, **9**, 5283–5291.

[32] D. Imbert, M. Cantuel, J.-C. G. Bünzli, G. Bernardinelli and C. Piguet, *J. Am. Chem. Soc.,* 2003, **125**, 15698–15699.

[33] B. N. Samoilov, *J. Exp. Theor. Phys.*, 1948, **18**, 1030–1039.

[34] C. A. Emeis and L. J. Oosterhoff, *J. Chem. Phys.*, 1971, **54**, 4809–4819.

[35] R. Carr, N. H. Evans and D. Parker, *Chem. Soc. Rev.*, 2012, **41**, 7673–7686.

[36] J. L. Lunkley, D. Shirotani, K. Yamanari, S. Kaizaki and G. Muller, *J. Am. Chem. Soc*., 2008, **130**, 13814–13815.

[37] L. E. MacKenzie, L.-O. Pålsson, D. Parker, A. Beeby and R. Pal, *Nat. Commun.*, 2020, **11**, 1676.

[38] J. Ohata, K. J. Bruemmer and C. J. Chang, *Acc. Chem. Res.,* 2019, **52**, 2841−2848.

[39] K. J. Bruemmer, O. Green, T. A. Su, D. Shabat and C. J. Chang, *Angew. Chem.,* 2018, **57**, 7508–7512.

[40] Y. Zuo, Y. Zhang, B. Dong, Z. Gou, T. Yang and W. Lin, *Anal. Chem.*, 2019, **91**, 1719–1723.

[41] D. G. Smith, I. L. Topolnicki, V. E. Zwicker, K. A. Jolliffe and E. J. New, *Analyst***,** 2017, **142**, 3549–3563.

[42] D. G. Smith, L. Mitchell and E. J. New, *Analyst*, 2019, **144**, 230–236.

[43] J. O. Moon, M. G. Choi, T. Sun, J.-I. Choe and S.-K. Chang, *Dyes and Pigments*, 2013, **96**, 170–175.

[44] M. C. Heffern, L. M. Matosziuk and T. J. Meade, *Chem. Rev.,* 2014, **114**, 4496−4539.

[45] J. R. Casey, S. Grinstein and J. Orlowski, *Nat. Rev. Mol. Cell Biol.*, 2010, **11**, 50–61.

[46] J. Leung and M. Crook, *J. Clin. Pathol.,* 2019, **72**, 741–747.

[47] S. Vasuvattakul, L. C. Warner and M. L. Halperin, *Am. J. Physiol. Regul. Integr. Comp. Physiol.*, 1992, **262**, R305–R309.

[48] M. Gowrishankar, K. S. Kamel and M. L. Halperin, *JASN*, 2007, **18**, 2278–2280.

[49] S. J. Choi and J. Lim, *J. Math. Anal. Appl*., 2009, **356**, 145–153.

[50] H. Bisswanger, *Perspectives in Science*, 2014, **1**, 41–55.

[51] S. Shuvaev, M. Starck and D. Parker, *Chem. Eur. J.*, 2017, **23**, 2–18.

[52] M. L. Schultz, L. Tecedor, M. Chang and B. L. Davidson, *Trends in Neuroscience*, 2011, **34**, 401–410.

[53] M. Starck, J. D. Fradgley, R. Pal, J. M. Zwier, L. Lamarque and D. Parker, *Chem. Eur. J.*, 2021, **27**, 766–777.

[54] Y. Urano, D. Asanum, Y. Hama, Y. Koyama, T. Barrett, M. Kamiya, T. Nagano, T. Watanabe, A. Hasegawa, P. L. Choyke and H. Kobayashi, *Nat. Med.,* 2009*,* **15**, 104–109.

[55] A. Loudet and K. Burgess, *Chem. Rev*., 2007, **107**, 4891–4932.

[56] D. Asanuma, Y. Takaoka, S. Namiki, K. Takikawa, M. Kamiya, T. Nagano, Y. Urano and K. Hirose, *Angew. Chem. Int. Ed*., 2014, **53**, 6085–6089.

[57] M. Beija, C. A. M. Afonso and J. M. G. Martinho, *Chem. Soc. Rev*., 2009, **38**, 2410–2433.

[58] M. Isa, D. Asanuma, S. Namiki, K. Kumagai, H. Kojima, T. Okabe, T. Nagano and K. Hirose, *ACS Chem. Biol.,* 2014, **9**, 2237−2241.

[59] G. V. Los, L. P. Encell, M. G. McDougall, D. D. Hartzell, N. Karassina, C. Zimprich, M. G. Wood, R. Learish, R. Friedman Ohana, M. Urh, D. Simpson, J. Mendez, K. Zimmerman, P. Otto, G. Vidugiris, J. Zhu, A. Darzins, D. H. Klaubert, R. F. Bulleit and K. V. Wood, *ACS Chem. Biol.*, 2008, **3**, 373–382.

[60] A. Grover, B. F. Schmidt, R. D. Salter, S. C. Watkins, A. S. Waggoner and M. P. Bruchez, *Angew. Chem. Int. Ed*., 2012, **51**, 4838–4842.

[61] C. Szent-Gyorgyi, B. F. Schmidt, Y. Creeger, G. W. Fisher, K. L. Zakel, S. Adler, J. A. J. Fitzpatrick, C. A. Woolford, Q. Yan, K. V. Vasilev, P. B. Berget, M. P. Bruchez, J. W. Jarvik and A. Waggoner, *Nat Biotechnol*., 2008, **26**, 235–240.

[62] N. V. Wasilewski, M. D. Lougheed and J. T. Fisher, *Curr. Opin. Pharmacol.*, 2014, **16**, 148–156.

[63] W. J. Koch, *Mol. Cell. Biochem*., 2004, **263**, 5–9.

[64] S. Sankaranarayanan, D. De Angelis, J. E. Rothman and T. A. Ryan, *Biophys. J.*, 2000, **79**, 2199–2208.

[65] D. G. Smith, B. K. McMahon, R. Pal and D. Parker, *Chem. Commun*., 2012, **48**, 8520–8522.

[66] R. Pal and D. Parker, *Chem. Commun*., 2007, **5**, 474–476.

[67] B. K. McMahon, R. Pal and D. Parker, *Chem. Commun*., 2013, **49**, 5363–5365.

[68] S. Shuvaev and D. Parker, *Dalton Trans*., 2019, **48**, 4471–4473.

[69] M. Giardiello, M. Botta and M. P. Lowe, *Inorg. Chem*., 2013, **52**, 14264−14269.

[70] J. D. Moore, R. L. Lord, G. A. Cisneros and M. J. Allen, *J. Am. Chem. Soc*., 2012, **134**, 17372−17375.

[71] K. Gupta and A. K. Patra, *Eur. J. Inorg. Chem*., 2018, **18**, 1882–1890.

[72] H. Xu, L.-H. Wang, X.-H. Zhu, K. Yin, G.-Y. Zhong, X.-Y. Hou and W. Huang, *J. Phys. Chem. B*, 2006, **110**, 3023–3029.

[73] M. Liu, Z. Ye, C. Xin and J. Yuan, *Anal. Chim. Acta*, 2013, **761**, 149–156.

[74] K. Gupta, M. Verma, P. Srivastava, S. Sivakumarb and A. K. Patra, *New J. Chem.*, 2020, **44**, 3570–3573.

[75] H. K. Hall, *J. Am. Chem. Soc.*, 1957, **79**, 5441–5444.

[76] R. J. Meier, J. M. B. Simbürger, T. Soukka and M. Schäferling, *Chem. Commun.*, 2015, **51**, 6682–6682.

CHAPTER TWO

Synthesis and Investigation of Parent Complexes

Chapter Two: Synthesis and Investigation of Parent Complexes

This chapter concerns the synthesis of the target parent complexes **[Eu.L$^{1\text{-}3}$]**, an evaluation of their photophysical properties, and assessment of their viability as 'core' complexes suitable for further development as pH-responsive lanthanide probes that are appropriate for use in a biological setting.

2.1. Target Parent Systems

In chapter one, a collection of pH-responsive luminescent probes has been documented and reviewed. At the beginning of this work, a target was set of designing a complex of europium(III) that shows a 100% change in lifetime over the pH range 8–4, accompanied by a change in emission intensity of two orders of magnitude. Such desirable properties require careful consideration of the mechanism of the process leading to emission quenching. Accordingly, the complexes **[Eu.L$^{1\text{-}3}$]** were proposed as candidates for study, in the expectation that the best examples would be taken forward as 'core' complexes for further development, (Figure 2.1). These complexes possess similar structural features, differing only in their number of antenna chromophores.

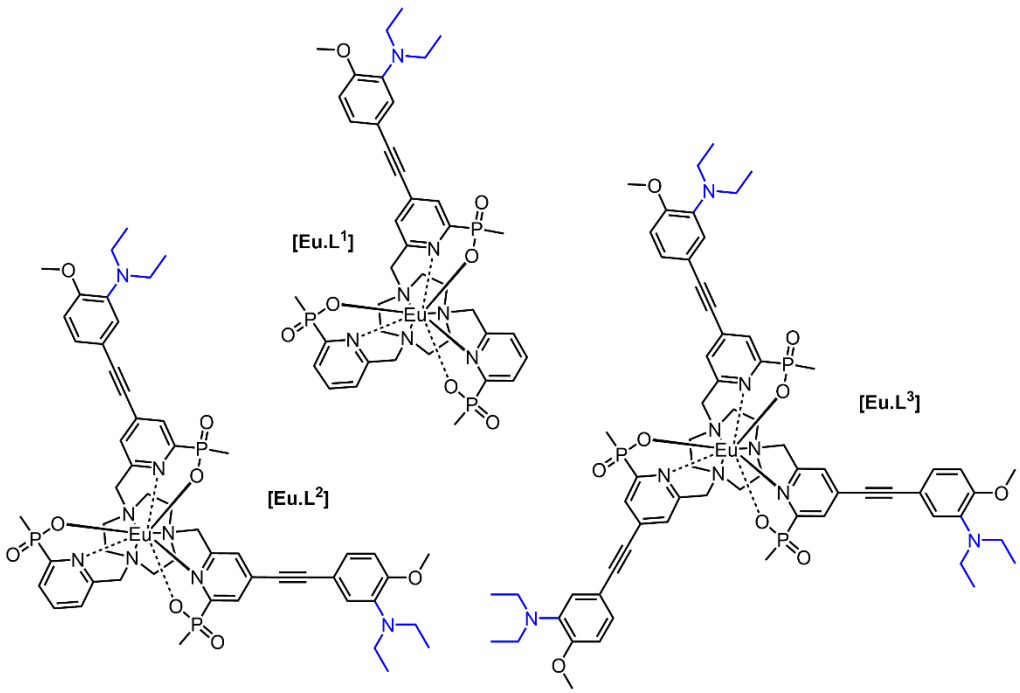

Figure 2.1. Structures of the target parent complexes **[Eu.L$^{1\text{-}3}$]**.

The design criteria for a successful luminescent sensor have been briefly reviewed and discussed (chapter one, section 1.3.1). Varying in their number of antennae, each of the europium complexes **[Eu.L$^{1\text{-}3}$]** feature pyridylalkynylaryl chromophores, functionalised with *para*-methoxy and *meta*-diethylamino groups. These highly conjugated antennae have been shown to sensitise europium emission efficiently, possess high ε values, and allow excitation above 330 nm, especially with electron-donating substituents in the aryl ring.[1] Europium binding has been reported with both phosphinate and carboxylate donor groups.[1-2] For this work, phosphinate donors were chosen, given the greater polarisability of the P-O bond and the higher ligand field strength. Where a chelating arm is not an extended antenna, a single pyridine moiety bearing a chelating phosphinate group was proposed, in order to preserve a high degree of local symmetry about the europium centre.

The substituents of the amino group were selected bearing in mind the reported pK_a values of simple anilines in aqueous media, with the aim of producing a system with a pK_a within the range 5.5 – 6. For each of these complexes, it was reasoned that acidification would lead to suppression of photo-induced electron transfer from the nitrogen lone pair to the excited europium ion, enhancing the intensity of europium emission by analogy to a plethora of published examples.[3-5] The complexes **[Eu.L$^{1\text{-}3}$]** vary in their number of diethylamino groups and it was considered necessary to investigate the full series to determine the impact on behaviour, if any, of the presence of multiple protonation sites.

Analogous europium complexes were prepared by Dr. Matthieu Starck in Durham at the outset of this work, featuring functionalised amine groups in differing locations on the aryl ring, (Figure 2.2). In this case, *para*-functionalisation of the aromatic ring with a conjugated dimethylamino group resulted in total quenching of emission, in both aqueous and methanolic solution. In the alternative structure, with functionalisation at the *meta* position and a methylene spacer, only a modest emission enhancement of 55% (pH 8 to 4) was observed on acidification in aqueous methanol. It was reasoned that substitution in the *meta* position should lead to a more favourable switching on of emission, when the amino group is in partial conjugation with the sensitising chromophore and in the absence of the spacer methylene group.

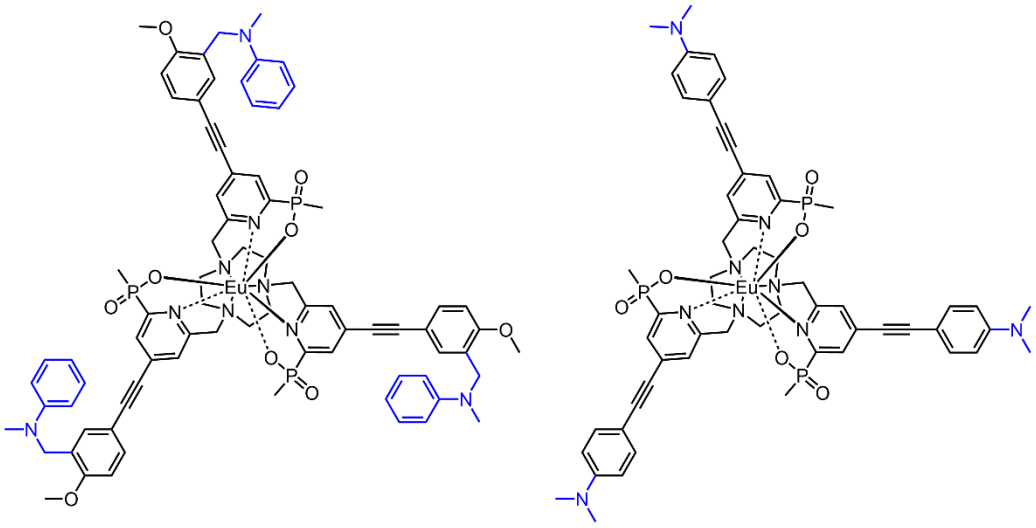

Figure 2.2. Structures of two europium(III) complexes, with variation in the functionalisation and position of the amine site (in blue) intended to induce pH sensitivity.

2.2. Synthesis of Parent Complexes

2.2.1. Retrosynthetic Analysis

A partial retrosynthetic analysis of **[Eu.L^1]** is shown (Figure 2.3) with a disconnection of the europium complex to appropriate synthetic equivalents and precursors and to the commercially available macrocycle 1,4,7-triazacyclononane (TACN).

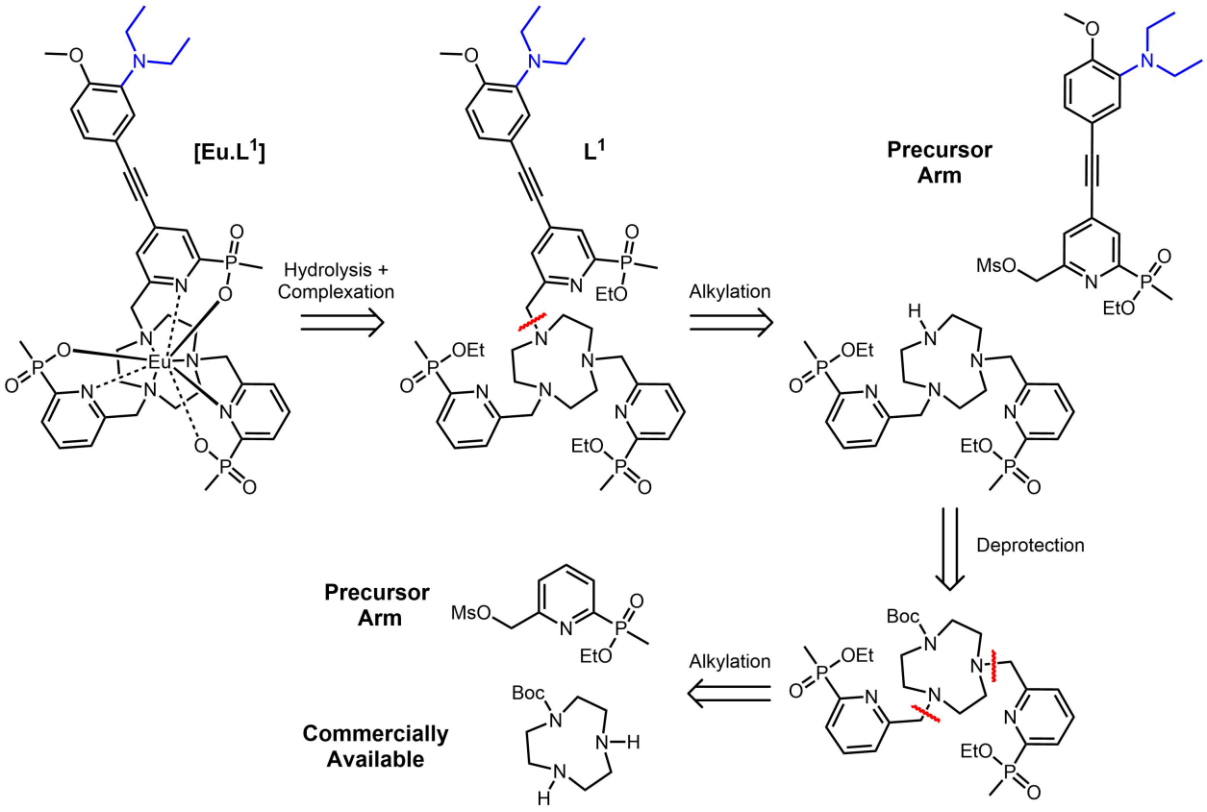

Figure 2.3. Disconnection of **[Eu.L^1]** by retrosynthesis to precursor compounds (Boc = *tert*-butyloxycarbonyl).

The synthesis of **L^1** was envisaged to proceed by the stepwise alkylation of the precursor arm units onto the TACN macrocycle, utilising a *tert*-butyloxycarbonyl (Boc) protecting group to control the extent of ring N-alkylation. Owing to the strongly acidic conditions required for the cleavage of the Boc protecting group in the subsequent deprotection step, it was planned to introduce the simple pyridine groups first,[6] to avoid undue exposure of the electron rich chromophore to such acidic conditions. This sequence circumvents potential complications with protonation of the alkyne functionality and subsequent capture of a vinyl cation by water.

Similarly, a retrosynthetic analysis was performed for the new chromophore arm. The simplification of the precursor structure to commercially available or previously described compounds is shown, (Figure 2.4). The synthesis of the extended chromophore was planned with a convergent approach to the ‘top’ and ‘bottom’

components of the compound. Here, preparation of the 4-bromopyridine derivative ('bottom' component) has been previously described.[7]

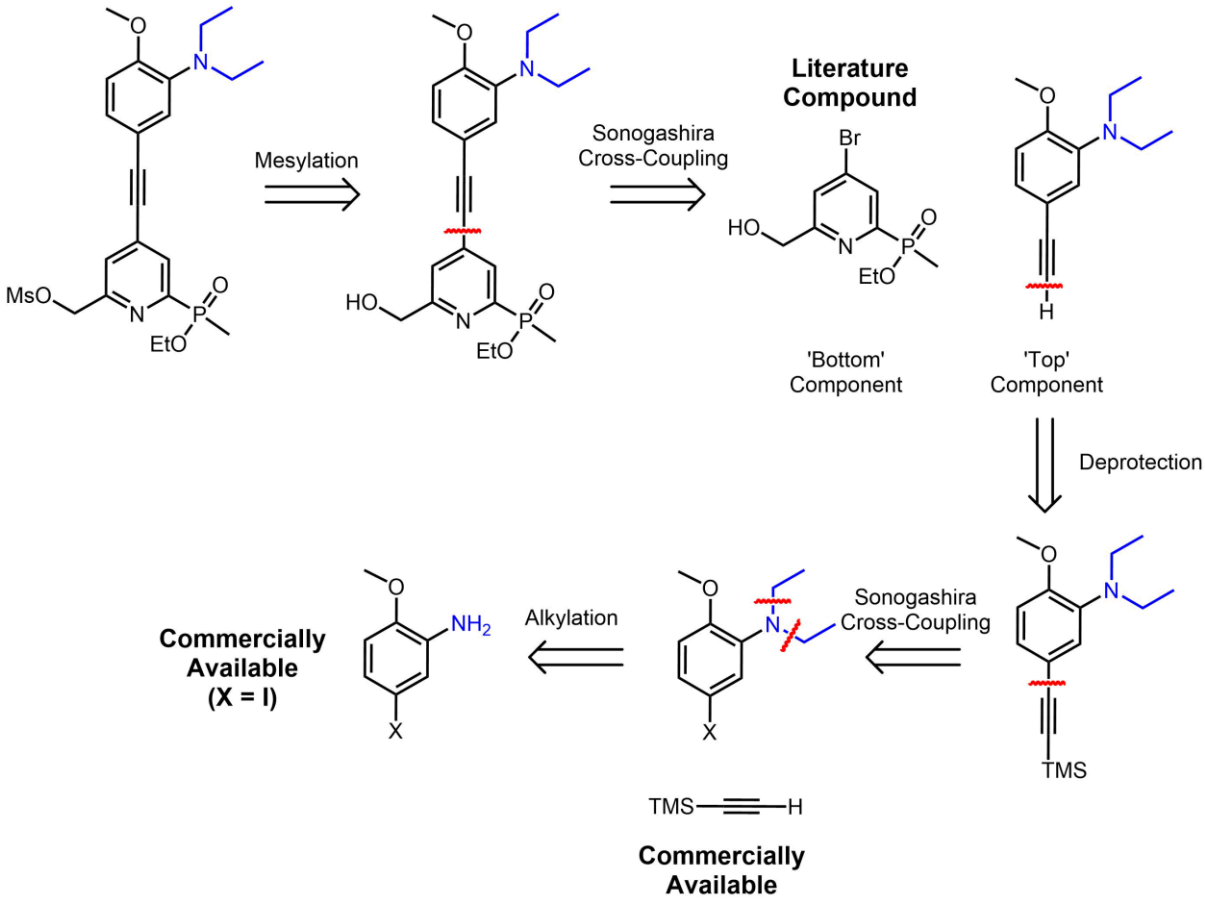

Figure 2.4. Retrosynthetic analysis performed on the extended chromophore precursor (TMS = trimethylsilyl, X = halogen).

2.2.2. Precursor Synthesis

The single pyridine precursor arm **1** was previously reported by Delbianco *et al.* and its synthesis has been described in a patent.[7] The compound was prepared in four steps from 2-bromo-6-methylpyridine, and only minor deviations to the reported procedure were made, (Figure 2.5).

In brief, controlled hydrolysis of methyldiethoxyphosphine gave MePO(OEt)H, liberating one equivalent of ethanol. This phosphinous ester was installed into the 2-position of the pyridine ring using a palladium-catalysed coupling reaction with 2-bromo-6-methylpyridine under forcing conditions. $Pd(dppf)Cl_2$.DCM was chosen as a palladium(II) source over the original catalyst $Pd(PPh_3)_4$ for a cleaner reaction,

avoiding the formation of triphenylphosphine oxide which can be awkward to separate during purification.

The pyridine N atom was then converted to the *N*-oxide using *m*CPBA followed by a [3,3]-sigmatropic Boekelheide rearrangement[8] with TFAA. Hydrolysis of the resulting trifluoroacetate ester yielded the pyridine precursor as the primary alcohol which was converted to the mesylate **1** using methanesulfonic anhydride and DIEA in THF. The anhydride reagent was preferred over the alternative mesyl chloride, in order to avoid the presence of chloride in the reaction. Earlier, it has been shown that chloride can substitute the reactive mesyl group to give the less reactive benzylic chloride derivative. The conversion of the alcohol to the mesylate was performed immediately prior to the use of the mesylate in the following alkylation reaction, because of the sensitivity of the mesylate towards hydrolysis.

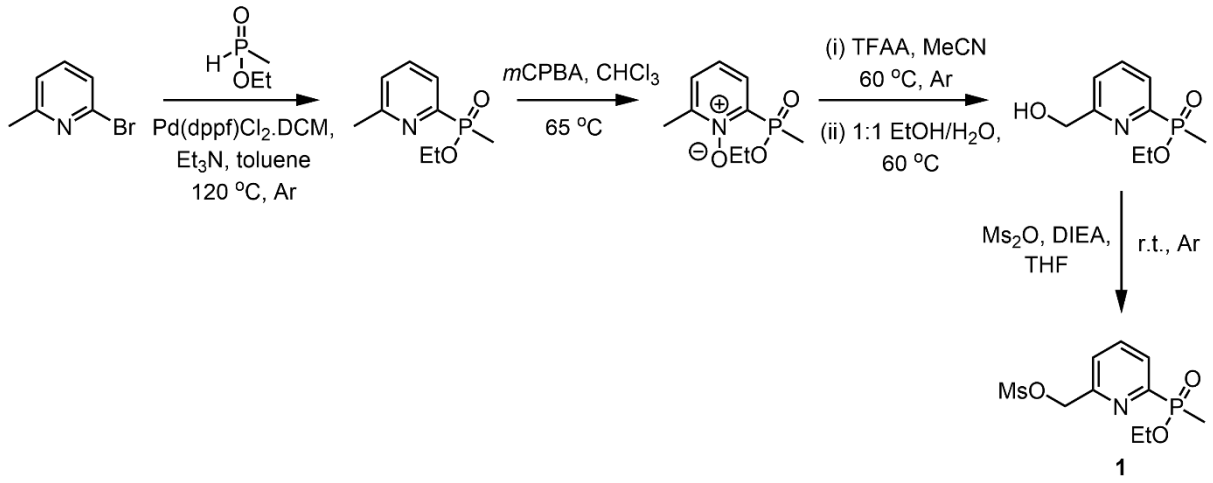

Figure 2.5. Synthesis of the single pyridine precursor arm **1**, (6-[ethoxy(methyl)phosphoryl]pyridine-2-yl)methyl methanesulfonate (dppf = 1,1'-bis(diphenylphosphino)ferrocene, *m*CPBA = *meta*-chloroperoxybenzoic acid, TFAA = trifluoroacetic anhydride, DIEA = diisopropylethylamine).

The chromophore precursor arm (Figure 2.4) was prepared via a convergent synthesis between the top and bottom components which were made, in turn, from commercially available compounds in three and eight steps, respectively.

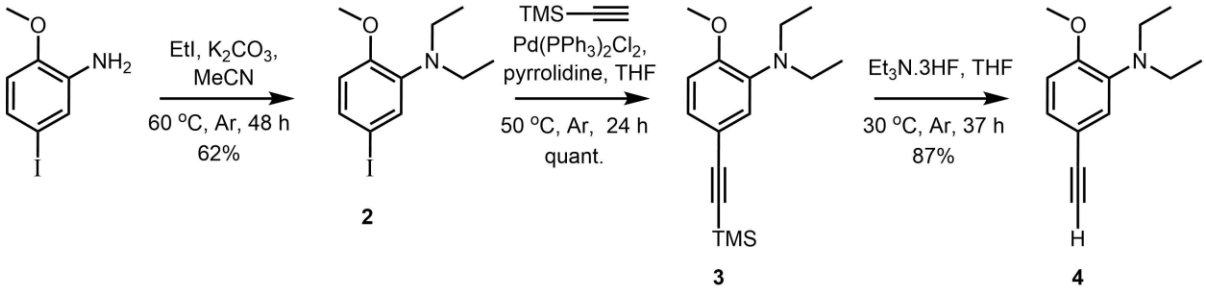

Figure 2.6. Synthesis of the top component of the chromophore, **4**.

Firstly, ethyl groups were introduced onto the commercially available 5-iodo-*o*-anisidine by an S_N2 alkylation reaction with iodoethane, using potassium carbonate as the base to give the diethylamine derivative, **2**. The second alkylation step was found to be rate-limiting, with evidence that the monoalkylated secondary amine formed rapidly as deduced by monitoring progress of the reaction using TLC and mass spectrometry. Iodoethane was chosen as a reagent over bromoethane due to its advantageous boiling point (72 °C *vs*. 38 °C), as well as the greater inherent reactivity of the electrophile in S_N2 reactions (average bond strength for C–I vs. C-Br at 273 K is 213 *vs*. 285 kJ mol^{-1})[9]. As a result of the bimolecular nature of S_N2 reactions and the rate dependence on the concentration of the species involved, the volume of solvent used was minimised. There was no evidence found by liquid chromatography mass spectrometry (LC/MS) for any undesired formation of a quaternary alkylated species. Such a reactivity profile is presumably a result of steric inhibition and the low nucleophilicity of the aromatic amine N atom, and allowed an excess of the iodoethane reagent to be used. Under these low volume, high concentration conditions, the desired dialkylated compound **2** was obtained cleanly after 48 hours, in reasonable isolated yield (62%) and no further purification beyond an aqueous work-up was required.

Next, the alkyne functionality protected by a trimethylsilyl (TMS) group was introduced through a Sonogashira metal cross-coupling reaction between **2** and trimethylsilylacetylene. These palladium-catalysed reactions are typically facilitated with a copper(I) co-catalyst. Although the effectiveness of this protocol is well-documented[10], the presence of copper leads to multiple drawbacks, including the formation of undesired homo-coupled alkyne side products and the need for strict exclusion of oxygen from the reaction.[11] A copper-free protocol avoids these issues. The latter approach was pursued with an eye on later cross-coupling reactions, where

the terminal alkyne is more ‘valuable’, requiring multiple steps to synthesise. The ‘copper-free’ cross-coupling reaction of **2** with trimethylsilylacetylene was achieved quantitatively using $Pd(PPh_3)_2Cl_2$ and pyrrolidine in THF. Success was also achieved using the catalyst $Pd(dppf)Cl_2$.DCM, albeit in lower yield (65%). The use of this latter catalyst avoids the formation of triphenylphosphine oxide which was found to be troublesome to separate from the desired product during chromatographic purification. Although maintenance of an inert atmosphere was not strictly necessary, the coupling reaction was performed under argon.

The exact mechanisms of the Pd/Cu catalysed and Cu-free Pd catalysed Sonogashira cross-coupling reactions are not known, (Figure 2.7a). Whilst the mechanism of the copper(I)-assisted Sonogashira reaction has seen little revision since its original proposition[12], there are several elements which are still debated and poorly understood, such as the interaction between the Cu and the alkyne, and the transmetallation step, (Figure 2.7b).[10] Accepted by general consensus, the Pd/Cu catalysed reaction involves oxidative addition of the C(sp^2)–X (X = halide) species onto the Pd(0) catalyst, which is typically generated *in-situ*. Transmetallation between the Pd(I) catalyst and the copper acetylide species, generated from the Cu-catalysed cycle, replaces the halide with the acetylene species. Finally, the Pd(II) catalyst undergoes reductive elimination to expel the coupled product and regenerate the Pd(0) catalyst.

The mechanism of the Cu-free Pd catalysed Sonogashira reaction is even more contested. A mechanism proposed by Soheili[13] has attained popularity where, similarly to the Pd/Cu catalysed Sonogashira, oxidative addition and reductive elimination of the Pd catalyst initiates and concludes the catalytic cycle, (Figure 2.7c). However, rather than a transmetallation step, formation of an intermediate complex is postulated involving the reversible p coordination (η^2) of the alkyne. This step is followed by base-mediated deprotonation of the acetylenic proton. Finding experimental proof for such mechanisms beyond reasonable doubt is difficult, partly due to the need to isolate or observe the key organometallic intermediates within a complex mixture. More recently, an alternative mechanism for the Cu-free Pd catalysed Sonogashira has been reported, (Figure 2.7d).[14] Here, a tandem Pd/Pd double-cycle is proposed where, similarly to the Pd/Cu catalysed Sonogashira, a

transmetallation step is proposed to follow oxidative addition with the Pd atom playing an almost identical role to the copper co-catalyst.

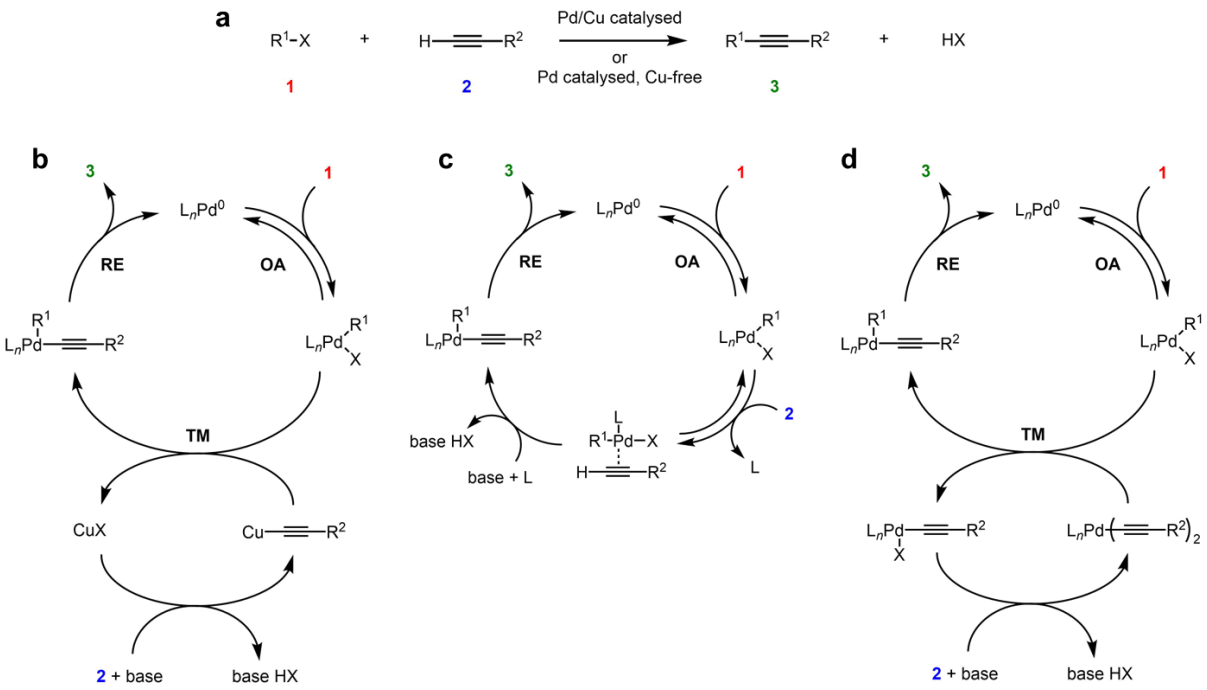

Figure 2.7. a A general representation of the Sonogashira cross-coupling reaction. **b** Consensus mechanism for the Pd/Cu catalysed Sonogashira reaction. **c** Proposed mechanism for the Cu free Pd catalysed Sonogashira reaction. **d** A recently proposed alternative mechanism for the Cu-free Pd catalysed Sonogashira reaction. X = halide, L = ligand, **OA** = oxidative addition, **TM** = transmetallation, **RE** = reductive elimination. *Cis–trans* isomerisation steps are not shown for clarity.

Removal of the TMS protecting group to yield the terminal alkyne **4** is readily achieved using a nucleophilic fluoride source, such as tetra-*n*-butylammonium fluoride or triethylamine trihydrofluoride. Deprotection of **3** with 25 equivalents of triethylamine trihydrofluoride with mild heating occurred over 37 h to give **4** in high yield (87%). The reaction proceeded cleanly with no further purification required other than an aqueous work-up to remove the excess hydrofluoride reagent and resulting salts.

The bottom part of the chromophore, ethyl (6-(hydroxymethyl)-4-(bromopyridin-2-yl)(methyl)phosphinate, **5**, was prepared following a procedure that has been described in detail elsewhere, (Figure 2.8).[7]

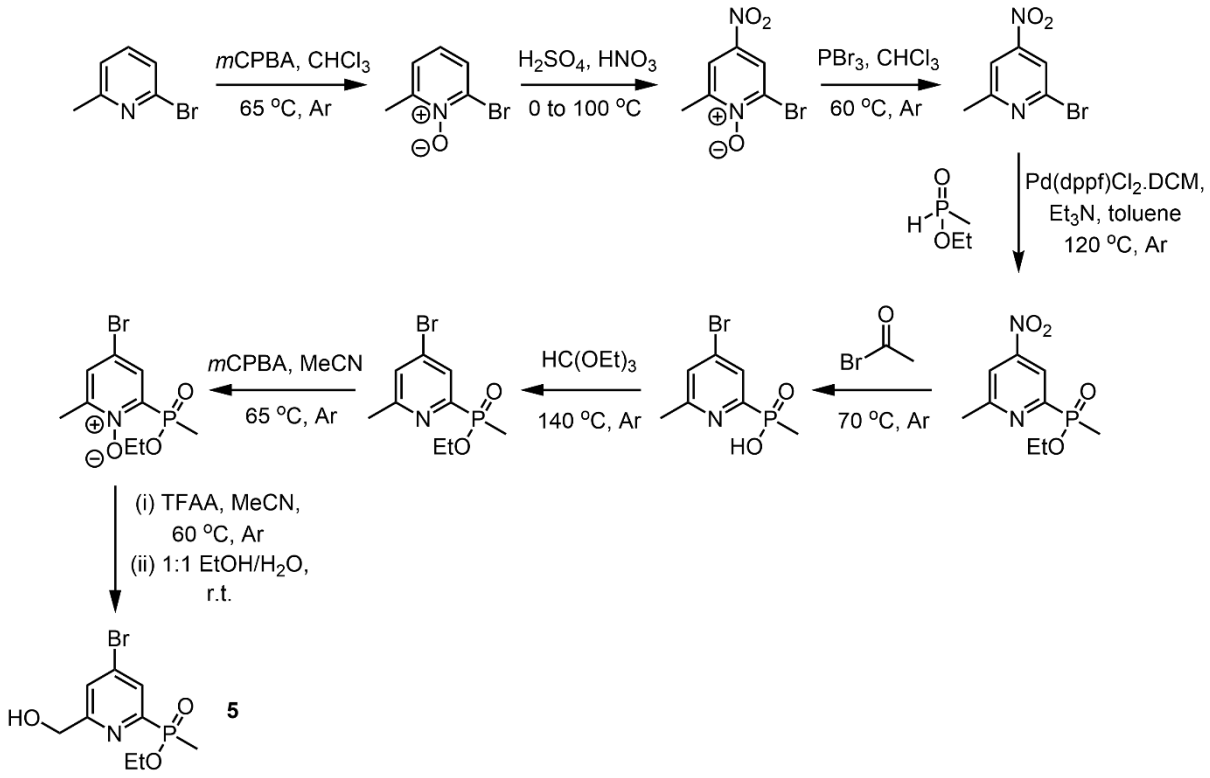

Figure 2.8. Synthesis of ethyl (6-(hydroxymethyl)-4-(bromopyridin-2-yl)(methyl)phosphinate, **5**.

In brief, 2-bromo-6-methylpyridine was reacted with *m*CPBA to install the *N*-oxide and raise the HOMO energy of the species, activating the pyridine ring towards electrophilic aromatic substitution by the $[NO_2]^+$ electrophile in the subsequent nitration reaction. This nitration reaction is believed to occur selectively in the *para* position to minimise electrostatic repulsion.[15] The *N*-oxide was removed using a trivalent phosphorus species, driven by the stability of the phosphorus-oxygen double bond in the by-product, $POBr_3$. Similarly to the preparation of the pyridine precursor **1**, the phosphinate moiety was introduced into the 2-position of the pyridine ring using a palladium-catalysed coupling reaction. Acetyl bromide was then reacted reversibly with the pyridine N atom to give the activated N-acetyl pyridinium cation. Subsequent nucleophilic attack by the liberated bromide anion at the pyridine 4-position results in a Meisenheimer intermediate which affords the product, following expulsion of the nitro leaving group and cleavage of the N-acetyl group on work up. The ethyl ester, which is hydrolysed in the previous step, was reformed through a transesterification reaction with triethyl orthoformate. To introduce the alcohol functional group, the pyridine N atom was converted to its *N*-oxide, followed by a Boekelheide rearrangement and hydrolysis, as described for **1**.

With the terminal alkyne **4** (top component) and 4-bromopyridine derivative **5** (bottom component) prepared, the two components were coupled together using a copper-free Sonogashira reaction to afford the extended chromophore as the primary alcohol. The coupling reaction was achieved using similar conditions to the first step, with no evidence for competitive homo-coupling of the alkyne, **4**. Purification of the alcohol **6** was found to be laborious by both silica and alumina column chromatography, but proved to be comparatively simple using reverse-phase high performance liquid chromatography (RP-HPLC) with an acetonitrile/water eluent gradient. A simple aqueous wash was performed prior to this, in order to remove some minor impurities and aid product separation during RP-HPLC. It was found that the 4-bromopyridine, **5**, possessed a similar retention time to the product **6**, under a variety of attempted different eluent gradients. Accordingly, a small excess (1.1 eq.) of the alkyne was used in the reaction to ensure complete consumption of the bottom component. The product was obtained in a yield of 48%. Although this yield is notably lower than that obtained for the first Sonogashira cross-coupling, the product **6** is considerably richer in functionality.

The alcohol **6** was converted to the mesylate **7** immediately prior to its use using methanesulfonic anhydride, as described earlier. The progression of the reaction was easily monitored using both TLC and mass spectrometry, and was found to be complete within 90 minutes in THF at room temperature.

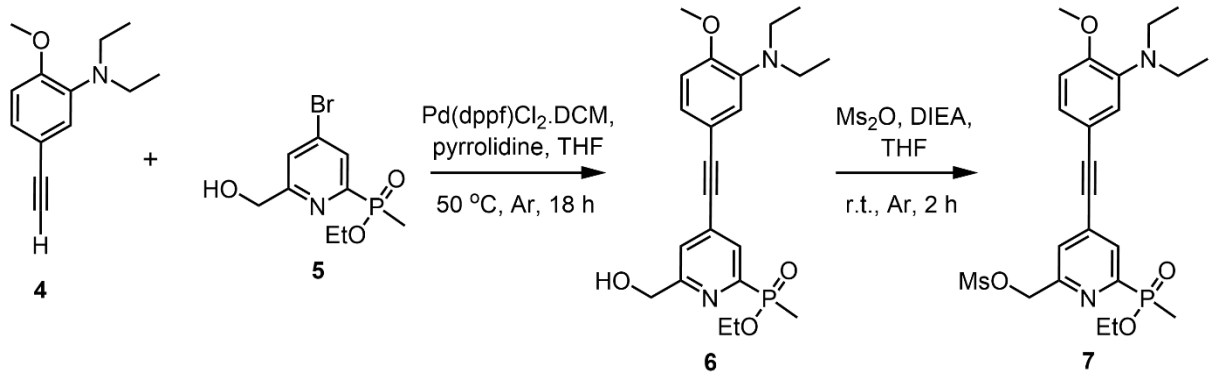

Figure 2.9. A copper-free Sonogashira cross-coupling reaction between compounds **4** and **5** yielded the alcohol **6**, that was converted to the mesylate ester, **7**.

2.2.3. Synthesis of ***[Eu.L^1]***

With the required precursor compounds prepared, the europium complex, **[Eu.L^1]**, was synthesised from a TACN scaffold. For this purpose, a TACN macrocycle bearing a single Boc protecting group was chosen to facilitate controlled stepwise alkylation of the precursor arms onto the scaffold. The macrocycle was used as the hydrochloride salt for convenience, without prior conversion to the free amine.

Introduction of the two single pyridyl arms onto the TACN scaffold was performed through an S_N2 alkylation reaction using the mesylate **1** in acetonitrile, in the presence of potassium carbonate, (Figure 2.10). The reaction was carried out under an inert atmosphere in order to strictly exclude water from the reaction, given the instability of the mesylate to adventitious hydrolysis. The progress of the reaction was conveniently monitored by LC/MS which showed distinct evidence of the stepwise alkylation of the TACN, with monoalkylation taking place within a few hours. A small excess of mesylate **1** was used (2.3 eq) and the reaction was left overnight to ensure completion. The dialkylated derivative of TACN, **8**, was obtained in an acceptable yield (57%) following RP-HPLC. It was isolated as a near 1:1 mixture of *RR*/*SS* and *RS* diastereoisomers, specifying chirality at the stereogenic P centres. In addition, restricted rotation about the carbamate NCO bond of the Boc group rendered the pyridyl arms non-equivalent on the NMR timescale at room temperature, as observed by both ^{1}H and ^{13}C NMR spectroscopy.

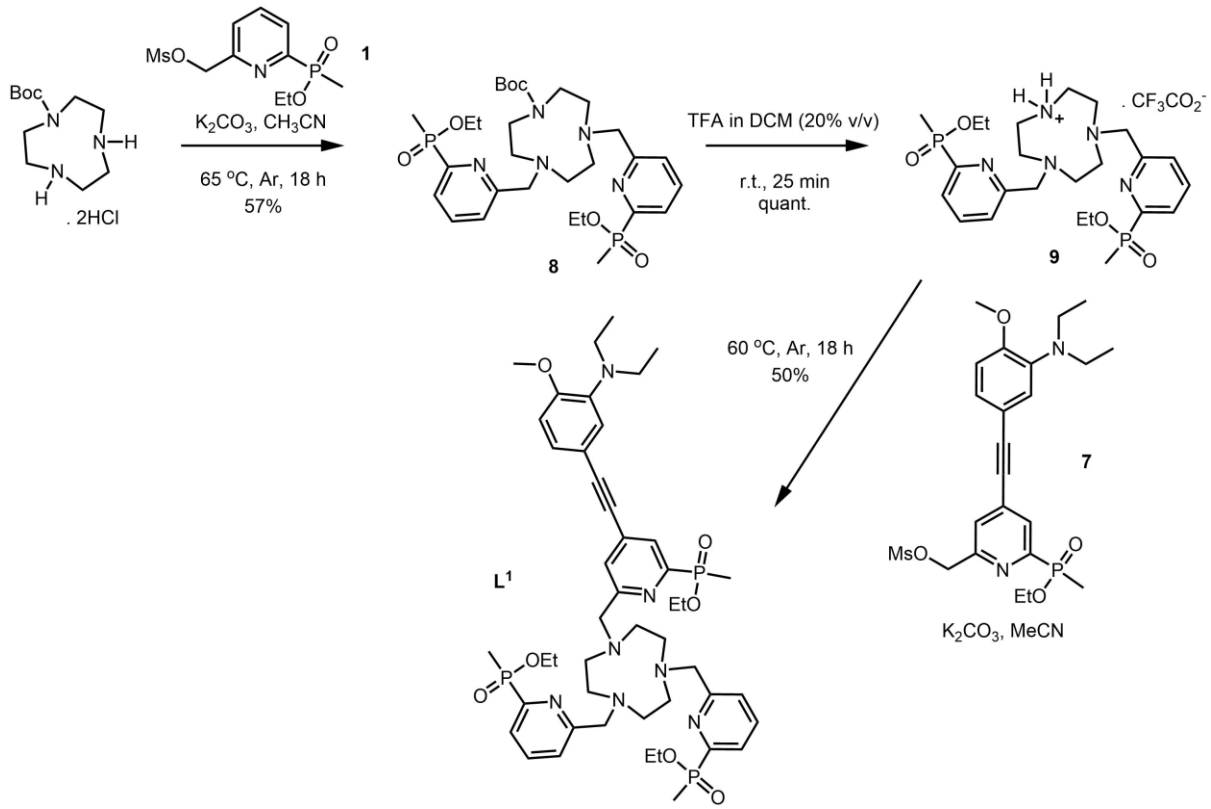

Figure 2.10. Synthesis of the ligand, **L[1]**.

Removal of the Boc protecting group using trifluoroacetic acid (TFA) in DCM (20% by volume) occurred rapidly, giving the secondary amine **9**, as its trifluoroacetate salt. This deprotection step proceeds via protonation of the Boc carbonyl oxygen by TFA and subsequent expulsion of a *tert*-butyl cation and carbon dioxide. The product was isolated in quantitative yield following repeated co-evaporation with DCM under reduced pressure to remove all of the residual TFA. The pyridyl groups were shift equivalent, as observed by ^{1}H NMR spectroscopy, supporting the earlier assumption that the NMR non-equivalence of the pyridyl group environments originated from restricted rotation about the carbamate NCO bond.

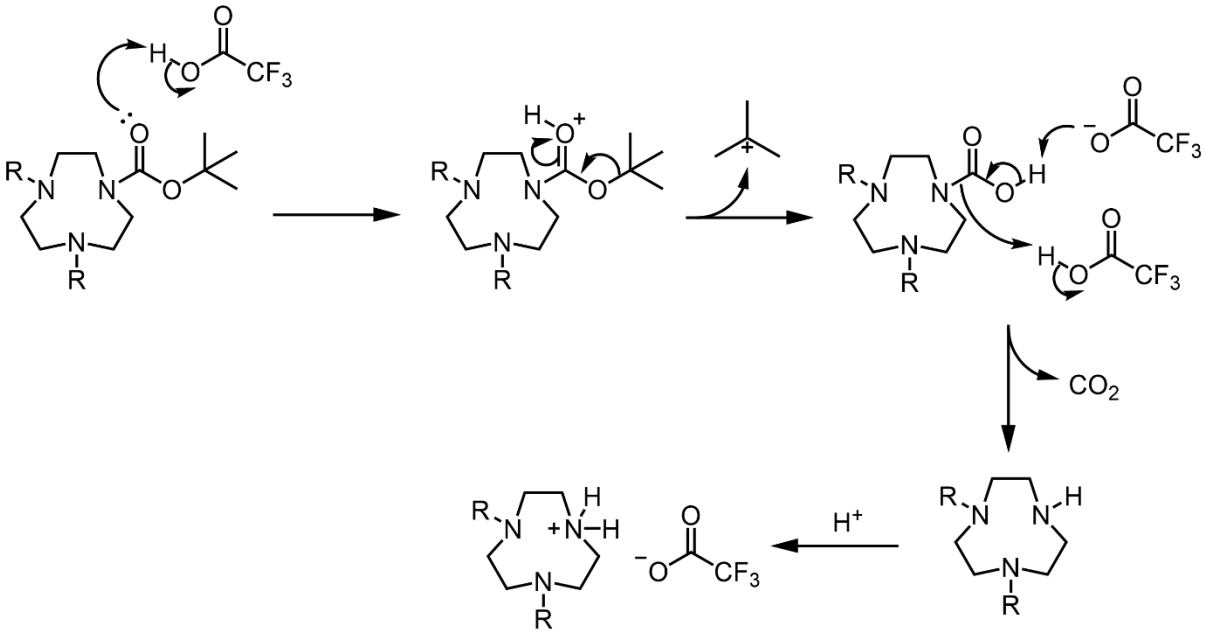

Figure 2.11. Mechanism for the removal of a Boc protecting group using TFA.

The macrocycle **9** was subsequently alkylated with the extended chromophore mesylate **7**, in acetontrile in the presence of potassium carbonate. The dialkylated macrocycle was used directly as its trifluoroacetate salt, without prior conversion to the free amine. Reaction monitoring by LC/MS indicated complete consumption of the dialkylated starting material within 3 hours, with the only UV-active species in the reaction mixture being the desired product and remaining hydrolysed mesylate, *i.e.* the parent alcohol. Purification by RP-HPLC yielded the ligand **L^1** in a modest yield (50%).

The target complex **[Eu.L^1]** was obtained through a well-established complexation protocol, (Figure 2.12).[16-19] Firstly, hydrolysis of the phosphinate ethyl esters was achieved under strongly basic conditions (addition of $NaOH_{(aq)}$ to pH 12) with heating at 60 °C. The hydrolysis reaction was easily monitored by LC/MS within a few hours, observing the appearance and disappearance of the partially hydrolysed esters. As the ligand framework is known to be stable to these reaction conditions, the hydrolysis reaction was allowed to proceed to completion overnight, to ensure complete hydrolysis of each phosphinate ester group. After this time, the pH of the reaction medium was adjusted to 6 using hydrochloric acid and a stoichiometric amount of $EuCl_3.6H_2O$ was added as a source of Eu(III). Metal complexation was found to be rapid by LC/MS and the reaction was left overnight to ensure completion. The desired

complex **[Eu.L^1]** was isolated in high yield (93%) as a pale yellow solid, following purification by RP-HPLC and subsequent lyophilisation.

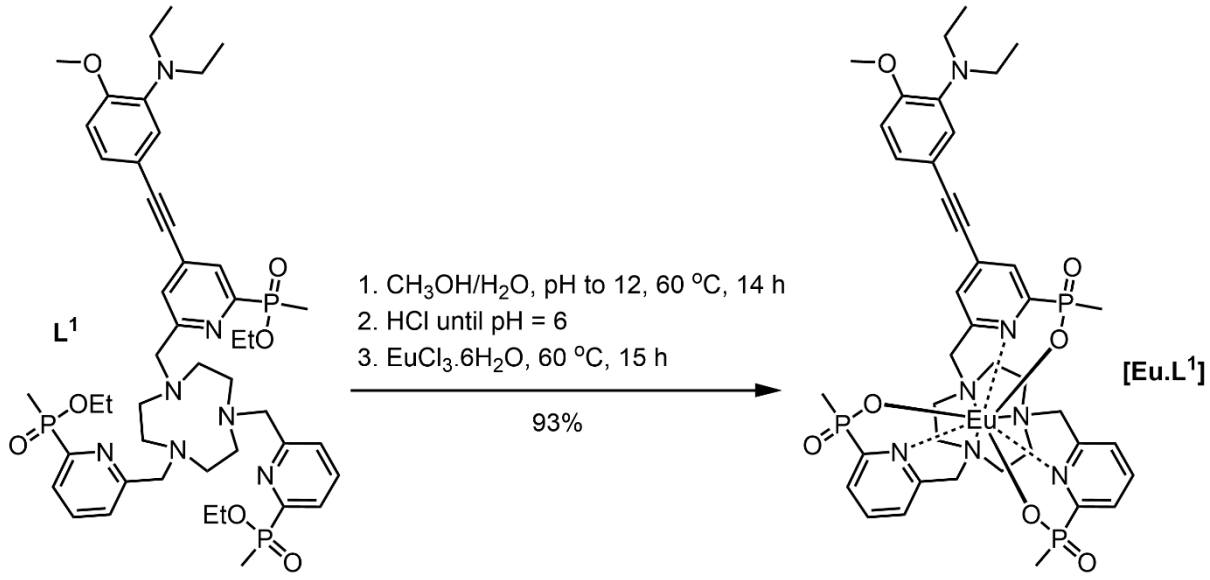

Figure 2.12. Hydrolysis of **L^1** followed by complexation with $EuCl_3.6H_2O$ at pH 6 to give **[Eu.L^1]**.

2.2.4. Synthesis of [Eu.L$^{2\text{-}3}$]

Initially, the synthesis of **[Eu.L^2]** was attempted by alkylation of the di-Boc-TACN macrocycle with the mesylate **1**. It was envisaged that this sequence, followed by deprotection of the Boc group, would avoid exposure of the alkyne triple bond to the acidic deprotection conditions, for reasons discussed previously. However, the use of di-Boc-triazacyclononane proved to be non-trivial and the alkylation gave rise to a complex product mixture, which did not simplify to a single species on Boc deprotection, as had been observed with **9**. The obvious, alternative approach was therefore pursued, involving dialkylation of mono-Boc-TACN with the chromophore antenna **7**.

It was necessary firstly to verify the assumption concerning the stability of the triple bond under the acidic Boc-deprotection conditions. This issue was probed by preparing a solution of the extended chromophore **6** in TFA/DCM (1:4 by volume) and monitoring changes by UV-Vis absorbance at room temperature. It was hypothesised that any acid mediated hydrolysis or general attack at the alkyne would reduce the

degree of conjugation within the molecule, resulting in a distinct and observable change in the UV-Vis absorbance profile. The solution was monitored over a period of 3 hours with little variation in the UV-Vis absorbance profile, suggesting that the chromophore is inert to these acidic conditions on this time-scale, (Figure 2.13). A plausible explanation for this behaviour is that protonation of the triple bond is electrostatically disfavoured when the diethylamino group is protonated.

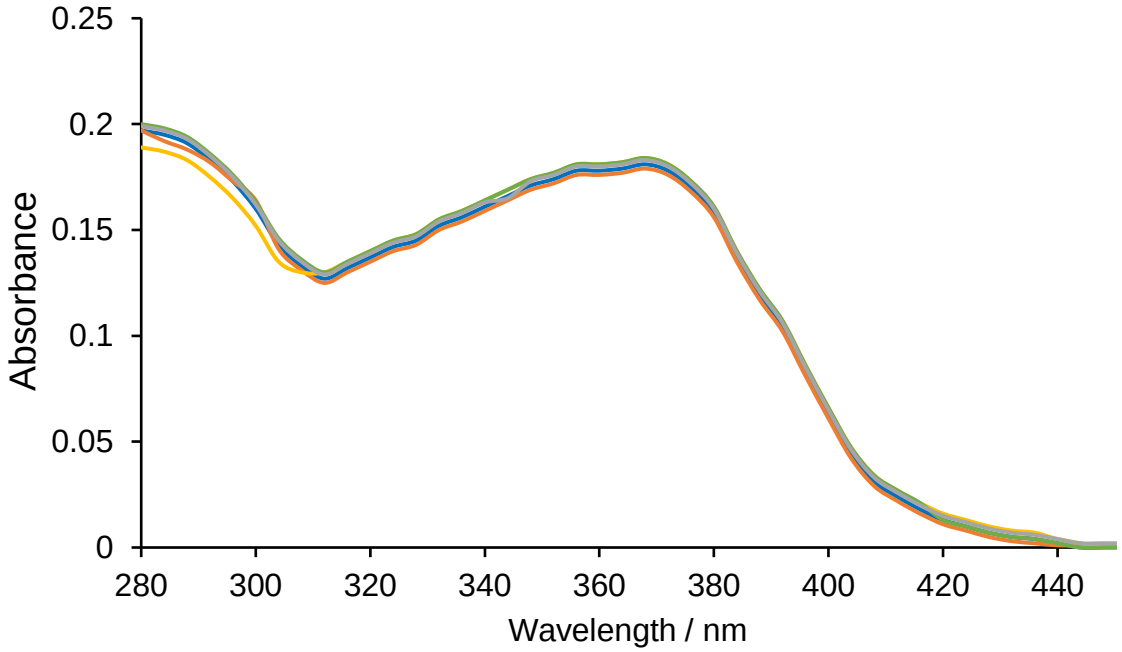

Figure 2.13. Absence of change in the UV-Vis absorbance profile of the chromophore, **6** (TFA/DCM, 1:4 v/v, 3 h, 20 ºC).

The di-chromophore complex, **[Eu.L^2]**, was therefore prepared with a procedure similar to that used for **[Eu.L^1]**, differing only in the sequence of alkylation of the precursor arms, (Figure 2.14). Firstly, alkylation of mono-Boc-TACN macrocycle with the extended chromophore mesylate **7** was achieved in reasonable yield (62%), after purification by RP-HPLC, and gave the di-alkylated product **10**. Next, the Boc group was removed using TFA in DCM and the dialkylated macrocycle **11** was reacted with the pyridyl mesylate, **1**, to give the target ligand **L^2** (55%). The ligand was subsequently hydrolysed under basic conditions and complexed with Eu(III) to give the neutral compound, **[Eu.L^2]**, in 58% overall yield.

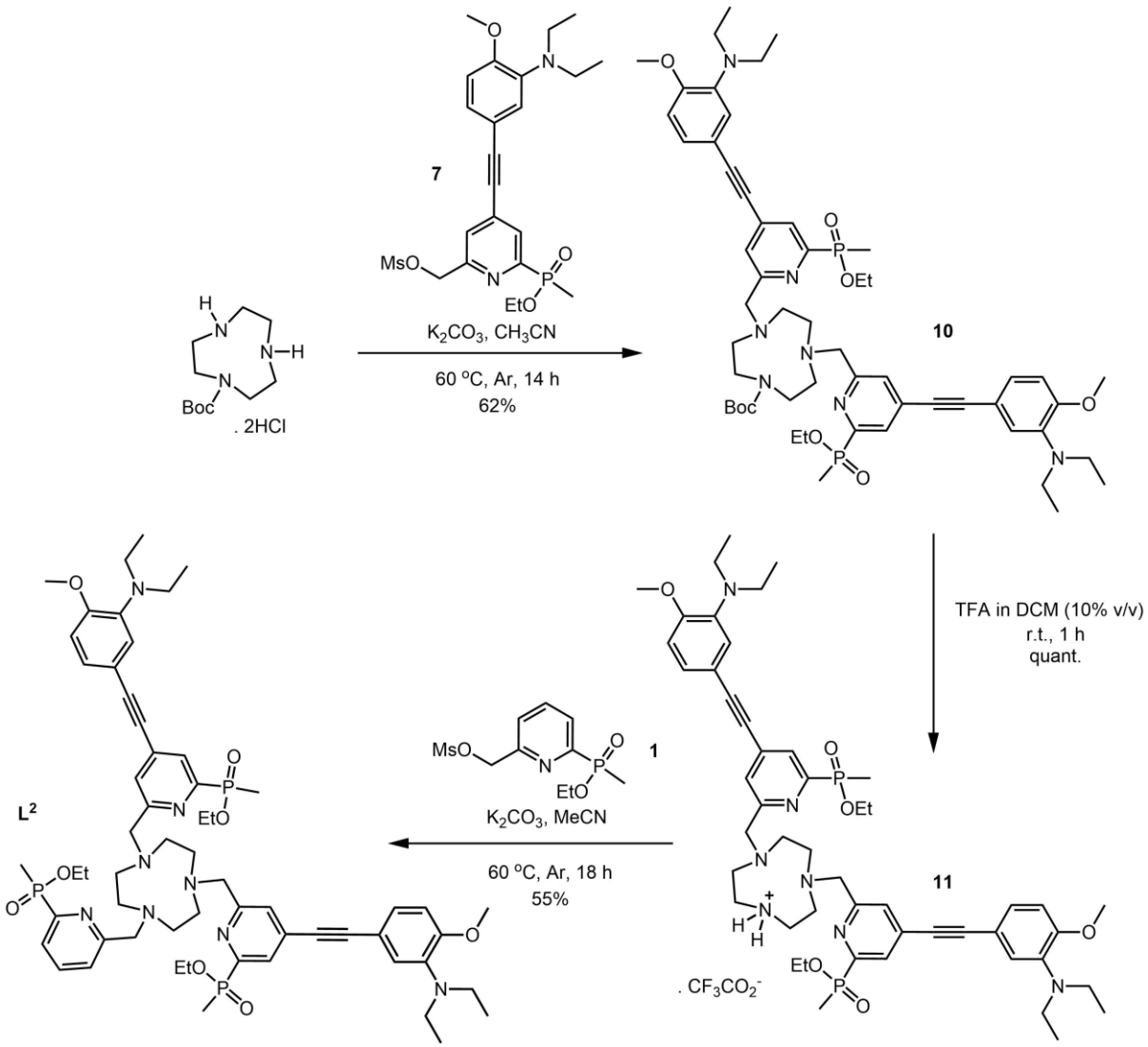

Figure 2.14. Synthesis of the ligand **L^2**.

The preparation of **[Eu.L^3]** is comparatively simple, as it possesses three identical chromophore groups, (Figure 2.15). The ligand **L^3** was synthesised by alkylation of triazacyclononane with the mesylate **7**, albeit in low yield (32%). This isolated yield is noticeably lower than that observed with **L^1** and **L^2** (50 and 55% respectively), possibly due to the increased steric bulk around the alkylation site in the final step. The complex **[Eu.L^3]** was obtained in moderate yield, after basic hydrolysis of the phosphinate esters and metal ion complexation at pH 6 using $EuCl_3.6H_2O$ (48% overall). .

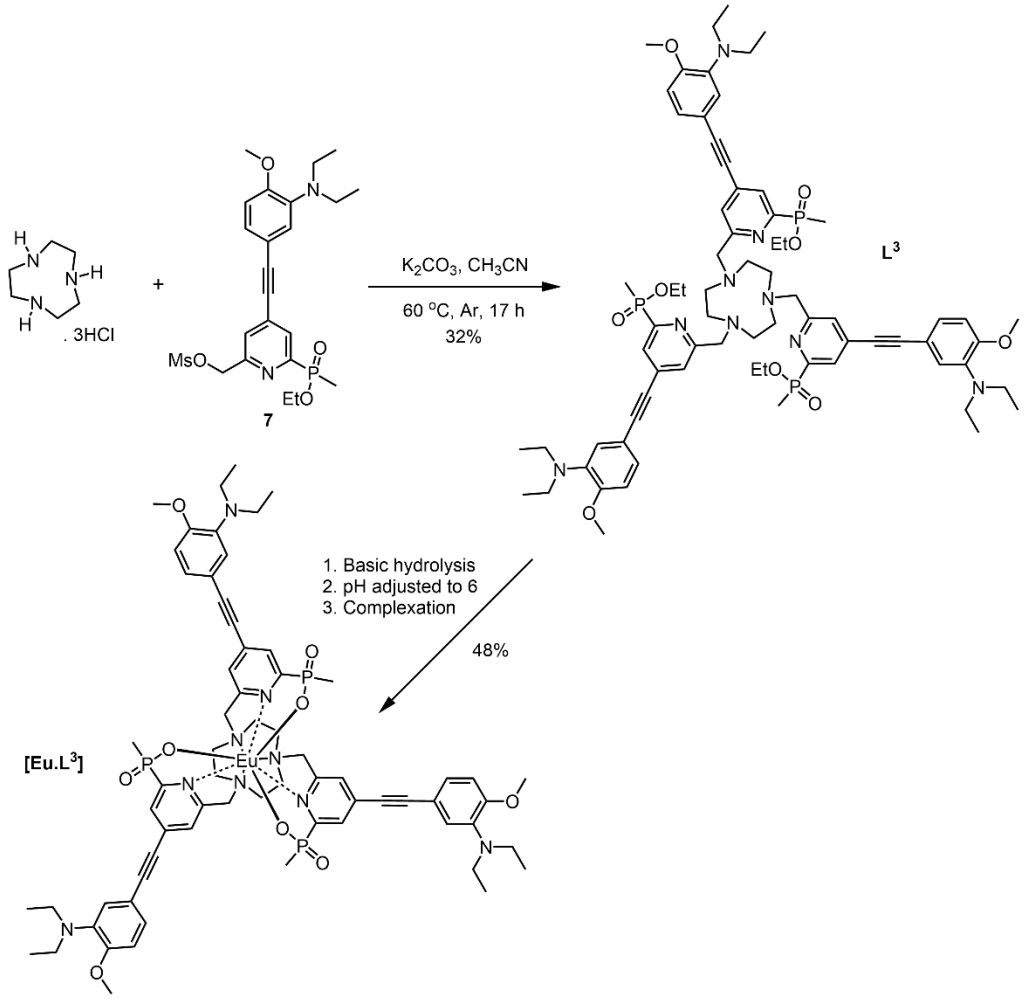

Figure 2.15. Synthesis of the complex **[Eu.L^3]**.

2.3. Photophysical Analysis of [Eu.L$^{1-3}$]

The pH dependence of absorption, emission, and excitation was examined for each of the three europium(III) complexes. In addition, measurements were made of the europium emission lifetime, τ, the absorption coefficients, ε, overall emission quantum yields, Φ, and europium hydration numbers, q. Data are summarised in Table 2.1.

Table 2.1. Summary of photophysical properties of **[Eu.L$^{1\text{-}3}$]** (295 K in 0.1 M NaCl).

Complex	λ_{exc} / nm	ε[a] / M^{-1} cm^{-1}	τ / ms	Φ[a] / %	q	B[a] / M^{-1} cm^{-1}
[Eu.L^1]	331	12,000	0.53[b] 1.16[c]	0.5[b] 17.0[c]	0	60[b] 2,040[c]
[Eu.L^2]	328	35,000	0.34[b] 1.00[c]	0.2[b] 17.6[c]	0	70[b] 6,160[c]
[Eu.L^3]	331	46,000[b] 60,000[c]	0.25[b] 0.84[c]	0.1[b] 17.0[c]	0	46[b] 10,200[c]

[a] Parameter calculated at the stated excitation wavelength, which is an isosbestic point where appropriate. [b] Values at pH 8. [c] Values at pH 4. Experimental errors of lifetime and quantum yields are ±5 and 15% respectively.

In the case of **[Eu.L^1]** which contains only a single amine group, protonation at N shifts the main p- p* transition from 340 nm to 320 nm, characterised by two isosbestic points at 331 nm and 278 nm, (Figure 2.16). A similar, albeit smaller, hypsochromic shift of the main band was also observed from 334 nm to 320 nm on protonation of the di-chromophore complex **[Eu.L^2]**, with isosbestic points at 328 nm and 284 nm. For **[Eu.L^3]** on the other hand, whilst a mirrored hypsochromic shift was observed (336 nm to 316 nm), no well-defined isosbestic points were seen. An increase in the relative intensity of the primary p- p* absorption band was seen for each complex following N-protonation.

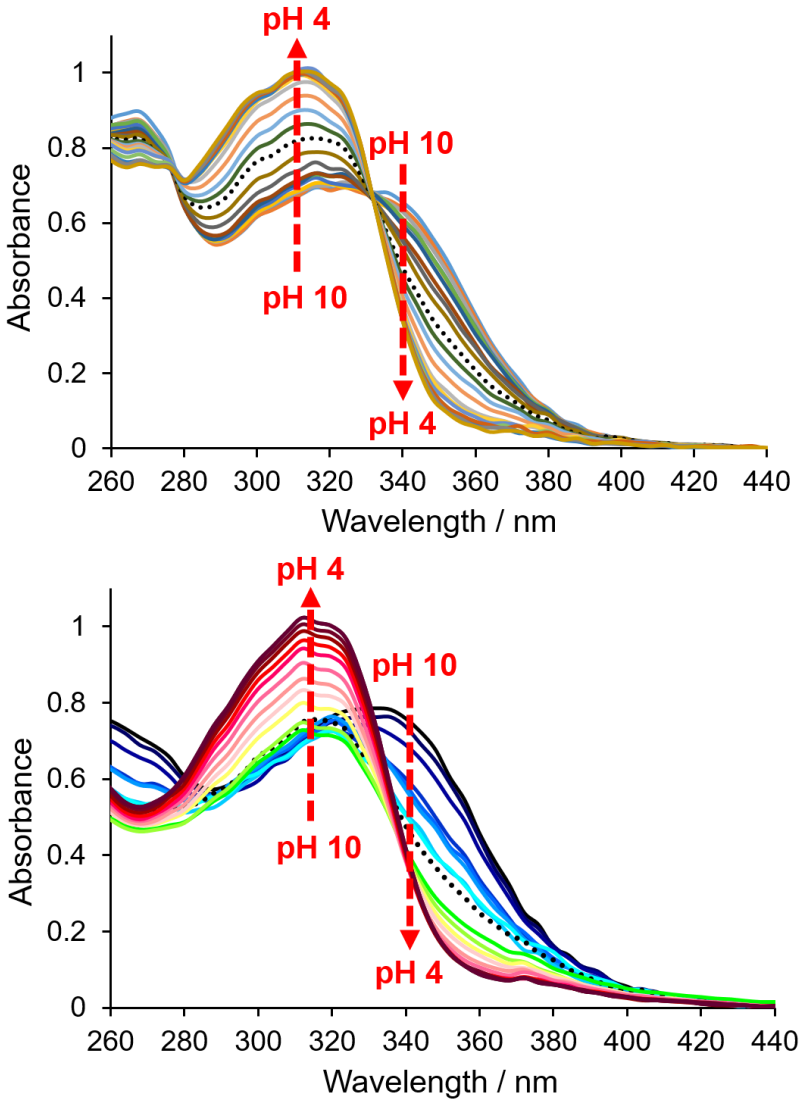

Figure 2.16. *(Top)* Variation of the absorption spectrum of **[Eu.L^{1}]** with pH, revealing the isosbestic points at 278 and 331 nm (295 K, $c_{complex}$ = 15 μM in 0.1 M NaCl). *(Bottom)* Variation of the absorption spectrum of **[Eu.L^{3}]** with pH (295 K, $c_{complex}$ = 15 μM in 0.1 M NaCl). The absorbance profile at pH 7 is indicated with black dots.

The europium emission intensity increased markedly for each complex as the pH was lowered from 10 to 4 (Figure 2.17), accompanied by an increase in europium emission lifetime. The change in lifetime was over a factor of three for **[Eu.L^{3}]**. Taking the hypersensitive Δ*J* = 2 transition as a reference point, emission was observed to increase 540-fold for **[Eu.L^{1}]** and by a factor of 560 for **[Eu.L$^{2\text{-}3}$]**. Emission spectra for **[Eu.L$^{1\text{-}3}$]** possessed a similar overall spectral form, as expected given the lack of change in the coordination environment of the europium ion. Only minor variations were observed between complexes in the intensity and form of the hypersensitive Δ*J*

= 2 and 4 transitions, *e.g.* a reversal of the relative intensity of the two main Δ*J* = 2 transitions in the region between 610 to 625 nm.

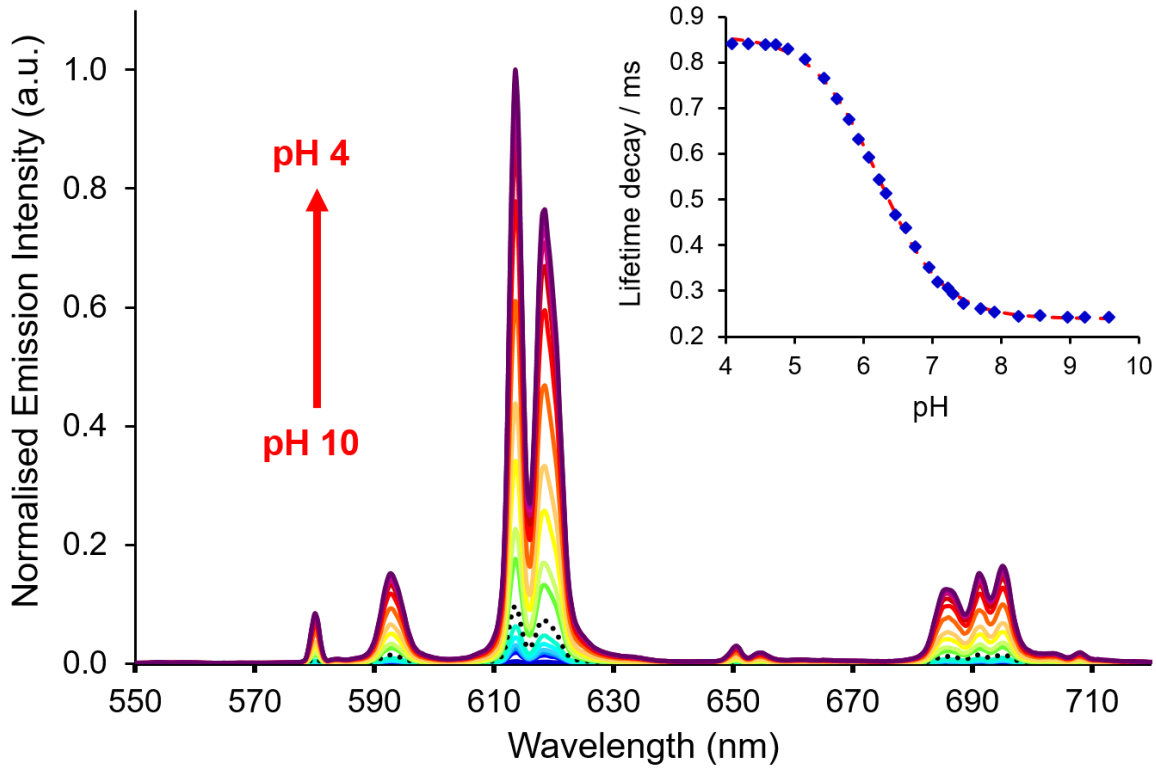

Figure 2.17. Variation of the europium emission spectrum and lifetime (*inset*) with pH for **[Eu.L^3]** (λ_{exc} 331 nm, 295 K, $c_{complex}$ = 15 μM, 0.1 M NaCl) showing the fit (*red dashed line*) to the experimental lifetime data. Emission spectrum at pH 7 is indicated with black dots. Similar plots were obtained following excitation at 337 or 355 nm.

Large increases in the europium emission lifetime accompanied the switching-on of emission, and these were measured to be 120, 200 and 240% respectively for **[Eu.L$^{1-3}$]** between the pH limits. Interestingly, the relative increase in lifetime increases significantly as a function of the number of antennae, with **[Eu.L^3]** returning the most significant change in emission lifetime.

The modulation of the europium emission lifetime following excitation implies some form of quenching of an excited state. Control experiments with each complex examining the concentration and oxygen-dependence of the europium emission lifetime revealed an absence of any lifetime change, eliminating the possibility of intermolecular quenching and quenching of an excited triplet state by oxygen. These experiments were performed by preparing each complex in acidic and basic solutions

of varying concentration (1 – 50 μM) and recording the emission lifetime before and after thorough degassing of each sample. A plausible explanation of the observed lifetime modulation is that quenching of the europium $^5D_0$ excited state is occurring by electron transfer from the (unprotonated) nitrogen atom of a proximate chromophore. The rate of protonation of this nitrogen atom is fast with respect to the emission timescale and is also fast with respect to the lifetime of the intermediate ligand excited states. This tentative hypothesis is supported by the decrease of the emission lifetime at the pH limits for **[Eu.L$^{1\text{-}3}$]** as the number of proximate antennae, and associated sites from which electron transfer can occur, is increased (*c.f.* 0.53/1.16 ms with 0.25/0.84 ms for **[Eu.L^1]** and **[Eu.L^3]** at pH 8/pH 4 respectively). This behaviour is further investigated and discussed within this chapter.

In each case, the variation of emission lifetime with pH gave data which could be fitted to a single protonation event using non-linear least squares regression analysis, notwithstanding the multiple protonation steps involved for **[Eu.L$^{2\text{-}3}$]**, (Figure 2.17 *inset*). The sites of protonation (*i.e.* the diethylamino groups) are separated in **[Eu.L$^{2\text{-}3}$]** by at least 15 Å and so can be considered to act independently. Fitting of the emission intensity *vs*. pH data allowed a pK_a value to be estimated in each instance, (Table 2.2). It is worthy of note that an identical dependence of europium emission lifetime with pH was found for both acidimetric and alkalimetric titrations, consistent with full reversibility of the protonation equilibrium.

Table 2.2. Summary of pK_a values (±0.05) determined for **[Eu.L$^{1\text{-}3}$]** ($c_{complexes}$ = 15 μM) in the stated media.

Complex	Conditions	pK_a
[Eu.L^1]	0.1 M NaCl	6.75
	0.1 M NaCl, 0.1 mM BSA	6.45
[Eu.L^2]	0.1 M NaCl	6.30
	0.1 M NaCl, 0.1 mM BSA	6.19
	NIH-3T3 cell lysate	6.25
[Eu.L^3]	0.1 M NaCl	6.21
	0.1 M NaCl, 0.1 mM BSA	6.20
	NIH-3T3 cell lysate	5.92

Apparent pK_a values for **[Eu.L$^{1\text{-}3}$]** were estimated to be 6.75, 6.30, and 6.21 (±0.05) respectively in aqueous solution (0.1 M NaCl). These pK_a values showed only a small variation in a 0.1% BSA solution in the case of **[Eu.L$^{2\text{-}3}$]** (pK_a 6.19 and 6.20, respectively), although a noticeable decrease was observed for **[Eu.L^1]** (pK_a 6.45).

This lack of change for **[Eu.L$^{2\text{-}3}$]** suggests little interaction between the complexes and this common serum protein. Given their favourable pK_a values, **[Eu.L$^{2\text{-}3}$]** were examined in cell lysate as a mimic of a biological setting. Similarly to the BSA medium, little change in pK_a was found for **[Eu.L^{2}]** in a cell lysate background. However, for **[Eu.L^{3}]** the pK_a value fell to 5.92. These results highlight the importance of considering the specific medium of a probe, and the need for appropriate calibration in each instance. It has been demonstrated that some species, such as proteins, are capable of perturbing the position of the protonation equilibrium. A contribution from the change in the local dielectric constant of the medium and associated solvation effects is also expected.

The variation of the Eu complex excitation spectra with pH was also examined and a uniform increase in intensity was observed for all complexes (illustrated using **[Eu.L^{2}]** in Figure 2.18). However, the complexes differ somewhat in their spectral form: a broad featureless profile was obtained for **[Eu.L^{1}]** with a maximum at 320 nm, whilst the spectra measured for **[Eu.L$^{2\text{-}3}$]** contained additional features. Both **[Eu.L$^{2\text{-}3}$]** display two main bands at 284/332 nm and 274/342 nm respectively, corresponding to the presence of more than one p- p* transition in the extended chromophore of the emissive species. Whilst this higher energy feature was not observed for **[Eu.L^{1}]**, the excitation spectrum is notably broader than those spectra obtained for **[Eu.L$^{2\text{-}3}$]**. Observation of this additional feature is expected and it is likely that this band is obscured by the main broad feature.

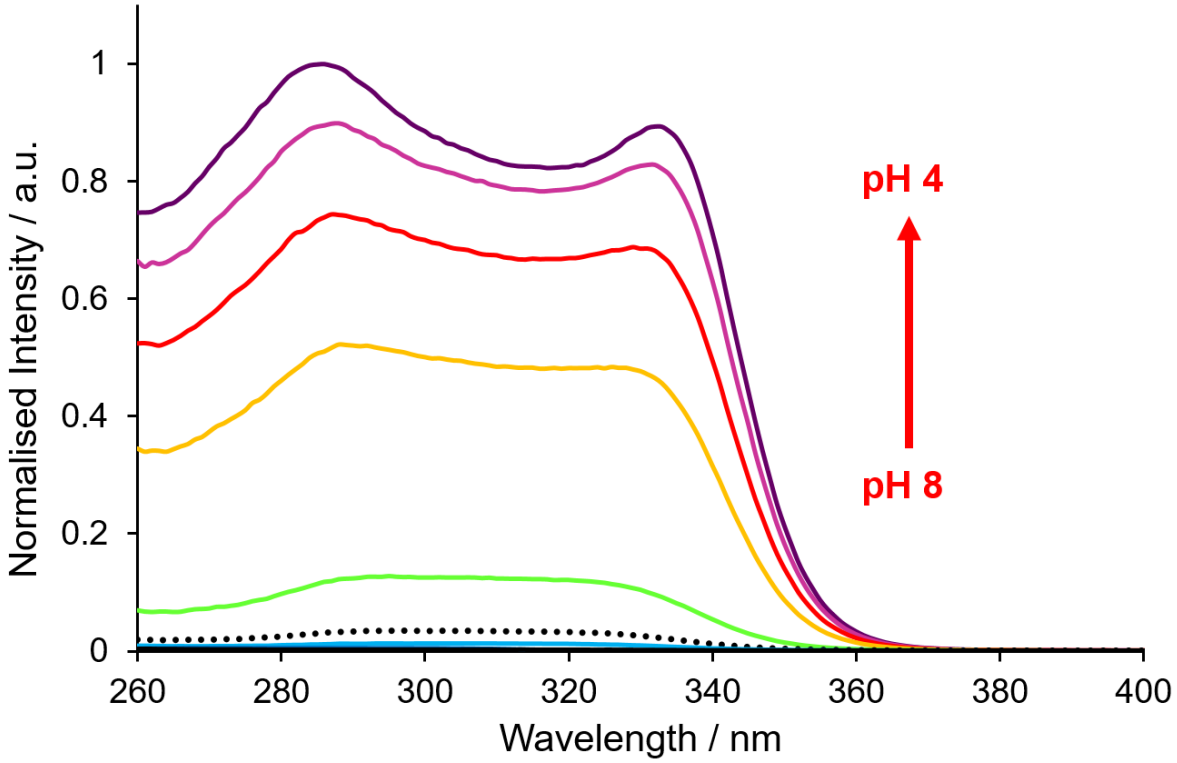

Figure 2.18. Variation in the excitation spectrum with pH for **[Eu.L^{2}]** (λ_{em} 613 nm, 295 K, $c_{complex}$ = 15 μM, 0.1 M NaCl). Excitation spectrum at pH 7 is indicated with black dots. Similar profiles were obtained for **[Eu.L^{1}]** and **[Eu.L^{3}]** under similar conditions.

These excitation spectra show the change in emission intensity as a function of the wavelength of the excitation light at the $\Delta J = 2$ band (the most emissive reference point of an europium complex). Through comparison of the absorption and excitation spectra, it is possible to deduce information about the emissive species. Due to the pH-responsive nature of **[Eu.L$^{1\text{-}3}$]** and the resulting equilibrium between the protonated and unprotonated forms, it is necessary to compare the absorption and excitation spectra at low and high pH, when the position of the equilibrium lies strongly in favour of the protonated and unprotonated forms, respectively. As discussed previously for **[Eu.L$^{2\text{-}3}$]**, the multiple protonation events are thought to occur independently of each other and give rise to multiply-charged species where antennae are both unprotonated and protonated within the same complex, complicating any rational analysis. For this reason, the absorption and excitation spectra are compared at pH 4 and 8 for **[Eu.L^{1}]**: the simplest complex, bearing a single chromophore antenna from which quenching by PeT can occur/be inhibited, (Figure 2.19). The lack of change in the excitation spectral form of **[Eu.L^{1}]** on changing pH from 8 to 4 and the consistency of the excitation and absorption spectra at pH 4 suggest that the

protonated form is the species leading to europium emission. This conclusion is also consistent with the hypothesis that PeT quenching in the unprotonated form is responsible for modulation of the emissive properties.

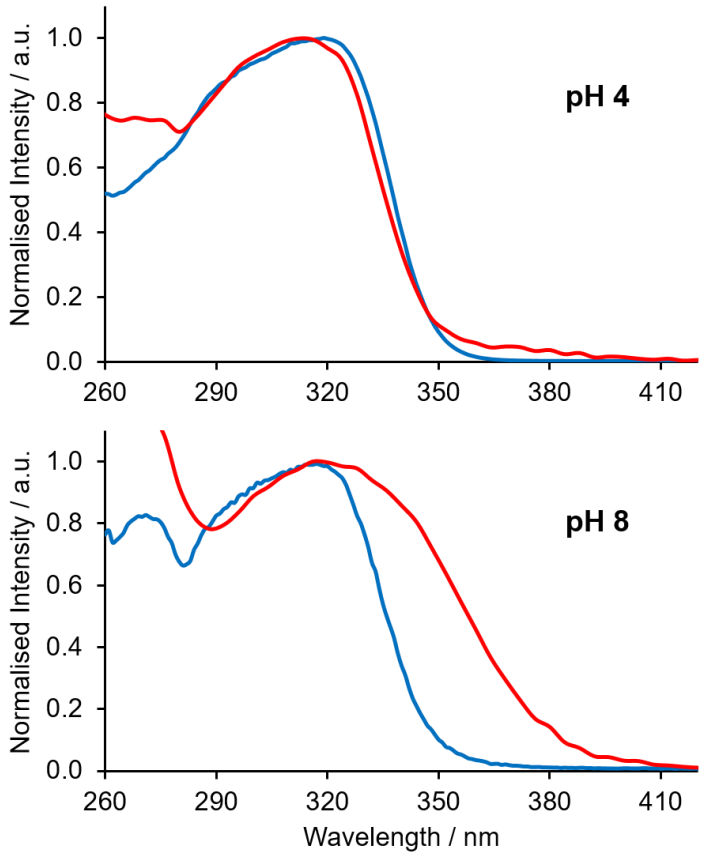

Figure 2.19. Normalised absorption (red line) and excitation (blue line, I_{em} 618 nm) spectra for **[Eu.L^{1}]** (295 K, 0.1 M NaCl) at pH 4 (*top*) and pH 8 *(bottom*).

Determination of photophysical parameters such as the molar extinction coefficient, ε, and quantum yield, Φ, allow an estimation of brightness to be made. For both **[Eu.L$^{1\text{-}2}$]**, the presence of isosbestic points allows for the convenient determination of ε, independent of pH. Thus, the molar extinction coefficient was evaluated and found to be 12,000 and 35,000 M^{-1} cm^{-1} respectively for **[Eu.L$^{1\text{-}2}$]**. Due to the lack of an isosbestic point(s), it was not possible to calculate a pH-independent value for ε in the case of **[Eu.L^{3}]**, as a result of the wavelength-dependence of ε. As an alternative, ε values were determined at the pH limits (46,000 and 60,000 M^{-1} cm^{-1} at pH 4 and 8 respectively) at the wavelength of minimal absorbance fluctuation.

As expected, the magnitude of the molar extinction coefficient increases from **[Eu.L^{1}]** to **[Eu.L^{3}]** with the increasing number of conjugated chromophores. **[Eu.L^{3}]** displays

an impressive ε value, particularly on acidification, rivalling the highest values observed for such lanthanide complexes, *e.g.* the series of EuroTracker® dyes.[20-21] Quantum yields at the pH limits were determined against the common reference $[Ru(bipy)_3]Cl_2$.[22] Similar values were returned for each complex with the emission quantum yield increasing from below 1% at pH 8 to approximately 17% at pH 4. The di-chromophore complex **[Eu.L^2]** was found to possess the highest emission quantum yield at pH 4 (17.6%). Subsequently, estimations of complex brightness in aqueous solution were made and the quoted values are summarised in Table 2.1. Unsurprisingly, a significant increase in brightness follows a decrease in pH from 8 to 4, with **[Eu.L^3]** displaying an appreciable brightness of 10,200 M^{-1} cm^{-1} (λ_{exc} 331 nm). This value is comparable to that of the terbium(III) complex, Tb-Lumi4 (~15,800 M^{-1} cm^{-1}, λ_{exc} 340 nm), a common benchmark.[23]

2.3.1. Time-gated Measurements

The increase of the europium emission lifetime that occurs on protonation with **[Eu.L^3]** is significant, allowing the apparent switching ratio between the 'on' and 'off' states to be varied, by changing the time delay in signal acquisition. Two cases were investigated in which either a fixed time delay was introduced, or a different time window for spectral acquisition was selected, (Table 2.3 and Figure 2.20). The emission intensities were measured in buffered solution at pH 4 and pH 8, and the ratios of the overall europium emission intensities were measured in each case using the integrated emission intensity of the hypersensitive $\Delta J = 2$ band.

Table 2.3. Ratios of emission intensities ('switch on' factors) for the stated single gate delay time or differing time gate periods, showing the effect on apparent pK_a values.

t / μs	pH 4/pH 8	app. pK_a
single gate delay times		
60	250	5.8
460	623	5.7
1000	650	5.6
differing time gate periods		
60–460	111	5.8
1000–2000	560	5.7
1500–2500	1334	5.6

[a] 295 K, $c_{complex}$ = 15 μM, 0.1 M NaCl; buffers, NH_4OAc (0.1 M, pH 4), NH_4HCO_3 (0.1 M, pH 8).

By changing the delay time from 0.06 ms to 1 ms, the 'switch-on' factor was found to increase from 250 to 650, with an apparent pK_a value of 5.7(0.1) under these different sets of experimental conditions. By choosing different time windows, a slightly greater increase in this factor was found, with the maximum ratio found for the time window 1.5 to 2.5 ms, notwithstanding the decrease in overall signal intensity that occurs using an acquisition period that is rather longer than the emission lifetime. Such behaviour is promising and augurs well for such conditions to be employed in either a time-gated assay, or in future time-resolved microscopy studies.

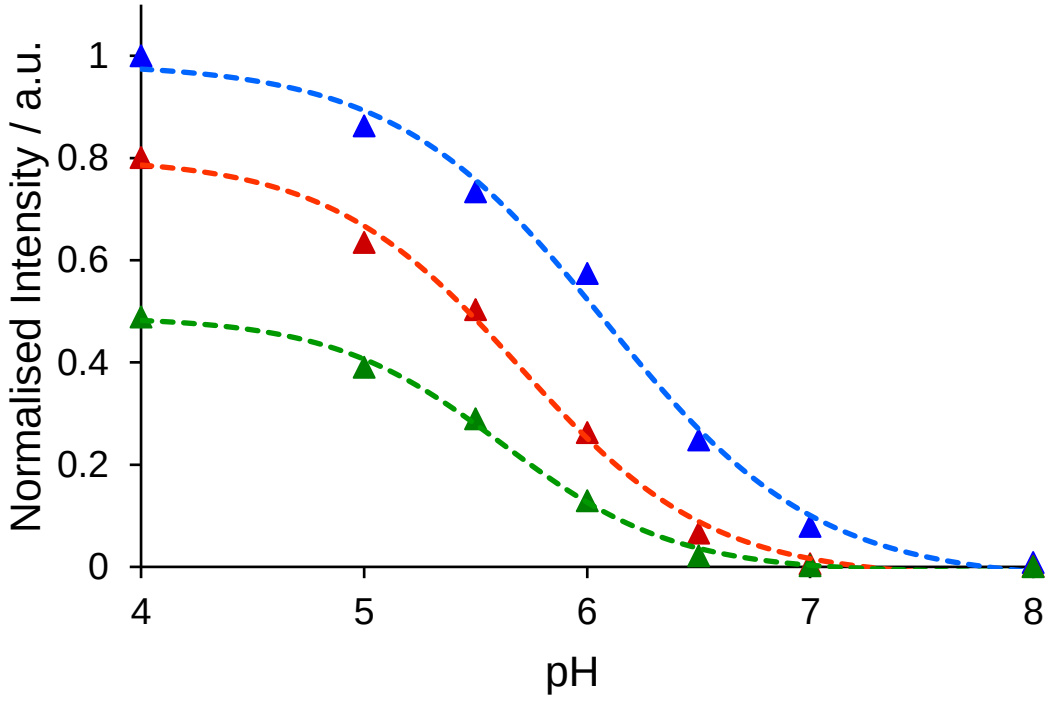

Figure 2.20. Emission intensity of **[Eu.L^3]** (λ_{em} 613 nm) as a function of pH with different time periods of acquisition (blue = 60 – 460 µs, red = 1000 – 2000 µs, green = 1500 – 2500 µs). Data are normalised to a 60 – 460 µs time window at pH 4. Measurements were taken in aqueous solutions of NH_4OAc (pH 4 and 5), MES (pH 5.5, 6 and 6.5), HEPES (pH 7), and NH_4HCO_3 (pH 8) buffers ($c_{complex}$ = 15 µM, 0.1 M buffer in 0.1 M NaCl).

2.4. [Eu.L^3] *in cellulo* Studies

Following examination of the photophysical properties of **[Eu.L$^{1\text{-}3}$]**, the trichromophore complex, **[Eu.L^3]**, was deemed the most suitable candidate for study in a living cell medium. Given its favourable pK_a value in aqueous media and high molar extinction

coefficient and quantum yield in the acidic pH regime, it was predicted that this complex would be the brightest for microscopy studies ($B = \varepsilon\Phi$).

Subsequently, cell uptake and co-localisation studies were undertaken (in collaboration with Dr. Robert Pal) and **[Eu.L^3]** was incubated in a cell growth medium independently with both living mouse skin fibroblasts (NIH-3T3) and human breast cancer cells (MCF-7), following established methods.[20,24-25] Owing to its broad absorption band, excitation of **[Eu.L^3]** *in cellulo* at 355 nm was possible and the extent of complex uptake was monitored by assessing image brightness as a function of time via laser scanning confocal microscopy. Uptake of **[Eu.L^3]** from the extracellular medium into the cells was observed to occur over a period of 1 to 2 hours, for complex incubation concentrations of 3 and 30 mM. Co-staining experiments using LysoTracker Green (LTG) verified that the complex localised in the lysosomes (Figure 2.21) with increasing Pearson's co-localisation coefficients (P) as the probe brightness increased, within a given cell cycle (P = 0.95 at 16 hours).

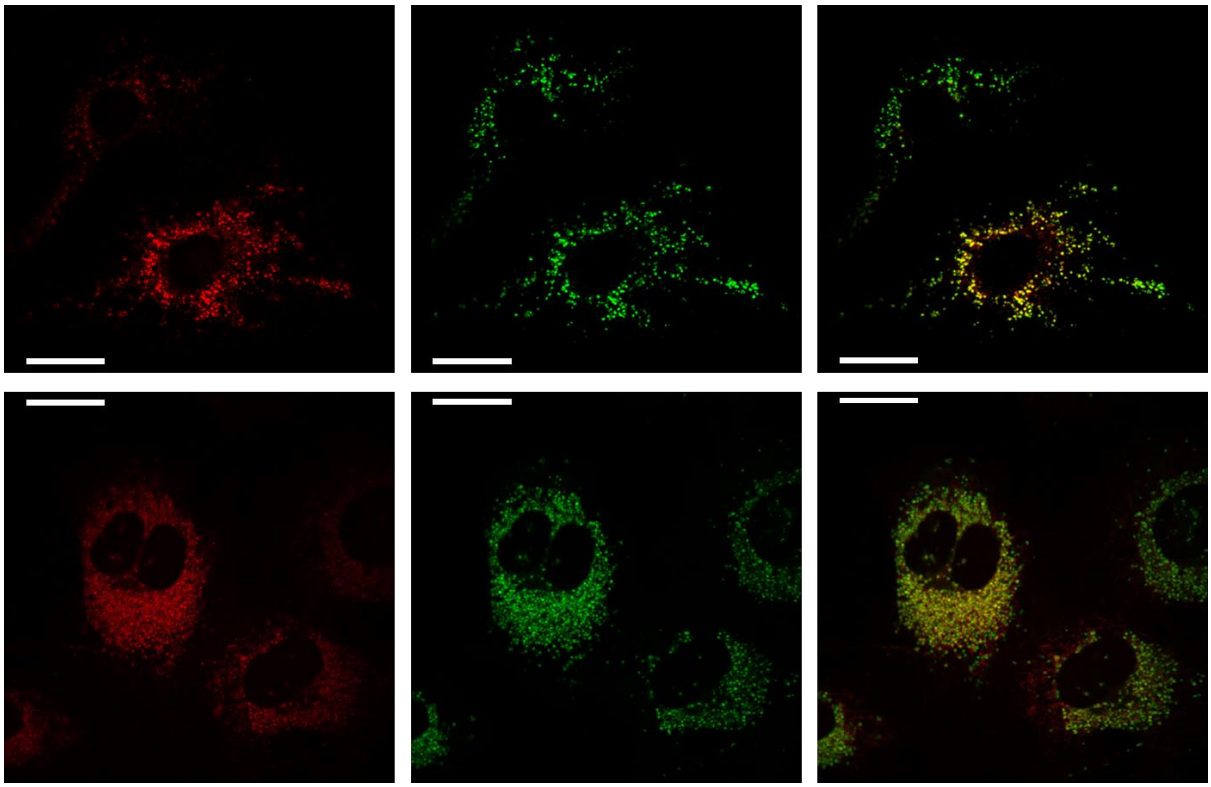

Figure 2.21. Live cell images (NIH-3T3) with **[Eu.L^3]** after 16 h. *(Left)* **[Eu.L^3]** (30 μM incubation concentration, λ_{exc} 355 nm, λ_{em} 600–720 nm). *(Centre)* Lysotracker Green (λ_{exc} 488 nm, λ_{em} 500–530 nm). *(Right)* Overlay shows co-localisation (P = 0.95). Note the observation of normal cell division at 16 h. Scale bar represents 20 microns.

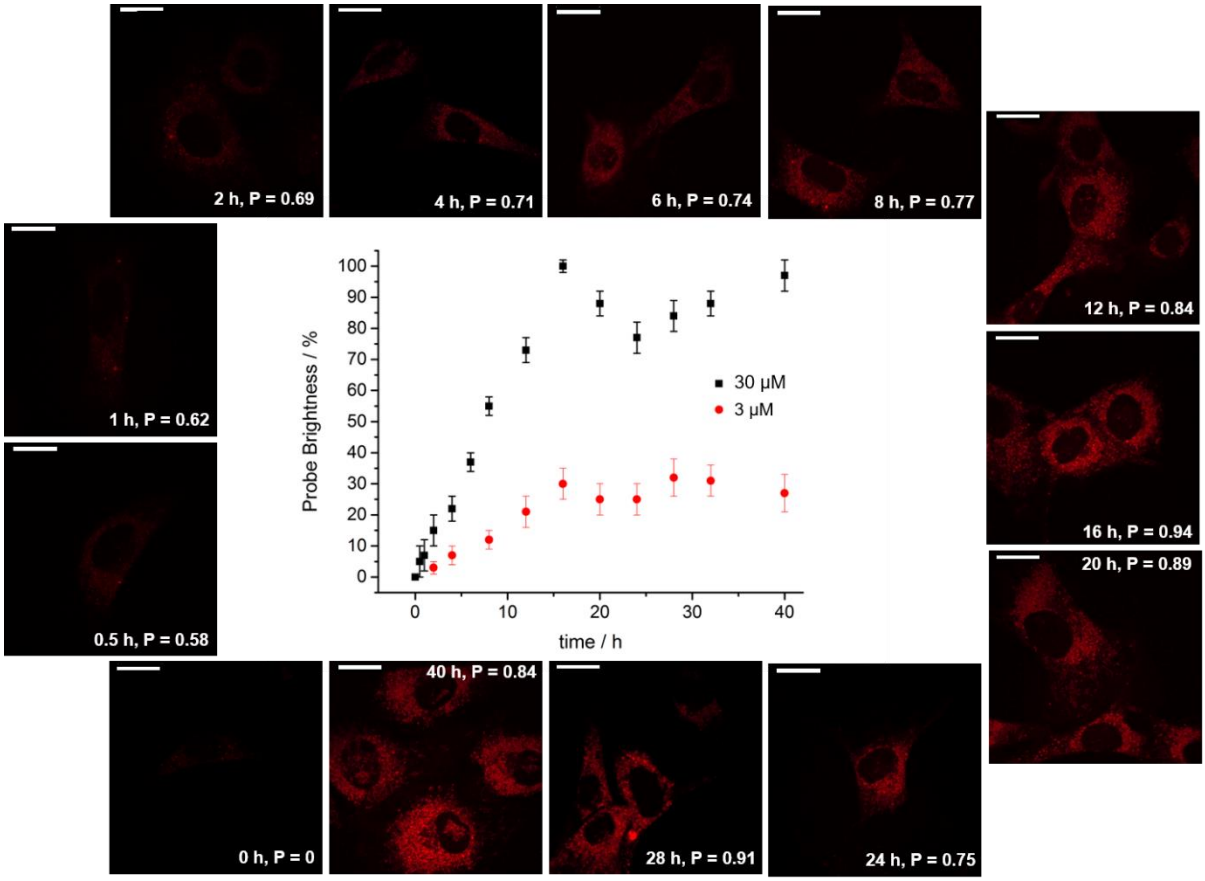

Figure 2.22. Brightness profile of **[Eu.L^3]** as a function of time for incubation concentrations of 30 µM (*black*) and 3 µM (*red*) in living NIH-3T3 cells; images shown are for 30 µM. Scale bar represents 20 microns. The cells were monitored for 72 h, at which time the cells were proliferating normally.

The microscopy study revealed a time dependent increase in brightness that maximised at around 16 to 18 hours, (Figure 2.22). A drop in brightness was then observed at both incubation concentrations. Such behaviour coincides with the time period of mitosis for NIH-3T3 cells which divide on average every 16 hours during unaltered proliferation. This process was indeed observed after 16 hours (Figure 2.22 at the 16 hour time point). Following cell division, the daughter cells appeared less bright, in line with the increase in cell volume. Each daughter cell possesses about 50% of the internalised complex of the parent cell, as they begin their independent life cycle. The concentration of complex found inside the cell then increases again, as the daughter cells mature and embark on homeostatic uptake of nutrients and of the **[Eu.L^3]** complex that is present in the cell growth medium. However, this process has a time lag, resulting in the observed time *vs.* brightness profile. Similar overall

behaviour was observed for both of the incubation concentrations of the europium complex examined, *i.e.* at 3 and 30 mM.

Regular cell function (division/proliferation) was observed to occur up to 72 hours, indicative of the minimal toxicity of **[Eu.L^3]** using the stated incubation concentrations. To verify this conclusion, cell toxicity was assessed in a separate study using live/dead assay image cytometry, (Figure 2.23). No evidence (±5%) for perturbation of natural cell homeostatic function and proliferation was found over a period of 24 hours, for complex concentrations of up to 100 µM.

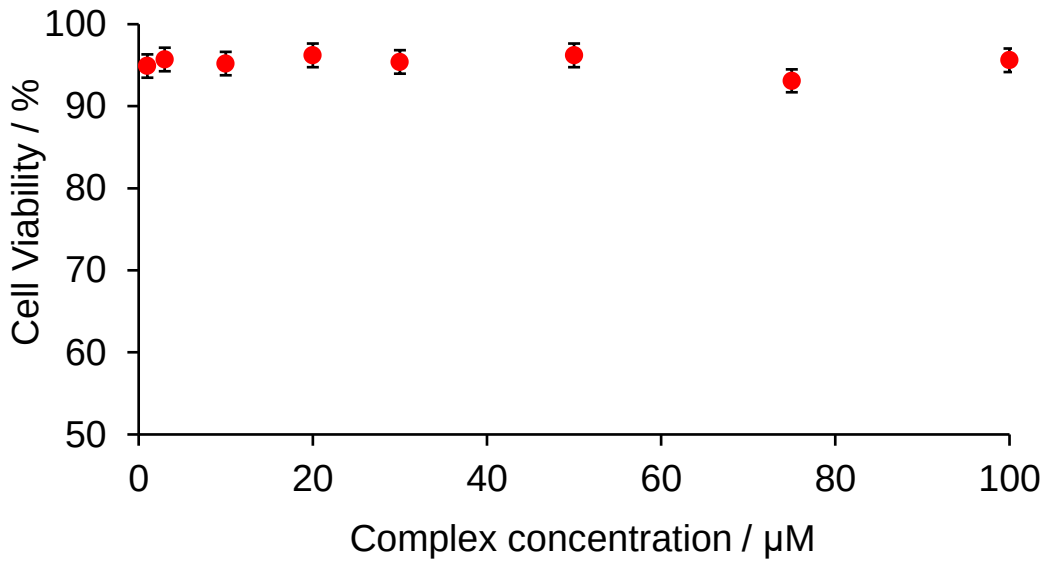

Figure 2.23. MTT assay showing the percentage of living viable cells as a function of complex concentration for a 24 h incubation.

The observed variation of **[Eu.L^3]** emission both *in vitro* and *in cellulo* is hypothesised to be attributed predominantly to the response to changes in the pH of the local environment. Whilst the impact of pH on the emissive properties of the complex has been demonstrated, it is necessary to validate the assumption that these observed changes are primarily a result of the pH variation, rather than perturbation following encounter with other common endogenous species whose concentration could hypothetically change in the same time period in the given organelles.

In a series of *in vitro* control experiments, the complex **[Eu.L^3]** was exposed to a range of selected endogenous analytes in acidic aqueous buffer at fixed pH (30 µM complex, 0.1 M NaCl, 0.1 M NH_4HCO_3 buffer, pH 5) and the emission lifetime and intensity of

the europium complex was measured. No significant changes in emission lifetime or intensity were observed following addition of up to 5 equivalents (corresponding to a limiting concentration of 150 μM) of the common cations Mg^{2+}, Ca^{2+} and Zn^{2+}, (Figure 2.24 *bottom*). Similarly, no changes were observed following addition of ascorbate, urate and glutathione. These are endogenous reductants that could potentially quench the excited state of the probe by electron transfer. Finally, no major variations (±10%) were found following the addition of BSA which is present in the cell incubation medium. For clarity, the total change in emission lifetime (blue) and intensity (red) with addition of 5 equivalents of each species is shown, relative to the change associated with pH change from 8 to 4 (normalised to 1).

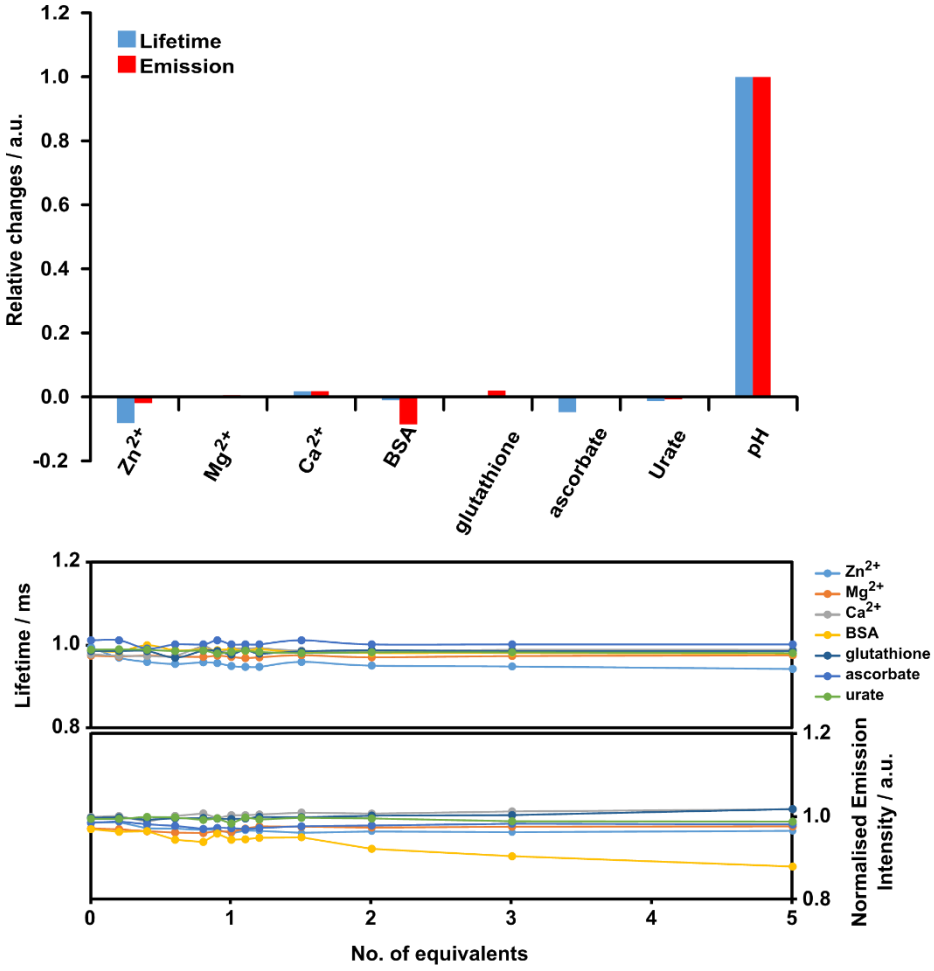

Figure 2.24. *(Top)* Total change in emission lifetime (*blue*) and emission intensity (*red*) following addition of 5 equivalents of analyte to **[Eu.L^3]** (30 μM complex, 0.1 M NaCl, 0.1 M NH_4HCO_3 buffer, pH 5) relative to the pH change observed from 8 to 4 (normalised to unity). *(Bottom)* Change in emission lifetime and emission intensity (normalised) of **[Eu.L^3]** (30 μM complex, 0.1 M NaCl, 0.1 M NH_4HCO_3 buffer, pH 5) with the number of equivalents of analyte added.

In a control experiment with a structurally analogous europium complex, ***D*-[Eu.L^4]** that shows no pH dependent emission behaviour and a predominant lysosomal localisation profile, very different *in cellulo* behaviour was observed, using identical incubation conditions with NIH-3T3 cells, (Figure 2.25).[26] In the case of this control complex, the mean image brightness reached a plateau after 4 hours after which it remained constant, with a minor inflection at around 16 – 18 hours. In stark contrast, the mean image brightness for **[Eu.L^3]** was observed to increase more gradually, only reaching a maximum at around 16 hours.

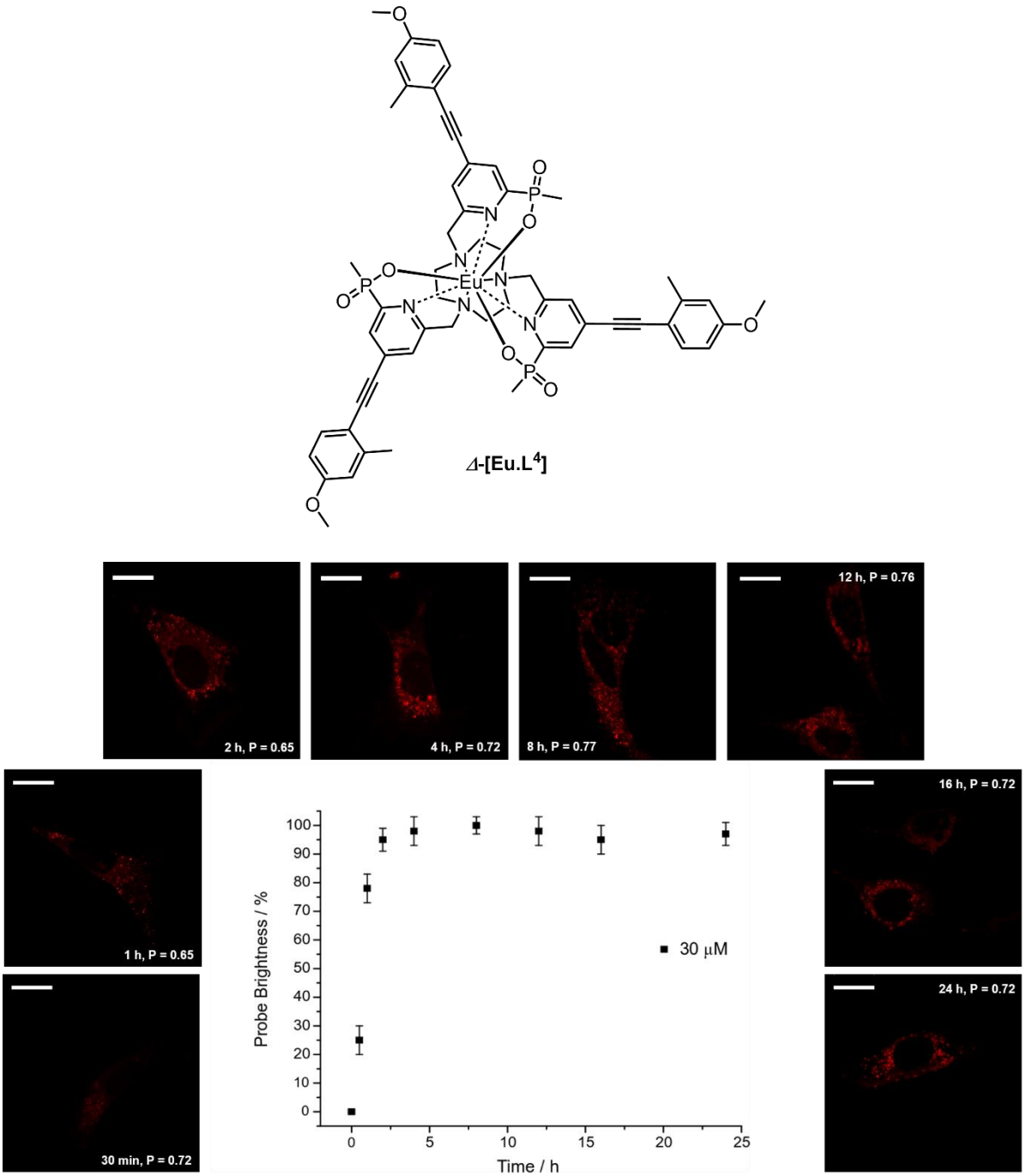

Figure 2.25. *(Top)* Structure of ***qp*[Eu.L^4]**; a pH-insensitive, enantiopure europium(III) complex, structurally analogous to **[Eu.L^3]**. *(Bottom)* Brightness profile of ***qp*[Eu.L^4]** as a function of time in live NIH-3T3 cells; images shown are for a 30 μM incubation. Scale bar represents 20 μM. The cells were monitored for 48 h and were proliferating normally.

The observed time dependent increase in brightness during cell experiments with **[Eu.L^3]** could in theory be attributed to both changes in the extent of uptake, which likely proceeds via macropinocytosis as found in related studies,[24,26] as well as the pH drop in the ageing endosomes as they transform into lysosomes. In parallel to the brightness *vs.* time microscopy study at 30 μM incubation concentration, control

experiments measuring the intracellular concentration of europium, (derived only from **[Eu.L^3]**) were undertaken at 2, 4, 8, 12, 16 and 24 hours. This analysis was undertaken by taking aliquots at these time points, preparing each sample for analysis by digestion in nitric acid for 24 hours at room temperature. These samples were then subjected to ICP-MS analysis to quantify the amount of europium (and hence the europium complex) present at each time point, (Figure 2.26).

These studies showed a significantly less steep increase in europium concentration, with the intracellular europium concentration doubling between 2 and 16 hours, while the observed mean image brightness increased by approximately two orders of magnitude over the same period. Such behaviour is consistent with the hypothesis that the brightness enhancement is not simply due to the slow increase in the total amount of complex internalised, but much more strongly relates to the effect of diminishing pH in the ageing lysosomes, with the associated large increase of europium emission intensity, as the percentage of the more emissive protonated complex increases. This hypothesis is also consistent with the observed time dependent increase in Pearson's co-localisation coefficient (*P*), in the parallel microscopy study using LysoTracker Green, (Figure 2.25).

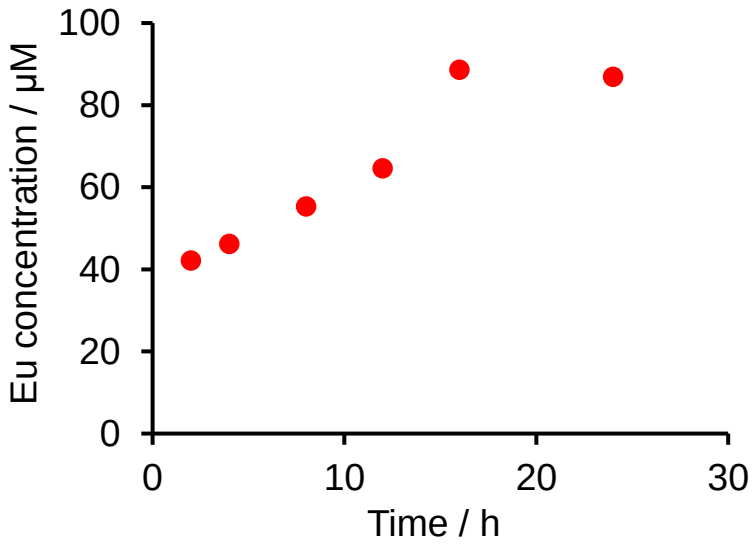

Figure 2.26. Eu concentrations determined by ICP-MS at the stated time points for **[Eu.L^3]** in NIH-3T3 cells showing the approximate doubling of complex uptake between 2 and 24 h.

As a further demonstration of the emissive response of **[Eu.L^3]** to pH *in cellulo*, nigericin (200 nM) was added, following a separate 16 hours incubation of **[Eu.L^3]** in

NIH-3T3 cells (30 μM complex incubation concentration). Nigericin is a K^+/H^+ ionophore that has been shown to increase lysosomal pH quickly, from approximately 4.5 to 6.5,[27] by promoting exchange of K^+ for H^+ across a cell membrane, in order to remove biological pH gradients across a cell.[28] After 5 minutes, confocal microscopy studies showed that the europium complex appeared to be considerably less bright overall, consistent with the increased size of the treated cell's lysosomes and the reduced probe brightness at the higher pH value. Whilst a very minor proportion of the complex was observed to migrate to the mitochondria as a result of this treatment, this shuttling behaviour is presumably a consequence of the swollen lysosome becoming leaky following the treatment with nigericin. Such behaviour was not seen during the earlier microscopy experiments where cellular function was regular and unperturbed. In a control experiment, the internalised complex concentration of treated and untreated cells, for a given time incubation time point, was found to be identical within experimental error, determining europium concentrations with ICP-MS.

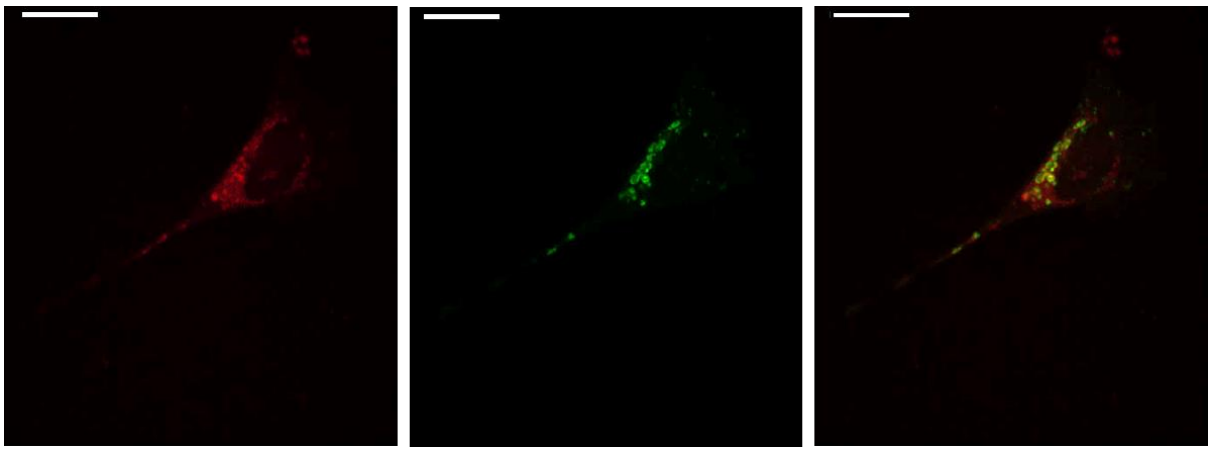

Figure 2.27. Living cell images (NIH-3T3 cells) taken during a nigericin experiment 16 h post incubation of **[Eu.L^3]** in the cellular medium. (*Left*) **[Eu.L^3]** (λ_{exc} 355 nm, λ_{em} 600–720 nm); (*Centre*) Lysotracker Green (λ_{exc} 488 nm, λ_{em} 500–530 nm); (*Right*) Overlay showing correspondence. Scale bar = 20 mm.

2.5. Low Temperature Studies of [Gd.L$^{1\text{-}3}$]

In several series of structurally related lanthanide complexes, europium sensitisation has been suggested to occur by an efficient intramolecular energy-transfer process involving a relaxed and fairly broad ICT excited state and not via a localized ligand triplet state, notably for systems with strongly electron donating groups on the aryl ring.[1,20-21] In the case of relatively weak donor groups on the aryl ring, such as alkyl

and alkoxy substituents, the ICT state lies at higher energy and consequently a contribution of the classical triplet-mediated sensitization process remains possible.[29-30] For the europium(III) complexes **[Eu.L$^{1-3}$]**, the europium emission lifetime was shown to be independent of complex concentration in water over the range 1 to 50 μM, and did not change on degassing the solution, for both acidic and basic solutions.

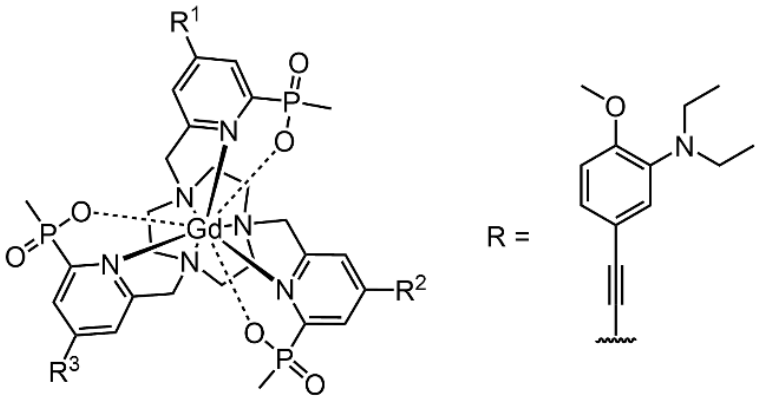

[Gd.L^{1}] $R^1 = R, R^2 = R^3 = H$

[Gd.L^{2}] $R^1 = R^2 = R, R^3 = H$

[Gd.L^{3}] $R^1 = R^2 = R^3 = R$

Figure 2.28. Structures of the gadolinium(III) analogues, **[Gd.L$^{1-3}$]**.

The corresponding gadolinium complexes, **[Gd.L$^{1-3}$]**, were prepared and investigated in order to study the influence of the number of conjugated chromophores and of protonation on the energies of the ligand based excited states, (Figure 2.28). At 77 K, each unprotonated complex exhibited a broad, structureless emission band with a maximum at 455 nm (21,980 cm^{-1}) that extended well beyond 500 nm (20,000 cm^{-1}), characteristic of an ICT state that overlapped with a more structured emission from the ligand-centred triplet state at 486 nm (20,575 cm^{-1}), (Figure 2.29). In the latter case, the first vibrational overtones were apparent for each Gd complex at 525 nm. At room temperature, only a broad structureless ICT emission was observed at around 460 nm.

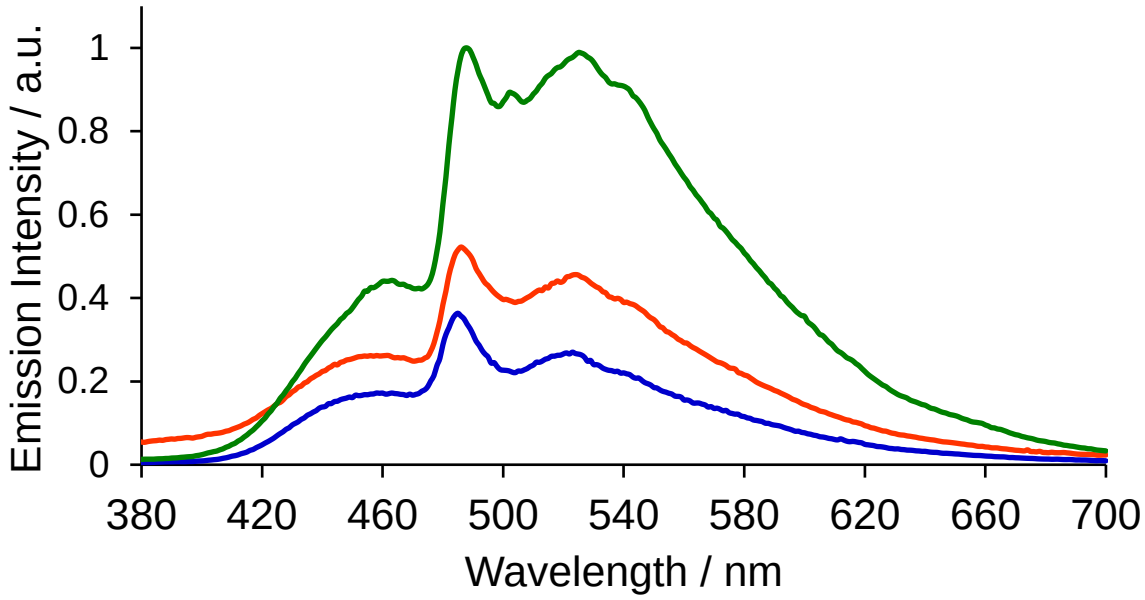

Figure 2.29. Emission spectra of **[Gd.L$^{1\text{-}3}$]** (*blue*, *red* and *green* respectively) at 77 K, prior to protonation. Recorded in an EPA glass (λ_{exc} 360 nm). The relative emission intensity values for the complexes are not to scale.

For the protonated complexes, examined *in situ* following addition of TFA, an unstructured band appeared at 370 nm (27,100 cm^{-1}), with the ligand triplet still evident as a weaker and structured emission band at 466 nm (21,460 cm^{-1}). Vibrational structure was evident, with overtones appearing at about 503 and 546 nm, possibly corresponding to harmonics of a pyridine ring vibration around 1580 cm^{-1}, (Figures 2.30 and 2.31).

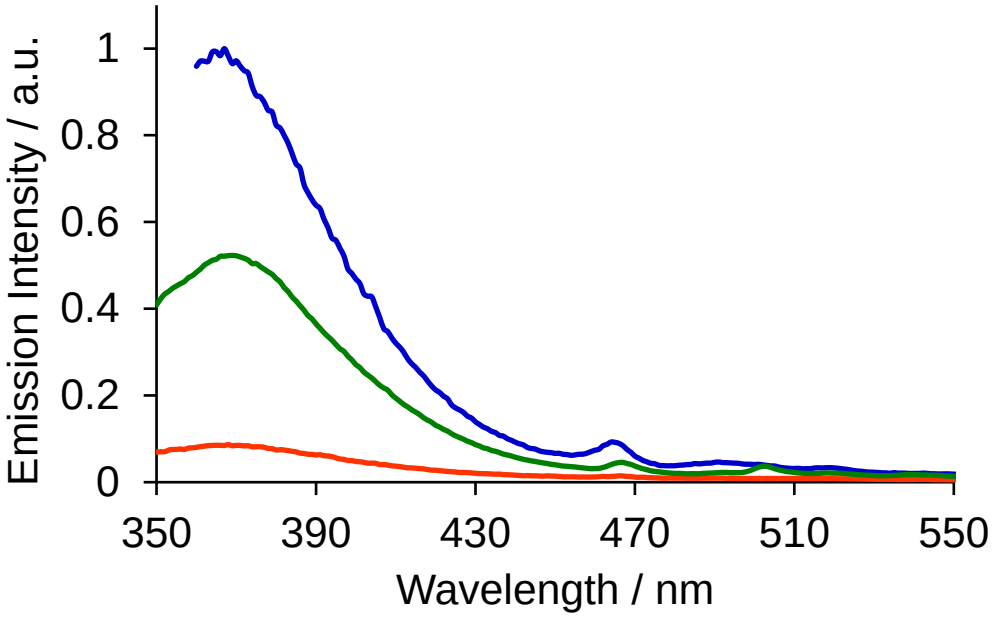

Figure 2.30. Emission spectra of **[Gd.L$^{1\text{-}3}$]** (*blue*, *red* and *green* respectively) at 77 K, following protonation with TFA (λ_{exc} 330 nm). Recorded in an EPA glass. The relative emission intensity values for the complexes are not to scale.

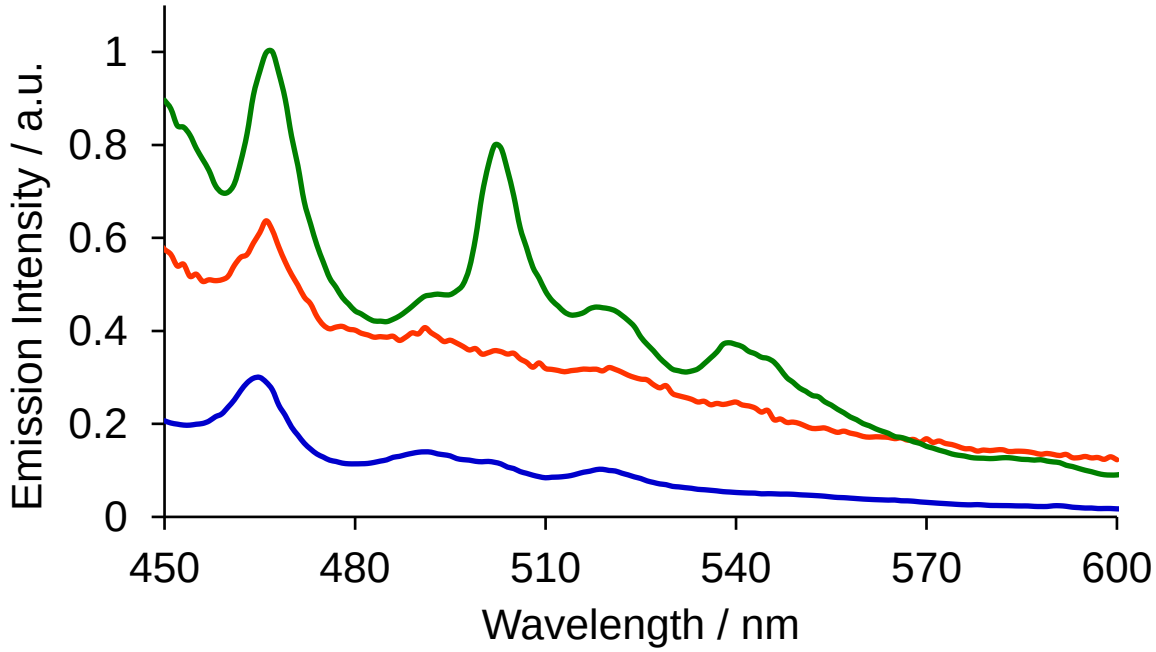

Figure 2.31. Emission spectra of **[Gd.L$^{1\text{-}3}$]** (*blue*, *red* and *green* respectively) at 77 K, following protonation with TFA (λ_{exc} 330 nm). Recorded in an EPA glass. A wider slit is used relative to Figure 2.32 for increased signal. The relative emission intensity values for the complexes are not to scale.

These variable-temperature (VT) measurements clearly indicate the presence of a triplet excited state at approximately the same energy as the ICT state for the unprotonated form which occurs at lower energy in the protonated form, (Figure 2.32). Consequently, whilst it is possible that the major sensitisation pathway for the corresponding europium(III) complexes involves the protonated ICT excited state, with energy transfer occurring directly from this excited state to the europium, it is not possible to rule out a classical ligand triplet excited state being involved in the sensitisation of europium luminescence, donating energy to the europium $^5D_1$ and $^5D_0$ excited states which lie at 19,100 and 17,200 cm^{-1} respectively. Further time-resolved pulsed fast laser experiments, *e.g.* observing transient absorption spectroscopy, are required to further probe and clarify this issue.

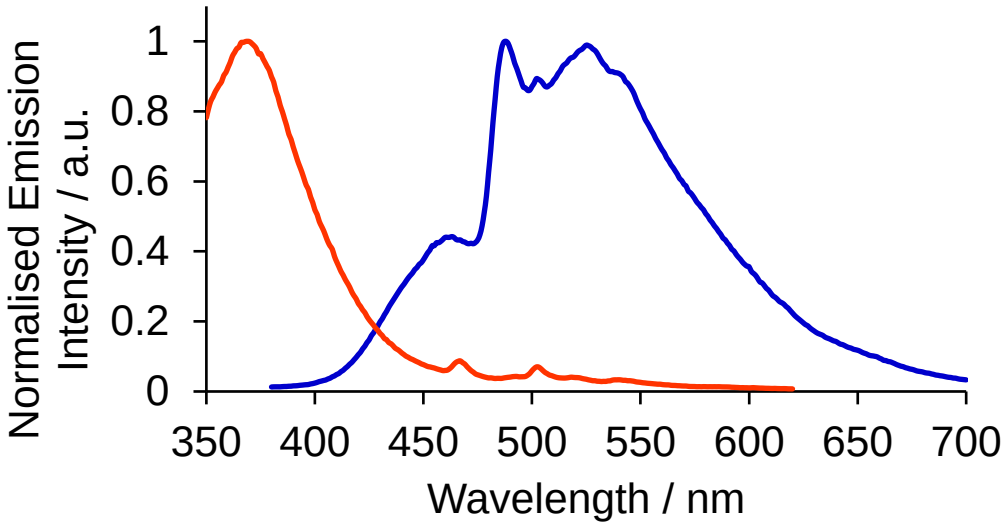

Figure 2.32. Comparison of the normalised emission spectra of **[Gd.L^3]**) at 77 K for the unprotonated (*blue*) and protonated forms (*red*) (λ_{exc} 330 and 360 nm respectively) showing the concomitant shift of the broad ICT band and the structured ligand triplet to higher energies. Recorded in an EPA glass.

Taken together with the europium emission spectral studies, their pH dependence, and insensitivity to dissolved oxygen and variation of complex concentration, the VT studies with **[Gd.L$^{1\text{-}3}$]** support the premise that the protonated europium complex is the observed emissive species in all cases. The europium excited state is prone to quenching by an intramolecular electron transfer process associated with the ligand amine N lone pair of the diethylamino group. The rate of proton transfer to and from N (typically 10^{11} s^{-1}) occurs much faster than the slow rate of decay of the excited

europium ion (10^3 s^{-1}) and of the intermediate ligand ICT or triplet excited states. Furthermore, the rate of electron transfer from N to the excited europium ion is usually much faster than the rate of energy transfer populating it or indeed of its own radiative rate of emission.

Thus, during the long lifetime of the Eu(III) $^5D_0$ excited state, deprotonation of the amine group will occur, allowing fast electron transfer to take place from the N lone pair to the europium ion, quenching emission and effectively shortening the 'time-averaged' observed lifetime. Such an effect is more likely to occur both as the mole fraction of the unprotonated complex increases and with the increase in the number of protonation sites, *i.e.* the number of chromophores bearing the amine group. Statistically, the mole fraction of the fully protonated complex where each amine group, from which electron transfer can occur, is protonated will decrease as the number of chromophores increases. This is consistent with the observation that the symmetrical trisubstituted complex, **[Eu.L^3]**, has the shortest observed lifetime of all, and the complex with one amine-containing chromophore, **[Eu.L^1]**, has the longest lifetime at both pH 4 and 8.

The likelihood of this hypothesised quenching by intramolecular electron transfer may be predicted using an approach adopted originally by Weller for PeT processes in the quenching of singlet excited states.[31]

$$\Delta_{ET} = ([_{ox} - _{red}] - _{s} - ^{2}/) \text{J mol}^{-1}$$

Here, E_{ox} and E_{red} are the oxidation and reduction potentials of the donor and acceptor respectively (*i.e.* the diethylamino lone pair and Eu^{3+} ion), E_s is the singlet excited state energy in eV, and $e^2/\varepsilon r$ is the attractive energy term corresponding to formation of a radical ion pair (typically <~0.2 eV).

The Weller equation considers the free energy of activation for an electron transfer process and can be applied here to assess the feasibility of the quenching of the europium excited state by intramolecular electron transfer from the diethylamino group(s) present on the antenna(e). The oxidation potential of an *N,N*-dialkylaniline (*e.g. N,N*-dimethylaniline) is approximately +0.53 V in acetonitrile (*c.f.* approx. +1.2 V for a trialkylamine such as triethylamine), whilst the reduction potential of the Eu(III)

ion lies in the range –0.8 to –1.2 V, when coordinated by a polar polydentate ligand (estimated as –1.1 V here).[5]

The energy of the excited Eu(III) $^5D_0$ state lies at 17,200 cm^{-1} (equivalent to +2.13 eV/+206 kJ mol^{-1}).

$$\Delta_{ET} = [(0.53 + 1.1] - 2.13 - 0.15]$$

$$\Delta_{ET} = -0.65 = -63\ kJ\ mol^{-1}$$

Given these values, the free energy for the electron transfer process from the donor nitrogen of a *N,N*-dialkylaniline to the europium(III) centre can be predicted to be energetically favourable, assuming the excited state reduction potential of the europium ion is of the same magnitude as the ground state.

2.6. Conclusions

Three new luminescent europium(III) complexes have been prepared and evaluated in a series of comparative studies, assessing their absorption and emission spectral behaviour as a function of pH. These complexes differ in their number of antenna chromophores (1-3), where an amine group is conjugated into the aryl ring at the periphery. Protonation of **[Eu.L$^{1\text{-}3}$]** resulted uniformly in a hypsochromic shift of the main absorption band and very large increases in europium emission lifetime of 120, 200 and 240% respectively. This behaviour was mirrored by increases in europium emission intensity for **[Eu.L$^{1\text{-}3}$]** of 540, 560 and 560-fold respectively ($\Delta J = 2$ analysis), by changing pH from 8 to 4. By varying the delay time or the time period for acquisition of europium spectral intensity data, it was demonstrated with **[Eu.L^3]** that the enhancement of emission intensity ratios of between 250 and 1300 was possible.

Europium lifetime and emission intensity were found to be more or less invariant with the concentration of biological cations (Ca^{2+}, Mg^{2+}, and Zn^{2+}), with naturally electron-rich reductants (ascorbate, urate, and glutathione), and with the protein BSA. Changes in the concentration of each of these species may potentially perturb the behaviour of a luminescent probe in a biological setting.

The europium emission lifetime was also determined to be independent of complex concentration over the range 1 – 50 μM and was unaffected by the presence or

absence of dissolved oxygen, ruling out the possibility of either intermolecular or oxygen mediated quenching processes. In an effort to elucidate this quenching behaviour further and probe the mechanism of europium sensitisation, the gadolinium(III) analogues **[Gd.L$^{1\text{-}3}$]** were prepared and low temperature emission behaviour was investigated. Whilst it was not possible to elucidate the europium sensitisation pathway unequivocally, the results from these studies, in addition to the spectral studies with **[Eu.L$^{1\text{-}3}$]**, strongly suggest that the fully protonated complex is the observed emissive species. Further investigation using time-resolved pulsed fast laser experiments, *e.g.* observing transient absorption spectroscopy, are proposed to test this hypothesis further.

The complex **[Eu.L^{3}]** was examined in two different cell lines and was observed to localise mainly in the cellular lysosomes, without compromising cellular viability or degree of proliferation. Using laser scanning confocal microscopy, exciting the complex at 355 nm, an increase in probe brightness was observed in the living cells as a function of time, over the period 2 to 16 hours. The observed brightness was 25 times greater than the change associated with the independently measured increase in probe uptake. In control experiments with a structurally related complex that exhibits no dependence of emission on pH, very different behaviour was observed and no significant changes in image brightness were observed, beyond the dependence on the extent of uptake. Taken together, such behaviour is consistent with the monitoring of the acidification of the cell's lysosomes as they age using this pH sensitive probe.

Such large pH induced 'switching on' factors, as displayed by these complexes, are well suited to assays where acidification needs to be monitored, as occurs during the maturation of endosomes or in the ageing of lysosomes, following uptake of a labelled protein or antibody.

Whilst the compatibility of **[Eu.L^{3}]** *in cellulo* has been demonstrated through living cell studies, currently none of these lanthanide systems permits the conjugation of the emissive probe to a targeting vector or protein. Such an approach is straightforward to devise and simply requires a suitable linkage site to be introduced into the ligand structure. This avenue of work is the subject of the next chapters in this thesis.

2.7. References

[1] M. Soulié, F. Latzko, E. Bourrier, V. Placide, S. J. Butler, R. Pal, J. W. Walton, P. L. Baldeck, B. Le Guennic, C. Andraud, J. M. Zwier, L. Lamarque, D. Parker and O. Maury, *Chem. Eur. J.*, 2014, **20**, 8636–8646.

[2] J. W. Walton, A. Bourdolle, S. J. Butler, M. Soulié, M. Delbianco, B. K. McMahon, R. Pal, H. Puschmann, J. M. Zwier, L. Lamarque, O. Maury, C. Andraud and D. Parker, *Chem. Commun*., 2013, **49**, 1600–1602.

[3] A. P. de Silva, H. Q. N. Gunaratne, T. Gunnlaugsson, A. J. M. Huxley, C. P. McCoy, J. T. Rademacher and T. E. Rice, *Chem. Rev.*, 1997, **97**, 1515–1566.

[4] C. M. G. dos Santos, A. J. Harte, S. J. Quinn and T. Gunnlaugsson, *Coord. Chem. Rev.*, 2008, **252**, 2512–2527.

[5] D. Parker, *Coord. Chem. Rev*., 2000, **205**, 109–130.

[6] J. W. Walton, R. Carr, N. H. Evans, A. M. Funk, A. M. Kenwright, D. Parker, D. S. Yufit, M. Botta, S. De Pinto and K.-L. Wong, *Inorg. Chem.*, 2012, **51**, 8042–8056.

[7] L. Lamarque, M. Delbianco, S. J. Butler and D. Parker, Nouveaux agents complexants hydrosolubles et complexes de lanthanide correspondants, WO201411166.

[8] V. Boekelheide and W. J. J. Linn, *J. Am. Chem. Soc.*, 1954, **76**, 1286–1291.

[9] J. E. Huheey, E. A. Keiter and R. L. Keiter, *Inorganic Chemistry,* 4th edition, 1993.

[10] R. Chinchilla and C. Nájera, *Chem. Rev.*, 2007, **107**, 874–922.

[11] B. Liang, M. Dai, J. Chen and Z. Yang, *J. Org. Chem.*, 2005, **70**, 391–393.

[12] K. Sonogashira, Y. Tohda and N. Hagihara, *Tetrahedron Lett.*, 1975, **50**, 4467–4470.

[13] A. Soheili, J. Albaneze-Walker, J. A. Murry, P. G. Dormer and D. L. Hughes, *Org. Lett.*, 2003, **5**, 4191–4194.

[14] M. Gazvoda, M. Virant, B. Pinter and J. Košmrlj, *Nat. Commun.*, 2018, **9**, 4814–4823.

[15] J. Clayden, N. Greeves and S. Warren, *Organic Chemistry*, Oxford University Press, United States, 2nd edition, 2012.

[16] M. Starck, J. D. Fradgley, R. Pal, J. M. Zwier, L. Lamarque and D. Parker, *Chem. Eur. J*., 2021, **27**, 766–777.

[17] L. B. Jennings, S. Shuvaev, M. A. Fox, R. Pal and D. Parker, *Dalton Trans.*, 2018, **47**, 16145–16154.

[18] S. Shuvaev, M. Fox and D. Parker, *Angew. Chem. Int. Ed.*, 2018, **57**, 7488–7492.

[19] M. Delbianco, V. Sadovnikova, E. Bourrier, G. Mathis, L. Lamarque and J. M. Zwier, *Angew. Chem. Int. Ed.*, 2014, **53**, 10718–10722.

[20] S. J. Butler, L. Lamarque, R. Pal and D. Parker, *Chem. Sci*., 2014, **5**, 1750–1756.

[21] S. J. Butler, M. Delbianco, L. Lamarque, B. K. McMahon, E. R. Neil, R. Pal, D. Parker, J. W. Walton and J. M. Zwier, *Dalton Trans*., 2015, **44**, 4791–4803.

[22] K. Nakamaru, *Bull. Chem. Soc. Jpn.,* 1982, **55**, 2697–2705.

[23] J. Xu, T. M. Corneillie, E. G. Moore, G.-L. Law, N. G. Butlin and K. N. Raymond, *J. Am. Chem. Soc.*, 2011, **133**, 19900–19910.

[24] E. J. New, A. Congreve and D. Parker, *Chem. Sci.*, 2010, **1**, 111–118.

[25] M. Starck, R. Pal and D. Parker, *Chem. Eur. J.*, 2016, **22**, 570–580.

[26] A. T. Frawley, H. V. Linford, M. Starck, R. Pal and D. Parker, *Chem. Sci.*, 2018, **9**, 1042–1049.

[27] M. O. Bevensee, E. Bashi and W. F. Boron, *J. Membrane Biol*., 1999, **169**, 131–139.

[28] B. K. Grillo-Hill, B. A. Webb and D. L. Barber, *Methods in Cell Biology*, 2014, **123**, 429–448.

[29] A. Picot, F. Malvolti, B. Le Guennic, P. L. Baldeck, J. A. G. Williams, C. Andraud and O. Maury, *Inorg. Chem*., 2007, **46**, 2659–2665.

[30] A. D'Aleo, A. Picot, A. Beeby, J. A. G. Williams, B. Le Guennic, C. Andraud and O. Maury, *Inorg. Chem*., 2008, **47**, 10258–10268.

[31] A. Weller, *Pure Appl. Chem*. 1968, **16**, 115–123.

CHAPTER THREE

The Development of Functionalised Hydrophilic Complexes for Bioconjugation

Chapter Three: The Development of Functionalised Hydrophilic Complexes for Bioconjugation

This chapter builds upon the studies described within chapter two of the parent series of pH responsive complexes, **[Eu.L$^{1\text{-}3}$]**. It is concerned with the development of two sets of functionalised hydrophilic europium(III) complexes bearing chemical functionality suitable for bioconjugation through thoughtful design and synthesis.

3.1. Methods of bioconjugation

When considering the conjugation of a lanthanide complex to an appropriate targeting vector or protein (bioconjugation), it is essential to ruminate on two important aspects concerning the linkage site in the design of the complex. Firstly, the physical location of the site within the structure of the ligand can have significant implications on the synthesis itself, in addition to the resulting properties of the complex, *e.g.* some photophysical parameters for luminescent europium(III) complexes, and therefore must be considered. Secondly, the specific chemical functionality of the linkage site will govern, to an extent, the compatibility of the system with the various available methods of bioconjugation. Further, the identity of the linkage site might require the use of a protecting group, and therefore a deprotection step, to avoid complications during synthesis.

Several approaches exist for the introduction of a suitable linkage site into the ligand structure of europium(III) complexes, such as those based on TACN discussed in chapter 2, (Figure 3.1). One option involves introducing the linking functionality onto the macrocyclic backbone, *e.g.* with the complex **[Eu.L^{5}]**. In this ring functionalisation strategy, a primary amine group is attached to the TACN macrocycle through a butyl chain.[1] This approach, however, does require the preparation of functionalised derivatives of the macrocycle. *C*-Functionalised derivatives of TACN are made in 5 steps from *S*-lysine for example, increasing the total number of synthetic steps.[2] Alternatively, the linkage site can be incorporated into the antenna in some way, and the unsubstituted macrocycle is then used.

A linkage point can be installed in a simple 4-substituted pyridine derivative to replace one of the alkynylaryl moieties, *e.g.* a terminal amine as shown with **[Eu.L^6]**.[3] Functionalisation with particular chemical groups can allow for site-selective displacement, *e.g.* nucleophilic substitution of the pyridyl *para*-NO_2 group of **[Eu.L^7]** by an appropriately functionalised vector.[3,4] The resulting di-sensitiser complex will suffer, however, from reduced values of particular photophysical parameters, *i.e.* the molar extinction coefficient, ε, and brightness, B (assuming Φ does not vary substantially between the di and triantenna species). Another approach is to introduce the linking moiety at the periphery of an extended antenna, *e.g.* chemical manipulation of a peripheral carboxylic acid group in the complex **[Eu.L^8]**.[5] Although the photophysical parameters of the resulting complexes are not expected to suffer the previously described penalties, the synthesis of these triantenna species may be additionally challenging.

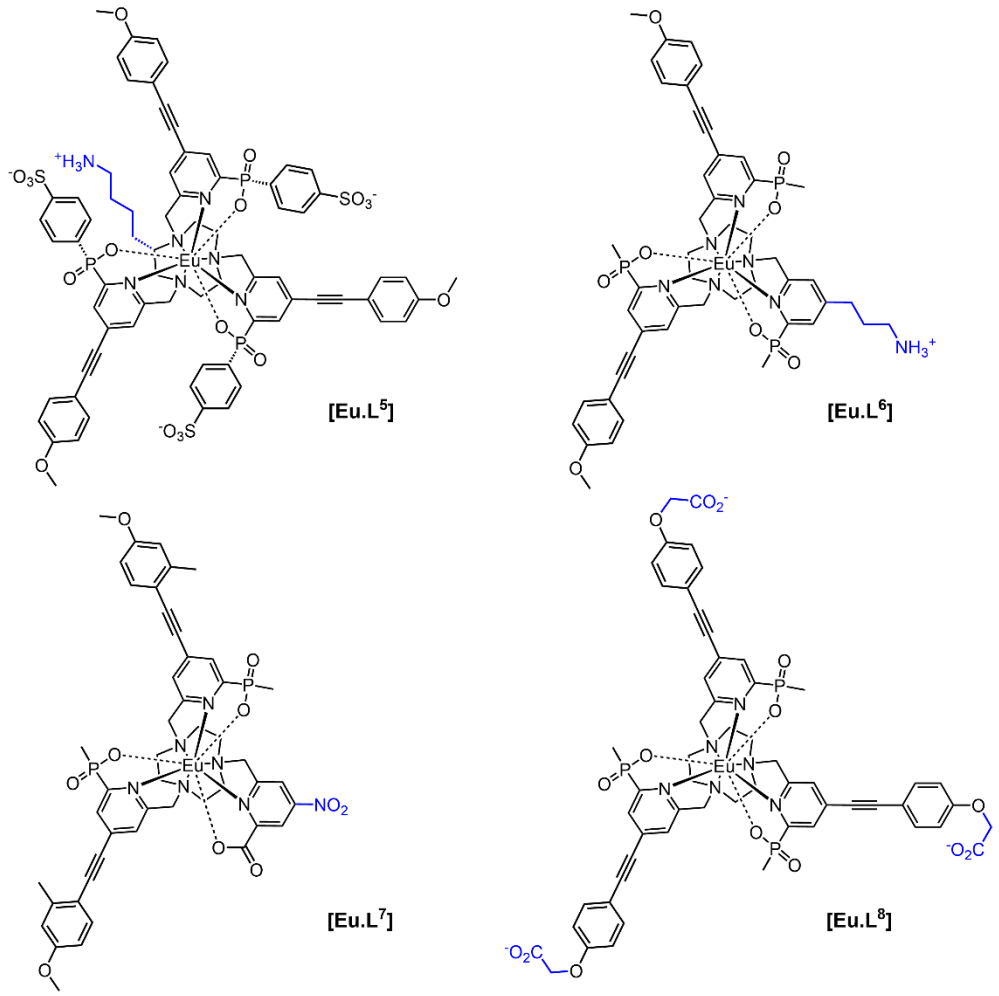

Figure 3.1. Selected literature examples[1,3-5] of functional groups used for the conjugation (*blue*) of the shown europium(III) complexes.

Typically, the bioconjugation step is performed once the complex itself has been prepared. There are various methods of accomplishing this, (Figure 3.2). For example, amine groups can be converted to maleimide intermediates through reaction with a bifunctional activated ester. These maleimides react quickly and selectively with thiols, such as the cysteine group in peptides and proteins. Similar reactivity profiles are shown by *para*-NO_2 pyridine derivatives, where the conjugation step is irreversible. Primary amines can also be converted to their benzyl guanine derivatives for bioconjugation using SNAP-tag methodology.

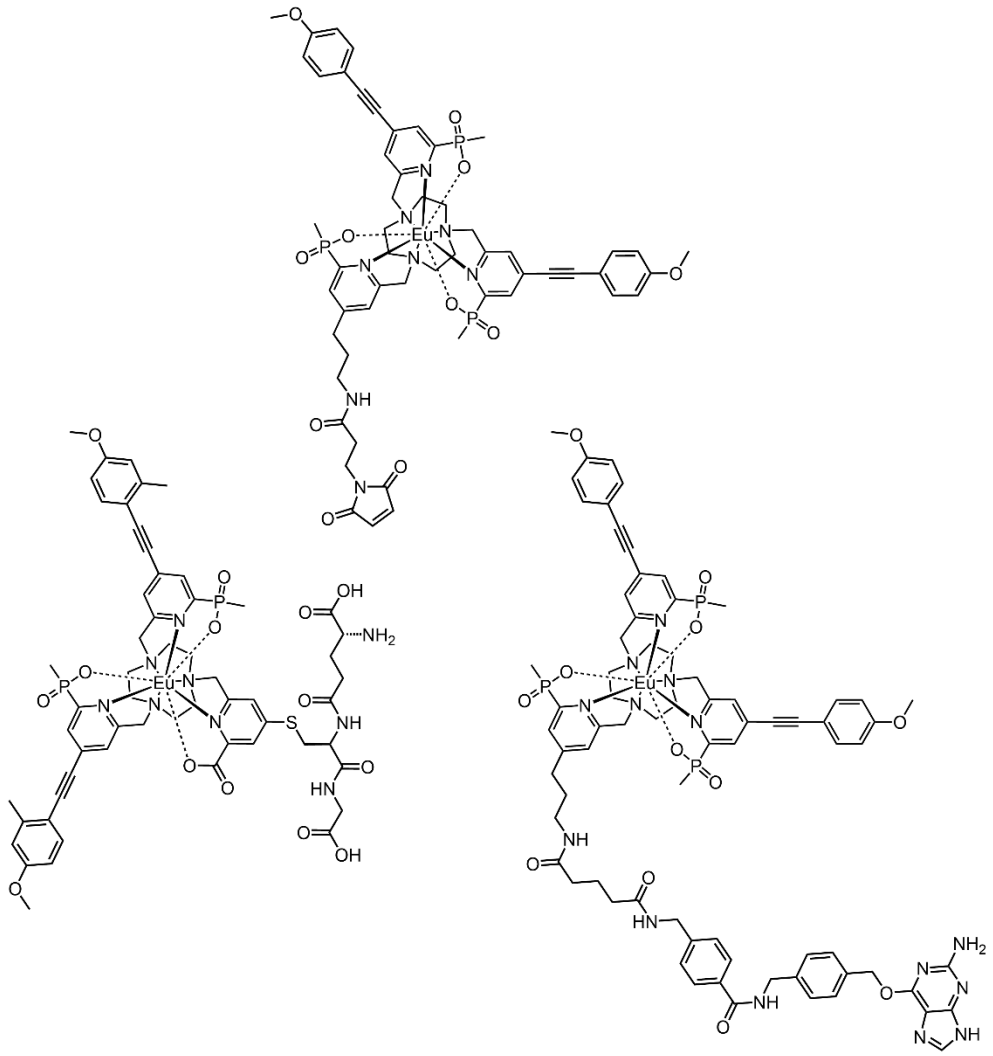

Figure 3.2. Examples of synthetic modifications enabling bioconjugation.

3.2. Discussion of the Structure of [Eu.L$^{9\ a\text{-}b\prime}$]

Early investigations into the pH dependence of the emission of the parent complexes, **[Eu.L$^{1\text{-}3}$]**, and subsequent *in cellulo* studies with **[Eu.L^{3}]** confirmed the viability of these systems as *in cellulo* pH probes. These systems must be modified thoughtfully, however, to introduce a linkage site suitable for conjugation and at the same time to improve critical properties, such as aqueous solubility. One such set of europium(III) complexes was proposed with this in mind, (Figure 3.3).

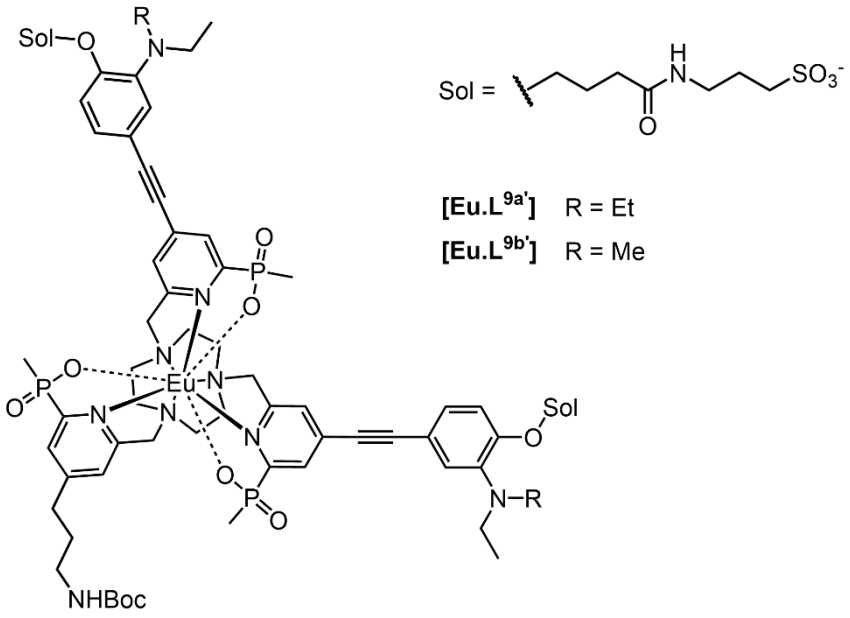

Figure 3.3. Structure of the proposed europium(III) complexes, **[Eu.L$^{9\ a\text{-}b\prime}$]**.

Comparative analysis of the photophysical behaviour of the parent systems **[Eu.L$^{2\text{-}3}$]** had suggested that the diantenna system was more well-behaved, *e.g.* the observation of an isosbestic point in the absorption *vs.* pH profile. For this reason, the decision was made to pursue a system featuring two antennae with a simple pyridine linkage site introduced at the expense of a third extended antenna.

Several modifications were required to the structure of the parent complex, **[Eu.L^{2}]**. Firstly, introduction of a long chain bearing a terminal sulfonate group to the head of each extended antenna was planned. The anticipated effect of these peripheral charged head groups is two-fold. Firstly, the presence of the anionic moieties was expected to increase the aqueous solubility of the complexes substantially. Secondly, the minimisation of unwanted non-selective binding with *in cellulo* species was envisaged, *i.e.* to endogenous proteins or membrane receptor sites. Whilst some

difficulties with the cellular uptake of anionic species bearing sulfonate groups have been reported,[6] such issues were not anticipated to be problematic here, due to the use of a high affinity targeting vector. The conjugation of the proposed systems to such a vector will result in their targeted localisation in a cellular system.

Secondly, modulation of the pK_a was proposed by varying the N-substituents (*e.g.* NEt_2 *vs.* NEtMe). Whilst the number of possibilities for functionalisation of the amine is large, inspection of literature pK_a values for substituted aniline suggested that the *N,N*-diethyl and *N*-ethylmethyl analogues be pursued first. Accordingly, they were examined.

Finally, a primary amine, protected as its carbamate with a Boc group, was proposed to enable conjugation of the europium(III) complex using SNAP-tag methodology.

3.3. Synthesis of [Eu.L$^{9\ a\text{-}b}$]

A partial retrosynthetic analysis for the proposed europium complexes **[Eu.L$^{9\ a\text{-}b}$]**, leads to the identification of appropriate synthetic equivalents and precursors, (Figure 3.4). The proposed synthetic pathway involves stepwise alkylation, analogous to that discussed for **[Eu.L^2]**, with one notable deviation being the introduction of peripheral sulfonic acid moieties in a final synthetic transformation, directly following metal ion complexation. It was foreseen to be advantageous to postpone the coupling of these aqueous-solubilising functionalities as late as possible in the synthesis. Such a strategy simplifies purification and minimises the handling of polar intermediates during the earlier synthesis stages, where high and low solubilities in organic and aqueous media, respectively, are preferable.

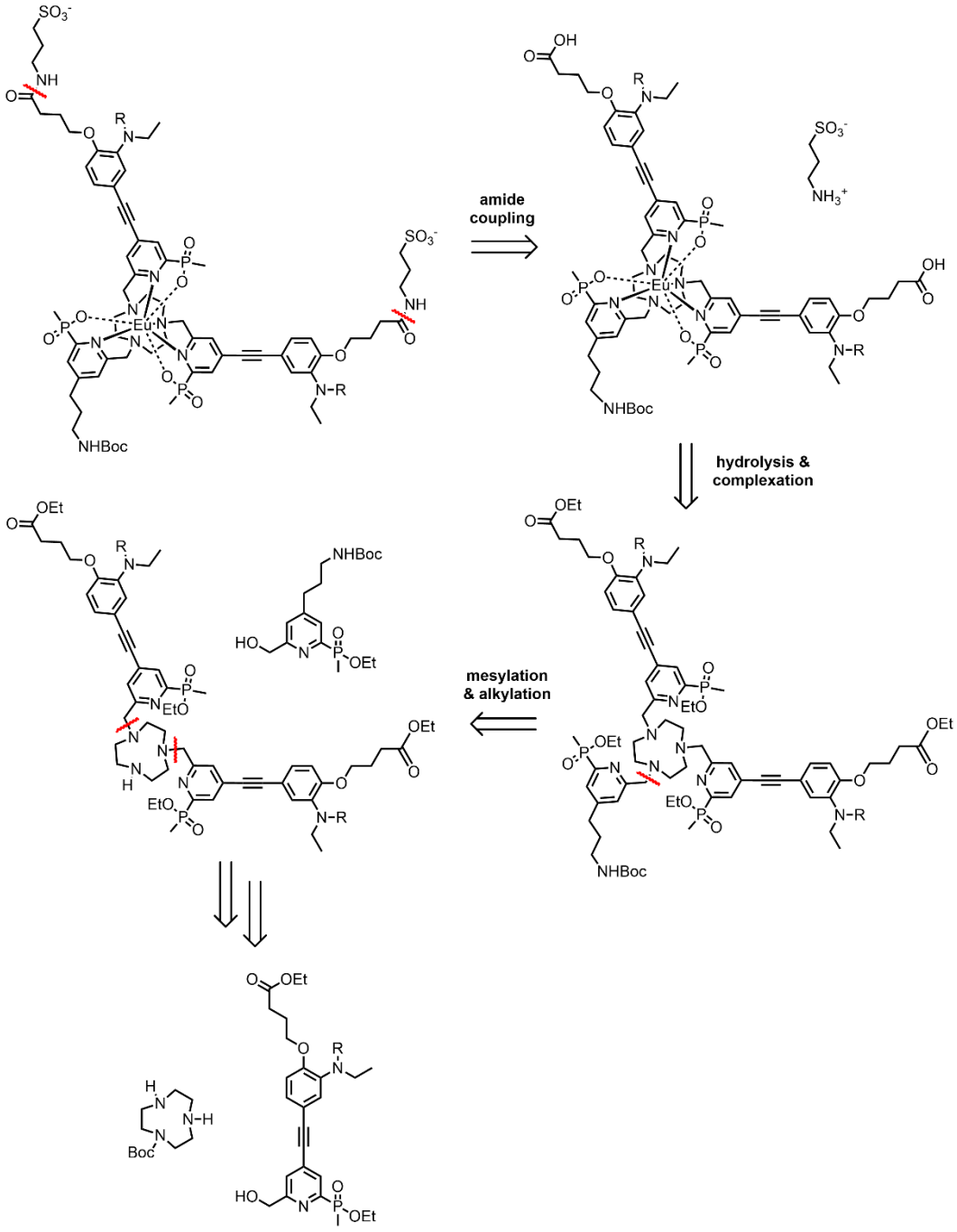

Figure 3.4. Retrosynthetic analysis of **[Eu.L$^{9\ a\text{-}b}$]** showing disconnections to mono-Boc-TACN and aromatic precursors (R = Et, Me).

The extended antennae were prepared in a convergent synthesis involving two main components, each of which was prepared in a linear manner. For the synthesis of the top components, where the identity of R differs, the commercially available 4-bromo-2-nitrophenol was selected as the starting material, (Figure 3.5). Whilst 2-amino-4-bromophenol is also available from commercial sources, the *o*-nitrophenol precursor

was preferred, as it allows direct O-alkylation without the need to protect the amine group.

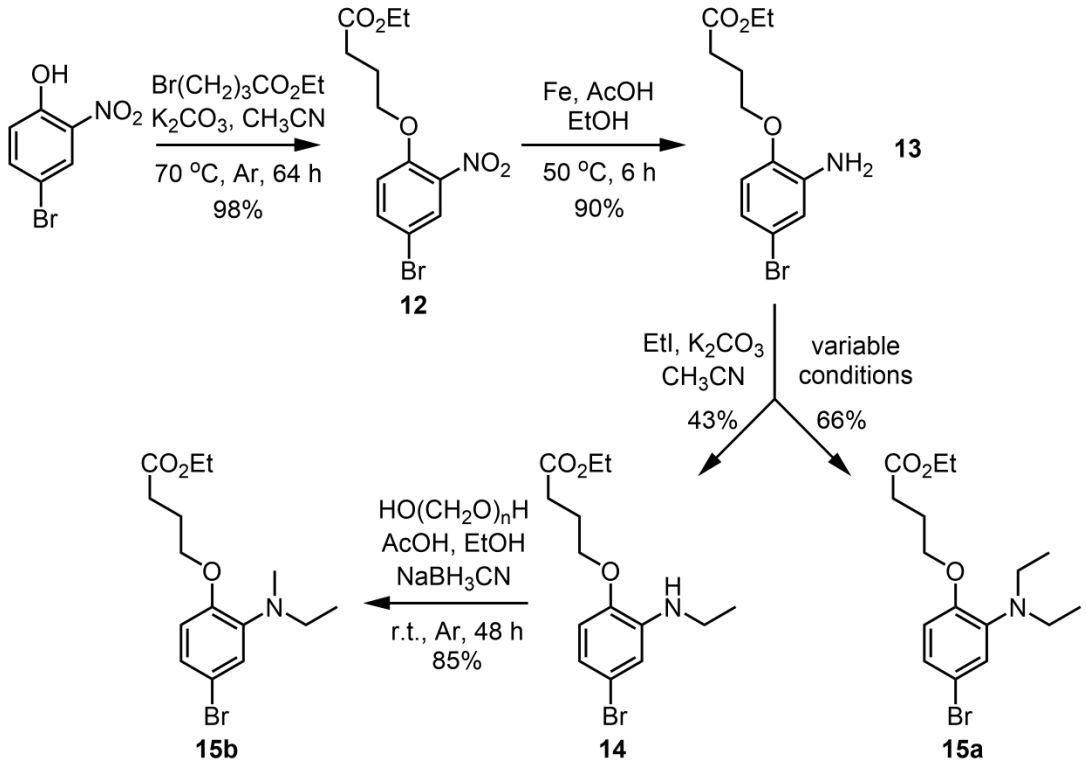

Figure 3.5. Functionalisation of the upper components by selective alkylation.

Alkylation of 4-bromo-2-nitrophenol by ethyl 4-bromobutyrate in the presence of potassium carbonate in acetonitrile, gave the ether **12** in near quantitative yield. A slightly larger solvent volume, compared with previous alkylation reactions (40 mL for 2.5 g starting material) was required, owing to the rather high viscosity of the reaction mixture. Only a small excess of ethyl 4-bromobutyrate (1.5 eq.) was used to facilitate separation of the product from the starting reagent in the ensuing silica column chromatography purification step. A prolonged reaction time was necessary (64 hours) to ensure consumption of the *o*-nitrophenol starting material.

Subsequent reduction of the nitro functionality of **12** by electron transfer using iron and acetic acid gave the amine **13**. Optimisation of the reduction conditions, work-up procedure, and reaction time was needed in order to maximise the yield and avoid side reactions, such as adventitious hydrolysis of the ethyl ester group. It was found that high yields (up to 90%) could be achieved within 4 hours by using increased equivalents of acid and iron, relative to the nitro compound (15 eq. AcOH, 5 eq. Fe). Longer reaction times (*e.g.* 14 hours), however, reduced the isolated yields to below

65% when using fewer equivalents of acid (*e.g.* 8 AcOH eq., 8 Fe eq.). The use of increased equivalents of AcOH and iron for prolonged reaction times (15 eq. AcOH, 5 eq. Fe, overnight reaction) resulted in competitive formation of several unidentified by-products.

Following reduction of the nitro group, the remaining iron salts were removed effectively by a work-up procedure using either the ion exchange resin CHELEX™ (Na^+ form) or by thorough aqueous washing with a saturated aqueous Na_4EDTA solution. Both work-up procedures yielded the amine **13** in a sufficiently pure form to be carried forward in the synthesis, as determined by TLC, ^1H NMR spectroscopy and LC/MS analysis.

The length of the alkyl chain installed in the first alkylation step was considered (*c.f.* three and one carbon atom(s)) with regard to the probability of competitive

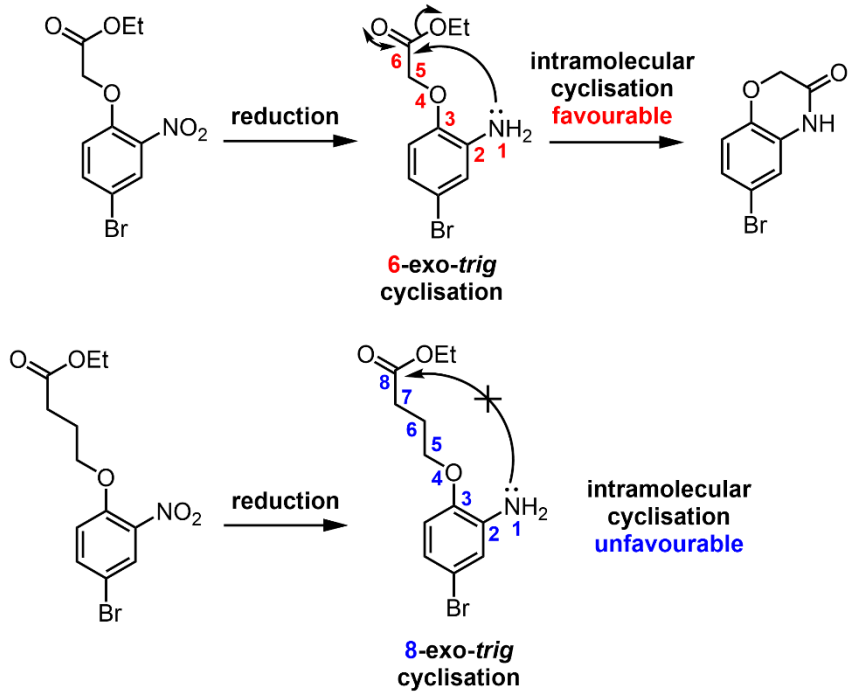

intramolecular cyclisation following reduction of the nitro group, (Figure 3.5). Guidelines for such intramolecular cyclisation processes have been postulated by Baldwin.[7] Attempts to prepare the top component with a shorter alkyl chain (Figure 3.6 *top*) served to emphasise the facility of the 6-exo-trig cyclisation reaction, as efforts to circumvent cyclisation were universally unsuccessful. Conversely, the desired product, **13,** was obtained without any complication arising from the disfavoured intramolecular cyclisation pathway.

Figure 3.6. Variation in the length of the alkyl chain introduced in the first synthetic step governs the facility of undesired intramolecular cyclisation (*c.f.* 6-exo-*trig* and 8-exo-*trig*).

As with the synthesis of the diethylamine derivative, **2**, the amine **13** was alkylated in acetonitrile with potassium carbonate. Iodoethane was again chosen as the electrophile, for reasons discussed previously. Previous synthetic work in chapter 2 had revealed the influence of varying reaction conditions on the rate of alkylation of the amine. In general, the first alkylation step was observed by TLC and mass spectrometry to be fast with respect to the second, which was rate-limiting. With this in mind, the mono- and di-alkylated amines, **14** and **15a,** were obtained in 43 and 66% yields, respectively, by varying the number of equivalents of iodoethane and the reaction temperature (1.5 eq. and 55 ºC *vs.* 5 eq. and 70 ºC). The reactions were carefully monitored by TLC and were stopped at an appropriate point, when the product and any by-products were deemed to be easily separable by silica column chromatography.

Methylation of the monoamine **14** by reductive amination in anhydrous ethanol gave the *N*-methylethyl functionalised amine **15b** and was high yielding (85%). Reaction with paraformaldehyde in the presence of acetic acid as a catalyst under ambient conditions gives rise to the intermediate imine, which was reduced *in situ* using $NaCNBH_3$. Alternatively, methylation could also be achieved by alkylation with iodomethane, using conditions similar to those already described (potassium carbonate and acetonitrile). This method afforded the product **15b** in a lower yield,

however, due to over-alkylation, leading to formation of the positively charged quaternary ammonium salt.

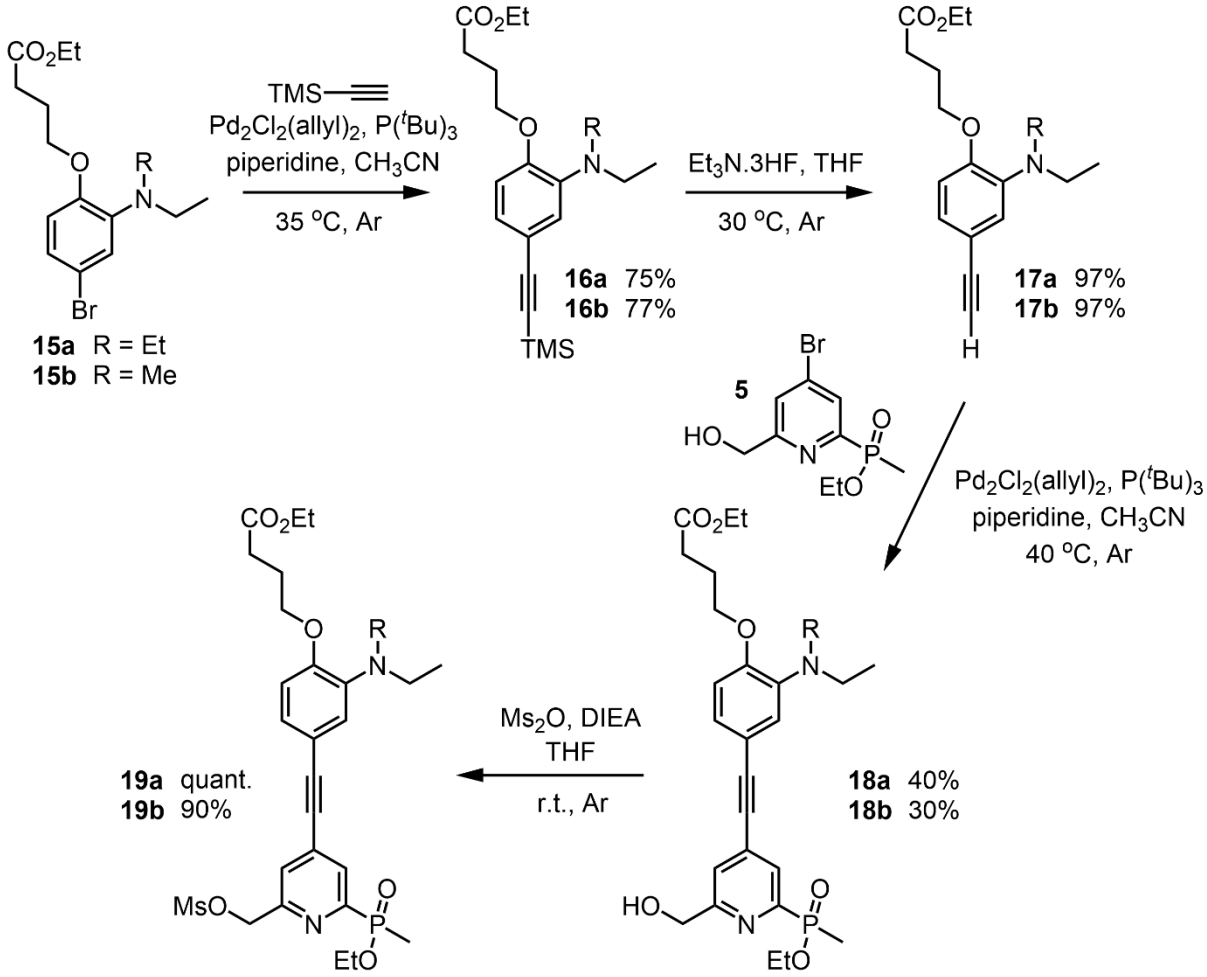

Figure 3.7. Synthesis of the extended antennae by successive metal cross coupling reactions.

With the appropriate functionality installed onto the upper aryl ring, the extended antennae were then constructed in a stepwise manner, (Figure 3.7). Identical conditions were used for each analogue (R = Et, Me), with no modification of reaction conditions required.

Preceding work in the Parker group had identified Pd(dppf)Cl_2.DCM as a preferred palladium catalyst for the Sonogashira metal cross coupling reaction, that allows introduction of the trimethylsilyl-protected acetylene moiety. This reaction has also been demonstrated to be effective within this work with the iodoaryl substrate, **2** (chapter two, section 2.2.2). Multiple sets of reagents and conditions for the Sonogashira cross coupling reaction between the bromoaryl substrate, **15a**, and trimethylsilylacetylene were trialled, varying the palladium catalyst, base, solvent,

presence of copper, and including the use of microwave irradiation, (Table 3.1). The majority of these trials were unsuccessful, with either zero or low yields of product formation at best (*e.g.* Table 3.1 entry 4). Success was achieved, however, with a palladium dimer catalyst $Pd_2Cl_2(allyl)_2$ using a mild, copper-free method reported by Soheili.[8]

Table 3.1. Summary of the reagents and conditions trialled for the Sonogashira cross coupling reaction between **15a** and trimethylsilylacetylene.

Reagents	Conditions	Yield / %
CuI, $Pd(PPh_3)_2Cl_2$, Et_3N, THF	Ar, 40 °C, 5 d	5
$Pd(PPh_3)_2Cl_2$, piperidine, THF	Ar, 50 °C, 1.5 d	-[a]
$Pd(dppf)Cl_2$.DCM, Et_3N, THF	Ar, 50 °C, 1.5 d	-[a]
$Pd(dppf)Cl_2$.DCM, pyrrolidine, THF	Ar, 50 °C, 1.5 d	22
$Pd(dppf)Cl_2$.DCM, Et_3N, DMF	Ar, 80 °C, 30 min[b]	11[b]
$Pd_2Cl_2(allyl)_2$, $P(^tBu)_3$, piperidine, MeCN	Ar, 35 °C, 1 d	75[c]

Anhydrous solvents were used for all reactions and thorough degassing with freeze-pump-thaw cycles was performed when using a copper(I) co-catalyst. [a] No product formation observed. [b] Microwave irradiation. [c] Complete starting material consumption and no nucleophilic attack on the ester by piperidine was observed.

The desired coupled product, **16a**, was obtained in good yield (75%) following purification by silica column chromatography. A similarly high yield (77%) was attained for the *N*-methylethyl analogue, **16b**. The various proposed mechanisms for the Sonogashira metal cross coupling reaction, with and without copper, have been discussed in detail previously (chapter two, section 2.2.2). The mechanism promulgated by Soheili *et al.* (Figure 3.8) is in line with the earlier discussion (*c.f.* Figure 2.7c).

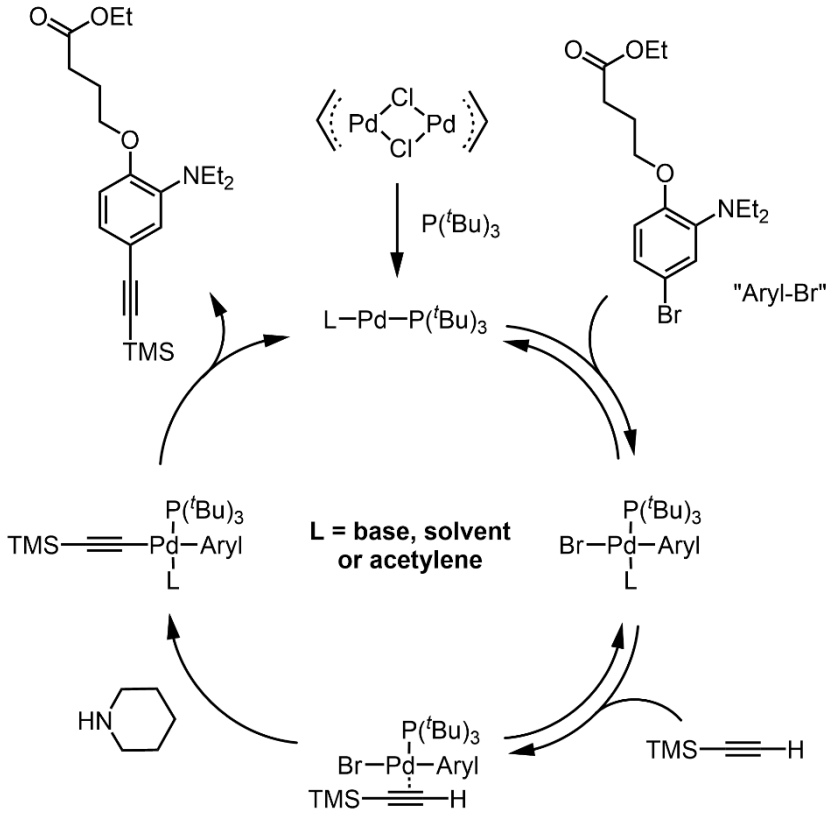

Figure 3.8. The mechanism proposed by Soheili[8] for the Sonogashira cross coupling reaction using $Pd_2Cl_2(allyl)_2$, $P(^tBu)_3$, and piperidine.

The proceeding synthesis to afford the extended antennae closely followed that of the antenna **6**. Removal of the TMS protecting group was achieved using an excess of $Et_3N.3HF$ (15 eq.) in anhydrous THF. The nucleophilic cleavage occurred in almost quantitative yield (97%), giving the free alkynes **17a-b**, following a simple aqueous wash work-up. These alkyne substrates, **17a-b**, were then coupled to the previously prepared 4-bromopyridine derivative, **5**, constructing the extended antennae through Sonogashira cross coupling reactions. Given the earlier success of the cross coupling reaction with the palladium dimer $Pd_2Cl_2(allyl)_2$, these reagents and reaction conditions

were implemented again here. In these instances, no issues were encountered with reactivity and the extended chromophores as the alcohols, **18a-b**, were successfully isolated in moderate yield (40 and 30%, respectively), following purification by RP-HPLC. Immediately prior to their use in the next synthetic step, the alcohols **18a-b** were converted to their reactive mesylate esters, by reaction with methanesulfonic anhydride at room temperature, using DIEA as base. Their rapid conversion was monitored by TLC and LC/MS, and the mesylates **19a-b** were isolated in high yields (90–100%) after one hour, following an aqueous work-up.

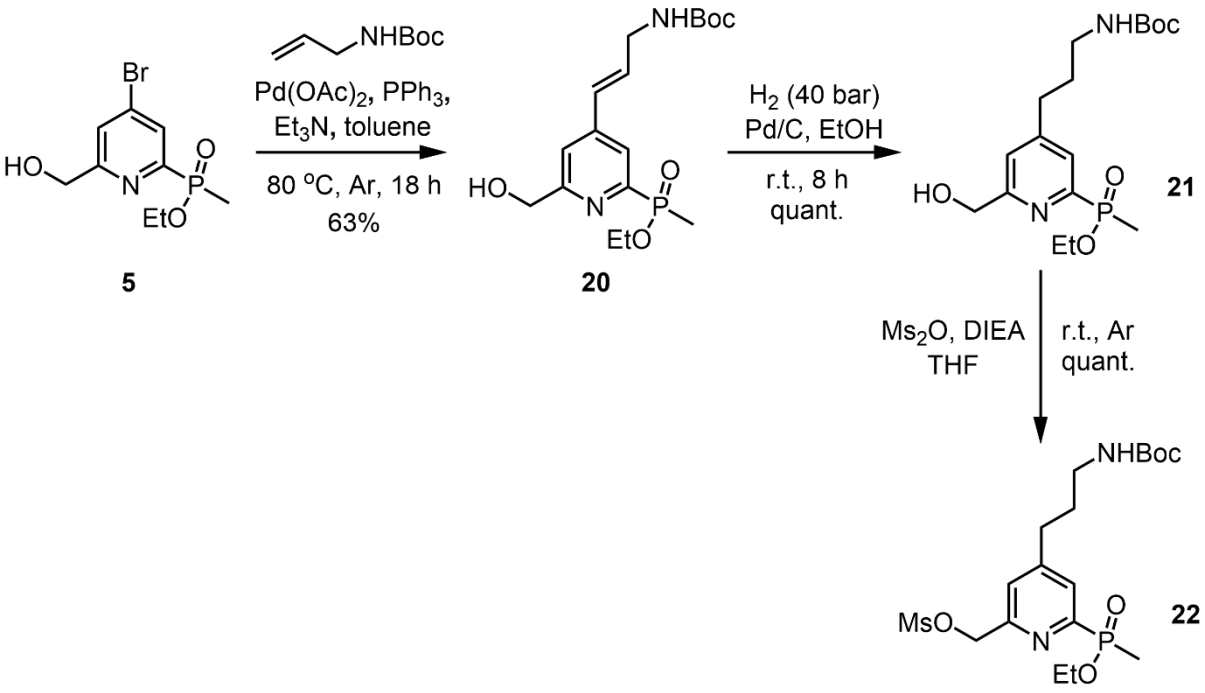

Figure 3.9. Synthesis of the 2,4,6-trisubstituted pyridine bearing a C_3 alkyl chain with a terminal NHBoc group to allow subsequent conjugation.

The alkyl chain bearing a chemical functionality suitable for conjugation (a Boc-protected primary amine in this case) was installed onto the 4-bromopyridine derivative, **5**, in two steps, (Figure 3.9). The successful coupling of *tert*-butyl *N*-allylcarbamate with a bromo-substituted PCTA system in a Heck reaction has been described in a patent.[9] The Heck reaction involves the formation of a single carbon-carbon bond through the coupling of an organohalide and alkene in the presence of a palladium(0) catalyst and base. The conditions described in the patent are somewhat similar to those used in the first report of the Heck reaction, involving the coupling of various aromatic halides with olefinic compounds.[10] A similar approach was

implemented for the Heck reaction between the 4-bromopyridine **5** and butyl *N*-allylcarbamate using palladium(II) acetate, a triphenylphosphine co-ligand and triethylamine. Under these conditions, the desired coupling was achieved in moderate yield (63%) to give the alkene **20** after purification by RP-HPLC. Both ^{1}H and ^{13}C NMR spectroscopic analysis of the product **20**, however, suggested the product was a mixture of the *E*- and *Z*- isomers. The mechanism of the Heck cross coupling reaction is given (Figure 3.10), highlighting how this *E*/*Z* isomer mixture may arise on initial coordination of the carbamate to the catalyst, followed by coupling to the aryl substrate. Due to the occurrence of the isomeric product mixture, it is reasonable to assume that the NHBoc functionality has insufficient steric bulk to induce any significant selectivity that may favour a particular isomer. No attempt was made to isolate the individual *E*- and *Z*- isomers, as it was anticipated that the subsequent hydrogenation of the alkene would yield the same product.

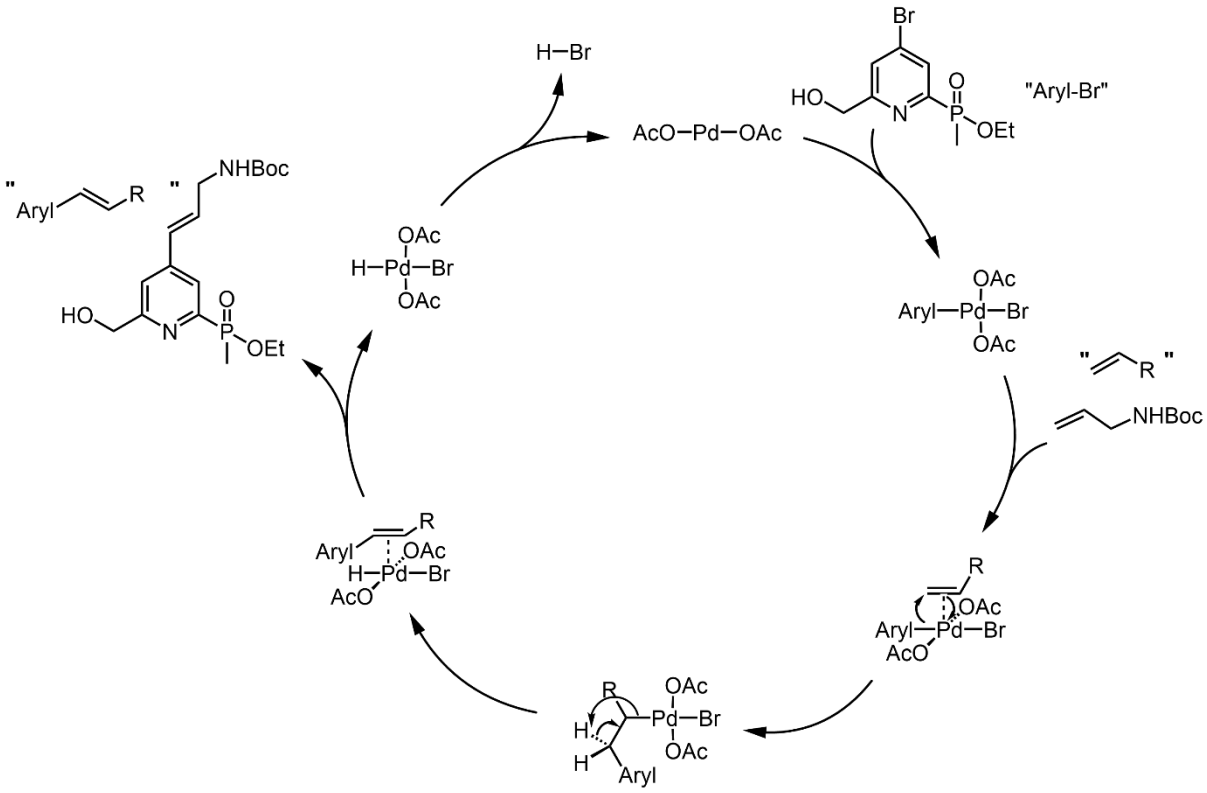

Figure 3.10. Proposed catalytic cycle for the Heck reaction.

Hydrogenolysis of the alkene **20** was performed using a Parr hydrogenator set-up under a medium pressure hydrogen atmosphere (40 bar) over palladium on carbon. The hydrogenolysis reaction was monitored over several hours by LC/MS and occurred in quantitative yield. It is noted that the phosphinate ester and the alcohol

were unaffected under these reduction conditions. Analysis of the product by ^{1}H and ^{31}P NMR spectroscopy indicated the existence of one species, consistent with the hypothesis of an *E*/*Z* mixture present in the previous step.

With the various arms prepared, the macrocyclic ligands were synthesised through successive alkylation and deprotection reactions with mono-Boc-TACN, (Figure 3.11). Alkylation of mono-Boc-TACN with the extended mesylates **19a-b** in anhydrous acetonitrile, in the presence of potassium carbonate under argon, was achieved in moderate to high yields (59–73%) to give the dialkylated macrocycles **23a-b**, following purification by RP-HPLC. As with the Boc-protected difunctionalised compound **10**, the assignment of resonances by NMR spectroscopic analysis proved challenging, owing to the non-equivalence of chromophore environments on the measurement timescale, induced by the restricted rotation about the carbamate NCO bond. Cleavage of the Boc protecting group was performed in a 10% TFA/DCM (by vol.) solution with complete removal of the protecting group observed by LC/MS after up to 1 hour stirring at room temperature. The deprotected macrocycles **24a-b** were obtained in quantitative yield as their trifluoroacetate salts.

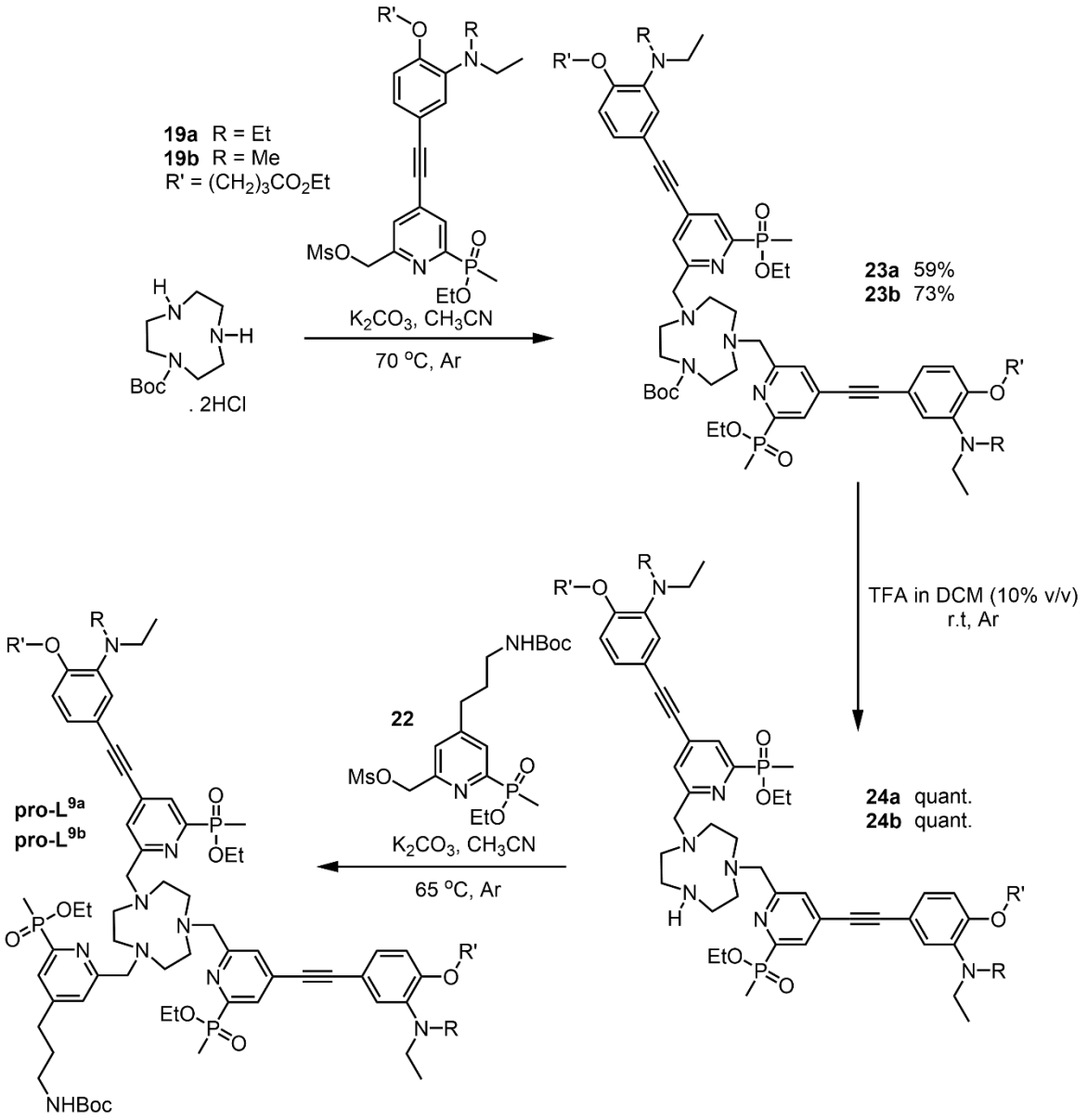

Figure 3.11. Synthesis of the ligands **pro-L^{9a-b}** by successive alkylation and deprotection steps.

A final alkylation reaction involving the pyridine mesylate **22** afforded the trisubstituted ligands **pro-L^{9a-b}**, as confirmed by LC/MS and NMR spectroscopy. Following removal of the inorganic salts, analysis of the crude products suggested a preponderance of the desired compounds **pro-L^{9a-b}** in each case, contaminated with the pyridine alcohol derivative, **21**, arising from hydrolysis of the excess mesylate **22**. Whilst purification of the crude ligand is possible, the loss of ligand in the purification process often occurs. Therefore, the ligand was taken on in this crude form to the subsequent hydrolysis and complexation steps.

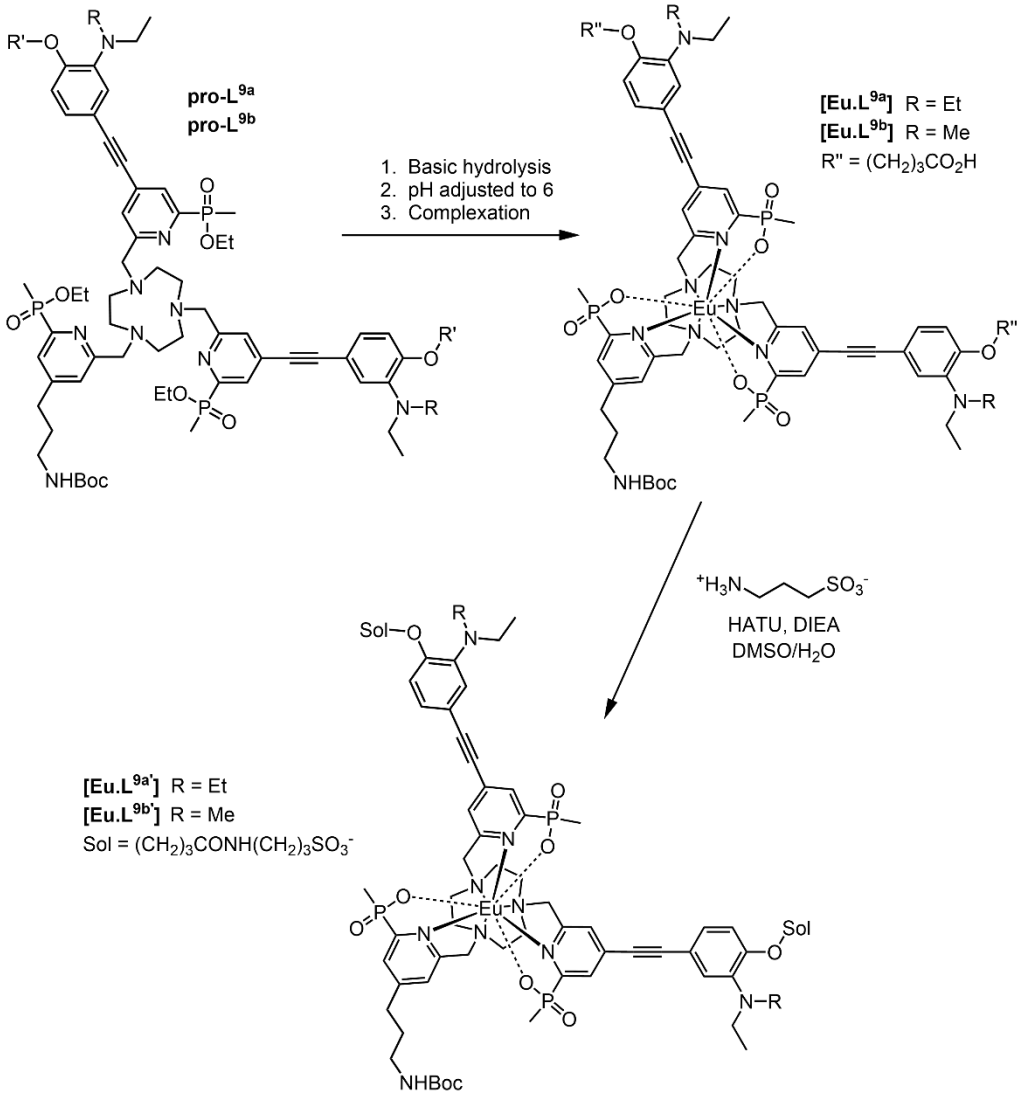

Figure 3.12. Synthesis of the europium(III) complexes **[Eu.L$^{9\ a\text{-}b}$]**.

The paramagnetic Eu(III) complexes were analysed using ^{1}H NMR spectroscopy measuring bulk magnetic susceptibility (BMS) shifts, and gave values for the concentration of Eu(III) present that were in agreement with ≥90% complex purity.

Figure 3.13. ESI LC/MS UV total absorption traces of the crude (a) ligand **pro-L^{9a}**, (b) hydrolysed ligand **L^{9a}**, and (c) complex **[Eu.L^{9a}]** (indicated by blue circles).

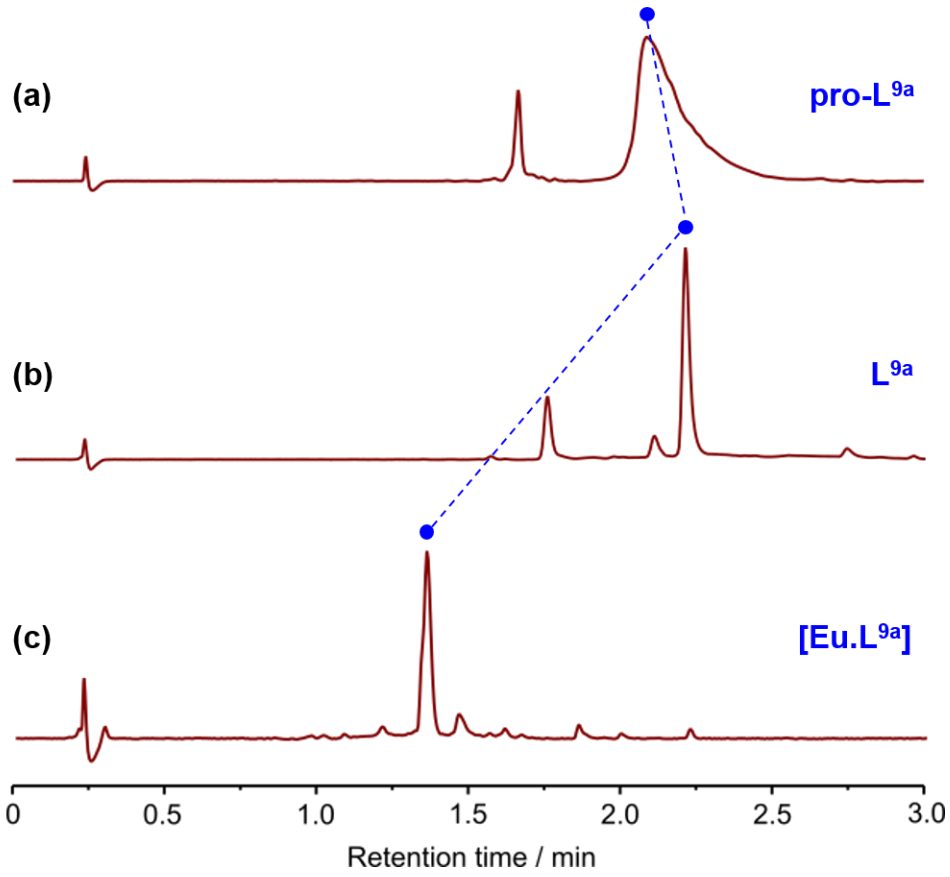

The final step to introduce the sulfonic acid moieties involved the coupling of the peripheral carboxylic acid groups with homotaurine to form the amide derivative. In reactions of this type, a coupling reagent that facilitates the reaction must be selected. The number of coupling reagents described in the literature for this purpose is vast; each one having its own advantages and downfalls.[11] The coupling reagent 1-[bis(dimethylamino)methylene]-1*H*-1,2,3-triazolo[4,5-*b*]pyridinium 3-oxid hexafluorophosphate (HATU) has been utilised successfully in related work for such couplings,[5,12] as well as more widely,[11,13-14] and therefore was selected.

The mechanism for this coupling with the HATU reagent is well known, (Figure 3.14). Following the deprotonation of the carboxylic acid with base, reaction with HATU

results in the activation of the conjugate base and formation of an ‘activated ester’. Nucleophilic attack by the amine onto this substrate is rapid to yield the coupled amide.

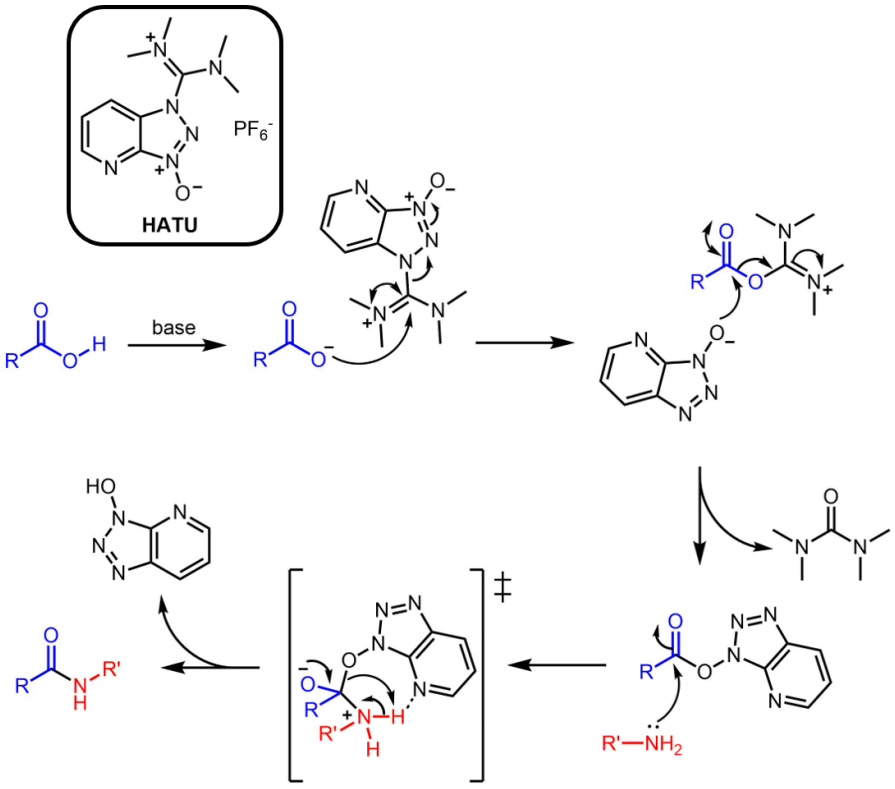

Figure 3.14. Mechanism of amide coupling between a carboxylic acid (*blue*) and an amine *(red)* using HATU. For the specific couplings to yield **[Eu.L^{9a-b}]**, R represents the rest of the europium(III) complex and R’ = $(CH_2)_3SO_3^-$.

On inspection of the coupling mechanism, it is reasonable to consider whether water can behave as a competing nucleophile to the amine and needs to be excluded. Previous work within the group has used DMSO as a solvent. However, attempts to couple the complexes **[Eu.L^{9a-b}]** with homotaurine in neat DMSO at room temperature were only partially successful, affording a mixture of coupled products. In this case, the uncoupled, mono-coupled, and the target complexes were easily isolatable by RP-HPLC. It is noted that a methanol/water eluent gradient allowed for good product separation, but the mono-coupled and target complexes co-eluted when using an analogous acetonitrile/water eluent with the same solvent gradient.

The incomplete coupling was attributed to the insolubility of the homotaurine reagent in neat DMSO, and the reaction was therefore repeated in various DMSO/water proportions to determine the minimum amount of water necessary to solubilise homotaurine. The coupling of homotaurine to complexes **[Eu.L^{9a-b}]** was successfully achieved after stirring overnight at room temperature to afford **[Eu.L^{9a-b}]** in 89 and

38% yield, respectively, using 10% water in DMSO. The formation of the desired products was easily monitored by LC/MS, with no starting material or mono-coupled complex remaining.

With the complexes **[Eu.L^{9a-b}]** prepared, the photophysical properties of these europium(III) complexes were studied. This work is described in chapter 4.

3.4. Design of N-Substituted Sulfonated Complexes

Following the synthesis and photophysical analysis of **[Eu.L^{9a-b}]** (this chapter and chapter four, respectively), a second set of hydrophilic pH responsive complexes, **[Eu.L$^{10a-b,11}$]**, was proposed where the solubilising sulfonate moiety is grafted directly onto the amine, (Figure 3.15).

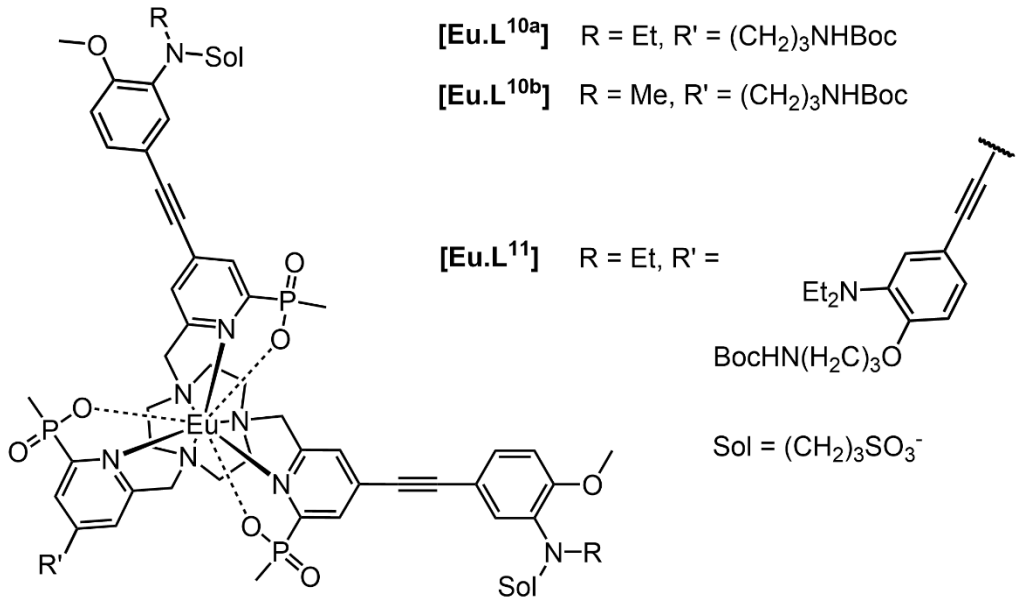

Figure 3.15. Structures of proposed complexes **[Eu.L$^{10a-b,11}$]**.

Movement of the sulfonate moiety from the periphery of the complex into close proximity to the amine is expected to have an impact on the pK_a value. In this case, protonation of the amine nitrogen will give rise to a zwitterion which was expected, on the basis of coulombic attraction, to stabilise protonation and increase the pK_a.

A final triantenna complex, **[Eu.L^{11}]**, was proposed, where a linkage site at the periphery removes the need to sacrifice an extended antenna (*c.f.* **[Eu.L^{9a-b}]**).[a] This complex was anticipated to possess an increased absorption coefficient, and therefore brightness value. The similarity of the structures of the complexes

[Eu.L^{10a,11}] allowed the europium(III) complex **[Eu.L^{11}]** to be prepared from a common intermediate.

3.5. Synthesis of [Eu.L$^{10a-b,11}$]

Firstly, it was necessary to functionalise the amine moiety of the top component of the antenna. It was reasoned that it was advantageous to introduce the propylsulfonate moiety at the outset due to the slow nature of the second alkylation step for conventional S_N2 alkylation, (Figure 3.16). This reaction rate behaviour would likely present issues if installing the propylsulfonate moiety second. Additionally, this order of alkylation would afford a common intermediate common for both synthetic pathways, reducing the synthetic effort required (*c.f.* 3 and 4 compounds). The decision was taken to protect the propylsulfonate arm with the lipophilic CH_2CF_3 group prior to alkylation at the amine nitrogen. The presence of the CH_2CF_3 group was expected to improve the solubility of the reagent in organic solvents for the subsequent alkylation reaction. Additionally, the lower cost of the starting reactant (3-bromopropanesulfonic acid sodium salt *vs.* 5-iodo-*o*-anisidine) and simpler work-up allowed the arm to be prepared easily on a multi-gram scale.

Conversely, if this protection reaction was performed after the initial alkylation, purification of the product and removal of any di-alkylated product would be complicated by the high and low solubilities of the substrate in aqueous and organic media, respectively. Whilst purification by HPLC is a possibility, purification on a large scale can be a time-consuming process for such amphiphilic compounds.

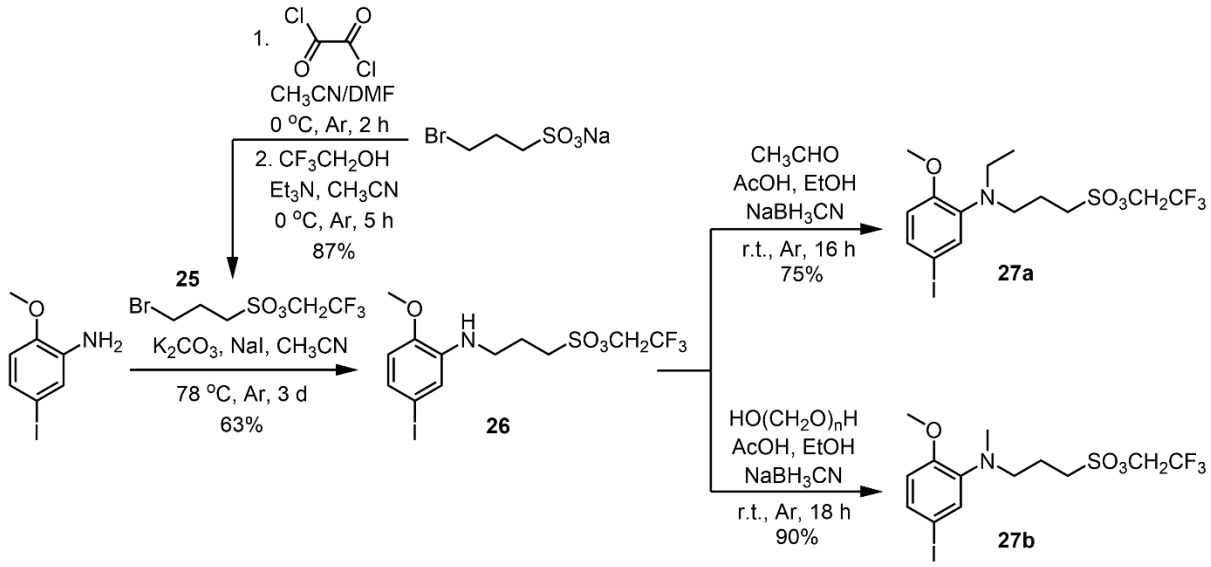

Figure 3.16. Functionalisation of the aniline N by successive alkylation reactions.

Protection of 3-bromopropanesulfonic acid was achieved in two steps. Firstly, the arm as the sodium salt was reacted with oxalyl chloride at 0 ºC in acetonitrile under argon in the presence of catalytic DMF, generating the sulfonyl chloride species. This reactive species was immediately reacted with 2,2,2-trifluoroethanol at 0 ºC with triethylamine as a base, affording the desired sulfonate ester, **25**. Maintenance of anhydrous reaction conditions and avoidance of heating (<20 ºC) when handling and reacting the sulfonyl chloride were necessary to eliminate undesired by-product formation, and allowed the pure arm **25** to be obtained efficiently (87%) after a simple aqueous work-up. In the subsequent alkylation reaction, only the monoalkylated product was desired. With the expectation that alkylation of 5-iodo-*o*-anisidine with **25** would be slow in rate relative to analogous reactions, four equivalents of the arm **25** were used, as well as the addition of sodium iodide in an effort to promote faster C-N bond formation following bromo/iodo halide exchange. Despite these measures, installation of **25** onto 5-iodo-*o*-anisidine with potassium carbonate in acetonitrile with significant heating (78 ºC) was slow with a reaction time of the order of days. This slow alkylation rate is likely due in some way to the steric bulk of the arm **25** and/or the electronic impact of the $SO_3CH_2CF_3$ moiety on the polarity of the C-Br bond. Nevertheless, the monoalkylated product **26** was isolated in reasonable yield (63%) following purification by silica column chromatography. The functionalisation of the amine nitrogen was completed using reductive amination reactions with either acetalaldehyde or paraformaldehyde, given their earlier success, to afford the *N*-ethyl-

(**27a**, 75%) and methyl-substituted (**27b**, 90%) compounds, respectively. Installation of an ethyl group by reductive amination using acetaldehyde was efficient, and could have been an alternative synthetic route when making the *N,N*-diethyl amines described earlier.

With the top components prepared, the antennae were constructed in a stepwise fashion, (Figure 3.17).

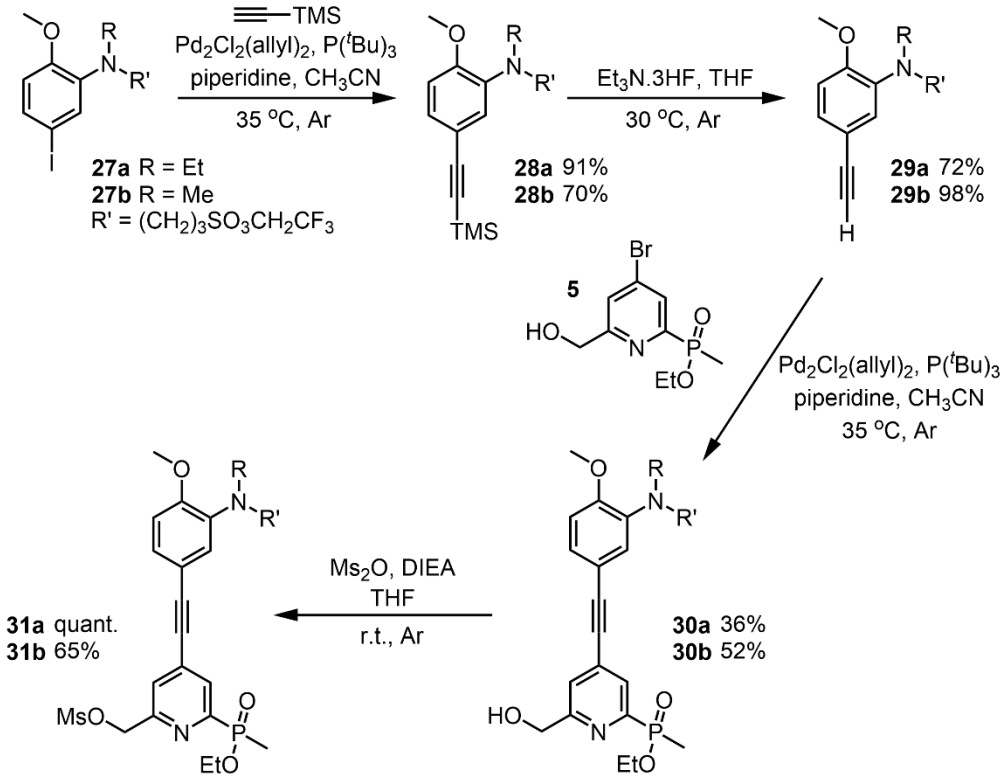

Figure 3.17. Synthesis of extended antennae with N-substituted sulfonate groups protected with a CH_2CF_3 group.

Cross coupling of the iodo-bearing aromatics **27a-b** with a TMS-protected alkynyl functionality was achieved using a Sonogashira reaction with the dimer catalyst $Pd_2Cl_2(allyl)_2$, to give the coupled products **28a-b** in high yield (91 and 70%, respectively). Following cleavage of the TMS protecting group with fluoride, a second Sonogashira cross coupling reaction with the aryl bromide **5** gave the antennae **30a-b** in low to moderate yields (36 and 52%, respectively). Immediately prior to the following alkylation step, the alcohols **30a-b** were converted to the reactive mesylate esters, **31a-b**.

Thorough analysis of each intermediate by NMR spectroscopy was performed. A full assignment of each resonance was achieved using a variety of two-dimensional NMR spectroscopy experiments including COSY, HSQC, HMBC, NOESY. These particular intermediates, *e.g.* **30a** (Figure 3.18), contain four different nuclei with I = 1/2 that are readily observed by NMR spectroscopy. The resulting NMR spectra feature varied J-coupled multiplets, arising from spin-spin coupling between these different nuclei. In many cases, the J-coupling pattern can serve as a fingerprint, aiding the assignment of resonances. Conversely, coupling of a nucleus to several other nuclei can overcomplicate interpretation and analysis, and in these cases the decoupling of spin active nuclei becomes a useful tool.

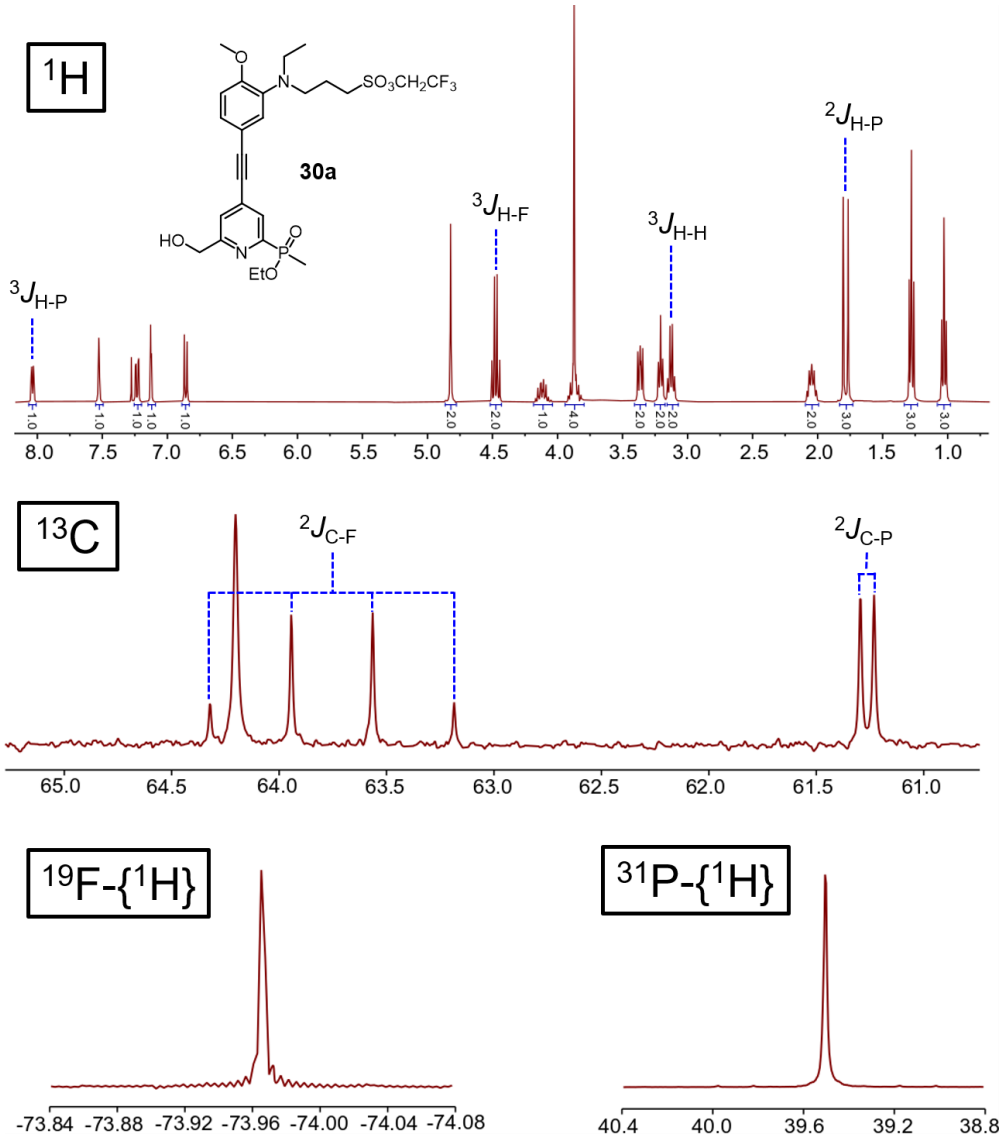

Figure 3.18. Excerpts from NMR spectra (^{1}H, ^{13}C, ^{19}F-{^{1}H} and ^{31}P-{^{1}H}) of the alcohol **30a**, highlighting selected J-coupling between NMR active nuclei.

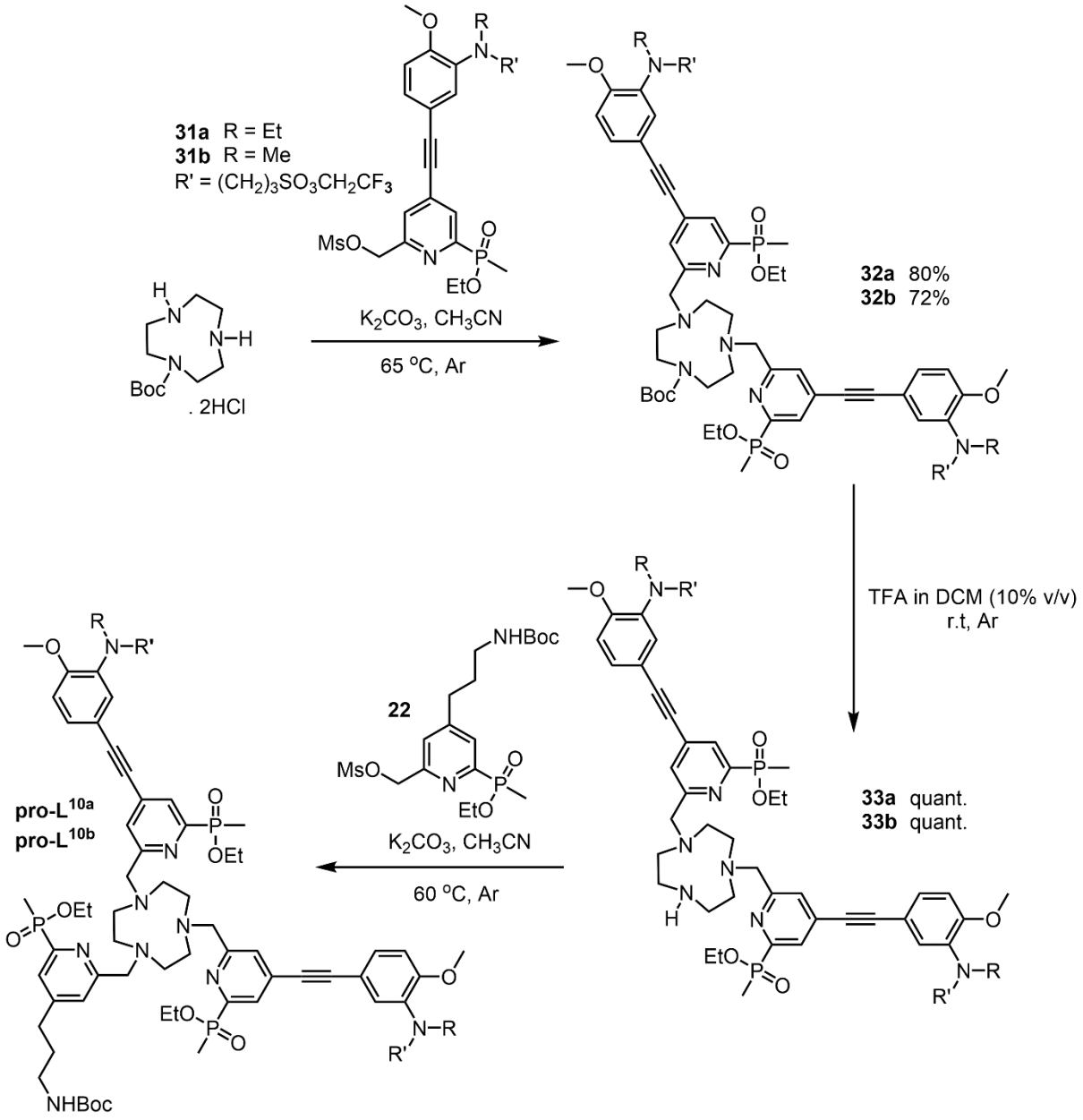

Figure 3.19. Synthesis of the pro-ligands, **pro-L^{10a-b}**, by stepwise alkylation reactions.

Grafting of the antennae onto the TACN macrocycle was performed using a bimolecular S_N2 alkylation reaction between the mesylates, **31a-b,** and mono-Boc protected TACN, (Figure 3.19). The dialkylated macrocycles **32a-b** were isolated by RP-HPLC in good yield, (80 and 72%, respectively). Removal of the Boc protecting group was efficient for each substrate using TFA/DCM before reaction of the secondary amines, **33a-b**, with the mesylate **22** to introduce the final arm onto the TACN backbone and give the ligands **pro-L^{10a-b}**. Analysis of the crude product by LC/MS and ^{1}H NMR spectroscopy revealed the major components to be the desired ligands, **pro-L^{10a-b}**, which were hydrolysed under basic conditions and complexed with

europium(III) at pH 6, (Figure 3.20). The hydrolysis step involved the additional cleavage of the 2,2,2-trifluoroethyl protecting groups present on the sulfonate groups. In an attempt to monitor this cleavage by NMR spectroscopy, the hydrolysis was trialled using CD_3OD/NaOD in D_2O. However, deuterium exchange was observed as a result of the prolonged heating at high temperature required to liberate the sulfonate groups, prohibiting characterisation by HRMS. Efforts to exchange the deuterium with hydrogen were unsuccessful. Isolation of the pure complexes **[Eu.L^{10a-b}]** was made possible by RP-HPLC in 27 and 11% overall yield.

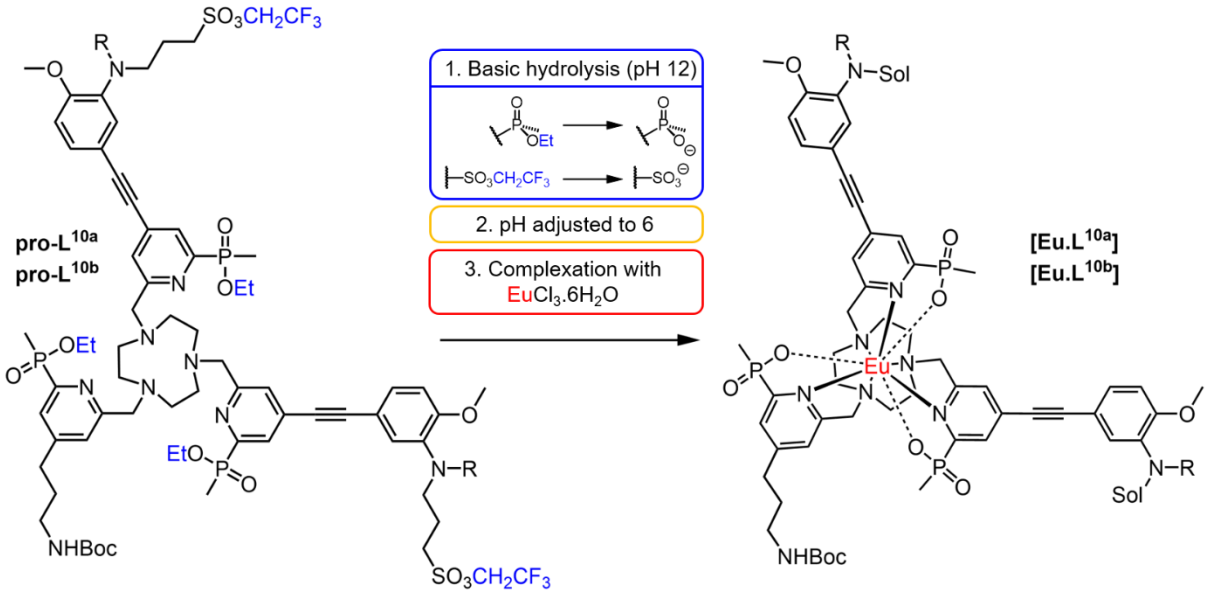

Figure 3.20 Hydrolysis of the phosphinate esters and CH_2CF_3 protecting groups of **pro-L^{10a-b}**, followed by complexation with $EuCl_3.6H_2O$ gave **[Eu.L^{10a-b}]** (R = Et, Me).

The final target complex **[Eu.L^{11}]** features three extended antennae, one of which bears a Boc protected amine suitable for deprotection and conjugation, and differs from the complex **[Eu.L^{10a}]** in the identity of the third N-substituent of the macrocycle. The extended antenna featuring a moiety appropriate for conjugation was prepared in three steps (Figure 3.21) from the TMS-protected upper component, **34**, provided by the company Cisbio. The TMS protecting group was cleaved by reaction of **34** with $Et_3N.3HF$ to give the free alkyne **35** in moderate yield (48%) following an aqueous work-up. This alkyne was coupled to the 4-bromo-pyridine substrate **5** using the catalyst $Pd_2Cl_2(allyl)_2$ affording the desired antenna, **36**, as the alcohol (24% yield). The yields observed for these deprotection and coupling steps were notably lower than those obtained for analogous reactions with substrates of differing functionality.

Quantitative conversion of the alcohol **36** to the mesylate **37** immediately prior to its use was achieved by reaction with methanesulfonic anhydride in THF, with DIEA as base.

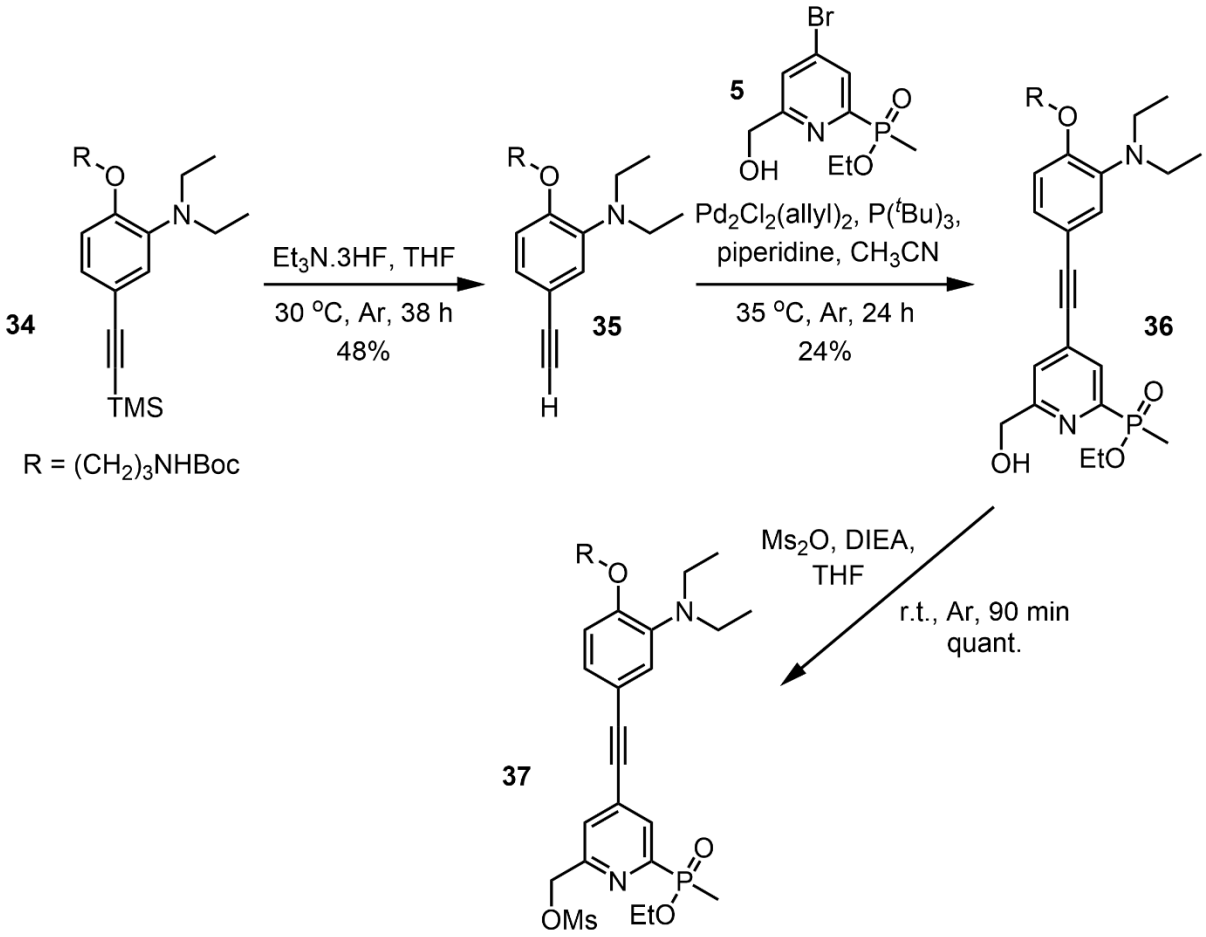

Figure 3.21. Preparation of the extended antenna bearing a protected amine (R = $(CH_2)_3NHBoc$).

With the extended antenna as the mesylate prepared, the pro-ligand **pro-L^{11}** was synthesised by an S_N2 alkylation reaction between the macrocyclic intermediate **33a** and the mesylate **37**, (Figure 3.22). The crude **pro-L^{11}** was subsequently hydrolysed under basic conditions, before complexation with europium(III) following adjustment of pH to 6. The hydrolysis of **pro-L^{11}** was performed in tandem with **pro-L^{10a-b}**, under similar deuterated conditions. Accordingly, similar deuteration issues were encountered, inhibiting characterisation by HRMS. Purification by RP-HPLC yielded the target complex **[Eu.L^{11}]** in 25% overall yield from the dialkylated intermediate **33a**.

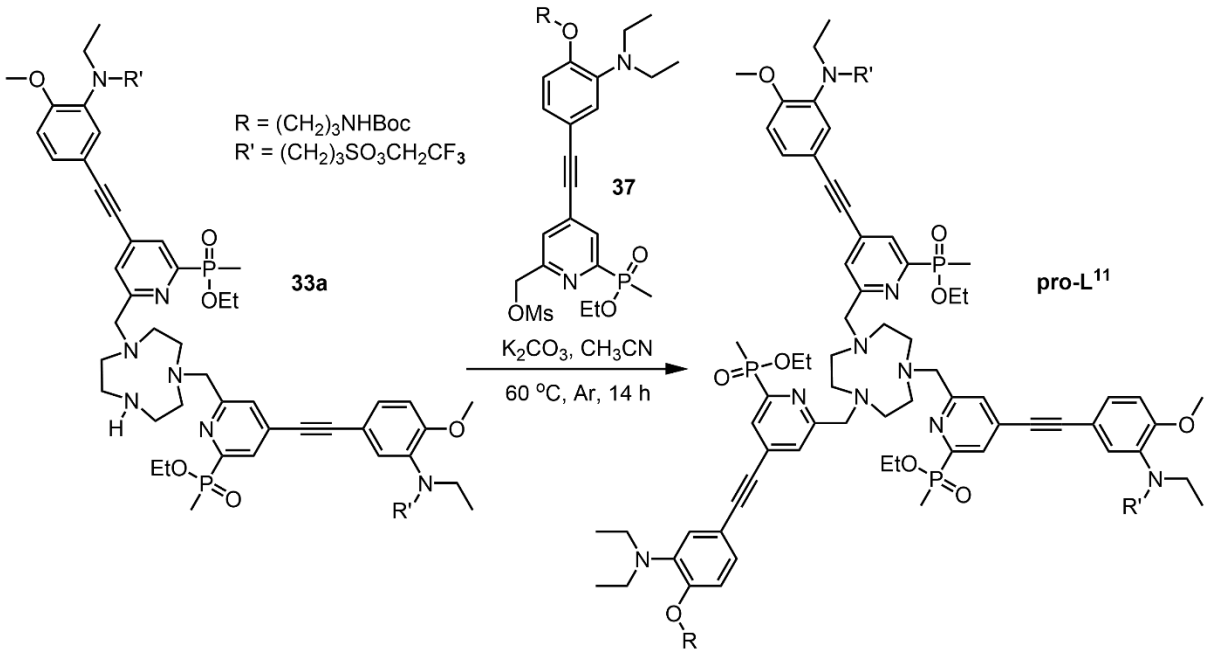

Figure 3.22. Synthesis of the ligand **pro-L^{11}** from the common macrocyclic intermediate **33a** (R = $(CH_2)_3NHBoc$, R' = $(CH_2)_3SO_3CH_2CF_3$).

3.6. Conclusions

Five hydrophilic europium(III) complexes have been designed containing a pH sensitive amino moiety and a Boc-protected primary amine, suitable for bioconjugation to a targeting vector following deprotection. These complexes vary primarily in the functionalisation at the aryl amino group, leading to modulation of its pK_a value. In particular, the location of the aqueous solubilising sulfonate groups (either grafted at the periphery of the complex, or installed as an N-propylsulfonate substituent) allows the complexes to be divided into two sets of structural analogues: **[Eu.L$^{9\ a\text{-}b}$]** and **[Eu.L$^{10a\text{-}b,11}$]**, respectively.

The synthesis of each highly conjugated antenna involved a convergent synthesis, where the top and bottom component were prepared before a copper-free Sonogashira cross-coupling reaction was used to link them. Preparation of the top component of the antenna required the appropriate functionalisation of the pH sensitive aryl amino group in a stepwise manner, exploiting a mixture of S_N2 alkylation and reductive amination reactions. In the synthesis of **[Eu.L$^{10a\text{-}b,11}$]**, the sulfonate moiety was introduced early in the synthetic route, protected as the 2,2,2-trifluoroethyl derivative. The use of a palladium-catalysed Heck reaction followed by hydrogenolysis

afforded a novel single pyridine arm bearing a propyl-Boc-amine group, common to the synthetic route of the dichromophore complexes.

With the various arms synthesised, the ligands were prepared through the mesylation of each arm followed by an alkylation reaction, allowing for stepwise grafting onto a TACN skeleton. The use of a Boc protecting group and timely deprotection using TFA yielded the target ligands, which were subsequently hydrolysed and complexed with europium(III) using well-established methods. A post-complexation amide coupling reaction using homotaurine and the coupling reagent HATU was necessary to install the sulfonate functionality for **[Eu.L^{9}]**.

Following the preparation of these synthetic targets, the photophysical properties and pK_a values of the europium complexes remained to be examined. Further, the viability of these probes in a context where the sensitive response to pH change is a useful information source, *e.g.* in monitoring the internalisation of membrane receptors, needed to be assessed. This work is explored within chapter four.

3.7. References

[1] M. Delbianco, L. Lamarque and D. Parker, *Org. Biomol. Chem*., 2014, **12**, 8061–8071.

[2] J. P. L. Cox, A. S. Craig, I. M. Helps, K. J. Jankowski, D. Parker, M. A. W. Eaton, A. T. Millican, K. Millar, N. R. A. Beeley and B. A. Boyce, *J. Chem. Soc., Perkin Trans. 1*, 1990, 2567–2576.

[3] M. Starck, J. D. Fradgley, S. Di Vita, J. A. Mosely, R. Pal and D. Parker, *Bioconjugate Chem.*, 2020, **31**, 229–240.

[4] K. L. Gempf, S. J. Butler, A. M. Funk and D. Parker, *Chem. Commun*., 2013, **49**, 9104–9106.

[5] S. J. Butler, L. Lamarque, R. Pal and D. Parker, *Chem. Sci*., 2014, **5**, 1750–1756.

[6] M. Starck, R. Pal and D. Parker, *Chem. Eur. J.*, 2016, **22**, 570–580.

[7] J. E. Baldwin, *J. Chem. Soc.*, *Chem. Commun.*, 1976, 734–736.

[8] A. Soheili, J. Albaneze-Walker, J. A. Murry, P. G. Dormer and D. L. Hughes, *Org. Lett.*, **5**, 4191–4194.

[9] M. Port, C. Robic, C. F. Leal and S. Chadel, Nanoemulsion Chelate for MRI, WO2006100305.

[10] R. F. Heck and J. P. Nolley, *J. Org. Chem.*, 1972, **37**, 2320–2322.

[11] E. Valeur and M. Bradley, *Chem. Soc. Rev.*, 2009, **38**, 606–631.

[12] S. J. Butler, M. Delbianco, L. Lamarque, B. K. McMahon, E. R. Neil, R. Pal, D. Parker, J. W. Walton and J. M. Zwier, *Dalton Trans*., 2015, **44**, 4791–4803.

[13] K. L. Wilson, J. Murray, C. Jamieson and A. J. B. Watson, *Org. Biomol. Chem.*, 2018, **16**, 2851–2854.

[14] J. R. Dunetz, J. Magano and G. A. Weisenburger, *Org. Process Res. Dev.*, 2016, **20**, 140–177.

CHAPTER FOUR

Photophysical Evaluation of Europium(III) Complexes and Bioconjugation Studies

Chapter Four: Photophysical Evaluation of Europium Complexes and Bioconjugation Studies

This chapter features the photophysical evaluation and comparative analysis of pH responsive behaviour of the europium(III) complexes described in chapter three. The preparation of the benzyl guanine derivatives **[Eu.L^{12a-b}]** and subsequent bioconjugation of these derivatives using SNAP-tag methodology to allow monitoring of receptor internalisation is also detailed.

4.1. Photophysical Analysis of Probe Candidates

Following the design and synthesis of the five hydrophilic pH responsive europium(III) complexes discussed in chapter three (Figure 4.1), the photophysical properties of these complexes were examined in detail. The complexes are divided into two groups for evaluation, based on the location of the aqueous solubilising sulfonate moiety (**[Eu.L$^{9\ a-b,10}$]** *vs.* **[Eu.L$^{10a-b,11}$]**), before an overall comparison is made.

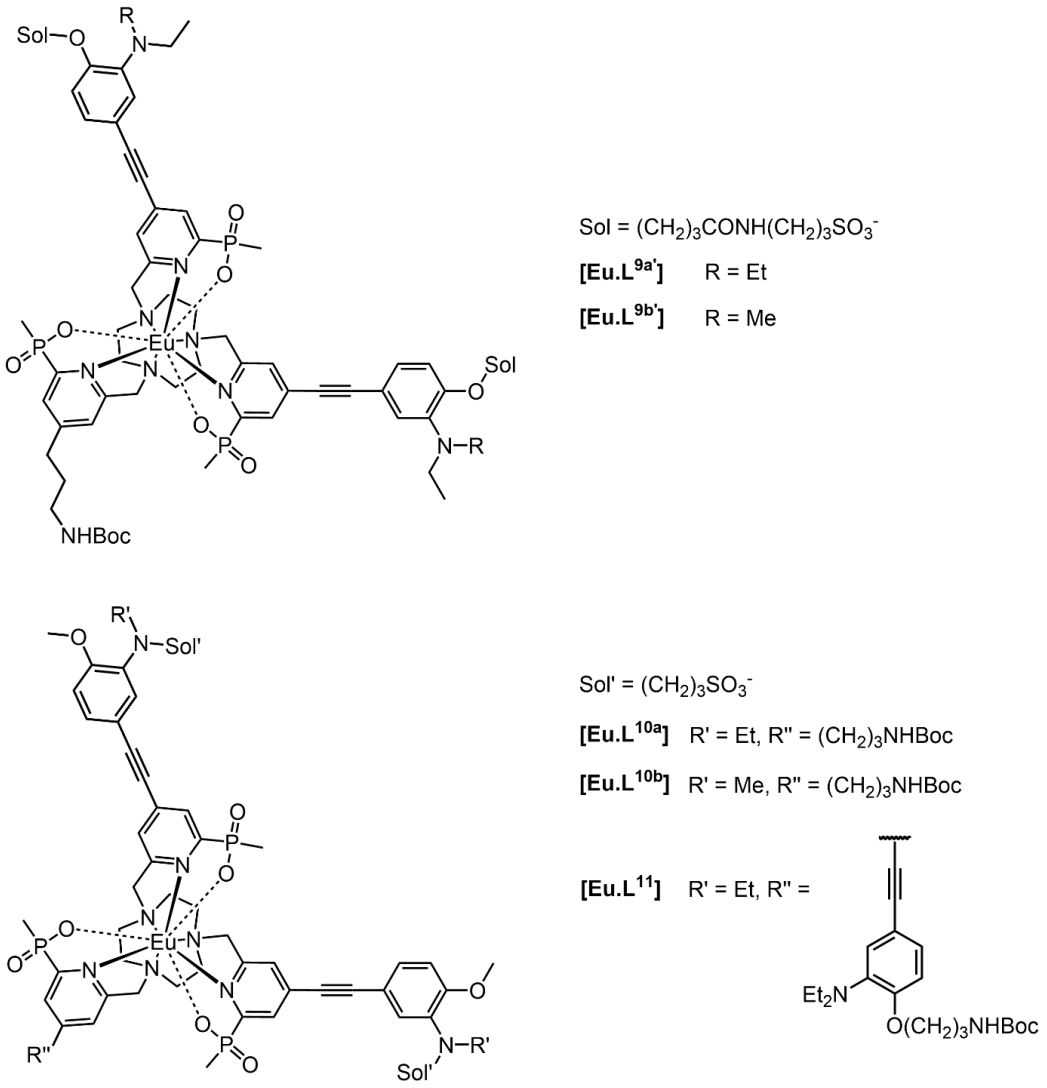

Figure 4.1. Structures of the hydrophilic europium(III) complexes evaluated within this chapter.

4.1.1. Evaluation of ***[Eu.L$^{9a-b'}$]*** *pH Responsive Behaviour*

a) Absorption Behaviour with pH

Absorption *vs*. pH profiles with similar general characteristics were obtained for **[Eu.L$^{9a-b'}$]** in 0.1 M NaCl solution, (Figure 4.2). A band absorbing at longer wavelength is observed at high pH (λ_{max} ~340-344 nm, pH 9) which decreases in intensity on lowering pH, as a shorter wavelength band of increased intensity becomes apparent (λ_{max} ~ 320 nm, pH 4). This general absorbance response to decreasing pH is identical to that observed for **[Eu.L$^{1-3}$]**. Originally, these dichromophore targets were pursued in preference to the more absorbing trichromophore analogue, in part due to the presence of an isosbestic point observed in the absorbance *vs*. pH profile of the

complex **[Eu.L^2]**, which was not seen for **[Eu.L^3]**. An isosbestic point is advantageous in these circumstances as excitation at that wavelength allows equal excitation of the unprotonated and protonated forms of the complex, which exist in equilibrium according to the pH of the system. Here, a single isosbestic point was revealed at 332 nm for the ethyl analogue complex, **[Eu.L^9 a]**, whilst two were found for the methyl complex, **[Eu.L^9 b]**, at 280 and 332 nm.

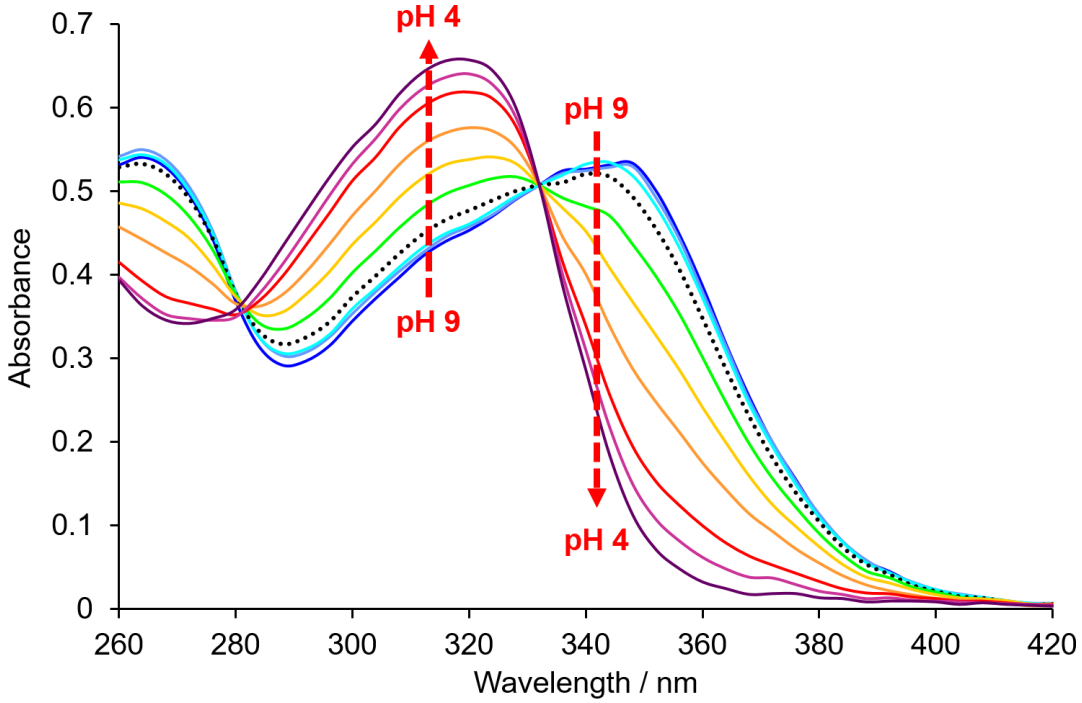

Figure 4.2. Variation of the absorption spectrum of **[Eu.L^9 b]** with pH, revealing isosbestic points at 280 and 332 nm (295 K, $c_{complex}$ = 20 µM, 0.1 M NaCl). The absorbance profile at pH 7 is indicated with black dots.

The longer wavelength band is ascribed to an ICT transition, which may be expected to show a pronounced solvent dependence both in energy and intensity (explored in chapter five), while the shorter wavelength band is a ligand p- p* transition, that does not normally show much variation with solvent.

b) Emission and Excitation Behaviour with pH

A significant increase in the total europium emission intensity was recorded with decreasing pH for both **[Eu.L^9 a,b]** in aqueous 0.1 M NaCl solution, (Figure 4.3). This signal intensity increase corresponds to the suppression of the europium excited state following protonation of the aryl amino nitrogen, as explored and discussed within chapter two.

By examining the emission signal at the pH limits, a 'switch-on' ratio can be calculated. Values of the switch-on ratios for **[Eu.L^{9a-b}]** were determined to be 585 and 1045, respectively, compared to 560 for the parent dichromophore complex **[Eu.L^{2}]**. The value obtained for the methyl analogue is 80% higher than that of the ethyl complex. Such a difference can be tentatively ascribed to the pK_a difference between the two complexes, where the pK_a of the methyl analogue is lower. The position of equilibrium for the methyl complex at pH 8 favours the unprotonated form to a greater extent than for the ethyl complex. Thus, emission from **[Eu.L^{9b}]** is more effectively quenched at this limit, giving rise to a slightly greater switch-on ratio.

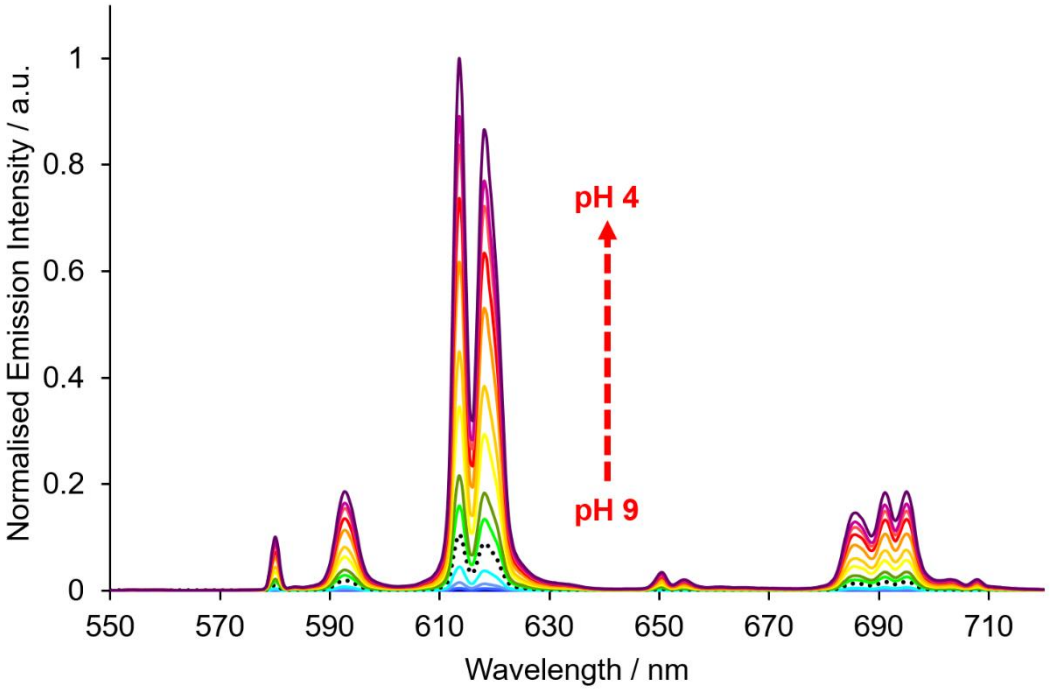

Figure 4.3. Variation of the europium emission spectrum with pH for **[Eu.L^{9a}]** (λ_{exc} 332 nm, 295 K, $c_{complex}$ = 20 μM, 0.1 M NaCl). Emission spectrum at pH 7 is indicated with black dots.

Examination of the excitation spectral profile on varying the pH, as expected, showed a uniform increase in intensity for **[Eu.L^{9a-b}]**. However, these spectra differ in their profile. Whereas the form of the excitation spectrum of the methyl analogue closely resembles that of the parent dichromophore complex, **[Eu.L^{2}]** (Figure 2.18), the excitation spectrum obtained for the ethyl analogue, **[Eu.L^{9a}]**, is broader and less well resolved, and similar to that of the monochromophore complex **[Eu.L^{1}]**, (Figure 2.19).

Previous analysis of the absorption and excitation spectra of the parent complex **[Eu.L^1]** (chapter 2, section 2.3) has suggested that the observed europium emission arises from the protonated form only for these pH responsive complexes. A similar observation is seen here for **[Eu.L^9 a]**, where the excitation spectral form resembles that of the protonated complex, (Figure 4.4).

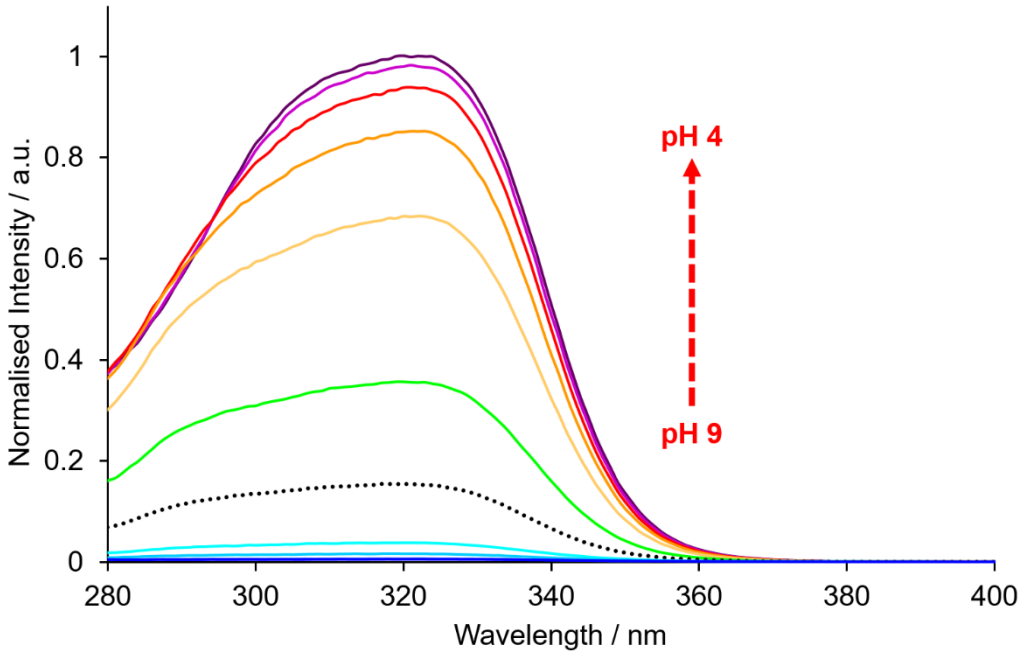

Figure 4.4. Variation in the excitation spectrum with pH for **[Eu.L^9 a]** (λ_{em} 613 nm, 295 K, $c_{complex}$ = 15 μM, 0.1 M NaCl). Excitation spectrum at pH 7 is indicated with black dots.

c) pH Dependent Emission Lifetime Behaviour

Modulation of the europium emission lifetime with pH was examined for each complex in 0.1 M NaCl solution, (Figure 4.5). The resulting sigmoidal lifetime *vs*. pH curves were fitted using non-linear least squares regression analysis, allowing an experimentally determined pK_a to be estimated in each case. Despite the presence of two protonation sites within each complex, the protonation events were treated as being mutually independent and the experimental curve was fitted to a single protonation event (chapter two, section 2.3). Accordingly, values for the pK_a of **[Eu.L^9 a, b]** in 0.1 M NaCl solution were estimated to be 6.18 ± 0.03 and 5.34 ± 0.03, respectively. The higher pK_a value obtained for the ethyl complex is in good agreement with the value obtained for the dichromophore parent **[Eu.L^2]** (6.30 ± 0.05), where the functionalisation of the amine is unchanged. The pK_a of the methyl analogue, however,

is lower in value than the ethyl analogue by ~0.85 of a pK_a unit, as anticipated. In the conjugate base, lone pair conjugation is increasingly favoured as the N-substituent decreases in size, owing to steric interactions between the nitrogen substituents and the *ortho*-groups present on the aryl ring (steric inhibition of resonance). In addition, the conjugate acid is more stabilised by solvation when the N-substituents are small.

Overall, acidification was accompanied by a large increase in the europium emission lifetime of each complex, with percentage increases of 323 and 274% for **[Eu.L$^{9\ a\text{-}b}$]**, respectively. The magnitude of these lifetime variations are notable in that they are greater than those measured for the parent series **[Eu.L$^{1\text{-}3}$]**, for which the corresponding changes were 120, 200 and 240%, respectively.

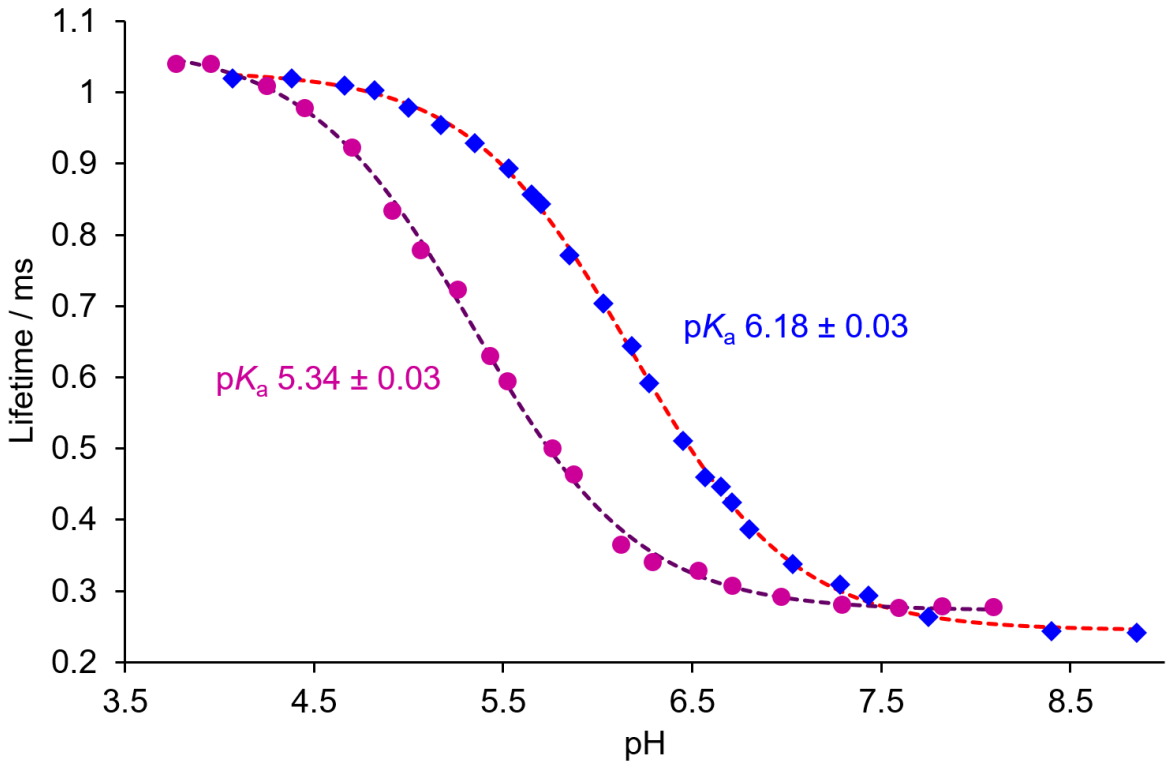

Figure 4.5. Variation in the europium emission lifetime with pH for **[Eu.L$^{9\ a\text{-}b}$]** (blue diamonds and purple circles, respectively, λ_{em} 613 nm, 295 K, $c_{complex}$ = 15 μM, 0.1 M NaCl). The data was fitted using non-linear least squares regression analysis (dashed lines).

The behaviour of the emission lifetime with pH was also examined in an NIH-3T3 cell lysate medium that is used to simulate an intracellular background, (Figure 4.6). Similar general behaviour with decreasing pH was observed in this medium, and a marginal decrease in the pK_a value was found (6.00 ± 0.04). Whilst the lifetime value at the pH limits was also found to decrease (~0.16 and 0.1 ms at pH 4 and 8,

respectively), the overall enhancement in the europium emission lifetime increased to 453%, due to the particularly low lifetime at high pH.

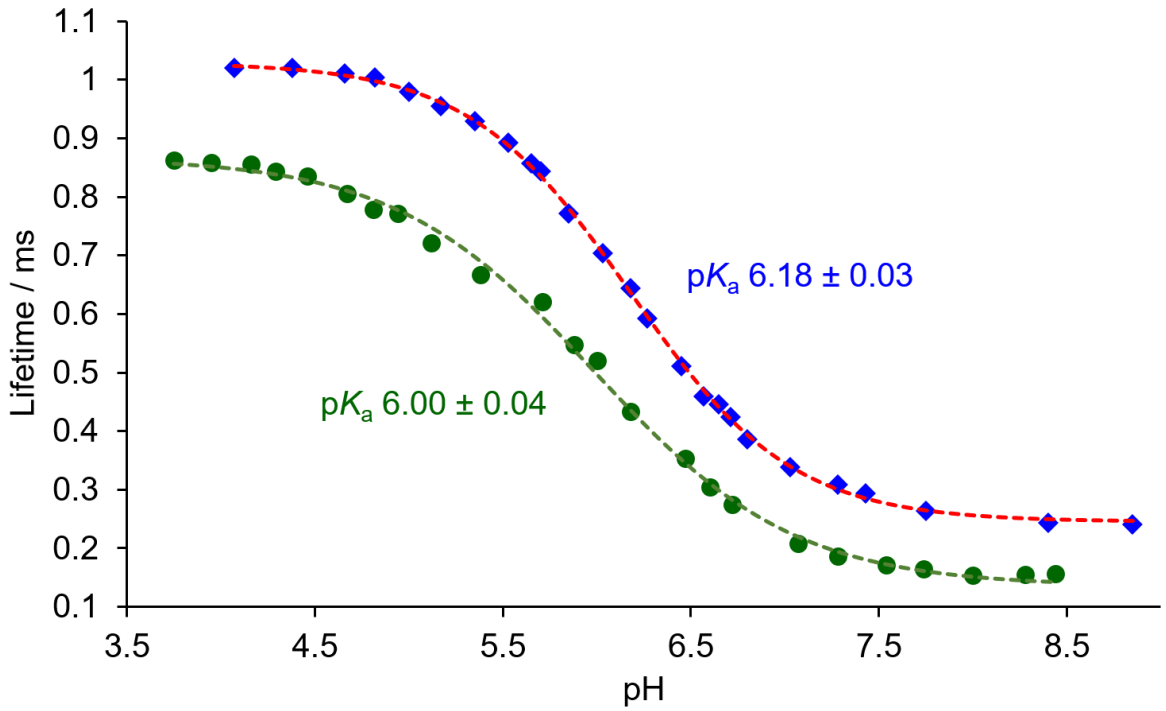

Figure 4.6. Variation in the europium emission lifetime with pH for **[Eu.L^{9} ª]**(/$_{em}$ 613 nm, 295 K, $c_{complex}$ = 15 μM, 0.1 M NaCl and NIH-3T3 cell lysate (blue diamonds and green circles, respectively)). The experimental data was fitted using non-linear least squares regression analysis (red and green dashed lines).

d) Time-gated Measurements

By varying the initial delay time or the time window of signal acquisition itself, the observed switch-on ratio for europium emission can be modulated. This observation arises from the large difference in lifetimes between the unprotonated and protonated complexes that exist in equilibrium at a given pH, where the emissive protonated species is the longer lived species.

Emission from the ethyl analogue complex **[Eu.L^{9} ª]**was examined, alongside the dichromophore complex **[Eu.L^{2}]**, in a series of time-gated measurements within aqueous buffer solutions, where the relative switch-on of emission (I_{rel}) was recorded between the limits using different time windows, (Table 4.1). The largest enhancement of the switch-on ratio was achieved using a delay time of 1.5 ms, acquiring signal for one millisecond to give I_{rel} values of 527 and 465 for **[Eu.L^{2}]** and **[Eu.L^{9} ª]**,respectively,

between the pH limits 4 and 8. As a general trend, the switch-on factor increased as the delay time was increased, at the expense of progressively diminishing signal strength. This increase in delay time is accompanied by a steady diminution in the apparent pK_a value. It is noted that the switch-on factors for **[Eu.L^2]** and **[Eu.L^9]** are comparable in magnitude within the selected time windows. These I_{rel} values are lower than those obtained for **[Eu.L^3]** in an analogous experiment, however, (Table 2.3).

Table 4.1. Ratios of emission intensities (I_{rel} = 'switch-on' factors) for **[Eu.L^2]** / **[Eu.L^9]** for differing time gate periods, showing the effect on the apparent pK_a values (295 K, $c_{complex}$ = 20 µM, 0.1 M NaCl; buffers, NH_4OAc (0.1 M, pH 4), NH_4HCO_3 (0.1 M, pH 8)).

	Time window		
	60 – 460 µs	1000 – 2000 µs	1500 – 2500 µs
I_{rel} : pH 4 / pH 8	34 / 32	266 / 227	527 / 465
Apparent pK_a[a]	6.21(04) / 6.57(05)	5.96(05) / 6.26(03)	5.86(04) / 6.16(03)

[a] pK_a values given are the mean of three replicates, at 295 K. Experimental errors are given in parentheses.

These time-gated experiments were also repeated for **[Eu.L^9]** in the NIH-3T3 cell lysate medium, (Figure 4.7). Within this medium, switch-on factors of 34, 311, and 651 were determined for the 60 – 460, 1000 – 2000, and 1500 – 2500 µs time windows, respectively. The I_{rel} values for the 1000 – 2000 and 1500 – 2500 µs time windows were enhanced relative to aqueous 0.1 M NaCl. This observation can be attributed to the reduced signal intensity at the higher pH limit when using these prolonged delay times. Inspection of the slopes of the 1000 – 2000 and 1500 – 2500 µs curves (Figure 4.7, red and green curves) provides some support for this rationale with the gradient being less steep within the cell lysate medium.

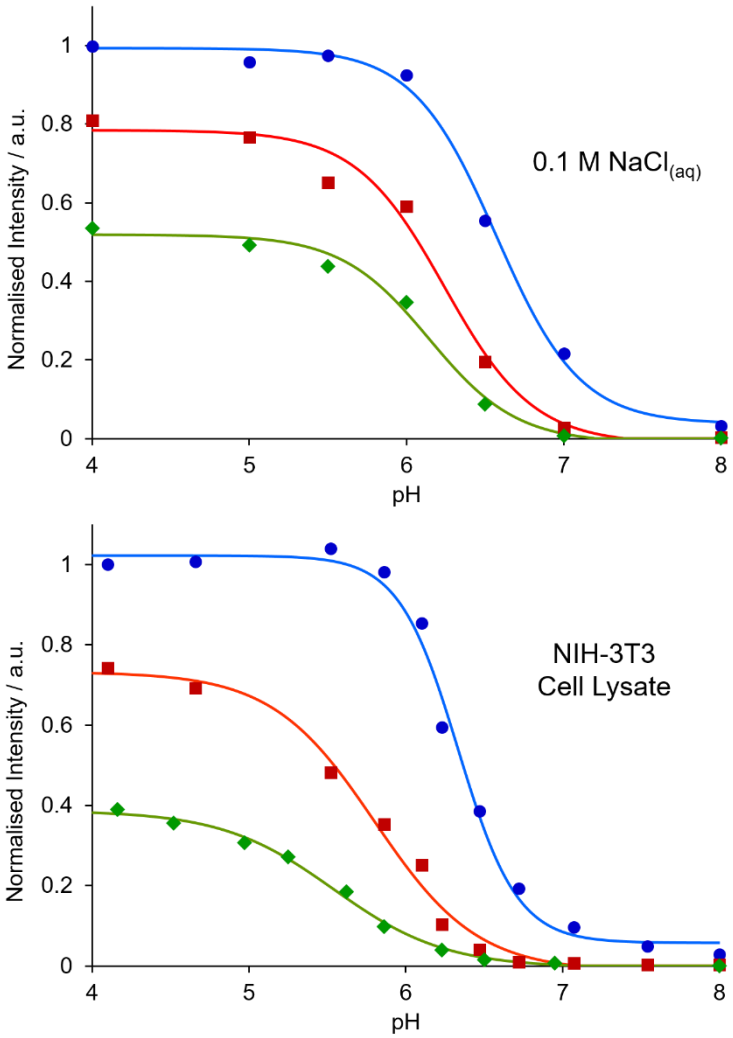

Figure 4.7. Relative emission intensity of **[Eu.L^{9} ^{a}]** (λ_{em} 613 nm) as a function of pH for different time periods of signal acquisition (*blue* = 60 – 460 µs, *red* = 1000 – 2000 µs, *green* = 1500 – 2500 µs). Data were normalised to a 60 – 460 µs time window at pH 4. Measurements were made in aqueous solutions of aqueous solutions of NH_4OAc (pH 4 and 5), MES (pH 5.5, 6, 6.5), HEPES (pH 7) and NH_4HCO_3 (pH 8) buffers ($c_{complex}$ = 20 µM, 0.1 M buffer in 0.1 M NaCl).

*4.1.2. Evaluation of **[Eu.L$^{10a\text{-}b,11}$]** pH Responsive Behaviour*

a) Absorption Behaviour with pH

The general absorption *vs*. pH behaviour observed for the complexes **[Eu.L$^{10a\text{-}b}$]** is very similar to the previously examined dichromophore complexes **[Eu.L^{2}**, **$^{9ba\hat{o}\hat{o}}$]**. on protonation, a hypsochromic shift of the main absorbance band was observed with an increase in intensity. These variations in absorbance with pH were characterised by the occurrence of isosbestic points at 332 nm, and 280 and 336 nm for **[Eu.L$^{10a\text{-}b}$]**,

respectively. Here, the ethyl functionalised analogues in both sets of complexes differ from their methyl analogues in displaying only a single isosbestic point.

Interestingly, examination of the absorption *vs*. pH behaviour for the trichromophore complex **[Eu.L^{11}]** revealed two isosbestic points at 280 and 332 nm (Figure 4.8), in stark contrast to the parent trichromophore complex **[Eu.L^{3}]** for which no isosbestic points were observed. Originally, the dichromophore system was selected for functionalisation in part due to the lack of an observed isosbestic point for **[Eu.L^{3}]**. Thus, this observation suggests that these trichromophore systems could be more appropriate for selection than first hypothesised. Whilst the general absorbance behaviour with pH profile (hypsochromic shift, intensity increase) was mirrored by **[Eu.L^{11}]**, the relative increase in intensity on acidification was somewhat lower, relative to the dichromophore complexes (*c.f.* Figures 4.2 and 4.8).

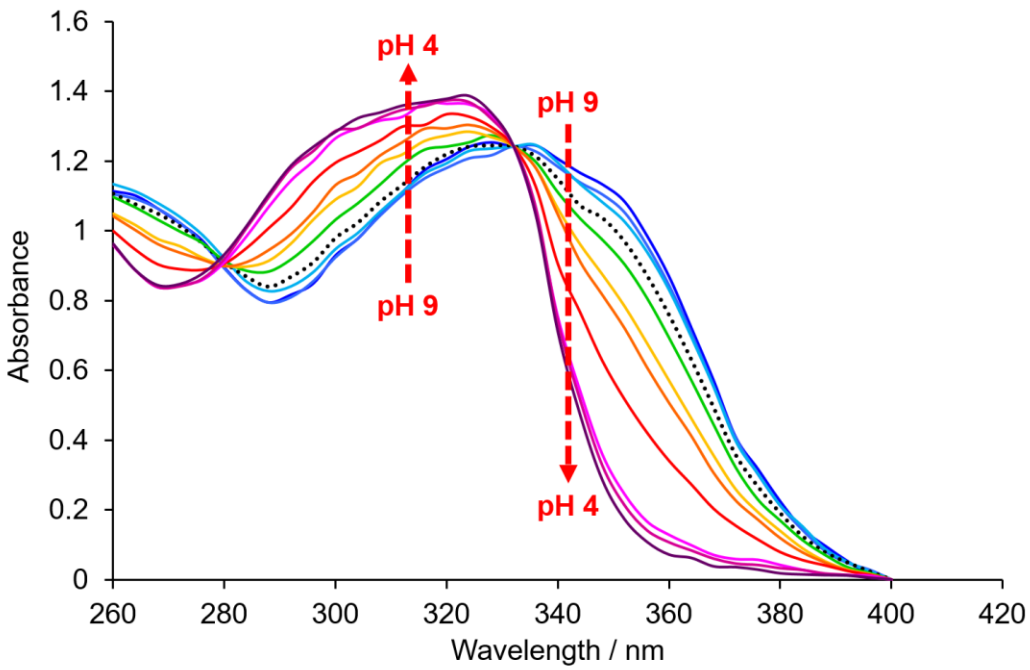

Figure 4.8. Variation of the absorption spectrum of **[Eu.L^{11}]** with pH, revealing isosbestic points at 280 and 332 nm (295 K, 0.1 M NaCl). The absorbance profile at pH 7 is indicated with black dots.

b) Emission and Excitation Behaviour with pH

In the case of total emission, the spectral form of **[Eu.L$^{10a\text{-}b,11}$]** was identical to the first set of complexes. This lack of change is predictable given the structural differences between the complexes occur away from the immediate coordination environment of

the europium(III) ion. A large increase in europium emission intensity on acidification was observed, with switch-on ratios of 925, 1040 and 1360 for **[Eu.L$^{10a\text{-}b,11}$]**, respectively. It is noted that the ratio for the methyl analogue, **[Eu.L^{10b}]**, is calculated between the pH limits 7 and 3, owing to the lower inherent pK_a, whereas the values for **[Eu.L^{10a,11}]** are calculated between pH 8 and 4.

Each complex displayed excitation spectra that increase in intensity without variation of spectral form, as the pH was lowered. Some variation in excitation spectral form between the complexes was evident, however. In the case of **[Eu.L^{10b}]** for example, a very broad profile was obtained with no distinctive features. In contrast, a broad profile featuring two clear overlapping bands at approximately 286 and 331 nm was displayed by the ethyl analogue, **[Eu.L^{10a}]**. These bands become more evident in more acidic pH conditions, given the broadness of the profile. Finally, the trichromophore complex **[Eu.L^{11}]** displayed a similar excitation profile to that of **[Eu.L^{10a}],** with two distinct bands at 281 and 338 nm, although, here the band at longer wavelength is more well-defined.

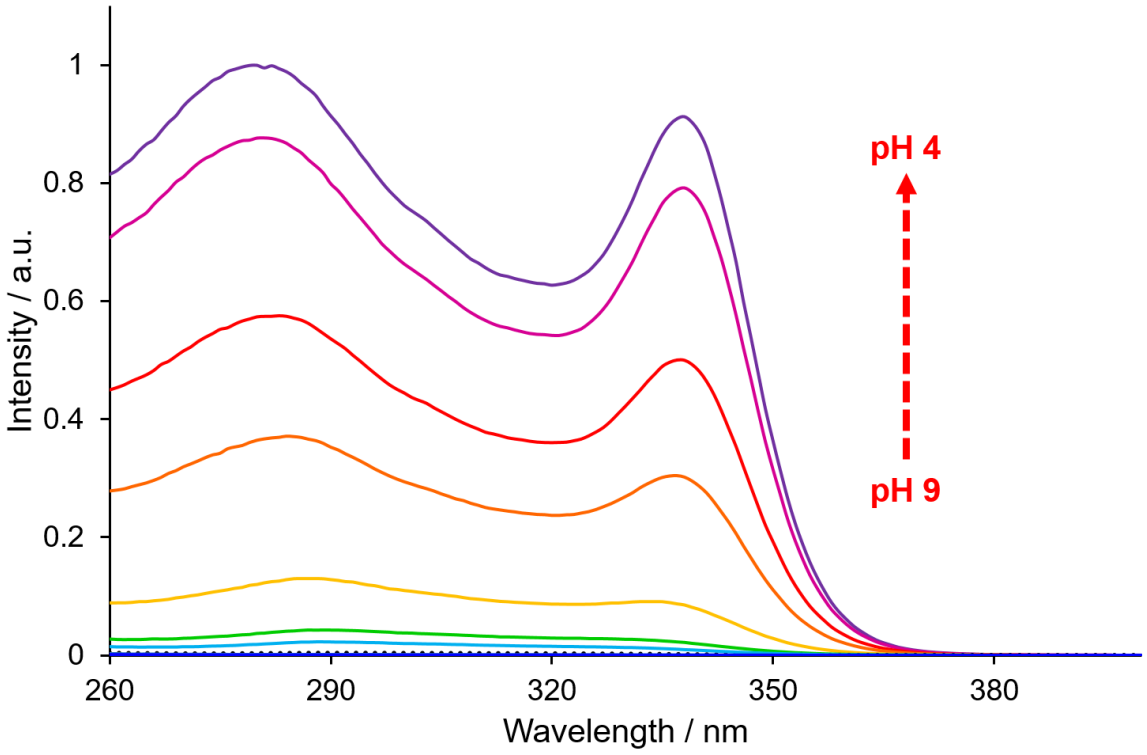

Figure 4.9. Variation in the excitation spectrum with pH for **[Eu.L^{11}]** (λ_{em} 613 nm, 295 K, $c_{complex}$ = 15 μM, 0.1 M NaCl). Excitation spectrum at pH 7 is indicated with black dots.

c) pH Dependent Emission Lifetime Behaviour

The variation of the europium emission lifetime with pH was probed for the complexes **[Eu.L$^{10a\text{-}b,11}$]** and the resulting sigmoidal curves fitted to determine an estimated pK_a value in 0.1 M NaCl, (Figure 4.10). Inspection of the curves in parallel clearly demonstrates the impact of substituting an ethyl for a methyl group on the pK_a through the decrease in pK_a of approximately 0.9 of a pK_a unit (5.21 to 4.32). Whilst the lower lifetime limiting value did not vary significantly between **[Eu.L$^{10a\text{-}b}$]**, the upper value decreased marginally for the methyl analogue. A general overall decrease in the lifetime curve was found for **[Eu.L^{11}]**, where a third, *N,N*-diethylamino protonation site is present on the third antenna. This third protonation site does not affect the value of the mean pK_a (*c.f.* **[Eu.L^{10a,11}]**). On acidification, the europium emission lifetime was enhanced by 248, 226 and 390% for **[Eu.L$^{10a\text{-}b,11}$]**, respectively.

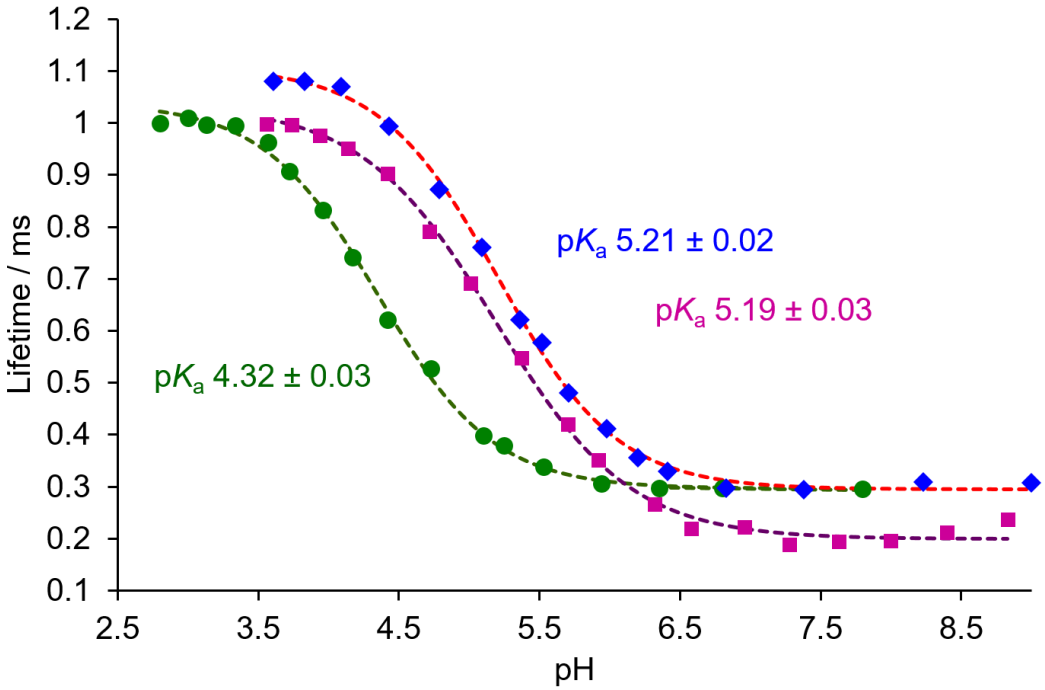

Figure 4.10. Variation in the europium emission lifetime with pH for **[Eu.L$^{10a\text{-}b,11}$]** (blue diamonds, green circles, and purple squares, respectively, λ_{em} 613 nm, 295 K, $c_{complex}$ = 15 μM, 0.1 M NaCl). The experimental data was fitted using non-linear least squares regression analysis (dashed lines).

4.1.3. Comparison and Summary

The photophysical properties of five new hydrophilic pH-responsive europium(III) complexes have been examined, (Table 4.2). These complexes consist of four

dichromophore and one trichromophore system(s), with modulation of the functionality at the amino protonation site.

Table 4.2. Summary of the photophysical properties of the key europium(III) complexes discussed within this work (295 K, 0.1 M NaCl).

Complex	λ_{exc} / nm	ε[a] / M^{-1} cm^{-1}	τ / ms	Φ[a] / %	q	B[a] / M^{-1} cm^{-1}
[Eu.L^{2}]	328	35,000	0.34[b]	0.2[b]	0	70[b]
			1.00[c]	17.6[c]		6,160[c]
[Eu.L^{9a}]	332	39,000	0.26[b]	0.3[b]	0	117[b]
			1.02[c]	16.0[c]		6,240[c]
[Eu.L^{9b}]	332	39,000	0.28[b]	0.01[b]	0	4[b]
			1.04[c]	15.0[c]		5,850[c]
[Eu.L^{10a}]	332	35,000	0.31[b]	0.06[b]	0	21[b]
			1.08[c]	13.4[c]		4,690[c]
[Eu.L^{10b}]	336	35,000	0.31[d]	0.06[d]	0	21[d]
			1.01[e]	13.0[e]		4,550[e]
[Eu.L^{3}]	331	46,000	0.25[b]	0.1[b]	0	46[b]
		60,000	0.84[c]	17.0[c]		10,200[c]
[Eu.L^{11}]	332	75,000	0.20[b]	0.01[b]	0	8[b]
			0.98[c]	15.9[c]		11,925[c]

[a] Parameter calculated at the stated excitation wavelength, which is an isosbestic point where appropriate. [b] Values at pH 8. [c] Values at pH 4. [d] Values at pH 7. [e] Values at pH 3. Experimental errors of lifetime and quantum yield are ±5 and 15%, respectively.

Values of the molar extinction coefficient, ε, and quantum yield, ϕ, for each complex excited at the stated isosbestic point, where possible, are shown. For each dichromophore complex, ε values were estimated using the Beer-Lambert Law and found to be consistent for structural analogues (*e.g.* **[Eu.L$^{9a\text{-}b}$]**), with values in the range 35,000 – 39,000 M^{-1} cm^{-1}. On examining the complex **[Eu.L^{11}]**, a more significant value of 75,000 M^{-1} cm^{-1} was estimated for ε, slightly greater than that estimated for the parent complex **[Eu.L^{3}]**. Quantum yields were estimated using the ruthenium complex $[Ru(bipy)_3]Cl_2$ as a standard.[1] For each complex, Φ was determined to be close to zero at the high pH limit, increasing to 13 – 16% at the low pH limit. These values are marginally lower than those determined for the di and trichromophore parent complexes **[Eu.L^{2,3}]**, respectively. This decrease can potentially be attributed to the increase in functional complexity within the molecule (*e.g.* long alkyl chains and sulfonate moieties) and additional associated non-radiative deactivation pathways.

With these two parameters determined, an estimation of complex brightness, B, can be made. Whilst the first set of complexes, **[Eu.L$^{9a\text{-}b}$]**, display comparable brightness values to the parent **[Eu.L^{2}]**, a brightness drop of approximately 20% is seen for

[Eu.L^{10a-b}], relative to the other dichromophore complexes. In contrast, an increased brightness value is estimated for **[Eu.L^{11}]** relative to the parent complex **[Eu.L^{3}]**.

By varying the nature of the substituents at the amino group, the pK_a has been modulated significantly from those of the original parent complexes, **[Eu.L$^{2-3}$]**, with values ranging from 4.32 – 6.18 in 0.1 M NaCl, (Table 4.3). The pK_a's of this set of five complexes cover two pH units, and are tuned to the pH range found in endosomes and lysosomes.

Table 4.3. Summary of pK_a values determined for the key europium(III) complexes discussed within this work in the stated media.

Complex	Conditions	pK_a[a]
[Eu.L^{2}]	0.1 M NaCl	6.30 (05)
	NIH-3T3 cell lysate	6.25 (05)
[Eu.L$^{9\,a}$]^{0}	0.1 M NaCl	6.18 (03)
	NIH-3T3 cell lysate	6.00 (04)
[Eu.L$^{9\,b}$]^{0}	0.1 M NaCl	5.34 (03)
[Eu.L^{10a}]	0.1 M NaCl	5.21 (02)
[Eu.L^{10b}]	0.1 M NaCl	4.32 (03)
[Eu.L^{3}]	0.1 M NaCl	6.21 (05)
	NIH-3T3 cell lysate	5.92 (05)
[Eu.L^{11}]	0.1 M NaCl	5.19 (03)

[a] pK_a values given are the mean of three replicates, at 295 K. Experimental errors are given in parentheses.

Substitution of an ethyl for a methyl group at the amino group reduced the pK_a by approximately 0.8 – 0.9 of a pK_a unit (*c.f.* **[Eu.L$^{9\,a-b}$]^{0}**). Additionally, by replacing one of the N-ethyl groups with the N-substituted propylsulfonate moiety, the pK_a was reduced by approximately one unit. This pK_a decrease occurred for both the ethyl and methyl complex analogues.

The behaviour of N-substituted sulfonate systems may be rationalised by considering several factors. Firstly, it is reasonable that, following protonation of the amino nitrogen, the presence of the anionic charge in close proximity to the positive charge will stabilise the protonated form electrostatically through a coulombic field effect. Here, the protonated species can be considered as a zwitterion. Overall stabilisation of the protonated form, *i.e.* the conjugate acid, would induce an increase in the pK_a accordingly. In contrast, the s-polarisation effect of the electron-withdrawing sulfonate

moiety will reduce the electron density at the N lone pair in the conjugate base. The reduced basicity of the free base is mirrored by an increase in the acidity of the protonated species, and results in a pK_a decrease. The degree of s-bond induction is distance-dependent, and the length of the propyl chain should be taken into consideration when considering the significance of this effect. A third factor to consider is the degree of solvation of the protonated form and the perturbation of this solvation by the charged sulfonate group. In the absence of the sulfonate group, solvation of the protonated complex is expected to stabilise the conjugate acid. The localisation of the negative charge on each oxygen atom of the sulfonate group gives rise to a highly ordered local solvation structure (termed a kosmotrope). Given the greater free energy of solvation observed for anions compared to the relatively lipophilic (a chaotropic) ammonium cation here, it is plausible that the relative free energy of solvation of the positive charge is decreased in the presence of the sulfonate group. It is tentatively hypothesised that such a differential solvation effect is significant and may be responsible for the overall increase in the acidity of the species.

4.2. Bioconjugation Studies

*4.2.1. Synthesis of the BG Derivatives **[Eu.L^{12a-b}]***

The benzyl guanine (BG) derivatives, **[Eu.L^{12a-b}]**, were prepared by our industrial collaborators (Cisbio, France) from the europium complexes **[Eu.L^{9}]**, (Figure 4.11). These syntheses were accomplished in two steps.

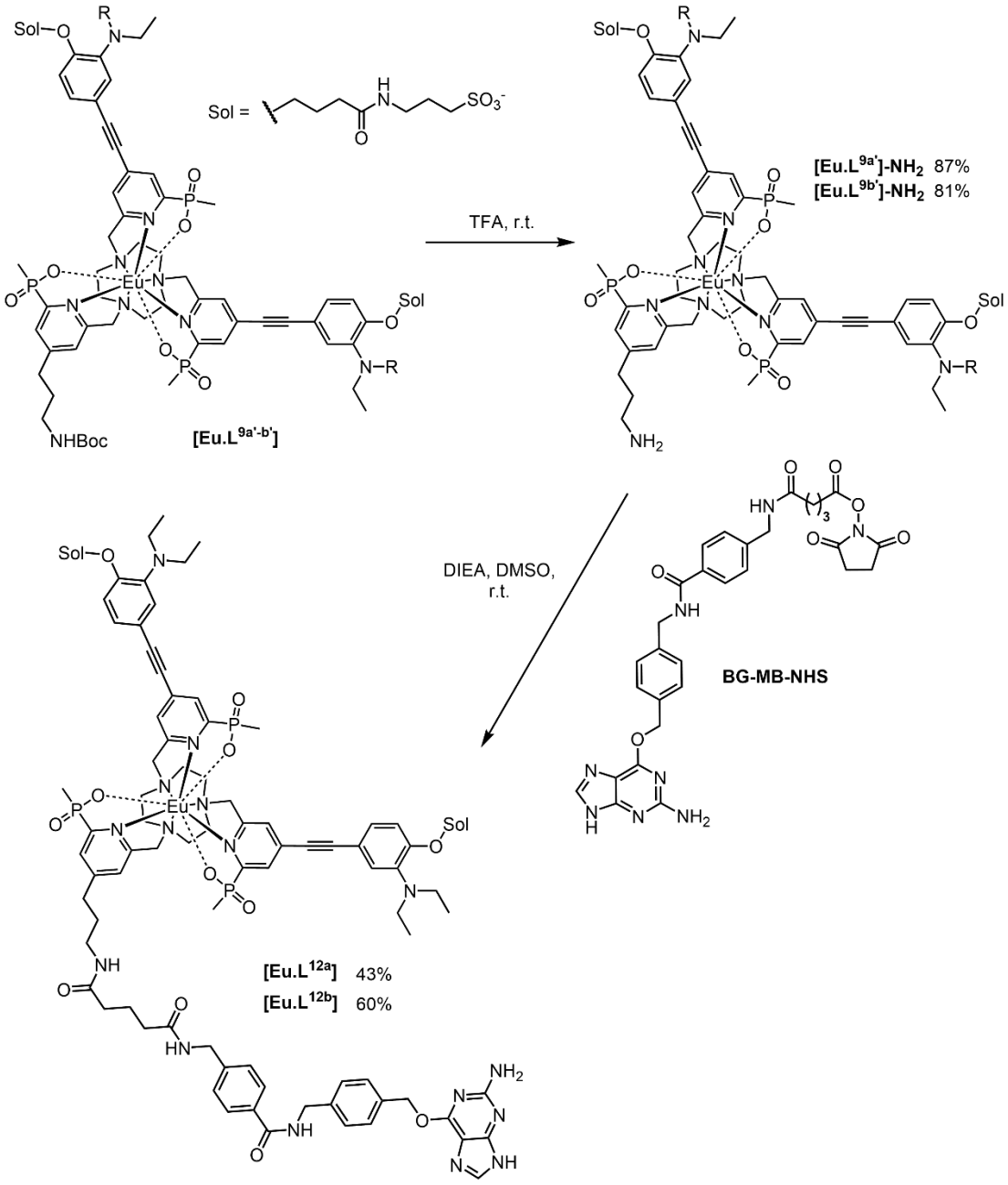

Figure 4.11. Synthesis of the BG derivatives, **[Eu.L^{12a-b}]**.

Firstly, deprotection of the peripheral Boc protected amine was achieved using TFA in each case and the deprotected complexes **[Eu.L$^{9\ a-b}$]-NH$_2$** were obtained in high yield (81 – 87%), following purification by RP-HPLC. The deprotected complexes were then reacted with the activated ester reagent **BG-MB-NHS** in the presence of the base DIEA to yield the BG-coupled derivatives **[Eu.L^{12a-b}]**. This activated ester reagent was prepared as described in earlier work.[2] These couplings were only moderate in yield (43 – 60%). Given the reactivity of the activated ester reagent, higher yields may be attainable with the use of anhydrous conditions and an inert reaction atmosphere. The

BG conjugates were isolated and their purity was confirmed by RP-HPLC, (Figure 4.12).

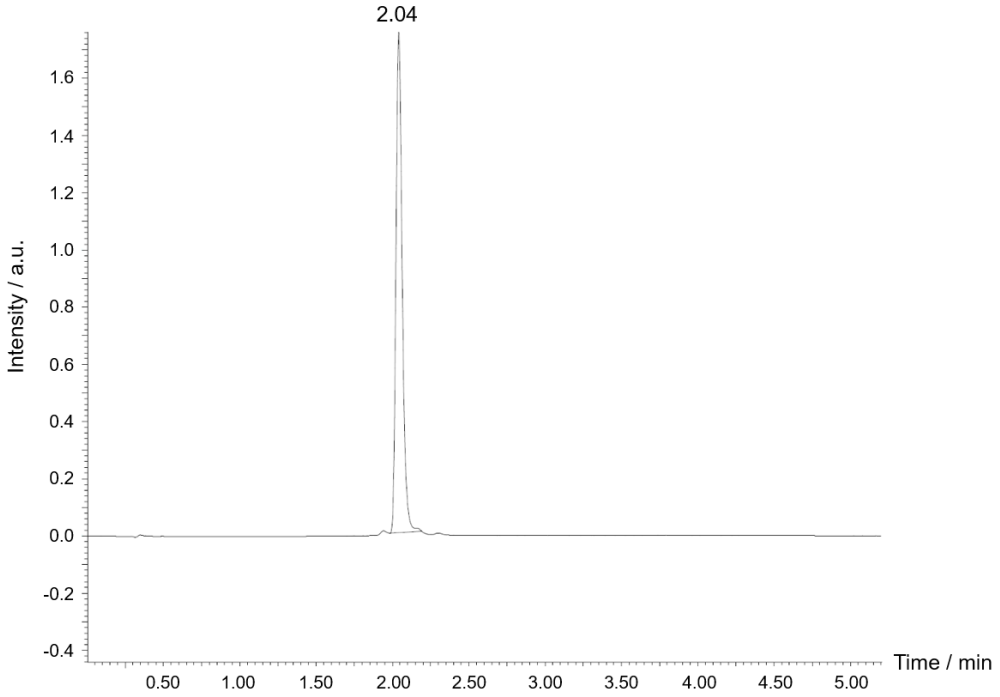

Figure 4.12. HPLC trace of the pure BG conjugate, **[Eu.L^{12a}]** (Acquity C_{18} Column, 300 Å, 1.7 µm, 2.1 × 50 mm; λ_{exc} 280 nm; 0.6 mL min^{-1}). The solvents (A) 5 mM $NH_4OAc_{(aq)}$ pH 5.5, and (B) MeCN were used with the following gradient: 5% B *t* 0 – 0.2 min then 5% to 100% B over 4.8 min.

Following the preparation and initial characterisation of the BG derivatives, the complexes **[Eu.L^{12a-b}]** were further characterised at Durham. Owing to the increasing molecular weight of these compounds, characterisation by HRMS was not possible during the lockdown period. As an alternative, the BG derivatives were examined through LC/MS-MS experiments, (Figure 4.13).

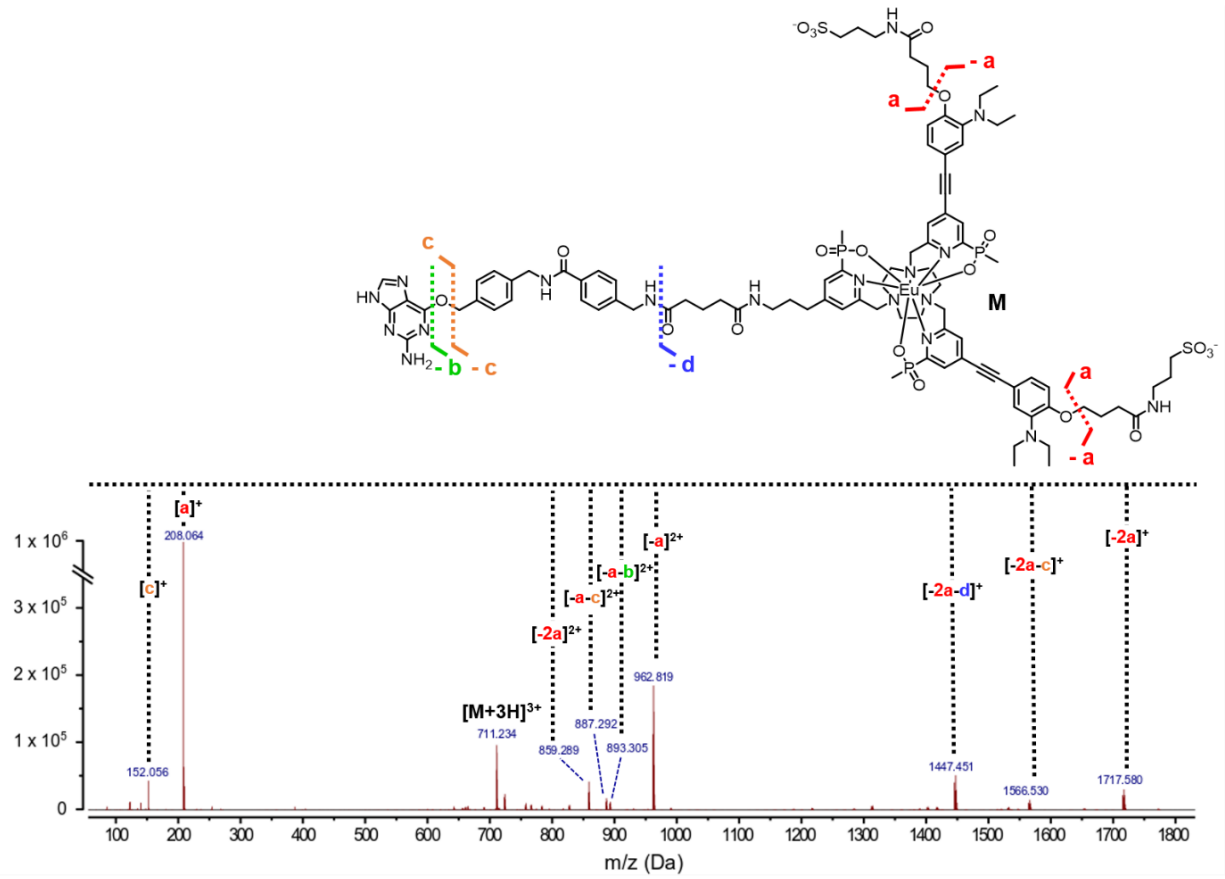

Figure 4.13. MS-MS analysis of the BG conjugate **[Eu.L^{12a}]**.

Proof of the constitution of the BG conjugate is possible through the assignment of the fragmentation patterns, as has been shown for other conjugates in related work.[3] Such an assignment is shown for the significant fragments generated in an LC/MS-MS experiment with **[Eu.L^{12a}]**. For example, a commonly observed bond breakage occurred at the ArO-CH_2 bond with cleavage of the peripheral head group (loss of fragment **a**). The corresponding charged **a** fragment was observed with high abundance. The occurrence of several fragmentations relating to bond cleavages within the BG moiety (fragmentations **b** and **c**) and the linker (fragmentation **d**) provide evidence for the conjugation of the BG to the complex. Similar results were obtained for LC/MS-MS experiments on the methyl conjugate analogue, **[Eu.L^{12b}]**.

4.2.2. Receptor Labelling Experiments

With the BG functionality introduced, these BG conjugates are appropriately functionalised to label the SNAP-tag (ST), a known self-labelling suicide enzyme[4] often utilised in the study of G-protein coupled receptors (GPCRs). The labelling of SNAP tagged receptors using europium(III)[5] and terbium(III)[6-7] derivatives has been exemplified within previous studies. Further work by others has seen the signalling of receptor internalisation through the labelling of a GPCR with the pH insensitive terbium(III) complex, Lumi4-Tb,[8] from which the Tag-lite technology® has subsequently emerged.

In a proof-of-concept study for membrane receptor labelling and monitoring of trafficking, the BG derivative **[Eu.L^{12a}]** was prepared as described. Given the literature precedent, a similar model is well suited to assess the behaviour and efficacy of these new europium pH responsive probes, (Figure 4.14).

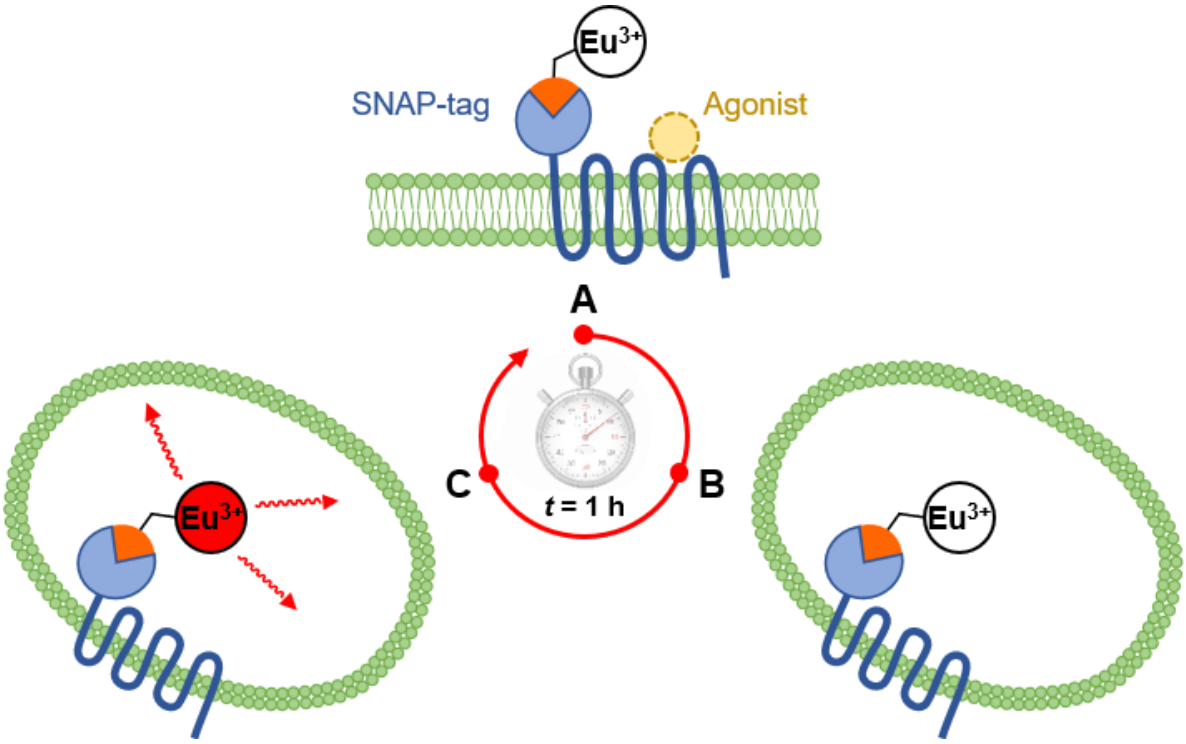

Figure 4.14. Graphical representation of the described proof-of-concept study. **A)** Labelling of a SNAP-tagged receptor (blue line) on the cell surface with a europium(III) complex through an appropriately functionalised linker (orange sector); **B)** internalisation of the receptor, and the conjugated complex, is induced by an agonist; **C)** luminescence from the europium(III) complex switches on as a result of a pH decrease.

The glucagon-like peptide-1 receptor (GLP-1R) is a receptor targeted for anti-diabetic drugs since it is involved in the metabolic pathway for insulin production. Tools to study its agonist-induced internalisation[9-11] are therefore in high demand. After labelling a HEK-293 cell line that stably expresses GLP-1R-ST with 200 nM of **[Eu.L^{12a}]** at pH 7.4, the excess europium complex was removed through successive washing steps, and an acetate buffer solution added (0.1 M, pH 4.5, +0.1% BSA) to the medium in order to induce luminescence. The europium luminescence was then recorded using a time-gated 60 – 460 µs acquisition window (Figure 4.15A), with specific monitoring of the hypersensitive Δ*J* = 2 band (λ_{em} 620 nm). A strong luminescence signal was observed. In contrast, no luminescence was recorded from non-transfected HEK-293 cells under identical conditions. This experiment serves as a useful control, demonstrating that labelling of the non-transfected cells is negligible under these conditions. Additionally, the labelling of the GLP-1R with **[Eu.L^{12a}]** on the cell surface is specific, and the species does not accumulate in endosomal particles, as this would give rise to an observable signal. As was originally designed, the presence of the anionic sulfonate groups in the probe structure suppresses any non-specific labelling to cells.

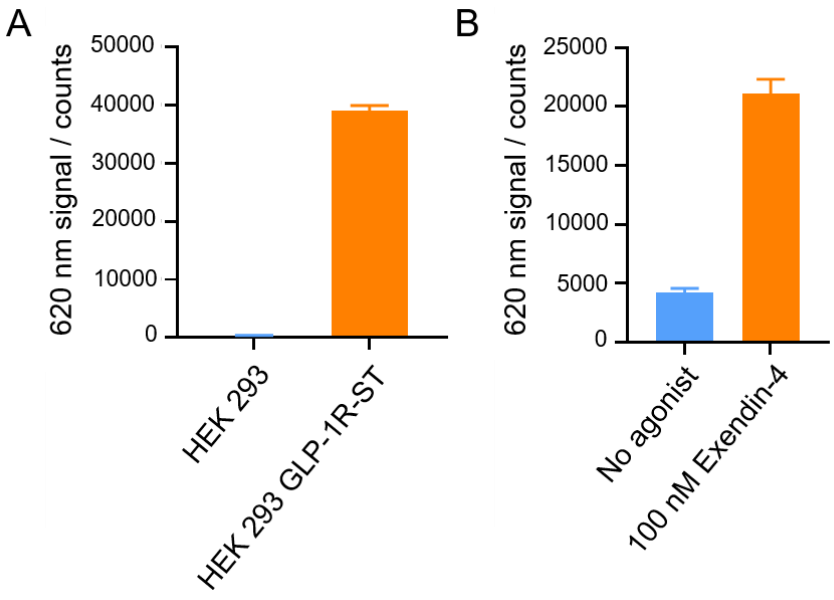

Figure 4.15. Time-gated luminescence measurements of the europium Δ*J* = 2 band intensity of: **A)** GLP-1R-ST receptor labelling, using **[Eu.L^{12a}]** (200 nM) on non-transfected and GLP-1R-ST expressing HEK 293 cells; **B)** GLP-1R-ST receptor internalisation, 1 h after addition of 100 nM of the peptide agonist, Exendin-4, versus a control with no agonist added. Experiments are performed in triplicate.

In order to follow receptor internalisation by monitoring endosomal acidification, 100 nM of Exendin-4, an agonist for the GLP-1R peptide, was added to the **[Eu.L^{12a}]** labelled receptors at pH 7.4. After a one hour incubation period, the time-gated luminescence at 620 nm was measured revealing a five-fold increase in luminescence intensity, (Figure 4.15B). This increase in luminescence is a result of receptor internalisation and acidification within the endosome. It is noted that significant optimisation of the experimental protocol or the reading parameters is yet to be investigated, and this will certainly allow for an enhancement of the luminescence switch-on. For example, measurement of the resulting luminescence from the **[Eu.L^{12a}]** labelled receptors following agonist-induced internalisation using a longer delay time and acquisition period (500 – 1000 *vs.* 60 – 460 µs) revealed a seven-fold increase in luminescence intensity.

A similar study was performed with **[Eu.L^{12b}]**, examining the specificity of labelling at the cell surface and the change in luminescence intensity on agonist induced internalisation, (Figure 4.16). Here, the specificity of the labelling at the cell surface was demonstrated once again. In contrast to the receptors labelled with **[Eu.L^{12a}]**, however, a significantly lower agonist-induced internalisation signal was recorded (2.1-fold increase on internalisation).

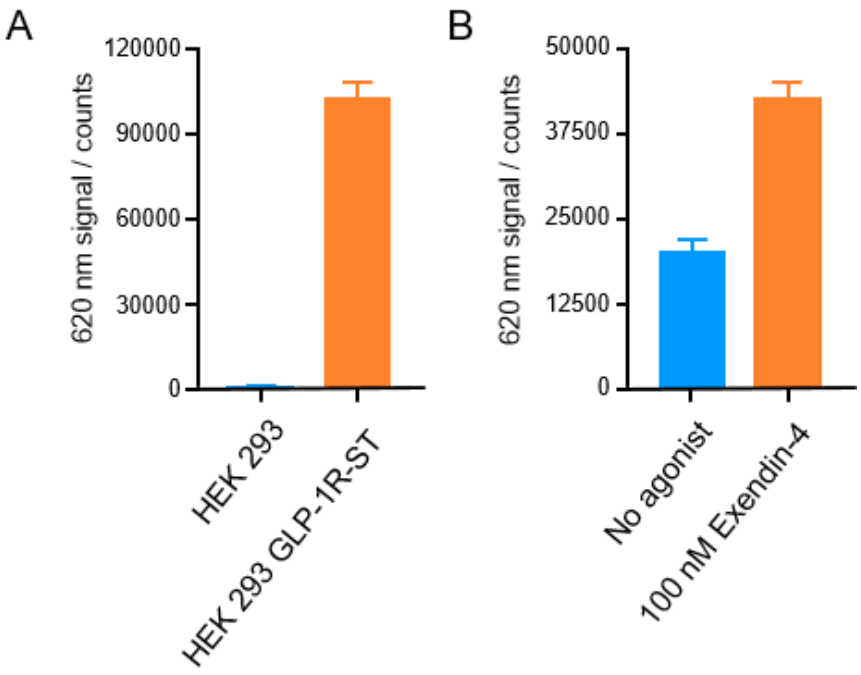

Figure 4.16. Time-gated luminescence measurements of the europium Δ*J* = 2 band intensity of: **A)** GLP-1R-ST receptor labelling, using **[Eu.L^{12b}]** (200 nM) on non-transfected and GLP-

1R-ST expressing HEK 293 cells; **B)** GLP-1R-ST receptor internalisation, 1 h after addition of 100 nM of the peptide agonist, Exendin-4, versus a control with no agonist added. Experiments are performed in triplicate.

In order to establish further the relative efficacy of the prepared europium complexes for monitoring receptor internalisation, a number of commercially available pH sensitive dyes (pHrodo iFL Red and Green, AcidiFluor Orange, pHAb, and CypHer5) were procured from various chemical suppliers. The BG conjugates of these commercial dyes were prepared and studied in a similar manner, examining: (1) the cell surface labelling onto GLP-1R-SNAP tagged receptors at low pH (4.5 – 5) and (2) the difference in luminescence with and without stimulation of the tagged receptor with an appropriate agonist. A summary of these results is tabulated below (Table 4.4), where I_{label} is the relative increase in luminescence intensity for the labelled receptors at low pH (4.5 – 5) relative to the non-transfected cell line, and $I_{agonist}$ is the relative increase in luminescence intensity for agonist-induced internalisation relative to no stimulation.

Table 4.4. Evaluation of several BG conjugates of commercial pH-sensitive dyes.

BG Conjugate	I_{label}	$I_{agonist}$
BG-pHrodo Red	3.6	1.2
BG-pHrodo Green	2.9	0[a]
BG-AcidiFluor Orange	2.3	1.8
BG-CypHer5	28	2.5
BG-pHAb (isomer A/B)	23/19	1.9/2.6
[Eu.L^{12a}]	108[b]	5[c]/7[d]
[Eu.L^{12b}]	72[b]	2.1[c]

[a] No luminescence change observed, within experimental error. [b] Observed luminescence from non-transfected HEK 293 cells is negligible. [c] Measurement is time-gated using a 60 – 460 µs acquisition window. [d] Measurement is time-gated using a 500 – 1000 µs acquisition window. Experiments were repeated in triplicate.

Whilst several commercial dyes are somewhat compatible with internalisation assays (*e.g.* Cypher5 and BG-pHAb), as shown by an observable agonist-induced internalisation signal, these $I_{agonist}$ values are notably less than those observed for **[Eu.L^{12a}]** using time-gated measurements. Additionally, it appears that the specificity for receptor labelling at the cell surface is uniquely high for **[Eu.L^{12a-b}]**, whereas for the commercial dyes luminescence from the non-transfected cell line is not negligible. The

observed luminescence from the non-transfected control is notably lower for BG-CypHer5 and BG-pHAb (isomers A and B), however, compared with the other dye conjugates where luminescence is significant. The structures of the dyes CypHer5 and pHAb are known to contain anionic sulfonate groups (one aromatic sulfonate and two butylsulfonate chains, respectively), and this selectivity can be tentatively attributed to the presence of these groups.

The inclusion of terminal sulfonate groups in the design of these europium complexes was proposed originally to achieve two purposes: firstly, to increase the aqueous solubility of these species significantly; and secondly, to minimise undesired non-selective interactions or binding with *in cellulo* species. These desired properties have been demonstrated qualitatively and quantitatively, respectively. The difficulty encountered by europium(III) complexes bearing anionic sulfonate groups to enter living cells, in the absence of bioconjugation, has been shown in related work with a lack of complex uptake by the cell.[12]

Confirmation of this uptake behaviour was sought through the separate incubation of the complexes **[Eu.L^{10a,11}]** with living NIH-3T3 cells, (Figure 4.17). After 24 hours, the uptake of the complex was examined using confocal microscopy. In each case, a lack of observed europium emission suggests no uptake of either complex into the cell (*top left* and *top right*, Figure 4.17). In comparison, the parent complex **[Eu.L^{3}]** entered the same cell line rapidly (~1-2 hours) and was clearly observable after 24 hours, (Figure 2.22). Given the literature precedent, the most probable explanation for this lack of luminescence is that the complexes have not entered the cell and are located outside in the non-emissive state. However, these observations can also be explained by the localisation of the complexes within a cellular compartment where the pH is appropriately high such that europium emission is thoroughly suppressed. Probing the concentration of europium complex in the extracellular medium using Eu-ICPMS would remove any doubt concerning complex uptake in this situation.

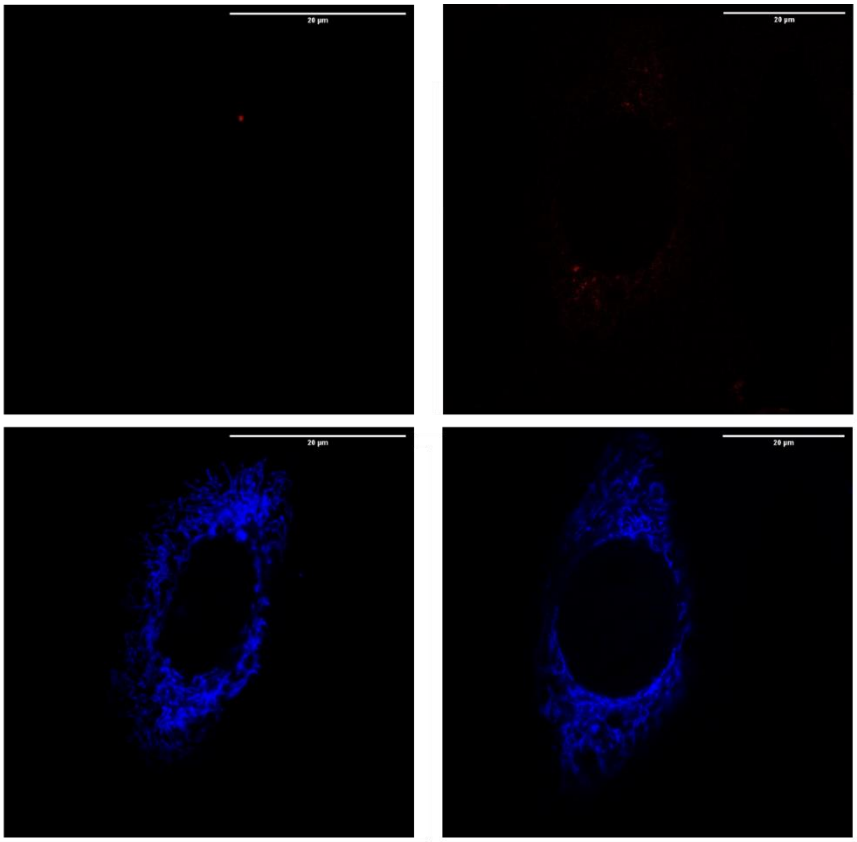

Figure 4.17. Live cell images (NIH-3T3) with **[Eu.L^{10a,11}]** (*top left* and *top right*, respectively) after 24 h (incubation concentration = 20 μM, λ_{exc} 355 nm, λ_{em} 605 – 720 nm). The corresponding autofluorescence (λ_{exc} 355 nm, λ_{em} 400 – 450 nm) is shown below. Scale bar represents 20 microns.

4.3. Conclusions

The photophysical properties of the five hydrophilic pH responsive europium(III) complexes discussed in chapter three have been evaluated in detail, with an examination of the absorption, emission, excitation, and emission lifetime behaviour as a function of pH. These complexes can be divided into two sets, based on the location of the aqueous solubilising sulfonate moiety (**[Eu.L$^{9\ a\text{-}b}$]** *vs.* **[Eu.L$^{10a\text{-}b,11}$]**).

Analysis of the absorbance *vs*. pH profiles revealed similar behaviour to that of the parent complexes **[Eu.L$^{1\text{-}3}$]** (chapter two), where a hypsochromic shift of the main absorption ICT band occurs on protonation, with the corresponding appearance of a ligand p- p* transition of increased intensity. Notably, the complexes each display an isosbestic point in the range 328 – 336 nm, including the trichromophore complex **[Eu.L^{11}]**, in contrast to the parent complex **[Eu.L^{3}]** that does not. On protonation, the europium emission intensity increased by 585 and 1045-fold for **[Eu.L$^{9\ a\text{-}b}$]**,

respectively (ΔJ = 2 analysis), between the appropriate pH limits. Introduction of the propylsulfonate group onto the amine was found to enhance the emission switch-on factor further with 925, 1040, and 1340-fold increases for **[Eu.L$^{10a\text{-}b,11}$]**, respectively. The enhancement of europium emission on lowering pH was mirrored by very large increases in the europium emission lifetime, ranging between 226 and 390% for the complexes in 0.1 M NaCl. In the case of **[Eu.L^{9a}]**, the relative increase in lifetime value was shown to be enhanced further to 453% within a cell lysate medium.

In an analogous manner to previous work (chapter two), the enhancement of emission intensity ratios was demonstrated for **[Eu.L^{2,9a}]** by varying the time window for acquisition of europium spectral intensity data. Enhancements of the switch-on factor from 34 to 527, and 32 to 465 were possible for **[Eu.L^{2,9a}]** in 0.1 M NaCl, respectively.

Fitting of the experimental lifetime data allowed the determination of pK_a values for the five europium(III) complexes, which were found to lie in the range 4.3 – 6.2 in 0.1 M NaCl. In line with the original design intent, varying the functionality at the aryl amino nitrogen had considerable impact on the pK_a value. A decrease in pK_a of approximately 0.8 – 0.9 of a unit (*c.f.* **[Eu.L$^{9a\text{-}b}$]** and **[Eu.L$^{10a\text{-}b}$]**) was seen with the exchange of an ethyl for a methyl group, and the introduction of a propylsulfonate resulted in a decrease of one unit. These changes can be rationalised by effects caused by the balance between steric inhibition of lone pair conjugation (ethyl *vs.* methyl), coulombic stabilisation, s-bond polarisation, and differential energies of solvation.

The benzyl guanine conjugates **[Eu.L$^{12a\text{-}b}$]** were prepared in two steps from the complexes **[Eu.L$^{9a\text{-}b}$]**, and the constitution of the conjugates confirmed using LC MS-MS experiments. The conjugates were utilised in a proof-of-concept study for the labelling of membrane receptors and monitoring of receptor internalisation. This study involved the labelling of a HEK-293 cell line capable of stably expressing the SNAP-tag functionalised glucagon-like peptide-1 receptor (GLP-1R). The high degree of labelling specificity at the cell surface, afforded by the sulfonate moieties, was demonstrated. Further, the possibility of monitoring of receptor internalisation was shown through the increase in europium emission, following the addition of the agonist Exendin-4, observed using time-gated measurements.

To assess the efficacy of these europium conjugates, a series of BG conjugates of commercial pH responsive dyes were prepared, and analogous receptor studies

performed. Initial comparative analysis suggests that, whilst some commercial dyes are compatible with such internalisation assays, the conjugate **[Eu.L^{12a}]** holds substantial promise against current commercial dyes. For example, europium emission was observed to increase seven-fold (500 – 1000 µs acquisition window) following agonist-induced internalisation, compared to 2.5-fold, the best result obtained with the dye CypHer5. Further optimisation of the methodology and measurement parameters should allow for further enhancement.

Given these initial favourable results, further pharmacological studies are currently underway on GLP-1R and other membrane receptors to assess the potential of these promising europium pH probes for studying receptor internalisation and its time dependence, both *in vitro* and in live cell assays.

4.4. References

[1] K. Nakamaru, *Bull. Chem. Soc. Jpn.,* 1982, **55**, 2697–2705.

[2] J. M. Zwier, H. Bazin, L. Lamarque and G. Mathis, *Inorg. Chem.*, 2014, **53**, 1854–1866.

[3] M. Starck, J. D. Fradgley, S. Di Vita, J. A. Mosely, R. Pal and D. Parker, *Bioconjugate Chem*., 2020, **31**, 229–240.

[4] A. Keppler, S. Gendreizig, T. Gronemeyer, H. Pick, H. Vogel and K. Johnsson, *Nat. Biotechnol.*, 2003, **21**, 86–89.

[5] M. Delbianco, V. Sadovnikova, E. Bourrier, G. Mathis, L. Lamarque, J. M. Zwier and D. Parker, *Angew. Chem. Int. Ed.*, 2014, **53**, 10718–10722.

[6] J. M. Zwier, H. Bazin, L. Lamarque and G. Mathis, *Inorg. Chem.*, 2014, **53**, 1854–1866.

[7] J. M. Zwier, T. Roux, M. Cottet, T. Durroux, S. Douzon, S. Bdioui, N. Gregor, E. Bourrier, N. Oueslati, L. Nicolas, N. Tinel, C. Boisseau, P. Yverneau, F. Charrier-Savournin, M. Fink and E. Trinquet, *J. Biomol. Screen.*, 2010, **15**, 1248–1259.

[8] J. Xu, T. M. Corneillie, E. G. Moore, G.-L. Law, N. G. Butlin and K. N. Raymond, *J. Am. Chem. Soc.*, 2011, **133**, 19900–19910.

[9] D. Donnelly, *Br. J. Pharmacol*., 2012, **166**, 27–41.

[10] S. N. Roed, P. Wismann, C. R. Underwood, N. Kulahin, H. Iversenn, K. A. Cappelen, L. Schäffer, J. Lehtonen, J. Hecksher-Soerensen, A. Secher, J. M. Mathiesen, H. Bräuner-Osborne, J. L. Whistler, S. M. Knudsen and M. Waldhoer, *Mol. Cell Endocrinol.*, 2014, **382**, 938–949.

[11] W. J. C. van der Velden, F. X. Smit, C. B. Christiansen, T. C. Møller, G. M. Hjortø, O. Larsen, S. P. Schiellerup, H. Bräuner-Osborne, J. J. Holst, B. Hartmann, T. M. Frimurer and M. M. Rosenkilde, *ACS Pharmacol. Transl. Sci.*, 2021, **4**, 296–313.

[12] M. Starck, R. Pal and D. Parker, *Chem. Eur. J.*, 2016, **22**, 570–580.

CHAPTER FIVE

Circularly Polarised Luminescence, Racemisation Kinetics and Solvatochromism Studies of [Eu.L^3]

Chapter Five: Circularly Polarised Luminescence, Racemisation Kinetics and Solvatochromism Studies of [Eu.L^3]

This chapter features the resolution of the parent complex **[Eu.L^3]** using chiral HPLC and the subsequent study of the circularly polarised luminescence (CPL) behaviour, arising from the pure enantiomers. The kinetics of racemisation for these enantiopure species were determined and solvatochromism studies with the complex performed.

5.1. Chiral Resolution of [Eu.L^3]

In addition to a 'switching-on' of emission and an increase in emission lifetime with decreasing pH, it was also expected that **[Eu.L^3]** would display strong CPL with the intensity of the signal being pH-dependent. As the complex exists as a racemic mixture of the *SSS-Δ(λλλ)* and *RRR-Λ(δδδ)* isomers, it was first necessary to separate them, before investigating their CPL behaviour. Previously, resolution of racemic europium(III) complexes has been achieved by chiral HPLC.

Successful separations of racemic europium(III) complexes featuring similar methoxy-substituents on the aryl ring have been performed using a CHIRALPAK-ID column.[1-2] Before attempting the separation of the complex of interest, the integrity of the chiral stationary phase (Figure 5.1, *left*) within the column was confirmed to be intact and functional. This was achieved through the successful resolution of a standard, 2,3-dihydroflavone (flavanone), into its enantiomers, (Figure 5.1, *right*).

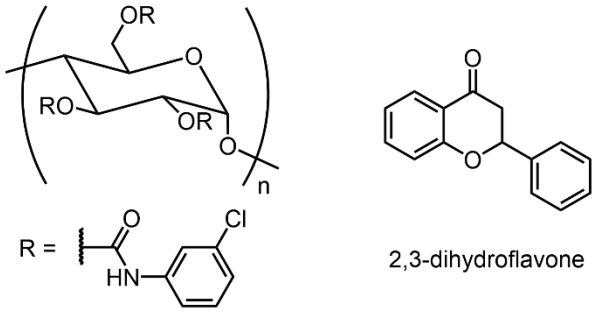

Figure 5.1. (*Left*) The chiral stationary phase within the CHIRALPAK-ID column. (*Right*) Structure of 2,3-dihydroflavone (flavanone).

The initial separation of **[Eu.L^3]** was trialled using a simple solvent gradient of isocratic methanol, which was successful in previous work. Initial experiments were performed on the analytical CHIRALPAK-ID column. Fortunately, these conditions resulted in a good separation of the *Δ* and *Λ* enantiomers, with retention times differing by over 20 minutes, with the *Δ* isomer being eluted first, (Figure 5.2). Following these results, the racemic complex **[Eu.L^3]** was separated on a 10 milligram scale using a semi-preparative column with an isocratic methanol eluent to yield the resolved enantiomers.

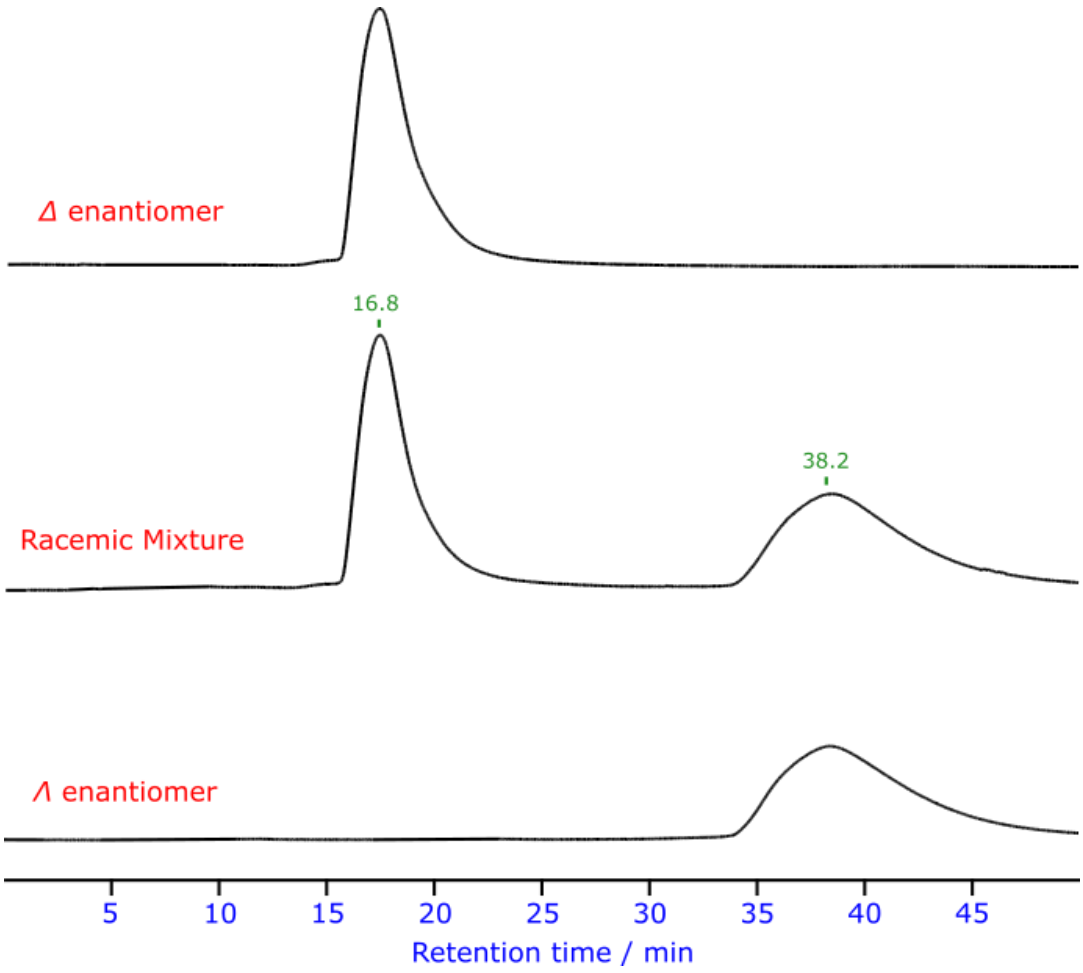

Figure 5.2. Chiral HPLC trace showing the resolution of the enantiomers of **[Eu.L^3]** using a CHIRALPAK-ID column (analytical, 295 K, CH_3OH, 1 ml min^{-1}, UV detector / = 330 nm). The retention times of the *Δ* and *Λ* enantiomers are given in green.

5.2. CPL Study of [Eu.L^3]

*5.2.1. Responsive CPL Behaviour of **[Eu.L^3]** with pH*

After isolation of the enantiomers, the CPL spectrum of each enantiomer was measured in a range of buffers at different pH values, (Figure 5.3). No discernible CPL signal was observed at pH 8 but a ‘switching-on’ of the CPL signal was evident as the pH decreased. An intense maximum CPL signal was observed at pH 4, under acidic conditions where >99% of the complex is fully protonated.

In an attempt to observe the higher Δ*J* bands, the CPL spectrum of each enantiomer at pH 4 was recorded out to 800 nm. It was not possible in this case, however, to detect the less intense bands of the Δ*J* = 5 or 6 transitions that sometimes can be observed beyond the Δ*J* = 4 manifold region (approx. 710 nm).

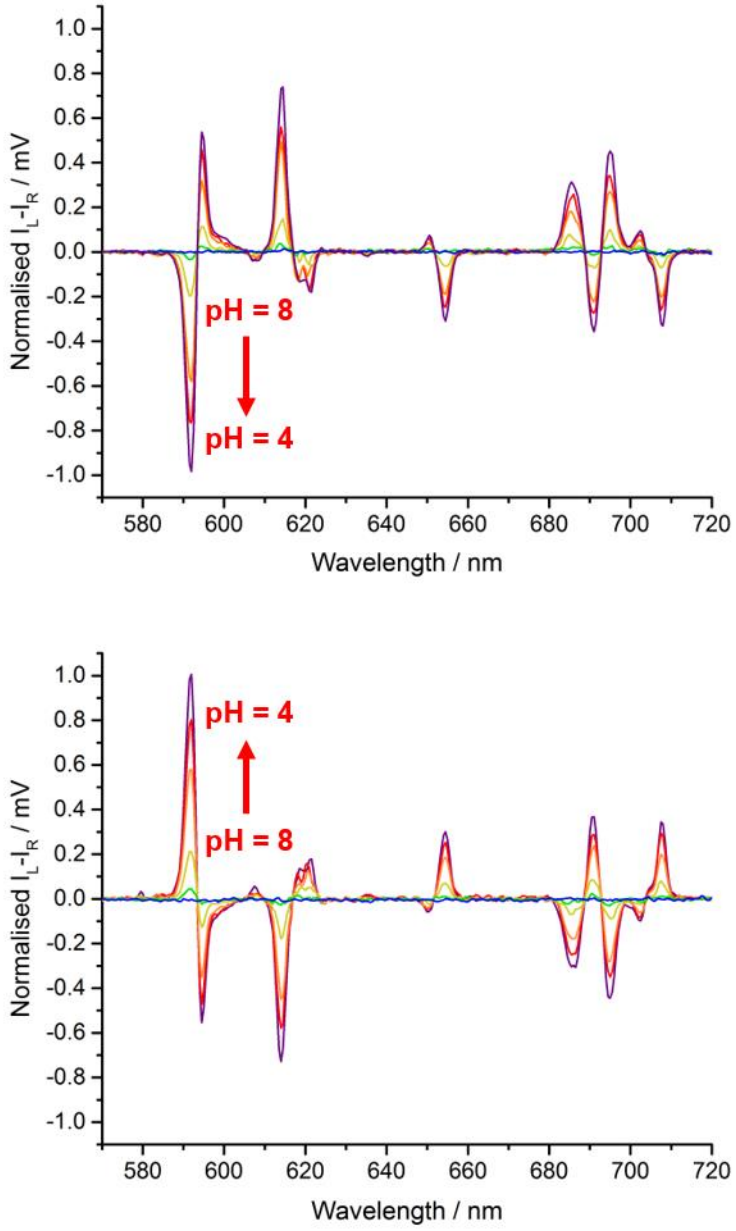

Figure 5.3. Evolution of the CPL spectrum for the *Δ* and *Λ* enantiomers (*top* and *bottom*, respectively) of **[Eu.L^3]** with pH (295 K, λ_{exc} 330 nm, 5 scans averaged). Measurements were taken in aqueous solutions of NH_4OAc, MES, HEPES, and NH_4HCO_3 buffers (0.1 M buffer in 0.1 M NaCl).

Comparison of the observed CPL from the *Δ* (red) and *Λ* (blue) enantiomers at pH 4 (Figure 5.4) highlights their high degree of similarity, where the spectra have mirror image forms. Particularly good resolution of five $\Delta J = 4$ band transitions was observed in the CPL spectrum, which is not seen in the total emission spectrum. The values calculated for the emission dissymmetry factor, g_{em}, are not very high but lie within the typical range for these sorts of complexes. The highest two values (-0.23 and -0.34)

were observed for transitions within the Δ*J* = 3 and Δ*J* = 4 bands, respectively, as found for structurally related chiral europium complexes.

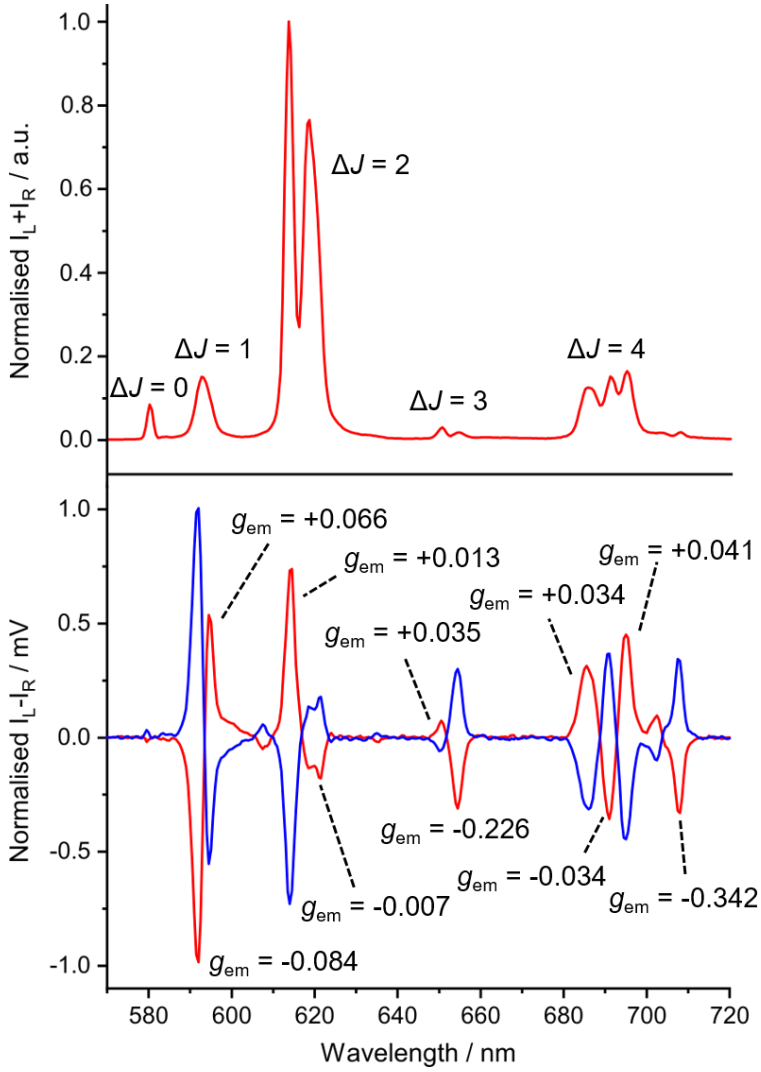

Figure 5.4. (*Top*) Normalised total emission spectrum of the racemic **[Eu.L^3]** complex (0.1 M ammonium acetate buffer, pH 4, 295 K, λ_{exc} 330 nm). (*Bottom*) Normalised CPL spectra of the *Δ* (red) and *Λ* (blue) enantiomers of **[Eu.L^3]** (0.1 M ammonium acetate buffer, pH 4, 295 K, λ_{exc} 330 nm, 5 scans averaged). Values of the dissymmetry factor at selected wavelengths are given for the *Δ* enantiomer.

*5.2.2. Study of Effect of Additives on **[Eu.L^3]** CPL and Total Emission*

Earlier work has investigated the reversible binding interaction between pH sensitive lanthanide complexes and biological serum proteins, such as α$_1$-AGP, HSA, and BSA.[3] It was hypothesised that an interaction between the chiral complex **[Eu.L^3]** and the chiral environment within the drug-binding pockets of such proteins might occur and evidence of this interaction could be observed using optical spectroscopy.

To probe this possibility, an aqueous buffered solution of **Ş-[Eu.L^3]** (15 μM, 0.1 M ammonium acetate, 0.1 M NaCl, pH 5) was prepared and both the CPL and total emission intensity recorded prior to and after the addition of two equivalents of a range of biological serum proteins (α_1-AGP, HSA, and BSA). In each instance, no discernible change was observed in either the CPL or total emission intensity.

Previous work has also examined the effect of addition of enantiopure acids, such as lactate or mandelate, to europium complexes, resulting in distinct changes in the total emission spectrum and an induced CPL signal.[4] It was hypothesised that the addition of a chiral acid to an enantiomer of **[Eu.L^3]** (*e.g.* the *Λ* enantiomer) could give rise to formation of diastereoisomeric acid-base pairs, which could be differentiated by examination of their CPL or total emission intensity.

As a preliminary experiment, the CPL and total emission intensity of **Ş-[Eu.L^3]** was monitored with addition of either the *R* or *S* enantiomer of 6-hydroxy-2,5,7,8-tetramethylchroman-2-carboxylic acid, (Trolox, Figure 5.5). The decision was made to use acetonitrile as the solvent over water, as it was reasoned that a less polar solvent, where ion solvation is less extensive, would be most favourable for the acid-base pair to occur. No noteworthy differences in CPL or emission intensity were observable, however, on the separate addition of *R*- and *S*-Trolox to **Ş-[Eu.L^3]**.

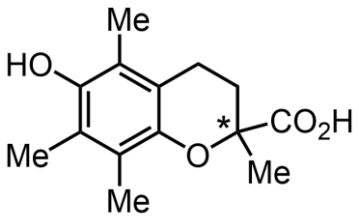

Trolox

Figure 5.5. Structure of 6-hydroxy-2,5,7,8-tetramethylchroman-2-carboxylic acid (Trolox).

Work probing the potential interaction between the chiral complex **[Eu.L^3]** and functionalised cyclodextrins was envisaged, but not carried out. It was hypothesised that an interaction between the enantiomer and a cyclodextrin, *e.g.* one of the antennae partially entering the inner pocket of a *β*-cyclodextrin, may be observable photometrically due to a change in the local solvation about the complex.

5.3. Determination of [Eu.L^3] Racemisation Kinetics

The kinetic stability of **[Eu.L^3]** with respect to enantiomer interconversion was assessed in an experiment monitoring the enantiomeric purity of the complex as a function of time. A solution of the resolved *Λ* enantiomer was prepared in different solvents and each solution was maintained at 60 ºC. Fixed aliquot samples of the solution were taken at successive time intervals and were examined by analytical chiral HPLC. Racemisation of the sample over time was anticipated, with a gradual change in the intensity ratio of the bands corresponding to the *Λ* and *Δ* enantiomers, reaching 1:1 in the racemic mixture.

Analysis of the ratio of the enantiomers with time allows a rate constant for enantiomeric interconversion, *k*, to be determined. Previously,[5] a kinetic relationship was derived to describe the racemisation process as an equilibrium between the *Λ* and *Δ* enantiomers. In this case, it is assumed that the racemisation kinetics experiment begins with the enantiopure *Λ* complex.

By examining the racemisation equilibrium,

$$\Lambda \underset{k_{-1}}{\overset{k_1}{\rightleftharpoons}} \Delta$$

and assuming the rate constants for enantiomeric interconversion between the enantiomers are equal ($k_1 = k_{-1} = k$), the rate of interconversion can be written as follows.

$$\frac{-\mathrm{d}[\ ]}{\mathrm{d}} = [\ ] - [\ ]$$

$$\frac{1}{[\ ] - [\ ]}\,\mathrm{d}[\ ] = -\ \mathrm{d}$$

An integrated rate law can be derived accordingly, since $[\Delta] = [\Lambda]_0 - [\Lambda]$.

$$\int_{[\ ]_0}^{[\ ]} \frac{1}{2[\ ] - [\ ]_0}\ [\ ] = \int_0 -\ \mathrm{d}$$

$$\frac{1}{2}\ln(2[\ ] - [\ ]_0) - \frac{1}{2}\ln(2[\ ]_0 - [\ ]_0) = -$$

$$\ln\left(\frac{2[\ ] - [\ ]_0}{[\ ]_0}\right) = -2$$

$$\ln\frac{[\ ]_0}{2[\ ] - [\ ]_0} = 2$$

By plotting $\ln\frac{[\ ]_0}{2[\ ]-[\ ]_0}$ against *t*, a linear correlation can be obtained with a gradient of 2*k*. An additional parameter, the half-life for racemisation, can be determined. It is defined as the time required for an enantiomeric excess (ee) of 50% to be reached.

$$^{1}/_{2} = \frac{\ln 2}{2}$$

This approach was used for the analysis of the rate of racemisation of **Ş-[Eu.L^3]** in acetonitrile, methanol, and 20% water in methanol, (Figure 5.6). Attempts to look at the kinetics in pure water were stymied by slow precipitation of the unprotonated complex, so a water/methanol mixture was used to avoid this happening.

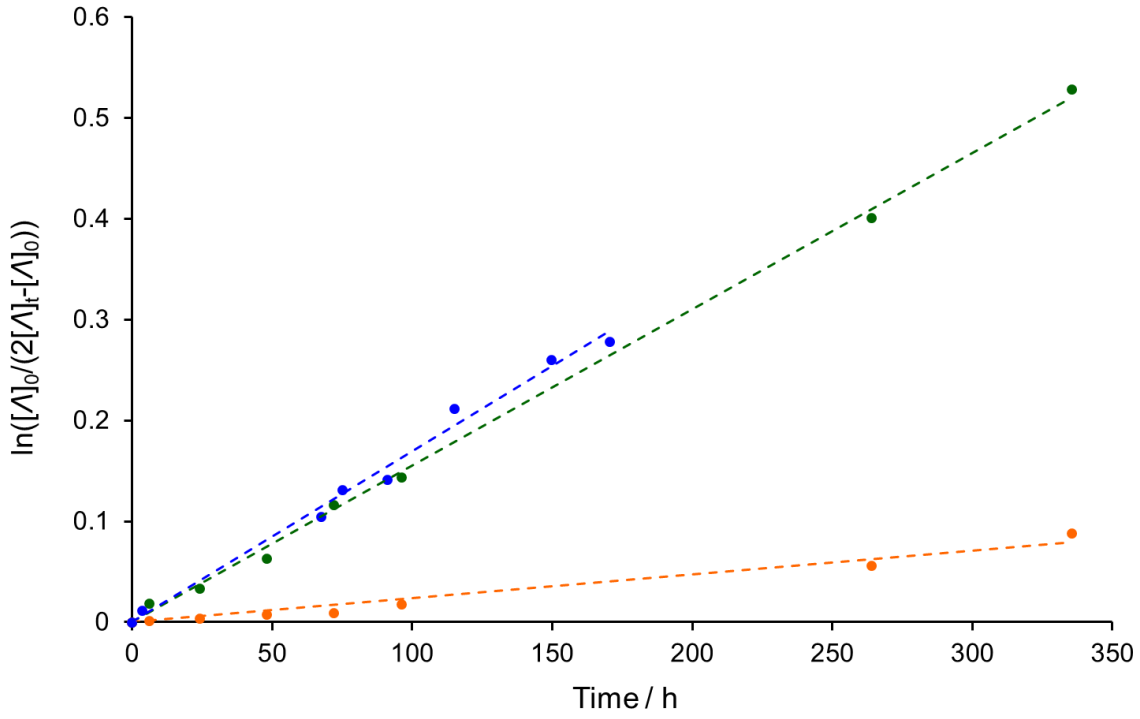

Figure 5.6. Kinetic plots of the rate of interconversion of enantiomers for **[Eu.L^3]** at 60 ºC in various solvents (*green*, *orange*, and *blue* data points correspond to acetonitrile, methanol, and methanol/water (4:1), respectively).

Analysis of the experimental data using the described mathematical treatment allowed the solvent dependence of the rate of enantiomeric interconversion to be probed. The half-lives for racemisation of **ş-[Eu.L^3]** in methanol and acetonitrile (orange and green plots, respectively) were found to be 3466 ± 10 and 462 ± 10 hours, respectively, at 60 ºC. Even for the smallest value in acetonitrile, the half-life is of the order of days. In pure methanol solvent, the half-life for racemisation approaches 0.4 years. Thus, a significant decrease in half-life on changing solvent from methanol to acetonitrile was observed.

The process of enantiomer interconversion for these complexes involves cooperative arm rotation, inversion of the macrocycle ring, and inversion of the configuration at each of the phosphorus atoms of the phosphinate donor groups. In order for the enantiomer to interconvert, there is a requirement for the sequential breaking of the bonds from the phosphinate oxygen to europium and for the complex to pass through a transient charged intermediate, where the coordination number of the europium is unsatisfied, and a short-lived ion pair exists. The order of magnitude difference in $t_{1/2}$ for enantiomer interconversion in **[Eu.L^3]** between methanol and acetonitrile clearly

suggests that the nature of the solvent influences this process in some manner. Given that the racemisation is a thermally activated process, it is prudent to consider the potential impact solvent could have on the energies of the ground or the transient state, thereby altering the activation energy barrier for the dissociative step that leads to inversion at the phosphorus centre. Stabilisation, or conversely destabilisation, of either state will modulate the overall energy barrier for the process, hence affecting the rate.

Whilst the water solubility of the complex **[Eu.L^{3}]** has been demonstrated,[6] issues with solubility were encountered on prolonged heating of the complex in water. It was, however, found that the solubility of the complex was sufficient in a water/methanol solution (1:4 by vol.) with heating over time. The value of $t_{1/2}$ was calculated in this medium and reduced to 408 ± 8 hours. This value is comparable to that obtained with acetonitrile. A tentative rationale for this decrease is that the addition of water assists the dissociative process through the stabilisation of the transient ion pair in the transition state, *e.g.* via hydrogen bonding or specific solvation. Water molecules are also efficient at coordinating to europium and are capable in this case of completing the coordination sphere about the europium ion, thereby lowering the energy of the transition state leading to its formation.

Values of half-lives for other methyl-substituted phosphinate europium(III) complexes (Figure 5.7) have been reported earlier, (Table 5.1).[5,7] Examination of the solvent effect on $t_{1/2}$ has not previously been investigated. Further, the available data is somewhat limited due to low solvent solubility of some complexes, *e.g.* the complex **[Eu.L^{14}]** is not water soluble, whereas **[Eu.L^{13}]** is soluble.

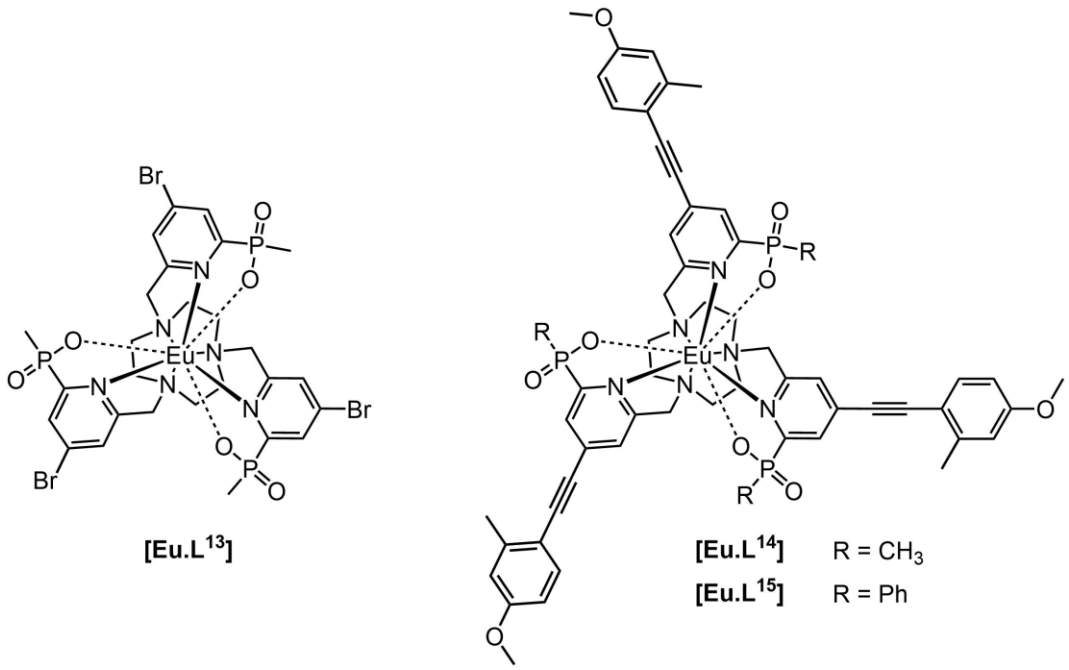

Figure 5.7. Structures of europium(III) complexes for which racemisation kinetics have been reported.

Table 5.1. Summary of the half-lives for racemisation, $t_{1/2}$, for triphosphinate europium(III) complexes in varying solvent systems.

Complex	$t_{1/2}$ / h			
	Methanol	Acetonitrile	20% Water/Methanol	Water
[Eu.L^{3}]	3466 (10)	462 (10)	408 (8)	-
[Eu.L^{13}]	-	-	-	74 (8)
[Eu.L^{14}]	180 (10)	-	-	-
[Eu.L^{15}]	>10^{5} [a]	-	-	-

Errors are given in parentheses. [a] No evidence for racemisation after 430 hours.

The smallest $t_{1/2}$ value was obtained for **[Eu.L^{13}]**[7] in water, in line with the earlier tentative hypothesis that water promotes the racemisation process. Additionally, this complex does not possess extended chromophore antennae, and so does not benefit from an enhanced ligand dipole which occurs in complexes such as **[Eu.L^{3}]**. In such extended systems, polarisation and subsequent enhancement of the Eu-N_{py} bond strength is expected to inhibit dissociation of the Eu-N_{py} bond and limit the rate of arm rotation.

Related to this aspect, three cationic triazacyclononane-based europium(III) complexes were prepared in other work.[8-9] Here, analogues of the parent amide complex, **[Eu.L^{16}]**, were synthesised by preparation of the *para*-bromo analogue, followed by exchange of the bromo substituent with NMe_2 via nucleophilic aromatic substitution.

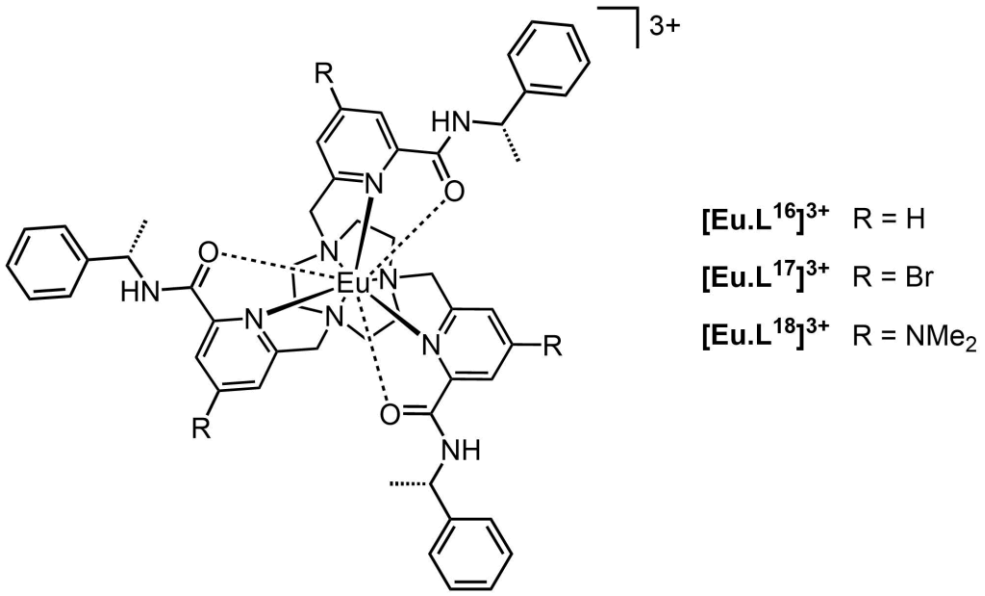

Figure 5.8. Structures of three cationic 9-N_3 europium(III) complexes, **[Eu.L$^{16\text{-}18}$]$^{3+}$** (R = H, Br, NMe_2, respectively).

Crystals of **[Eu.L$^{16\text{-}18}$]X_3** were grown from methanol, where X is a counter anion such as triflate or bromide, and a crystallographic analysis undertaken in each case. The europium ion is coordinated by the three N atoms of the triazacyclononane ring, each pyridyl N atom, and the O atoms of the amide to give a coordination number of nine. On analysis of the lanthanide-donor bond lengths, it is evident that there is no variation in the length of the Eu-O and Eu-N_{ring} bonds with the identity of the *para* substituent, (Table 5.2). Whilst there is no change in the Eu-N_{py} bond length on introducing the bromo group into the *para* position, it decreases by 0.05 Å on substitution with the NMe_2 group. Introduction of the NMe_2 group generates a significant charge transfer transition, confirmed by the appearance of a broad absorption band at 348 nm. This CT interaction results in a shortening of the Eu-N_{py} bond length with concomitant enhancement of the bond strength, offering insight into the earlier discussion.

Table 5.2. Selected mean distances of ligand donor atoms to the lanthanide ion (Å, ±<0.01) for **[(*S*)-*q*(///)-Eu.L$^{16\text{-}18}$]X$_3$** (X = counter anion).

Bond	**[Eu.L^{16}]X$_3$**[a]	**[Eu.L^{17}]X$_3$**[b]	**[Eu.L^{18}]X$_3$**[b]
Eu-O	2.41	2.41	2.41
Eu-N_{py}	2.57	2.57	2.52
Eu-N_{ring}	2.63	2.63	2.63

Complexes of L^{17} and L^{18} were crystallised as the simple triflate salt in R3, and L^{16} as the mono-triflate-dibromide in P21. [a] Ref. [8]. [b] Ref. [9].

The complex **[Eu.L^{14}]** differs structurally from **[Eu.L^{3}]** in the functionalisation of the aryl groups of the antennae. Despite this modest structural variation (*o*-methyl *vs. m*-diethylamino), a significant decrease of the half-life from 3466 to 180 hours was observed in methanol.

Notably, the identity of the substituent at the phosphorus stereogenic centre has a dramatic impact on the rate of racemisation. Exchange of the methyl substituent at the phosphorus for a phenyl ring (**[Eu.L^{14}]** *vs.* **[Eu.L^{15}]**) significantly increases the activation barrier to racemisation.[5] Indeed, no discernible evidence for racemisation was observed with heating at 60 ºC in methanol after 430 hours. This behaviour can be attributed to the enhanced rigidity of the complex and greater steric bulk of the phenyl group *vs.* a methyl group (A values are 12 and 7.4 kJ mol^{-1}, respectively) disfavouring epimerisation at the phosphorus centre. In related work on 9-N_3 triphosphinate complexes, DFT calculations carried out with a phenylphosphinate yttrium complex suggests that P-phenyl groups have a strongly preferred geometry that directs the phenyl ring away from the macrocyclic ring.[10] Movement away from this preferred geometry can be expected to disfavour racemisation.

Clearly, further study is required to elucidate these findings further, *e.g.* by acquiring additional $t_{1/2}$ data for complexes across different solvents, such as **[Eu.L^{15}]** in other non-aqueous media, to allow for comparison and trends to be established. Despite this, it is evident that two significant conclusions may be drawn. It has been shown that the nature of the solvent has a pronounced effect on racemisation kinetics. Also, the nature of the substituent at the phosphorus atom (Me *vs.* Ph) and the strength of the Ln-N_{py} bond may also have an influence.

Additionally, examination of the effect of photo-irradiation on racemisation kinetics may be of interest. Other work has shown the impact of photo-irradiation on the integrity of

the coordinating bonds within europium(III) complexes, *e.g.* in labilising the Eu-N_{py} bond.[11] It is hypothesised that photo-irradiation of the heated solution may increase the rate of racemisation in a given solvent.

5.4. Solvatochromism Studies

The term solvatochromism was originally introduced by Hantzsch to refer to the well-documented phenomenon where changes in the UV-Vis and NIR absorption spectra of chemical species were brought about by variation of the solvent.[12] Now, the term solvatochromic effect is used more broadly to refer to the reversible change in spectral characteristics of a species induced by variation in the energy difference between the ground and first excited states as a result of the local solvent. Typically, these changes are observed in the λ_{max} value, intensity of bands/transitions, and/or general shape of spectral profiles, *e.g.* in absorption or emission spectra.

This phenomenon arises from the existence of both electron-donating and electron-withdrawing moieties and their mutual conjugation within a molecule, creating a local dipole moment. Excitation of such species generates an instant charge separation in the excited state, where the associated energy of this highly polar state is highly sensitive to changes in the polarity of the surrounding environment, *i.e.* the solvation ability of the medium.

Reichardt's empirical spectroscopic scale of solvent polarity is widely used and has been accepted as a standard method of ordering solvents by polarity. For this scale, a betaine dye with a longest wavelength intramolecular CT absorption band is utilised as a standard, (Figure 5.9).[13] This dye possesses a significant permanent dipole moment (*ca.* 15 Debye) as a result of the charge separation within the molecule, and the visible absorption of the species is highly solvatochromic, suitable as a solvent-dependent reference.

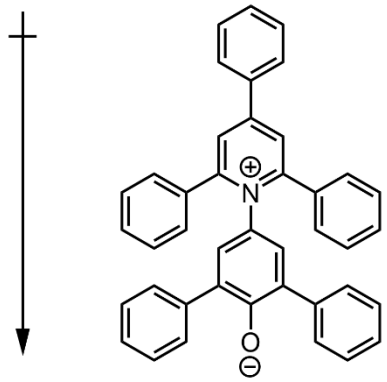

Figure 5.9. Molecular structure of the betaine dye (2,6-diphenyl-4-(2,4,6-triphenylpyridinium-1-yl)phenolate) used as a solvatochromic standard in the determination of $E_T(30)$ values.

The $E_T(30)$ scale ascribes a value to a solvent pertaining to the molar transition energy of the standard betaine dye in that particular solvent, at room temperature and atmospheric pressure. This $E_T(30)$ value is estimated using the equation:

$$(30) = \quad \tilde{}_{max\ A} = 28591(\ _{max})$$

The values yielded by this equation are in kilocalories per mole (1 kcal = 4.184 kJ) and a dimensionless normalised scale has since been introduced, where water and tetramethylsilane have $^{N}_{T}$ values of 1.00 and 0.00, respectively:

$$^{N}_{T} = \frac{[\ _T(\text{solvent}) - \ _T(\text{TMS})]}{[\ _T(\text{water}) - \ _T(\text{TMS})]} = \frac{[\ _T(\text{solvent}) - 30.7]}{32.4}$$

Table 5.3. A summary of the normalised solvent polarity parameters for the solvents used within this work.	
Solvent	Reichardt solvent polarity parameter,[14]
Water	1.000
2,2,2-Trifluoroethanol (TFE)	0.898
Methanol (MeOH)	0.762
Ethanol (EtOH)	0.654
Isopropanol (^{i}PrOH/IPA)	0.546
Acetonitrile (MeCN)	0.460
Dimethylsulfoxide (DMSO)	0.444
N,N-Dimethylformamide (DMF)	0.404
Tert-butanol (^{t}BuOH)	0.389
Dichloromethane (DCM)	0.309
Chloroform	0.259

Previous work has examined the solvatochromic effect with macrocyclic europium(III) complexes, (Figure 5.10). Study of the complex **[Eu.L^{19}]** across ten different solvents was possible ($\frac{N}{T}$ value ranging from 0.259 to 0.898), owing to the presence of the phenyl substituent and the associated solubility increase in organic solvents.[5] The absorbance, total emission, and circularly polarised emission were examined as a function of solvent polarity and solvatochromism was observed in each instance. Notably, significant changes were observed in the spectral form of the **[Eu.L^{19}]** emission, in particular the hypersensitive $\Delta J = 2$ and $\Delta J = 4$ manifolds. Closer inspection of the variation in intensity ratios and energies of the transitions within these manifolds allowed for trends to be identified. As part of a separate study with the cyclen-based complex **[Eu.L^{20}]**, the absorption, total emission, and excitation spectra were inspected over a smaller range of solvents.[15-16] Here, both the absorption and excitation spectra were found to be insensitive to change in solvent polarity, whilst the intensity of europium emission was strongly dependent.

Other work has probed the solvatochromic effect with complexes of non-macrocyclic chelating ligands. For example, others have examined the variation of the UV-Vis absorption, total emission, and quantum yield of the complex **[Eu.L^{21}]** with solvent polarity.[17] Unfortunately, in this case, the coordination environment of the europium

ion is changed by more polar solvents with increasing solvent nucleophilicity, leading to the displacement of the tridentate dipyrazolyltriazine ligand possessing the ICT band. Thus, the validity and integrity of any meaningful conclusions are confounded by the lack of clarity concerning the europium complex speciation in different solvents. It is noted that here, interestingly, the emission lifetime of the $^5D_0$-$^7F_2$ transition was observed to vary with solvent polarity, contrary to the study of **[Eu.L^{19}]**. This variation of emission lifetime, however, is likely to be associated with the changing coordination environment about the europium ion. Solvatochromism effects for a series of p-conjugated tris-dipicolinate europium complexes bearing PEG groups have also been investigated in UV-Vis and emission over a number of chlorinated solvents.[18] Here, the variation of the CT energy level separation with solvent polarity was also demonstrated.

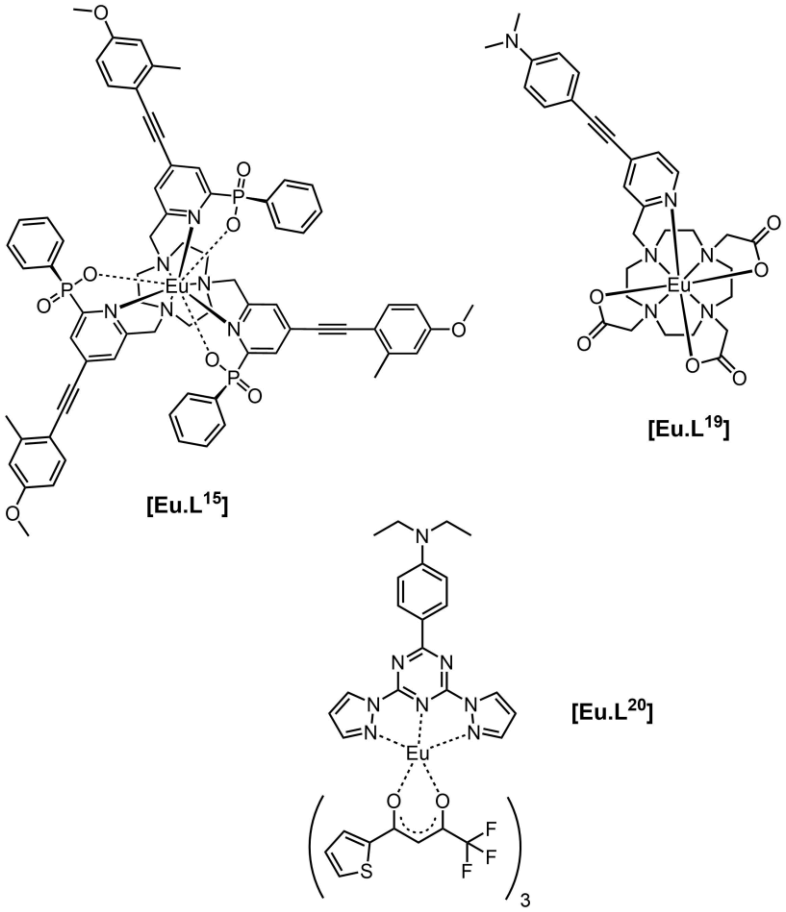

Figure 5.10. Europium(III) complexes exhibiting solvatochromism.

The behaviour of the europium complex **[Eu.L^3]** across a series of eleven solvents was studied, with $\frac{N}{T}$ values ranging from 0.259 to 1.000, (Table 5.3). The pH sensitivity of this complex is known and has already been discussed, as well as the

variation of the photophysical properties on acidification (chapter two). Thus, the complex was studied in each solvent before and after the addition of TFA in order to probe the solvatochromism of the “neutral” and protonated species.

a) Absorption Spectral Behaviour

The absorption spectrum of **[Eu.L^3]** in the absence of acid was found to be highly solvent dependent, with increasing solvent polarity resulting in a hypsochromic shift in $/_{max}$ of 30 nm, from 350 nm in chloroform (28,570 cm^{-1}) to 320 nm in water (31,250 cm^{-1}). Plotting the inverse of $/_{max}$ (*i.e.*, its frequency) against the normalised Reichardt polarity parameter, $\frac{N}{T}$, resulted in a positive linear correlation, (R^2 = 0.98, Figure 5.11). This behaviour is termed *negative* solvatochromism, with the more polar solvents stabilising the ground state more than the excited state. On addition of TFA, however, very similar absorption spectra were obtained in every solvent examined, where the overall intensity was observed to increase with a corresponding hypsochromic shift in $/_{max}$ to 320 – 324 nm.

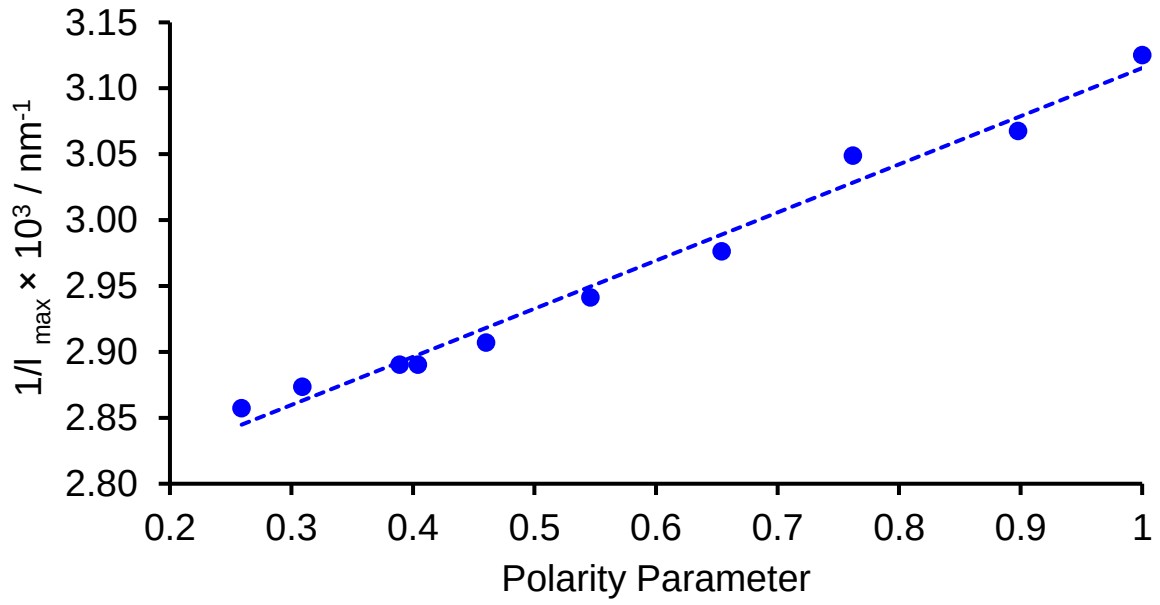

Figure 5.11. Negative solvatochromism exhibited by **[Eu.L^3]**, comparing the absorption band frequency to the the normalised Reichardt polarity parameter (R^2 = 0.983).

b) Emission Spectral Behaviour

On inspection of the normalised total emission spectrum, variation in the spectral form of **[Eu.L^3]** with solvent polarity was observed both prior to and following the addition of TFA, particularly in the energy splitting and relative intensity ratios of the transitions within the hypersensitive Δ*J* = 2 and Δ*J* = 4 manifolds, (Figure 5.12).

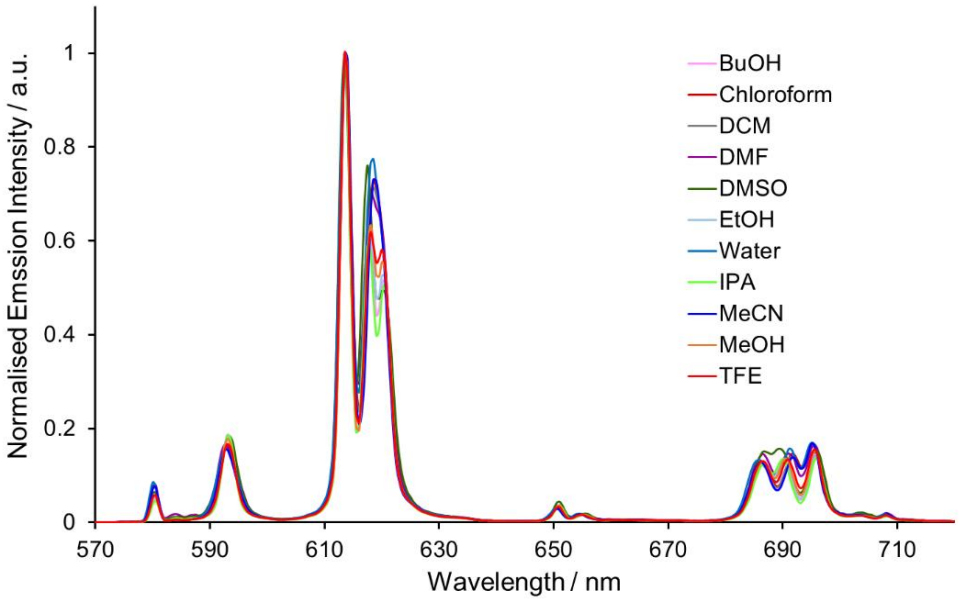

Figure 5.12. Total emission spectra of **[Eu.L^3]** in various solvents after addition of TFA (295 K, excitation at the absorption maximum value in each solvent).

The solvatochromic effect was observed to be most prominent in the Δ*J* = 2 manifold prior to the addition of TFA. In the absence of acid, the quenching of emission by PeT is more significant, and the strength of the luminescence signal becomes dependent on the pK_a value for **[Eu.L^3]** that may vary somewhat for each solvent. Despite a weaker signal strength in some solvents (DMSO, methanol, and ethanol), the intense nature of the hypersensitive Δ*J* = 2 band allowed for analysis of the “neutral” species in most solvents.

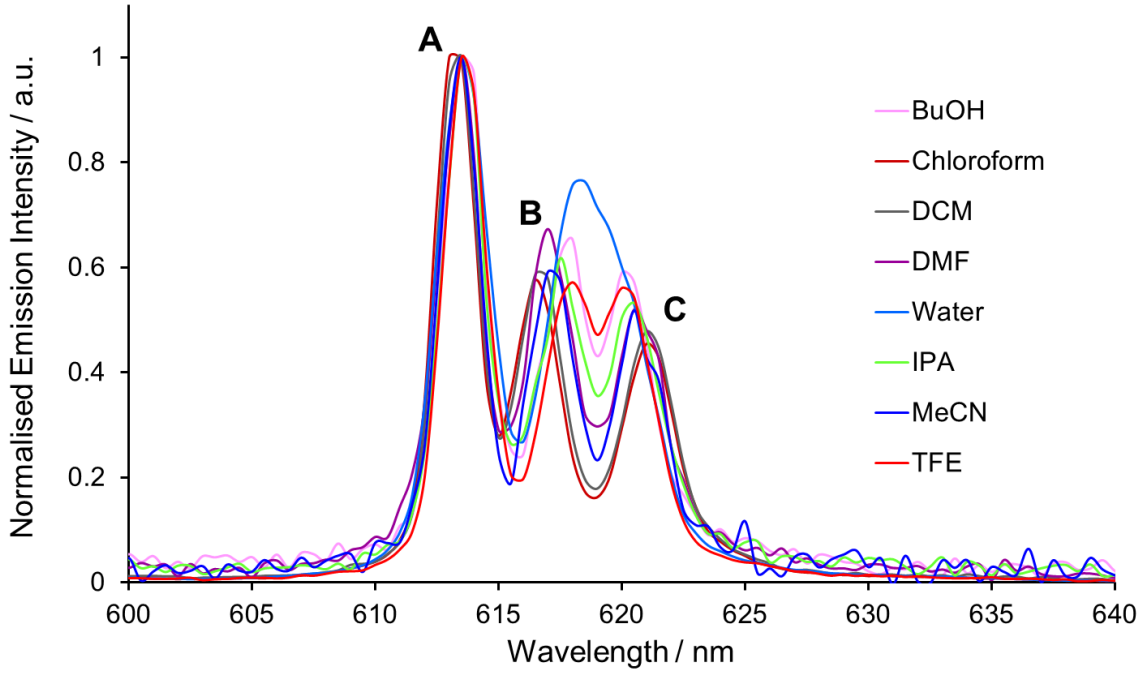

Figure 5.13. Expanded emission spectra of **[Eu.L^3]** in various solvents, showing the Δ*J* = 2 manifold. Spectra for DMSO, methanol, and ethanol are excluded for clarity. Transitions are labelled as described in the text.

The strongest transition in the Δ*J* = 2 manifold (component A, at shortest wavelength, Figure 5.13) showed minimal variation in the energy of the transition, whilst the two longer wavelength transitions (components B and C) show variation in both their intensity and energy as a function of solvent polarity. On inspection of the intensity of the transitions, a clear trend relating to solvent polarity was not apparent. This conclusion was confirmed by considering the different intensity ratios between the three components (A *vs.* B, A *vs.* C, and B *vs.* C) as a function of solvent polarity. Again, the absence of any significant correlation was evident, (Figure 5.14).

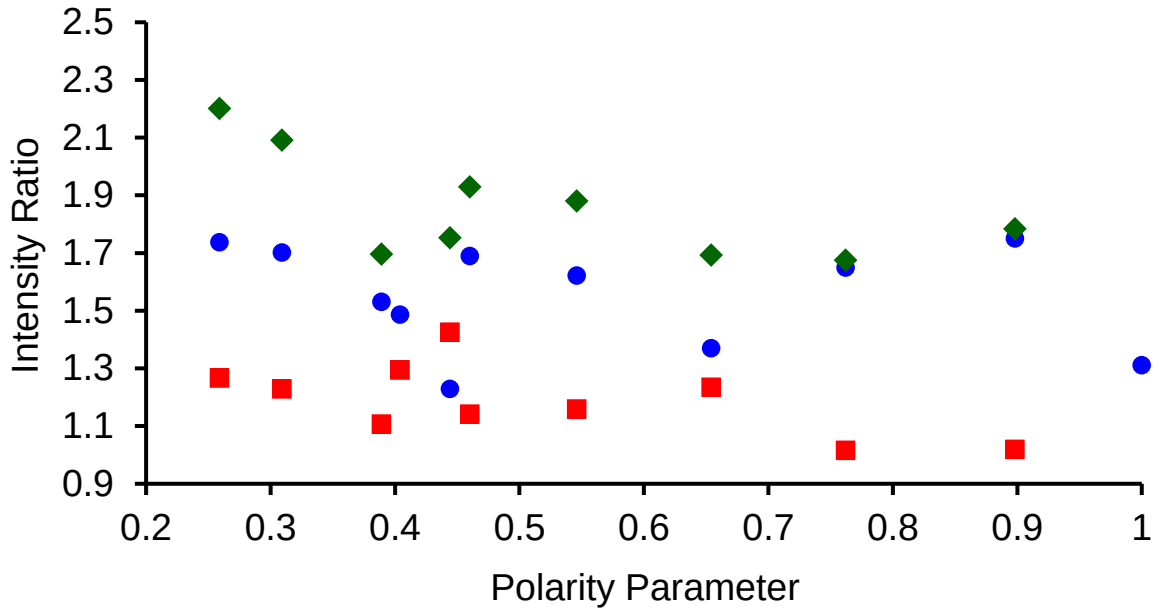

Figure 5.14. Ratios of the intensity of the emissive transitions A *vs.* B (*blue*), A *vs.* C (*green*), and B *vs.* C (*red*) for **[Eu.L^3]** as a function of the normalised Reichardt polarity parameter.

On considering the *difference* in energies of these transition components with solvent polarity, however, a strong negative correlation (positive solvatochromism) was obtained, (Figure 5.15). With increasing solvent polarity from chloroform to water, the energy difference between the B and C components decreased. In other words, the degree of splitting, *i.e.* the relative energies of the m_J sub-levels in the $^7F_2$ manifold, increased as the solvent polarity is decreased.

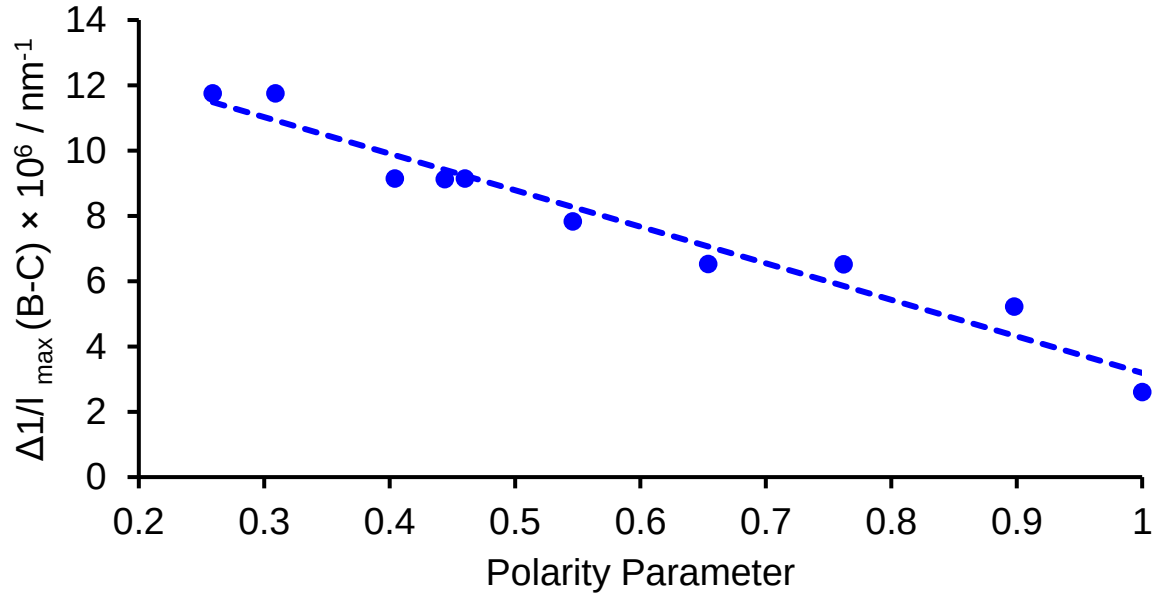

Figure 5.15. Plot of the difference in inverse wavelength of the B and C emissive transitions as a function of the normalised Reichardt polarity parameter (R^2 = 0.953).

The spectral form of the Δ*J* = 2 manifold is observed to change considerably with solvent polarity. This variation in spectral form is illustrated examining the Stark splittings of the $^7F_2$ manifold in both water and non-polar chloroform, (Figure 5.16). Whilst theoretically five Stark sub-levels exist in the $^5D_0 \rightarrow {}^7F_2$ transition, in practice only three are observed here, presumably due to some being forbidden.[19]

These three levels are more evident on examining the Δ*J* = 2 manifold in the CPL spectrum, (Figure 5.4).

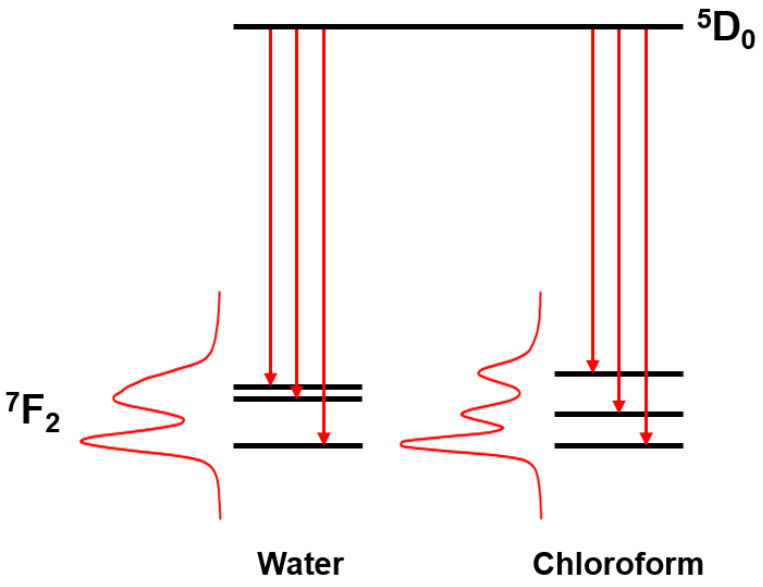

Figure 5.16. Representation of the change in the Stark splittings of the $^7F_2$ manifold in water and chloroform ($\frac{N}{T}$ = 1.000 and 0.259, respectively, 298 K, λ_{exc} at the absorption maximum).

Analysis of the Δ*J* = 4 manifold in the absence of acid proved more problematic due to the low signal strength and high signal-to-noise ratio. Some variation in the relative intensity and energy of the components (D, E, and F) was also evident following the addition of acid, where signal strength is not an issue, (Figure 5.17). Accordingly, the Δ*J* = 4 manifold was examined for **[Eu.L^3]**, following protonation by TFA in each solvent.

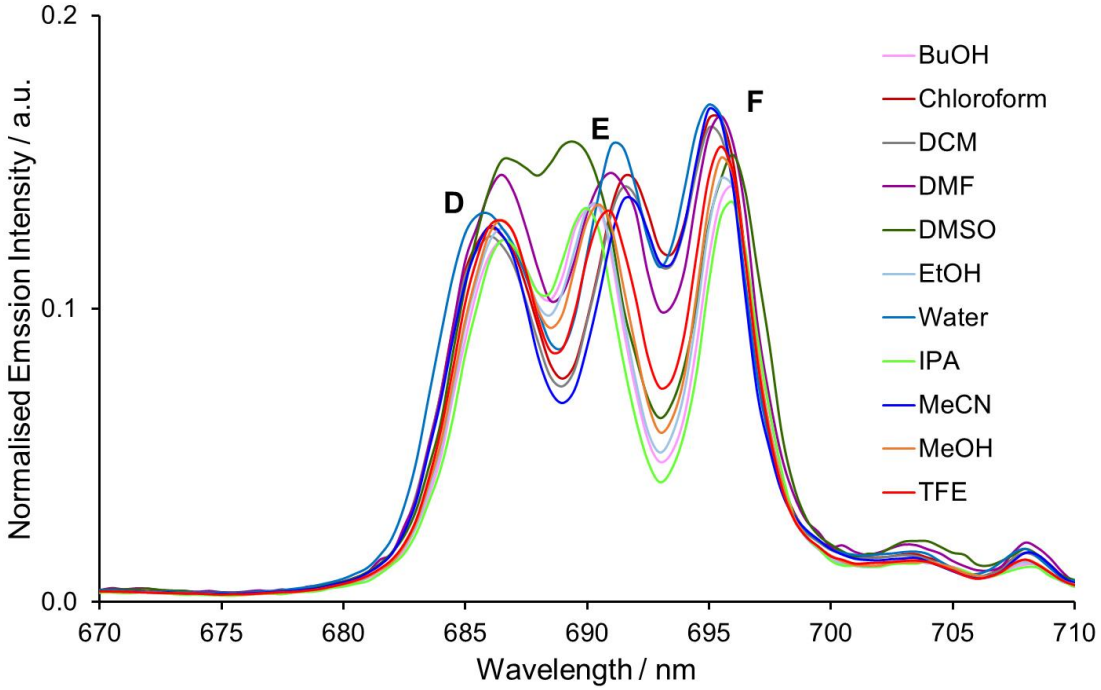

Figure 5.17. Expanded emission spectra of **[Eu.L^3]** in various solvents following addition of TFA, showing the Δ*J* = 4 manifold. Transitions are labelled as described in the text.

In each solvent, three components (D, E, and F) were identified within the Δ*J* = 4 manifold, (Figure 5.17). On examination of the change in the respective intensity ratios of these components with solvent polarity, no discernible trend was evident, (Figure 5.18). A similar result was found for the energies of the manifold components.

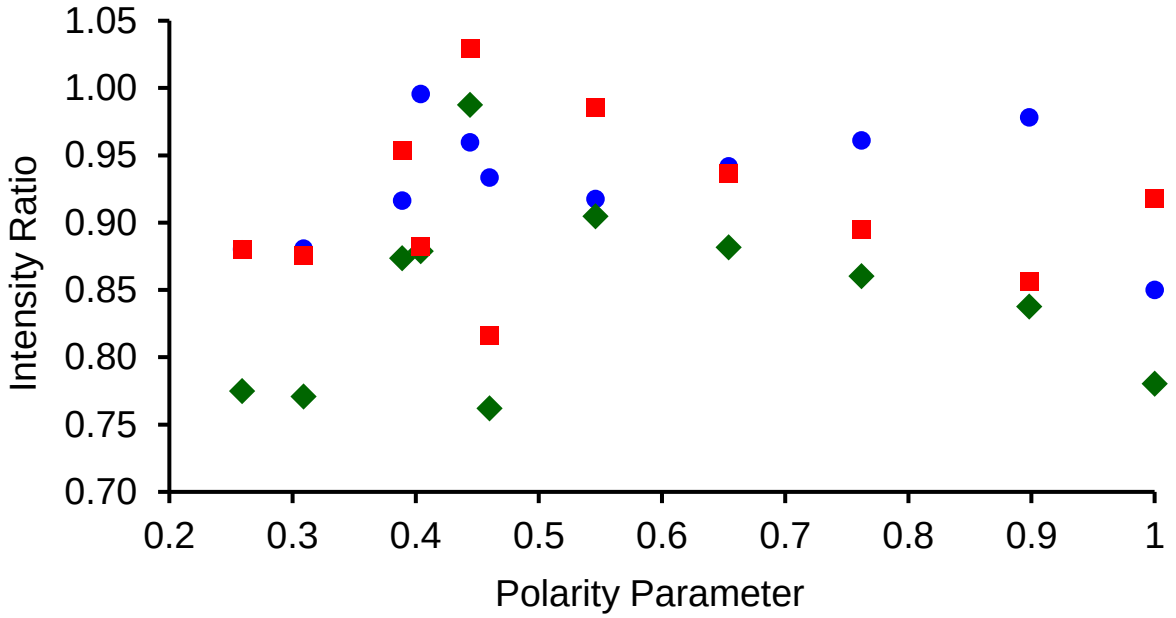

Figure 5.18. Ratios of the intensity of the emissive transitions D *vs.* E (*blue*), D *vs.* F (*green*), and E *vs.* F (*red*) for **[Eu.L^3]** as a function of the normalised Reichardt polarity parameter.

5.5. Conclusions

Resolution of the *Δ* and *Λ* enantiomers of the racemic europium(III) complex **[Eu.L^3]** has been achieved by chiral HPLC, with an impressive separation of over 20 minutes using a CHIRALPAK-ID column and an isocratic methanol eluent. The CPL behaviour of these resolved enantiomers and their response to pH variation was probed at different pH values. A strong 'switching-on' of the CPL intensity was observed on acidification from pH 8 to pH 4, mirroring the total emission response observed previously (chapter 2). Particularly good resolution of the Δ*J* = 4 manifold in this case allowed for the five major transitions to be resolved.

In light of previous work, the effect of additives on the CPL and total emission intensity of **[Eu.L^3]** was studied, whereby the interaction with several biological serum proteins was examined. No variation in either the CPL or total emission intensity was observed following addition of excess α_1-AGP, HSA, or BSA. A preliminary experiment probing the possibility of forming a diastereoisomeric acid-base pair was also carried out, involving the addition of both the *R* and *S* forms of the chiral acid Trolox to **ȿ-[Eu.L^3]** in acetonitrile. Here, no notable differences in the CPL or total emission intensity were observable.

The kinetics of enantiomeric interconversion for **[Eu.L^3]** were assessed across a small number of different solvents at 60 ^{o}C, using a mathematical kinetic relationship derived in earlier work. The half-life for racemisation for **[Eu.L^3]** was determined to vary significantly with solvent ($t_{1/2}$ = 3466 ± 10, 462 ± 10, and 408 ± 8 in methanol, acetonitrile, and 20% water in methanol, respectively). Comparison of these $t_{1/2}$ values with those of other triphosphinate europium(III) examples allowed some preliminary conclusions to be drawn. It is evident that the nature of the solvent can affect the activation energy barrier for dissociation of the Eu-O bond, through its stabilisation or destabilisation of the ground or transient state. In the case of water, stabilisation of the transient state by hydrogen bonding and solvent coordination following dissociation is proposed. Comparison with previous examples suggests that the rate of enantiomeric conversion can also be affected by other factors, such as the strength of the Eu-N_{py} bond. Additionally, functionalisation at the stereogenic phosphorus centre, where epimerisation must occur, with sterically demanding groups (*e.g.* phenyl) dramatically disfavours the racemisation process.

Finally, the solvatochromic effect was explored with **[Eu.L^3]** by examining the absorption and total emission spectral behaviour over a series of eleven solvents of differing polarity ($\frac{N}{T}$ = 0.259 – 1.000). This study was performed both with and without the addition of TFA, to allow the protonated and neutral species to be investigated, respectively. Clear negative solvatochromism was exhibited in the absorption spectral form in the absence of TFA (*i.e.*, the separation of the ground and excited states increased as solvent polarity increased), and a linear positive correlation (R^2 = 0.98) was determined on plotting the inverse of λ_{max} (a frequency term) against the normalised Reichardt polarity parameter. This is consistent with a larger dipole moment in the ICT ground state electronic structure. Likewise, positive solvatochromism was identified by considering the difference in $(\lambda_{max})^{-1}$ between two varying components within the ΔJ = 2 manifold, as a function of solvent polarity.

Thus, well-defined solvatochromic effects are apparent for the neutral europium(III) complex both in absorption and europium emission spectra. Such behaviour is consistent with the involvement of a low energy ICT state in the former case, as suggested by the mechanistic studies discussed in chapter two. In the latter case, there must be an important solvent effect on the degree of dipolar solvation of the Eu $^7F_2$ energy levels, associated with a strong electrostatic interaction between the

induced dipole on the ligand extended pyridyl moiety and the lanthanide quadrupole moment.[20-21]

A similar rationale has also been put forward to explain the exquisite sensitivity of the paramagnetic NMR pseudocontact shift to solvent variation with a class of TACN coordination complexes that possess small ligand field splittings.[22]

5.6. References

[1] A. T. Frawley, H. V. Linford, M. Starck, R. Pal and D. Parker, *Chem. Sci.*, 2018, **9**, 1042–1049.

[2] A. T. Frawley, R. Pal and D. Parker, *Chem. Commun., 2016,* **52**, 13349–13352.

[3] S. Shuvaev, E. A. Suturina, K. Mason and D. Parker, *Chem. Sci.*, 2018, **9**, 2996–3003.

[4] E. R. Neil, PhD Thesis, Durham University, 2015.

[5] A. T. Frawley, PhD Thesis, Durham University, 2017.

[6] M. Starck, J. D. Fradgley, R. Pal, J. M. Zwier, L. Lamarque and D. Parker, *Chem. Eur. J.*, 2021, **27**, 766–777.

[7] N. H. Evans, R. Carr, M. Delbianco, R. Pal, D. S. Yufit and D. Parker, *Dalton Trans*., 2013, **42**, 15610–15616.

[8] N. Bolier, MChem Thesis, Durham University, 2019.

[9] E. R. Neil, A. M. Funk, D. S. Yufit and D. Parker, *Dalton Trans*., 2014, **43**, 5490–5504.

[10] M. Soulié, F. Latzko, E. Bourrier, V. Placide, S. J. Butler, R. Pal, J. W. Walton, P. L. Baldeck, B. Le Guennic, C. Andraud, J. M. Zwier, L. Lamarque, D. Parker and O. Maury, *Chem. Eur. J*., 2014, **20**, 8636–8646.

[11] H. Li, R. Lan, C.-F. Chan, L. Jiang, L. Dai, D. W. J. Kwong, M. H.-W. Lam and K.-L. Wong, *Chem. Commun.*, 2015, **51**, 14022–14025.

[12] C. Reichardt, *Chem. Rev.*, 1994, **94**, 2319–2358.

[13] C. Reichardt, *Green Chem.*, 2005, **7**, 339–351.

[14] C. Reichardt, Solvents and Solvent Effects in Organic Chemistry, VCH, Weinheim, 1988.

[15] S. V. Shuvaev, PhD Thesis, Durham University, 2017.

[16] S. Shuvaev, R. Pal and D. Parker, *Chem. Commun.*, 2017, **53**, 6724–6727.

[17] W.-S. Lo, W.-T. Wong and G.-L. Law, *RSC Adv.*, 2016, **6**, 74100–74109.

[18] A. D'Aléo, A. Picot, A. Beeby, J. A. G. Williams, B. Le Guennic, C. Andraud and O. Maury, *Inorg.* Chem., 2008, **47**, 10258–10268.

[19] K. Binnemans, *Coord. Chem. Rev.*, 2015, **295**, 1–45.

[20] S. F. Mason, R. D. Peacock and B. Stewart, *Molecular Physics,* 1975, **30**, 1829–1841.

[21] S. F. Mason, *The ligand polarization model for the spectra of metal complexes: The dynamic coupling transition probabilities*, In *Electrons and Transitions*, Springer, 1980, 43–81.

[22] K. Mason, A. C. Harnden, C. W. Patrick, A. W. J. Poh, A. S. Batsanov, E. A. Suturina, M. Vonci, E. J. L. McInnes, N. F. Chilton and D. Parker, *Chem. Commun.*, 2018, **54**, 8486–8489.

CHAPTER SIX

Conclusions and Future Work

Chapter Six: Conclusions and Future Work

A detailed summary of the findings within this thesis can be found at the conclusion of each chapter. Additionally, designs for further work are discussed, where relevant, within the text. For clarity, these conclusions and opportunities for further work are summarised below.

6.1. General Conclusions

At the outset of this work, we set out to design and synthesise a luminescent europium(III) complex suitable for the monitoring of GPCR internalisation. A series of criteria was identified to which a successful probe must conform to be viable for this purpose; these properties are specified below:

i. **Appropriate pH responsive luminescent behaviour**
ii. **Long luminescence lifetime**
iii. **Suitable absorption wavelength**
iv. **High brightness**
v. **Defined speciation**
vi. **Low toxicity**
vii. **High complex stability**
viii. **High aqueous solubility**
ix. **Suitable linker for conjugation**
x. **Negligible non-specific binding**

With these criteria and previous work in mind, a parent series of target complexes, **[Eu.L$^{1\text{-}3}$]**, was prepared, devoid of a point of conjugation in the pursuit of the desired photophysical properties. The complexes **[Eu.L$^{1\text{-}3}$]** consist of a 1,4,7-triazacyclononane macrocyclic ring bearing three pyridyl methylphosphinate chelating groups, affording a nine coordinate ligand to satisfy the europium(III) coordination sphere. The 4-position of the pyridyl moieties is functionalised with either a hydrogen or substituted alkynylaryl sensitising group, and the complexes **[Eu.L$^{1\text{-}3}$]** vary in their number of extended antennae (one to three, respectively). The pH sensitivity of luminescence is induced through incorporation of an amine functionality in the *ortho*

position of the peripheral aryl group of the antenna. This responsive mechanism was designed to arise through the quenching of an excited state by PeT transfer, which is only possible when the amine is unprotonated. The desired pH limits of the luminescence response (*i.e.* at what pH values the luminescence of the probe is switched on or switched off/quenched) may be controlled by appropriate functionalisation of the amine group; a *N,N*-diethylamino group is used in **[Eu.L$^{1\text{-}3}$]**.

The complexes **[Eu.L$^{1\text{-}3}$]** displayed the desired pH responsive behaviour with significant increases in europium emission intensity observed (540, 560, and 560-fold increase, respectively) on changing from pH 8 to 4 in 0.1 M NaCl. An associated increase in europium emission lifetime of 120, 200, and 240% over the same pH change was also recorded. The long-lived nature of the europium lifetime at low pH allows the use of time-gated measurements. Here, modulation of the length and timing of the acquisition window was demonstrated to produce enhancements of the emission 'switching on' ratio of between 250 and 1300, boding well for applications in biological environments. The use of the highly conjugated pyridylalkynylaryl antennae allows efficient sensitisation of the europium(III) ion with excitation in the range 320 – 355 nm, and results in high molar absorptivities, increasing with the number of antennae (e = 60,000 M^{-1} cm^{-1} for **[Eu.L^{3}]**, pH 4, λ_{exc} 331 nm). Coupled with the reasonable quantum yields recorded for these complexes at pH in the absence of quenching (F = 17.0 – 17.6%), an appreciable brightness value was obtained for **[Eu.L^{3}]** (B = 10,200 M^{-1} cm^{-1}, λ_{exc} 331 nm), comparable to the common terbium(III) benchmark, Tb-Lumi4 (B = ~15,800 M^{-1} cm^{-1}, λ_{exc} 340 nm).

A detailed control experiment revealed the selectivity of the PeT mechanism to pH and the lack of dependence on a range of biological cations, electron-rich reductants, and serum albumin. Additionally, the lack of quenching of the luminescence signal by either intermolecular or oxygen mediated processes was demonstrated. In an effort to elucidate the quenching behaviour further and probe the mechanism of europium sensitisation, the gadolinium(III) analogues, **[Gd.L$^{1\text{-}3}$]**, were prepared. These studies, in addition to spectral studies with **[Eu.L$^{1\text{-}3}$]**, strongly suggest the emissive species is the fully protonated complex in each instance. Direct excitation of **[Eu.L$^{1\text{-}3}$]** and study of the observed luminescence response with pH indicated that the excited state quenched by PeT is indeed the europium excited state.

To assess the biological compatibility of these probes, living cell experiments were performed with the brightest parent complex, **[Eu.L^{3}]**, using laser scanning confocal microscopy to study two different cell lines. Through these experiments, the negligible toxicity of the complex over 72 hours was confirmed, as well as the successful real-time monitoring of lysosomal aging, with the complex localising in the lysosome cellular compartment. The use of a pH insensitive control complex, Eu-ICPMS measurements, and deliberate perturbation of the system using nigericin allowed for the origin of the observed pH changes to be attributed unambiguously to the switching on of europium emission from **[Eu.L^{3}]**.

Following these promising results, five derivatised probes were designed, **[Eu.L$^{9\,a-b,\,10,\,11a}$]**, differing primarily in the functionalisation of the aryl amino group, leading to modulation of the pK_a. Each of these probes feature both a Boc-protected primary amine group, suitable for conjugation following deprotection, and possess terminal sulfonate groups to enhance aqueous solubility, grafted either at the complex periphery or installed at the aryl amino group as an N-propylsulfonate substituent. The presence of the sulfonate moieties was hypothesised to suppress non-specific binding of the complex for the subsequent *in vivo* studies.

The stepwise synthesis of these targets was pursued accordingly and the five probe candidates were prepared. Analysis of the photophysical properties of **[Eu.L$^{9\,a-b,\,10,\,11a-b}$]**, revealed generally similar behaviour, with significant switching on of europium emission (ranging between 585 and 1340-fold) and emission lifetime (ranging between 226 and 390%) between the respective pH limits. As anticipated, varying the functionality at the aryl amino nitrogen has considerable impact on the pK_a value. Such changes may be rationalised by considering the balance between numerous factors, *i.e.* the steric inhibition of nitrogen lone pair conjugation into the aryl system, Coulombic and s-bond stabilisation of the protonated nitrogen, and the differential energies of solvation of the base and its conjugate acid.

Two of these complexes, **[Eu.L$^{9\,a-b}$]**, were converted to their benzyl guanine (BG) derivatives, **[Eu.L^{12a-b}]**, and used in a series of proof-of-concept studies exploring GPCR internalisation. These experiments involved the expression of a HEK-293 cell line with the SNAP-tag functionalised glucagon-like peptide-1 receptor, and subsequent labelling of the receptor with the complexes **[Eu.L^{12a-b}]**. Here, the high

degree of labelling specificity at the cell surface, afforded by the sulfonate moieties, was clearly demonstrated and negligible non-specific binding was observed. Further, the capability of monitoring of receptor internalisation was shown through a seven-fold increase in europium emission on addition of the agonist Exendin-4, using a 500 – 1000 μs acquisition window. To assess the efficacy of these europium conjugates, a series of BG conjugates of commercial pH responsive dyes were prepared, and analogous experiments performed highlighting their inferior behaviour. Comparative analysis indicates that these europium probes hold substantial promise for the purpose of monitoring GPCR internalisation; the observed magnitude of switching on of europium emission and specificity of binding are superior for the europium conjugates over any of the commercial competitors tested.

Whilst not directly relevant to the main aim of this PhD work, the CPL and racemisation kinetics of the parent complex **[Eu.L^3]** were investigated, following the successful resolution of the racemic complex into its *Δ* and *Λ* enantiomers. The CPL signal was pH responsive and particularly good resolution of the Δ*J* = 4 band was found allowing identification of five major transitions. The kinetics of enantiomeric interconversion were shown to be strongly solvent dependent, reflecting the influence of the solvent nature on the activation energy barrier for Eu-O bond dissociation. Other factors, such as the steric demand of substituents or the strength of the Eu-N_{py} bond, are also relevant when investigating racemisation kinetics.

The solvatochromic effect with **[Eu.L^3]** was also explored by examining the absorption and total emission spectral behaviour over a range of eleven solvents of differing polarity. Clear negative and positive solvatochromic trends were found for the absorption and emission spectral form, respectively, for the neutral species, where the energy of the transitions was considered ($/_{max}^{-1}$). This absorption behaviour offered further evidence of the involvement of a low energy ground ICT electronic state, consistent with earlier mechanistic studies.

6.2. Further Work

Possessing a complete understanding of the energy levels, pathways, and species involved in photophysical processes is highly desirable. Our efforts to probe the mechanism of the PeT quenching process, giving rise to the observed pH sensitivity, has revealed the identity of the emissive species and the quenched excited state. However, further work is necessary to elucidate the nature and energy of the excited states involved in the sensitisation of the europium(III) ion. Low temperature studies examining **[Gd.L$^{1\text{-}3}$]** were unable to unequivocally dismiss a classical ligand triplet excited state (*vs.* a ligand ICT state) in the europium sensitisation pathway. The use of time-resolved fast laser experiments, *e.g.* observing transient absorption spectroscopy, may shed light here.

Given the initial favourable results of the internalisation studies with **[Eu.L$^{12a\text{-}b}$]**, further efforts will focus on the synthesis of the BG derivatives of **[Eu.L$^{10a\text{-}b,11}$]**. Analogous receptor internalisation experiments are required to assess whether incorporation of the sulfonate moiety onto the aryl amino group impacts the observed switching of emission on receptor internalisation and the specificity of binding. It is possible that these complexes may display enhanced properties to those described in this thesis. As a priority, further attention should seek to optimise the methodology and measurement parameters used in the time-gated monitoring of receptor internalisation: it is highly likely that additional enhancement of the signal switch on can be achieved given the precedent set by the time-gated measurements throughout this work. Finally, the receptor internalisation experiments performed within this work serve as an effective proof-of-concept. Further pharmacological studies are necessary to identify the context where these probes are best applied, *e.g.* the identity of GPCR, and to assess the overall commercial viability of these bright pH responsive probes.

CHAPTER SEVEN

Experimental Methods

Chapter Seven: Experimental Methods

7.1. General Procedures

Commercially available reagents were used as received. Solvents were laboratory grade and were dried over appropriate drying agents when required. Where appropriate, solvents were degassed using freeze-pump-thaw cycles.

Thin layer chromatography (TLC) was carried out on aluminium-backed silica gel plates with 0.2 mm thick silica gel 60 F254 (Merck), and visualised by UV irradiation at 254 nm or 366 nm. Preparative flash column chromatography was performed using flash silica gel 60 (230-400 mesh) from Merck or Fluorochem.

^{1}H, ^{13}C, ^{19}F, ^{29}Si and ^{31}P NMR spectra were recorded in commercially available deuterated solvents on a Bruker Avance-400 (^{1}H at 400.06 MHz, ^{13}C at 100.61 MHz, ^{19}F at 376.50 MHz, ^{29}Si at 79.49 MHz and ^{31}P at 161.95 MHz), a Mercury 400 (^{1}H at 399.95 MHz), a Varian VNMRS-600 (^{1}H at 599.67 MHz, ^{13}C at 150.79 MHz and ^{31}P at 242.75 MHz), or a Varian VNMRS-700 (^{1}H at 699.73 MHz, ^{13}C at 175.95 MHz and ^{31}P at 283.26 MHz). All chemical shifts are in ppm and coupling constants are in Hz.

Electrospray mass spectra were obtained on a TQD mass spectrometer equipped with an Acquity UPLC system, an electrospray ion source and an Acquity photodiode array detector (Waters Ltd., UK). Accurate masses were recorded on an LCT Premier XE mass spectrometer or a QToF Premier Mass spectrometer, both equipped with an Acquity UPLC, a lock-mass electrospray ion source and an Acquity photodiode array detector (Waters Ltd., UK). Methanol or acetonitrile were used as the carrier solvents.

7.2. HPLC Analysis

Reverse phase HPLC (RP-HPLC) was performed at 295 K using a Shimadzu system comprising of a Degassing Unit (DGU-20A5R), a Prominence Preparative Liquid Chromatography pump (LC-20AP), a Prominence UV-Vis Detector (SPD-20A) and a Communications Bus Module (CBM-20A). For preparative HPLC, an XBridge C_{18} OBD column was used (19 × 100 mm, 5 µm) with a flow rate of 17 mL min^{-1}. For analytical HPLC, a Shimadzu Shim-Pack VP-ODS column was used (4.6 × 150 mm, 5 µm) with a flow rate of 2.0 mL min^{-1}. Fraction collection was performed manually. The solvent

system used to achieve purification is specified in the text. In general, a solvent system of H_2O / CH_3CN or H_2O / CH_3OH (with or without 0.1% formic acid) was used with gradient elution as follows:

Step	Time / min	% H_2O	% CH_3CN/CH_3OH
0	0	90	10
1	4	90	10
2	14	0	100
3	19	0	100
4	22	90	10

Chiral HPLC analysis was carried out on a Perkin Elmer Series 200 system comprising of a Perkin Elmer Series 200 pump, autosampler, and UV-Vis detector, using a Daicel CHIRALPAK-ID column (4.6 × 250 mm for analytical with a flow rate of 1.0 mL min^{-1}, 10 × 250 mm for preparative with a flow rate of 4.4 mL min^{-1}, all 5 µm particle size). Isocratic methanol was used as the mobile phase. Fraction collection was automated.

7.3. Optical Measurements

All solution state optical analyses were carried out in quartz cuvettes with a path length of 1 cm. UV-Vis absorbance spectra were measured on an ATI Unicam UV-Vis spectrometer (Model UV2) using Vision software (version 3.33). Emission spectra were recorded using either an ISA Jobin-Yvon Spex Fluorolog-3 luminescence spectrometer using DataMax software (version 2.2.10) or a HORIBA Jobin-Yvon Fluorolog-3 luminescence spectrometer equipped with an iHR320 module, which selects either a HORIBA FL-1073 (Hammatsu R928P) photomultiplier tube or a HORIBA Synapse BIDD CCD for detection of emitted light, using FluorEssence software (based on Origin® software). Quantum yields were recorded using against the reference standard $[Ru(bipy)_3]Cl_2$, as described elsewhere.[1-2] Lifetime measurements were carried out using a Perkin Elmer LS55 spectrometer using FL Winlab software. Low temperature emission spectra were recorded in the above

instruments using a Janis VNF-100 cryostat coupled to a LakeShore 332 temperature controller, and cooled with liquid nitrogen.

Time-gated lanthanide emission measurements were performed using an in house-built time-gated spectrophotometer (www.fscanltd.com). This was designed to maximise europium(III) emission detection sensitivity and reduce physical size. A pulsed LED excitation source (Nichia: 365 nm, 50 s, 200 Hz, 250 mW) was placed in a purpose built sample chamber, designed to accommodate commercially available cuvettes (*e.g.* 12 mm × 12 mm). Luminescence from the sample was collected at 90 to the excitation source and focussed onto the entrance slit of a monochromator (Acton), adjusted to provide a 2 nm band-pass. The emission was detected using a photon counting photomultiplier module (Hamamatsu) and the signal acquired using a PC-based National Instruments data acquisition card. Europium(III) emission spectra were obtained in the range 550–720 nm in 1 nm increments. A 10 s time-delay was applied prior to a 1 ms time-gate for the spectral acquisition, in order to eliminate scattered light, avert auto-fluorescence and avoid any residual short-lived fluorescence.

CPL spectra were recorded on a custom-built spectrometer consisting of a laser driven light source (Energetiq EQ-99 LDLS, spectral range 170 – 2100 nm) coupled to an Acton SP2150 monochromator (600 g nm^{-1}, 300 nm Blaze) that allows excitation wavelengths to be selected with a 6 nm FWHM band-pass. The collection of the emitted light was facilitated (90° angle setup) by a Lock-In Amplifier (Hinds Instruments Signaloc 2100) and Photoelastic Modulator (Hinds Instruments Series II/FS2AA). The differentiated light was focused onto an Acton SP2150 monochromator (1200 g nm^{-1}, 500 nm Blaze) equipped with a high sensitivity cooled Photo Multiplier Tube (Hamamatsu H10723-20 PhotoSensor). Red correction is embedded in the detection algorithm and was constructed using a calibrated Ocean Optics lamp. Spectra were recorded with 0.5 nm spectral intervals and 500 µs integration time, using a 5 spectral average sequence for europium(III) complexes. The monochromators, PEM control unit and lock-in amplifier were interfaced with a desktop PC and controlled by LabView code.

7.4. Cell Culture Protocols

Cells used for simple microscopy studies were cultured as follows. Cells were grown in a 12-well plate on a sterilised (autoclaved at 121 °C for 45 min) glass coverslip in phenol red 3-containing DMEM/F12 cell growth medium (pH 7.6) supplemented with sodium pyruvate, glucose, 0.25 mM HEPES buffer and 10% fetal bovine serum. The cells were allowed to grow to 70-80% confluence at which point the medium was removed and replaced with medium containing complex. The cells were incubated at 37 °C at 5% CO_2 and 10% humidity. For co-staining experiments, MitoTracker Green (0.2 μM) was added to the medium 30 min before imaging, while LysoTracker Green (0.2 μM) was added 5 min before imaging. Prior to imaging, the coverslips were washed with fresh medium three times and fixed to glass slides for imaging.

Cells used for ICP-MS studies were prepared as follows. Cells were cultured in a 6-well plate to 90% confluence. Cells were then counted (107 cells based on a cell volume of 4000 μm^3) and incubated with medium containing the complex before being washed three times with phosphate-buffered saline (PBS). The cells were then trypsinated and harvested and diluted to 1 mL with PBS. Concentrated nitric acid (0.6 mL) was added and the samples were digested for 24 h at 37 °C. These digested samples were submitted for ICP-MS measurements (Department of Earth Sciences, Durham University). The samples were run against a series of Eu standards, and the measured concentration was back calculated to find the total Eu concentration present in the original counted cells.

7.5. Confocal Microscopy and Imaging

Cell images and co-localisation experiments were obtained using a Leica SP5 II microscope equipped with PhMoNa.[3] In order to achieve excitation with maximal probe emission, the microscope was coupled by an optical fibre to a coherent 355 nm CW (Nd:YAG) laser (3rd harmonic), operating at 8 mW power. A HeNe or Ar ion laser was used when commercially available organelle-specific stains (e.g. MitoTracker Green and LysoTracker Green) were used to corroborate cellular compartmentalisation. The microscope was equipped with a triple channel imaging detector, comprising two conventional PMT systems and a HyD hybrid avalanche photodiode detector. The latter part of the detection system, when operated in the

BrightRed mode, is capable of improving imaging sensitivity above 550 nm by 25%, reducing signal to noise by a factor of 5. The pinhole was determined by the Airy disc size, calculated from the objective in use (HCX PL APO 63x/1.40 NA Lbd Blue), using the lowest excitation wavelength (355 nm) and was set to 0.6 Airy unit. Scanning speed was adjusted to 200 Hz in a unidirectional mode, to ensure both sufficient light exposure and enough time to collect the emitted light from the lanthanide based optical probes (1024 × 1024 frame size, a pixel size of 120 × 120 nm and depth of 0.772 µm) but sufficiently fast to prevent movement of cellular compartments due to natural homeostasis. Spectral imaging in cells was achieved using a custom built microscope (modified Zeiss Axiovert 200M), using a Zeiss APOCHROMAT 63x/1.40 NA objective combined with a low voltage (24 V) 365 nm pulsed UV LED focused, collimated excitation source (1.2 W). For rapid spectral acquisition the microscope was equipped at the X1 port with a Peltier cooled 2D-CCD detector (Maya Pro, Ocean Optics) used in an inverse 100 Hz time gated sequence. Spectra were recorded from 400-800 nm with a resolution of 0.24 nm and averaged using a 10,000 scan duty cycle. Probe lifetimes were measured on the same microscope platform using a novel cooled PMT detector (Hamamatsu H7155) interchangeable on the X1 port, with the application of pre-selected interference filters. Both the control and detection algorithm were written in LabView2014, where probe lifetime was determined by using a single exponential fitting algorithm to the monitored signal intensity decay.

7.6. Internalisation Study Protocols

The assays were run in black 96 well cell culture treated plates (GREINER 655086). Each well was precoated with 50 µl of poly-L-ornithine for 30 minutes at 37 °C and were plated at 100,000 cells per well. HEK293 cells stably expressing GLP-1R-ST were obtained from Cisbio Bioassays (HEK293 SNAP-GLP1, #C1SU1GLP1) and non-transfected HEK293 (CLS) cells were plated at 100,000 cells per well in DMEM Glutamax and then placed at 37 °C under 5% CO_2 during 24 hours. These adherent cells were used for the following labeling procedure.

After removal of the cell culture medium, a 50 µL solution of 200 nM of the BG derivative in Tag-lite labeling medium (Cisbio Bioassays, Catalog LABMED) was added and incubated for 1.5 hours at room temperature. After removal of the buffer,

the excess europium complex was removed by three washing steps, using 100 µL of Tag-lite labeling medium. Finally, a solution of 0.1 M of acetate buffer at pH 4.5 (+0.1% BSA) was added to the wells to reveal the luminescence. Each experiment was repeated in triplicate. The plates were read on a PheraStarFS (BMG) plate reader, using the HTRF setting. The 620 nm signal was measured over a 400 µs period, with a 60 µs delay time.

For the internalization study, the same procedure was followed for the SNAP-GLP1 cells. After the three washing steps to remove the excess europium complex, either 50 µL of Tag-lite medium was added or a solution of 100 nM of Exendin-4 (Tocris Cat. No. 1933) in Tag-lite medium. After incubation for 1 hour at room temperature the cells were washed once with Tag-Lite medium (100 µL), after which 100 µL of Tag-Lite medium was added to the wells. Each plate was read as described above.

7.7. Synthetic Procedures

The compounds **1**[4], **5**[5] and **BG-MB-NHS**[6] were prepared as reported elsewhere.

7.7.1. Synthesis of the Parent Complexes

7.7.1.1. Synthesis of L^{1-3}

(6-(Ethoxy(methyl)phosphoryl)pyridine-2-yl)methyl methanesulfonate, 1[4]

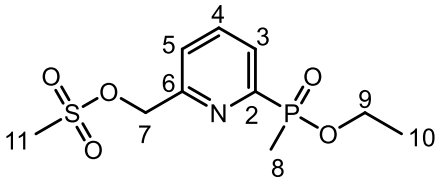

Compound **1** was synthesised in five steps from 2-bromo-6-methylpyridine following a procedure described in the literature; **^{1}H-NMR** (400 MHz, $CDCl_3$) δ 8.07–8.01 (1H, m, H^3), 7.91 (1H, ddd, $^3J_{H\text{-}H}$ 7.8, $^4J_{H\text{-}P}$ 4.2, H^4), 7.64 (1H, d, $^3J_{H\text{-}H}$ 7.8, H^5), 5.39 (2H, s, H^7), 4.17–3.81 (2H, m, H^9), 3.12 (3H, s, H^{11}), 1.78 (3H, d, $^2J_{H\text{-}P}$ 15, H^8), 1.27 (3H, t, $^3J_{H\text{-}H}$ 7.1, H^{10}); **ESI-LRMS** (+) *m/z* 294 $[M+H]^+$; **ESI-HRMS** (+) calc. for $[C_{10}H_{17}NO_5SP]^+$ 294.0565, found 294.0575.

2-*N,N*-Diethylamino-4-iodo-methoxybenzene, 2

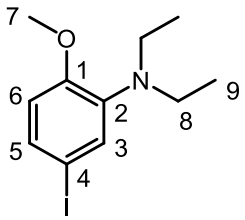

5-Iodo-2-methoxyaniline (2.83 g, 11.4 mmol), iodoethane (7 mL, 87 mmol) and K_2CO_3 (6.3 g, 45.6 mmol) were combined in anhydrous CH_3CN (15 mL) under argon. The reaction mixture was heated at 60 °C for 48 h. After this time, the solvent was removed under reduced pressure and the residue dissolved in DCM (30 mL), washed with H_2O (5 × 20 mL) and dried over K_2CO_3. Removal of the solvent under reduced pressure yielded a pale orange oil (2.16 g, 62%); **^{1}H-NMR** (600 MHz, $CDCl_3$) δ 7.24 (1H, dd, $^3J_{H\text{-}H}$ 8.5, $^4J_{H\text{-}H}$ 1.9, H^5), 7.15 (1H, d, $^4J_{H\text{-}H}$ 1.9, H^3), 6.58 (1H, d, $^3J_{H\text{-}H}$ 8.5, H^6), 3.81 (3H, s, H^7), 3.12 (4H, q, $^3J_{H\text{-}H}$ 7.1, H^8), 1.02 (6H, t, $^3J_{H\text{-}H}$ 7.1, H^9); **^{13}C-NMR** (151 MHz, $CDCl_3$) δ 153.5 (C^1), 141.0 (C^2), 131.0 (C^5), 130.0 (C^3), 113.4 (C^6), 83.0 (C^4), 55.4 (C^7), 45.9 (C^8), 11.9 (C^9); **ESI-LRMS** (+) *m/z* 306 $[M+H]^+$; **ESI-HRMS** (+) calcd for $[C_{11}H_{17}NO^{127}I]^+$ 306.0355, found 306.0363.

2-*N,N*-Diethylamino-4-trimethylsilylethynyl-methoxybenzene, 3

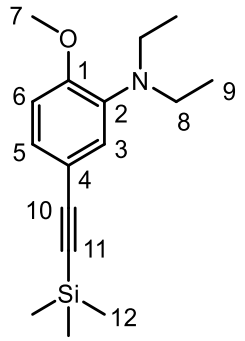

The tertiary amine **2** (548 mg, 1.80 mmol), trimethylsilylacetylene (0.5 mL, 3.6 mmol), $Pd(dppf)Cl_2$.DCM (150 mg, 0.184 mmol) and pyrrolidine (0.45 mL, 5.4 mmol) were combined under argon in anhydrous THF (3 mL). The reaction mixture was heated at 50 °C for 19 h before removal of the solvent under reduced pressure. The subsequent residue was dissolved in DCM (30 mL), washed with H_2O (4 × 30 mL) and dried over K_2CO_3. Removal of solvent under reduced pressure gave the crude product which was purified by column chromatography (SiO_2, 100% hexane to 6% EtOAc in hexane) to yield a pale orange oil (323 mg, 65%); **^{1}H-NMR** (700 MHz, $CDCl_3$) δ 7.12 (1H, d, $^3J_{H\text{-}H}$

8.5, H^5), 7.03 (1H, s, H^3), 6.75 (1H, d, $^3J_{H\text{-}H}$ 8.5, H^6), 3.85 (3H, s, H^7), 3.14 (4H, q, $^3J_{H\text{-}H}$ 7.1, H^8), 1.01 (6H, t, $^3J_{H\text{-}H}$ 7.1, H^9), 0.24 (9H, s, H^{12}); **^{13}C-NMR** (176 MHz, $CDCl_3$) δ 154.5 (C^1), 139.1 (C^2), 127.2 (C^5), 125.3 (C^3), 115.1 (C^4), 111.2 (C^6), 105.9 (C^{10}), 91.9 (C^{11}), 55.6 (C^7), 46.1 (C^8), 12.1 (C^9), 0.3 (C^{12}); **^{29}Si-NMR** (139 MHz, $CDCl_3$) δ -18.3; **ESI-LRMS** (+) *m/z* 276 $[M+H]^+$; **ESI-HRMS** (+) calcd for $[C_{16}H_{26}NOSi]^+$ 276.1784, found 276.1790; **R_f** = 0.40 (SiO_2, 10% EtOAc in hexane).

2-*N,N*-Diethylamino-4-ethynyl-methoxybenzene, 4

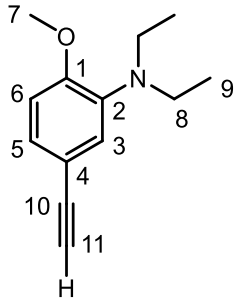

Triethylamine trihydrofluoride (0.75 mL, 3.28 mmol) was added to a solution of compound **3** (115 mg, 0.306 mmol) in anhydrous THF (3 mL) under argon. The solution was heated to 30 °C for 37 h before removal of solvent under reduced pressure. The resulting oil was dissolved in DCM (30 mL) and washed with H_2O (3 × 40 mL). The combined aqueous layers were extracted with DCM (5 × 40 mL) and the organic layers combined and dried over K_2CO_3. Removal of the solvent under reduced pressure yielded a pale orange oil (81 mg, 87%); **^{1}H-NMR** (700 MHz, $CDCl_3$) δ 7.14 (1H, dd, $^3J_{H\text{-}H}$ 8.4, $^4J_{H\text{-}H}$ 2.0, H^5), 7.06 (1H, d, $^4J_{H\text{-}H}$ 2.0, H^3), 6.78 (1H, d, $^3J_{H\text{-}H}$ 8.4, H^6), 3.86 (3H, s, H^7), 3.15 (4H, q, $^3J_{H\text{-}H}$ 7.1, H^8), 2.98 (1H, s, H^{11}), 1.02 (6H, t, $^3J_{H\text{-}H}$ 7.1, H^9); **^{13}C-NMR** (176 MHz, $CDCl_3$) δ 154.6 (C^1), 139.2 (C^2), 127.1 (C^5), 125.3 (C^3), 113.9 (C^4), 111.3 (C^6), 84.4 (C^{10}), 75.3 (C^{11}), 55.7 (C^7), 46.1 (C^8), 12.1 (C^9); **ESI-LRMS** (+) *m/z* 204 $[M+H]^+$; **ESI-HRMS** (+) calcd for $[C_{13}H_{18}NO]^+$ 204.1388, found 204.1401.

Ethyl (4-bromo-6-hydroxymethylpyridin-2-yl)methylphosphinate, 5[5]

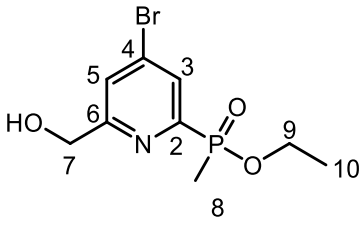

Compound **5** was synthesised in nine steps from 2-bromo-6-methylpyridine following a procedure described in the literature; **^{1}H-NMR** (400 MHz, $CDCl_3$) δ 8.05 (1H, d, $^{3}J_{H\text{-}P}$ 6, H^{3}), 7.71 (1H, s, H^{5}), 4.78 (2H, s, H^{7}), 4.33 (1H, br s, OH), 4.12–3.80 (2H, m, H^{9}), 1.73 (3H, d, $^{2}J_{H\text{-}P}$ 15, H^{8}), 1.24 (3H, d, $^{3}J_{H\text{-}H}$ 7, H^{10}); **^{13}C-NMR** (101 MHz, $CDCl_3$) δ 163.5 (d, $^{3}J_{C\text{-}P}$ 20, C^{6}), 154.7 (d, $^{1}J_{C\text{-}P}$ 156, C^{2}), 134.6 (d, $^{3}J_{C\text{-}P}$ 13, C^{4}), 129.4 (d, $^{2}J_{C\text{-}P}$ 22, C^{3}), 126.5 (d, $^{4}J_{C\text{-}P}$ 3, C^{5}), 64.3 (C^{7}), 61.8 (d, $^{2}J_{C\text{-}P}$ 6, C^{9}), 16.6 (d, $^{3}J_{C\text{-}P}$ 6, C^{10}), 13.8 (d, $^{1}J_{C\text{-}P}$ 104, C^{8}).

2-*N,N*-Diethylamino-4-(2-(ethoxy(methyl)phosphoryl)-6-(hydroxymethyl)pyridine-4-yl)ethynyl)methoxybenzene, 6

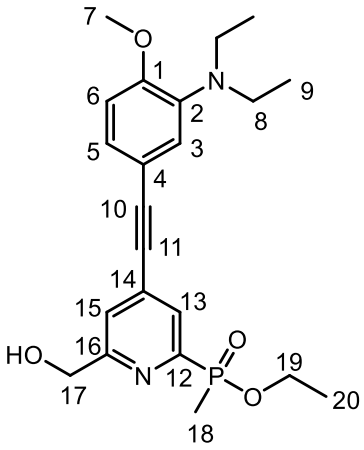

To a solution of compounds **4** (120 mg, 0.59 mmol) and **5** (175 mg, 0.60 mmol) in anhydrous THF (2.5 mL) under argon was added pyrrolidine (0.1 mL, 1.22 mmol) and Pd(dppf)Cl_2.DCM (60 mg, 0.073 mmol). The reaction mixture was subsequently heated at 50 °C for 18 h when the solvent was removed under reduced pressure and the resulting residue dissolved in DCM (40 mL) and washed with H_2O (3 × 40 mL). The organic layer was dried over K_2CO_3 and the solvent removed to yield a brown residue that was purified by RP-HPLC (10 to 100% CH_3CN in H_2O over 10 min, $\mathbf{t_R}$ = 10.7 min) to afford a pale yellow oil (118 mg, 48%); **^{1}H-NMR** (600 MHz, $CDCl_3$) δ 8.03 (1H, d, $^{3}J_{H\text{-}P}$ 6.0, H^{13}), 7.49 (1H, s, H^{15}), 7.18 (1H, d, $^{3}J_{H\text{-}H}$ 8.5, H^{5}), 7.09 (1H, s, H^{3}),

6.82 (1H, d, $^{3}J_{H\text{-}H}$ 8.5, H^{6}), 4.80 (2H, s, H^{17}), 4.14–3.82 (2H, m, H^{19}), 3.87 (3H, s, H^{7}), 3.16 (4H, q, $^{3}J_{H\text{-}H}$ 6.9, H^{8}), 1.77 (3H, d, $^{2}J_{H\text{-}P}$ 15, H^{18}), 1.26 (3H, t, $^{3}J_{H\text{-}H}$ 7.0, H^{20}), 1.03 (6H, t, $^{3}J_{H\text{-}H}$ 6.9, H^{9}); **^{13}C-NMR** (151 MHz, $CDCl_3$) δ 160.8 (d, $^{3}J_{C\text{-}P}$ 19, C^{16}), 155.2 (C^{1}), 153.2 (d, $^{1}J_{C\text{-}P}$ 155, C^{12}), 139.5 (C^{2}), 133.3 (d, $^{3}J_{C\text{-}P}$ 11, C^{14}), 128.3 (d, $^{2}J_{C\text{-}P}$ 22, C^{13}), 127.2 (C^{5}), 125.0 (C^{3}), 124.1 (d, $^{4}J_{C\text{-}P}$ 3, C^{15}), 113.5 (C^{4}), 111.5 (C^{6}), 97.0 (C^{10}), 84.9 (C^{11}), 64.2 (C^{17}), 61.3 (d, $^{2}J_{C\text{-}P}$ 6, C^{19}), 55.7 (C^{7}), 46.0 (C^{8}), 16.5 (d, $^{3}J_{C\text{-}P}$ 6, C^{20}), 13.6 (d, $^{1}J_{C\text{-}P}$ 105, C^{18}), 12.0 (C^{9}); **^{31}P{^{1}H}-NMR** (243 MHz, $CDCl_3$) δ +39.4; **ESI-LRMS** (+) *m/z* 417 $[M+H]^+$; **ESI-HRMS** (+) calcd for $[C_{22}H_{30}N_2O_4P]^+$ 417.1943, found 417.1954.

2-*N*,*N*-Diethylamino-4-((2-(ethoxy(methyl)phosphoryl)-6-(((methylsulfonyl)oxy)methyl)pyridine-4-yl)ethynyl)methoxybenzene, 7

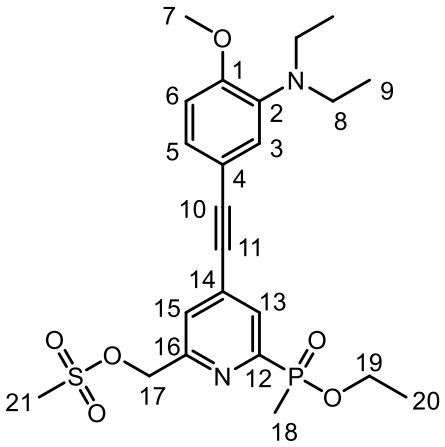

Compound **6** (67 mg, 0.161 mmol), methanesulfonic anhydride (56 mg, 0.322 mmol) and DIEA (0.07 mL, 0.402 mmol) were combined in anhydrous THF (1.5 mL) under argon and stirred at room temperature for 90 min. After this time, the solvent was removed under reduced pressure. To the resulting residue was added DCM (30 mL) and H_2O (30 mL). The organic layer was separated and washed with H_2O (2 × 30 mL), before the combined aqueous layers were extracted with DCM (1 × 30 mL). The combined organic layers were dried over K_2CO_3 and the solvent removed under reduced pressure to afford a pale orange oil that was used directly in the next step without further purification (69 mg, 87%); **^{1}H-NMR** (400 MHz, $CDCl_3$) δ 8.09 (1H, dd, $^{3}J_{H\text{-}P}$ 6.0, $^{4}J_{H\text{-}H}$ 1.5, H^{13}), 7.64–7.62 (1H, m, H^{15}), 7.19 (1H, dd, $^{3}J_{H\text{-}H}$ 8.5, $^{4}J_{H\text{-}H}$ 2.1, H^{5}), 7.10 (1H, d, $^{4}J_{H\text{-}H}$ 2.1, H^{3}), 6.84 (1H, d, $^{3}J_{H\text{-}H}$ 8.5, H^{6}), 5.36 (2H, s, H^{17}), 4.19–3.81 (5H, m, H^{7} & H^{19}), 3.17 (4H, q, $^{3}J_{H\text{-}H}$ 7.1, H^{8}), 3.13 (3H, s, H^{21}), 1.77 (3H, d, $^{2}J_{H\text{-}P}$ 15, H^{18}), 1.27 (3H, t, $^{3}J_{H\text{-}H}$ 7.0, H^{20}), 1.04 (6H, t, $^{3}J_{H\text{-}H}$ 7.1, H^{9}); **ESI-LRMS** (+) *m/z* 495 $[M+H]^+$.

Compound 8

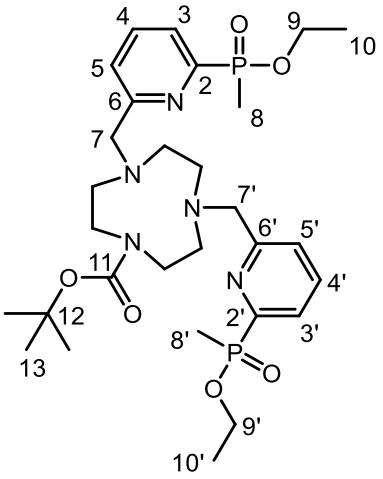

The dihydrochloride salt of 1-(*tert*-butoxycarbonyl)-1,4,7-triazacyclononane (28 mg, 0.093 mmol), compound **1** (64 mg, 0.22 mmol) and K_2CO_3 (40 mg, 0.29 mmol) were combined in anhydrous CH_3CN (2 mL) under argon and heated at 65 °C for 18 h. After this time, the solution was separated from the inorganic salts and purified by RP-HPLC (10 to 100% CH_3CN in H_2O over 10 min, $\mathbf{t_R}$ = 11.8 min) to yield a pale yellow oil (33 mg, 57%); **^{1}H-NMR** (700 MHz, $CDCl_3$) δ 7.92–7.88 (2H, m, H^3 & $H^{3'}$), 7.78–7.72 (2H, m, H^4 & $H^{4'}$), 7.62 (1H, d, $^3J_{H\text{-}H}$ 7.9, H^5), 7.55 (1H, d, $^3J_{H\text{-}H}$ 7.9, $H^{5'}$), 4.11–4.03 & 3.87–3.79 (4H, m, H^9 & $H^{9'}$), 3.95–3.90 (4H, m, H^7 & $H^{7'}$), 3.40–3.29 (4H, m, 9-N_3 ring), 3.11–2.96 (4H, m, 9-N_3 ring), 2.72–2.59 (4H, m, 9-N_3 ring), 1.75 (3H, d, $^2J_{H\text{-}P}$ 15, H^8), 1.74 (3H, d, $^2J_{H\text{-}P}$ 15, $H^{8'}$), 1.44 (9H, s, H^{13}), 1.25–1.21 (6H, 2 × t, $^3J_{H\text{-}H}$ 7.1, H^{10} & $H^{10'}$); **^{13}C-NMR** (176 MHz, $CDCl_3$) δ 161.3 (br s, C^6 and $C^{6'}$), 155.7 (C^{11}), 153.9 (d, $^1J_{C\text{-}P}$ 160, C^2), 153.7 (d, $^1J_{C\text{-}P}$ 160, $C^{2'}$), 136.5 (d, $^3J_{C\text{-}P}$ 10, C^4), 136.4 (d, $^3J_{C\text{-}P}$ 10, $C^{4'}$), 125.9 (2 × d, $^2J_{C\text{-}P}$ 20, C^3 & $C^{3'}$), 125.5 (C^5), 125.3 ($C^{5'}$), 79.5 (C^{12}), 63.4 ($C^{7'}$), 63.1 (C^7), 61.0 (2 × d, $^2J_{C\text{-}P}$ 6, C^9 & $C^{9'}$), 56.4 (9-N_3 ring), 55.3 (9-N_3 ring), 54.8 (9-N_3 ring), 54.2 (9-N_3 ring), 50.1 (9-N_3 ring), 49.7 (9-N_3 ring), 28.7 (C^{13}), 16.6 ($C^{10'}$), 16.5 (C^{10}), 13.5 (d, $^1J_{C\text{-}P}$ 104, $C^{8'}$), 13.4 (d, $^1J_{C\text{-}P}$ 104, C^8); **^{31}P{^{1}H}-NMR** (162 MHz, $CDCl_3$) δ +40.3, +40.2; **ESI-LRMS** (+) *m/z* 624 $[M+H]^+$; **ESI-HRMS** (+) calcd for $[C_{29}H_{48}N_5O_6P_2]^+$ 624.3080, found 624.3105.

Compound 9, trifluoroacetate salt

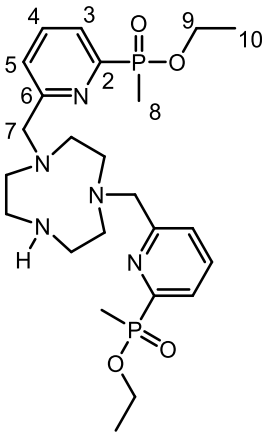

A solution of compound **8** (33 mg, 0.053 mmol) in TFA and DCM (20% v/v, 4 mL total) was prepared. The solution was stirred at room temperature for 25 min before removal of the solvent under reduced pressure to give an orange residue. To this residue was added DCM (30 mL) before removal of the solvent under reduced pressure once again. This procedure was repeated five times to afford the trifluoroacetate salt as a pale orange oil (28 mg, quant.); **^{1}H-NMR** (700 MHz, $CDCl_3$) δ 7.84–7.79 (4H, m, H^3 & H^4), 7.48–7.43 (2H, m, H^5), 4.30 (4H, s, H^7), 4.14–3.87 (4H, m, H^9), 3.57–3.38 (8H, m, 9-N_3 ring), 3.30–3.17 (4H, m, 9-N_3 ring), 1.73 (6H, d, $^{2}J_{H\text{-}P}$ 15, H^8), 1.28 (6H, t, $^{3}J_{H\text{-}H}$ 7.0, H^{10}); **^{13}C-NMR** (176 MHz, $CDCl_3$) δ 156.8 (d, $^{3}J_{C\text{-}P}$ 20, C^6), 153.2 (d, $^{1}J_{C\text{-}P}$ 160, C^2), 137.6 (d, $^{3}J_{C\text{-}P}$ 10, C^4), 126.2 (d, $^{2}J_{C\text{-}P}$ 21, C^3), 62.0 (d, $^{2}J_{C\text{-}P}$ 6, C^9), 59.9 (C^7), 51.6 (9-N_3 ring), 49.4 (9-N_3 ring), 44.5 (2 × s, 9-N_3 ring), 16.3 (d, $^{3}J_{C\text{-}P}$ 6, C^{10}), 13.6 (d, $^{1}J_{C\text{-}P}$ 102, C^8); **^{31}P{^{1}H}-NMR** (162 MHz, $CDCl_3$) δ +40.8, +40.7; **ESI-LRMS** (+) *m/z* 524 $[M+H]^+$; **ESI-HRMS** (+) calcd for $[C_{24}H_{40}N_5O_4P_2]^+$ 524.2556, found 524.2563.

L[1]

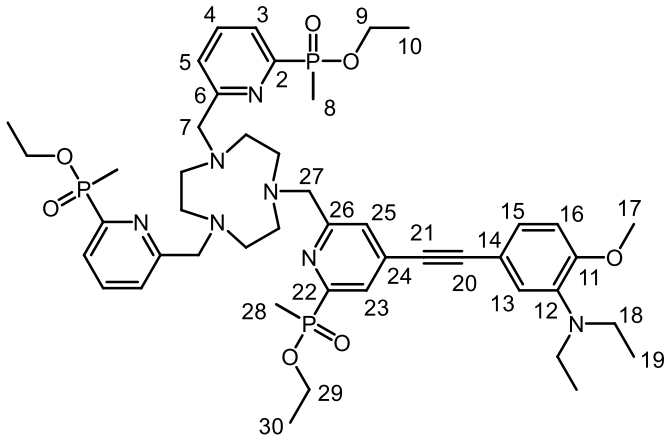

Compound **9** (8.5 mg, 16.2 µmol), compound **7** (16 mg, 32.4 µmol) and K_2CO_3 (5 mg, 35.4 µmol) were combined in anhydrous CH_3CN (1 mL) under argon and heated at 60 °C for 18 h. After this time, the crude mixture was separated from the inorganic salts by filtration. The resulting solution was subjected directly to RP-HPLC (10 to 100% CH_3CN in H_2O over 10 min, t_R = 11.0 min) to afford a pale yellow oil (7.4 mg, 50%); **^{1}H-NMR** (400 MHz, $CDCl_3$) δ 8.01 (1H, d, $^3J_{H\text{-}P}$ 6.0, H^{23}), 7.94–7.87 (2H, m, H^3), 7.82–7.74 (2H, m, H^4), 7.67–7.61 (3H, m, H^5 & H^{25}), 7.18 (1H, d, $^3J_{H\text{-}H}$ 8.4, H^{15}), 7.09 (1H, s, H^{13}), 6.84 (1H, d, $^3J_{H\text{-}H}$ 8.4, H^{16}), 4.18–3.76 (15H, m, H^7, H^{17}, H^{19}, H^{27} & H^{29}), 3.17 (4H, q, $^3J_{H\text{-}H}$ 6.9, H^{18}), 2.97–2.80 (12H, m, 9-N_3 ring), 1.76 (3H, d, $^2J_{H\text{-}P}$ 15, H^{28}), 1.75 (3H, d, $^2J_{H\text{-}P}$ 15, H^8), 1.29–1.20 (9H, m, H^{10} & H^{30}), 1.04 (6H, t, $^3J_{H\text{-}H}$ 6.9, H^{19}); **^{13}C-NMR** (101 MHz, $CDCl_3$) δ 161.5 (2 × d, $^3J_{C\text{-}P}$ 12, C^6 & C^{26}), 155.0 (C^{11}), 153.6 (2 × d, $^1J_{C\text{-}P}$ 159, C^2 & C^{22}), 139.4 (C^{12}), 136.4 (d, $^3J_{C\text{-}P}$ 9, C^4), 133.3 (d, $^3J_{C\text{-}P}$ 16, C^{24}), 127.8 (d, $^2J_{C\text{-}P}$ 22, C^{23}), 127.0 (C^{15}), 126.4 (d, $^4J_{C\text{-}P}$ 4, C^5), 125.9 (C^{25}), 125.6 (d, $^2J_{C\text{-}P}$ 20, C^3), 124.8 (C^{13}), 113.4 (C^{14}), 111.3 (C^{16}), 96.4 (C^{20}), 85.1 (C^{21}), 64.4 (2 × s, C^7 & C^{27}), 60.9 (2 × d, $^2J_{C\text{-}P}$ 6, C^9 & C^{29}), 55.6 (C^{17}), 45.9 (C^{18}), 16.5 (2 × d, $^3J_{C\text{-}P}$ 6.0, C^{10} & C^{30}), 13.4 (2 × d, $^1J_{C\text{-}P}$ 104, C^8 & C^{28}), 11.9 (C^{19}); **^{31}P{^{1}H}-NMR** (162 MHz, $CDCl_3$) δ + 40.2 (2P), +40.0 (1P); **ESI-LRMS** (+) *m/z* 922 $[M+H]^+$; **ESI-HRMS** (+) calcd for $[C_{46}H_{67}N_7O_7P_3]^+$ 922.4315, found 922.4355.

Compound 10

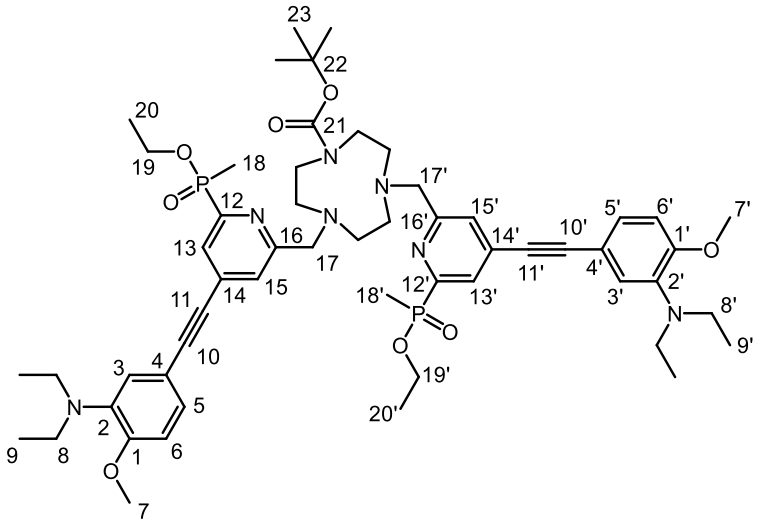

The dihydrochloride salt of 1-(*tert*-butoxycarbonyl)-1,4,7-triazacyclononane (31 mg, 0.10 mmol), the mesylate **7** (122 mg, 0.26 mmol) and K_2CO_3 (60 mg, 0.43 mmol) were combined in anhydrous CH_3CN (2 mL) under argon. The resulting mixture was heated to 60 °C for 14 h before separation of the crude solution from the inorganic salts and removal of the solvent under reduced pressure yielded an orange oil that was purified by RP-HPLC (10 to 100% CH_3CN in H_2O over 10 min, $\mathbf{t_R}$ = 15.6 min) to afford a pale yellow oil (66 mg, 62%); **^{1}H-NMR** (400 MHz, $CDCl_3$) δ 8.03–7.96 (2H, m, H^{13} & $H^{13'}$), 7.66 (1H, s, H^{15}), 7.58 (1H, s, $H^{15'}$), 7.17 (2H, d, H^5 & $H^{5'}$), 7.08 (2H, s, H^3 & $H^{3'}$), 6.82 (2H, d, H^6 & $H^{6'}$), 4.15–4.02 & 3.91–3.78 (10H, m, H^{19}, $H^{19'}$, H^7 & $H^{7'}$), 3.94 (4H, 2 × s, H^{17} & $H^{17'}$), 3.44–3.29 (4H, m, 9-N_3 ring), 3.20–3.04 (12H, m, H^8, $H^{8'}$ & 9-N_3 ring), 2.76–2.61 (4H, m, 9-N_3 ring), 1.76 (6H, 2 × d, H^{18} & $H^{18'}$), 1.48 (9H, s, H^{23}), 1.24 (6H, 2 × t, H^{20} & $H^{20'}$), 1.02 (12H, t, H^9 & $H^{9'}$); **^{13}C-NMR** (101 MHz, $CDCl_3$) δ 161.7 (d, $^3J_{C\text{-}P}$ 21, C^{16}), 161.5 (d, $^3J_{C\text{-}P}$ 21, $C^{16'}$), 155.7 (C^{21}), 155.1 (C^1), 155.0 ($C^{1'}$), 153.8 (d, $^1J_{C\text{-}P}$ 157, C^{12}), 153.6 (d, $^1J_{C\text{-}P}$ 157, $C^{12'}$), 139.9 (2 × s, C^2 & $C^{2'}$), 132.8 (d, $^3J_{C\text{-}P}$ 12, C^{14}), 132.7 (d, $^3J_{C\text{-}P}$ 12, $C^{14'}$), 128.0 (d, $^2J_{C\text{-}P}$ 22, C^{13}), 127.9 (d, $^2J_{C\text{-}P}$ 22, $C^{13'}$), 127.1 (C^5 & $C^{5'}$), 126.4 (d, $^4J_{C\text{-}P}$ 3, C^{15}), 126.1 (d, $^4J_{C\text{-}P}$ 3, $C^{15'}$), 125.0 (2 × s, C^3 & $C^{3'}$), 113.7 (C^4), 113.6 ($C^{4'}$), 111.4 (2 × s, C^6 & $C^{6'}$), 96.5 (C^{10}), 96.2 ($C^{10'}$), 85.3 (d, $^4J_{C\text{-}P}$ 2, C^{11}), 85.1 (d, $^4J_{C\text{-}P}$ 2, $C^{11'}$), 79.5 (C^{22}), 62.9 (C^{17}), 62.6 ($C^{17'}$), 61.1 (2 × d, $^2J_{C\text{-}P}$ 6, C^{19} & $C^{19'}$), 56.1 (9-N_3 ring), 55.7 (C^7 & $C^{7'}$), 55.0 (9-N_3 ring), 54.6 (9-N_3 ring), 54.0 (9-N_3 ring), 50.0 (9-N_3 ring), 49.7 (9-N_3 ring), 46.0 (C^8 & $C^{8'}$), 28.8 (C^{23}), 16.6 (d, C^{20} & $C^{20'}$), 13.5 (d, $^1J_{C\text{-}P}$ 150, C^{18}), 13.4 (d, $^1J_{C\text{-}P}$ 150, $C^{18'}$), 12.0 (C^9 & $C^{9'}$); **^{31}P{^{1}H}-NMR** (162 MHz, $CDCl_3$) δ

+ 40.2 (1P), +40.1 (1P); **ESI-LRMS** (+) *m/z* 1027 $[M+H]^+$; **ESI-HRMS** (+) calcd for $[C_{55}H_{78}N_7O_8P_2]^+$ 1026.539, found 1026.543.

Compound 11, trifluoroacetate salt

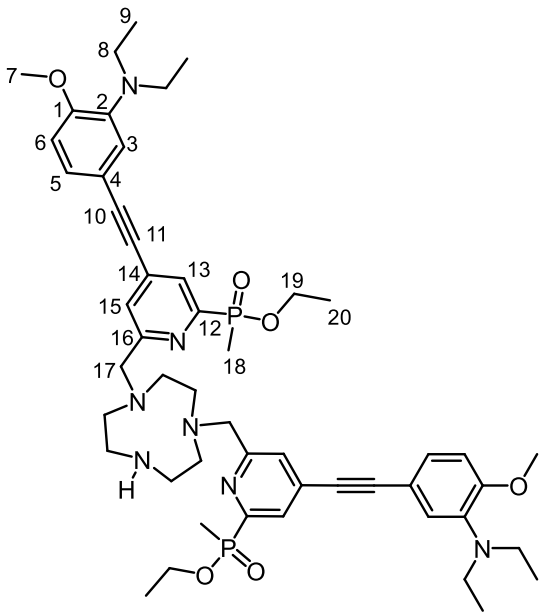

A solution of compound **10** (66 mg, 0.064 mmol) in TFA and DCM (10% v/v, 3 mL total) was prepared. The solution was stirred at room temperature for 1 h before removal of the solvent under reduced pressure to give an orange residue. To this residue was added DCM (30 mL) before removal of the solvent under reduced pressure once again. This procedure was repeated five times to afford a pale orange oil (67 mg, quant.); **^{1}H-NMR** (600 MHz, CD_3OD) δ 7.97 (2H, s, H^3), 7.95 (2H, dd, $^3J_{H\text{-}P}$ 6, $^4J_{H\text{-}H}$ 1.0, H^{13}), 7.79 (2H, dd, $^3J_{H\text{-}H}$ 8.7, $^4J_{H\text{-}H}$ 1.9, H^5), 7.72–7.70 (2H, m, H^{15}), 7.41 (2H, d, $^3J_{H\text{-}H}$ 8.7, H^6), 4.24 (4H, s, H^{17}), 4.17–4.10 & 4.01–3.95 (4H, m, H^{19}), 4.07 (6H, s, H^7), 3.70 (8H, q, $^3J_{H\text{-}H}$ 7.2, H^8), 3.42–3.35 (4H, m, 9-N_3 ring), 3.29–3.23 (4H, m, 9-N_3 ring), 3.06–2.99 (4H, m, 9-N_3 ring), 1.82 (6H, d, $^2J_{H\text{-}P}$ 15, H^{18}), 1.30 (6H, t, $^3J_{H\text{-}H}$ 7.0, H^{20}), 1.12 (12H, t, $^3J_{H\text{-}H}$ 7.2, H^9); **^{13}C-NMR** (151 MHz, CD_3OD) δ 160.8 (d, $^3J_{C\text{-}P}$ 20, C^{16}), 155.6 (C^1), 155.2 (d, $^1J_{C\text{-}P}$ 159, C^{12}), 136.8 (C^5), 133.8 (d, $^3J_{C\text{-}P}$ 12, C^{14}), 128.6 (C^{15}), 128.5 (d, $^2J_{C\text{-}P}$ 24, C^{13}), 127.5 (C^3), 126.2 (C^2), 116.9 (C^4), 114.9 (C^6), 94.6 (C^{10}), 87.3 (d, $^4J_{C\text{-}P}$ 2, C^{11}), 63.1 (d, $^2J_{C\text{-}P}$ 7, C^{19}), 60.6 (C^{17}), 57.7 (C^7), 55.0 (C^8), 52.3 (9-N_3 ring), 49.9 (9-N_3 ring), 45.5 (9-N_3 ring), 16.8 (d, $^3J_{C\text{-}P}$ 6.2, C^{20}), 13.6 (d, $^1J_{C\text{-}P}$ 103, C^{18}), 10.4 (C^9), **^{31}P{^{1}H}-NMR** (162 MHz, CD_3OD) δ +40.8; **ESI-LRMS** (+) *m/z* 926 $[M+H]^+$,

464 $[M+2H]^{2+}$, 309 $[M+3H]^{3+}$; **ESI-HRMS** (+) calcd for $[C_{50}H_{70}N_7O_6P_2]^+$ 926.4863, found 926.4865.

L²

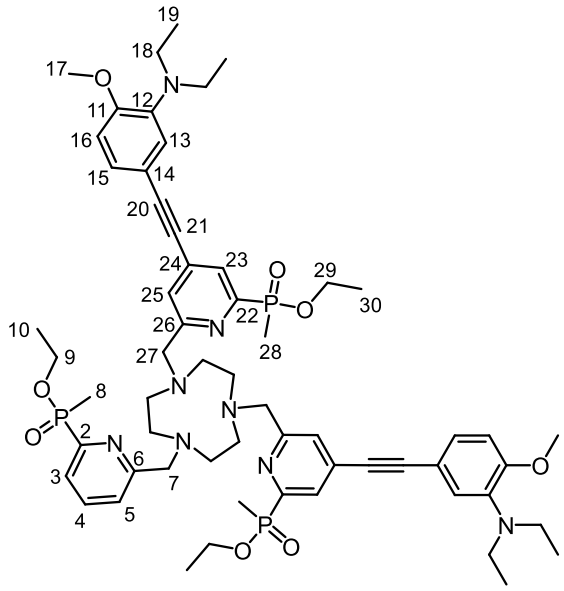

Compound **11** (39 mg, 0.038 mmol), compound **1** (36 mg, 0.12 mmol) and K_2CO_3 (30 mg, 0.22 mmol) were combined in anhydrous CH_3CN (2 mL) under argon and heated at 60 °C for 18 h. After this time, the crude mixture was separated from the inorganic salts by centrifugation and the resulting solution was subjected directly to RP-HPLC (10 to 100% CH_3CN in 25 mM ammonium bicarbonate buffer over 10 min, $\mathbf{t_R}$ = 11.8 min) to yield a pale yellow oil (23 mg, 55%); **^{1}H-NMR** (600 MHz, $CDCl_3$) δ 8.00 (2H, dd, $^3J_{H\text{-}P}$ 6.0, $^4J_{H\text{-}H}$ 1.3, H^{23}), 7.93–7.88 (1H, m, H^3), 7.83–7.76 (1H, m, H^4), 7.73–7.67 (1H, m, H^5), 7.65 (2H, s, H^{25}), 7.18 (2H, dd, $^3J_{H\text{-}H}$ 8.5, $^4J_{H\text{-}H}$ 1.8, H^{15}), 7.09 (2H, d, $^4J_{H\text{-}H}$ 1.8, H^{13}), 6.83 (2H, d, $^3J_{H\text{-}H}$ 8.5, H^{16}), 4.14–4.04 & 3.90–3.82 (12H, m, H^9, H^{17} & H^{29}), 4.01–3.91 (4H, m, H^7 & H^{27}), 3.16 (8H, q, $^3J_{H\text{-}H}$ 7.1, H^{18}), 3.07–2.83 (12H, m, 9-N_3 ring), 1.76 (6H, d, $^2J_{H\text{-}P}$ 15, H^{28}), 1.75 (3H, d, $^2J_{H\text{-}P}$ 15, H^8), 1.25 (6H, t, $^3J_{H\text{-}H}$ 7.0, H^{30}), 1.23 (3H, t, $^3J_{H\text{-}H}$ 7.0, H^{10}), 1.03 (12H, t, $^3J_{H\text{-}H}$ 7.1, H^{19}); **ESI-LRMS** (+) *m/z* 1124 $[M+H]^+$, 563 $[M+2H]^{2+}$, 375 $[M+3H]^{3+}$; **ESI-HRMS** (+) calcd for $[C_{59}H_{82}N_8O_8P_3]^+$ 1123.547, found 1123.548.

L^3

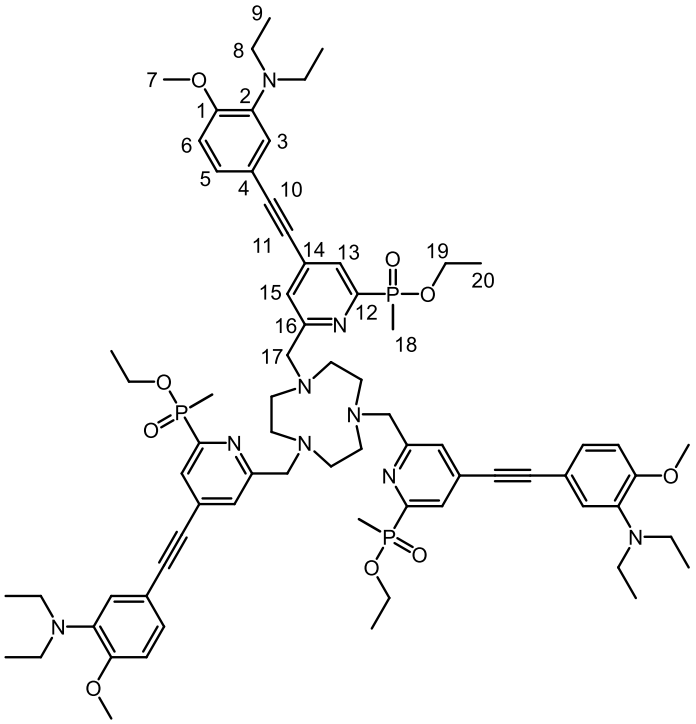

The trihydrochloride salt of 1,4,7-triazacyclononane (4.5 mg, 0.019 mmol), compound **7** (33 mg, 0.067 mmol) and K_2CO_3 (20 mg, 0.15 mmol) were combined in anhydrous CH_3CN (1.5 mL) under argon and heated at 60 °C for 17 h. After this time, the crude mixture was separated from the inorganic salts by filtration. The resulting solution was subjected directly to RP-HPLC (10 to 100% CH_3CN in H_2O over 10 min, $\mathbf{t_R}$ = 16.5 min) to yield a pale yellow oil (8 mg, 32%); **^{1}H-NMR** (600 MHz, $CDCl_3$) δ 8.01 (3H, d, $^3J_{H\text{-}P}$ 5.0, H^{13}), 7.68 (3H, s, H^{15}), 7.18 (3H, dd, $^3J_{H\text{-}H}$ 8.5, $^4J_{H\text{-}H}$ 1.9, H^5), 7.09 (3H, d, $^4J_{H\text{-}H}$ 1.9, H^3), 6.82 (3H, d, $^3J_{H\text{-}H}$ 8.5, H^6), 4.13–4.05 & 3.87–3.81 (6H, m, H^{19}), 3.92 (6H, s, H^{17}), 3.88 (9H, s, H^7), 3.16 (12H, q, $^3J_{H\text{-}H}$ 7.2, H^8), 2.94 (12H, br s, 9-N_3 ring), 1.76 (9H, d, $^2J_{H\text{-}P}$ 15, H^{18}), 1.24 (9H, t, $^3J_{H\text{-}H}$ 7.0, H^{20}), 1.03 (18H, t, $^3J_{H\text{-}H}$ 7.2, H^9); **^{13}C-NMR** (151 MHz, $CDCl_3$) δ 161.9 (d, $^3J_{C\text{-}P}$ 20, C^{16}), 155.4 (C^1), 154.0 (d, $^1J_{C\text{-}P}$ 157, C^{12}), 139.8 (C^2), 133.0 (d, $^3J_{C\text{-}P}$ 12, C^{14}), 128.0 (d, $^2J_{C\text{-}P}$ 23, C^{13}), 127.3 (C^5), 126.8 (C^{15}), 125.2 (C^3), 113.9 (C^4), 111.7 (C^6), 96.6 (C^{10}), 85.5 (C^{11}), 64.2 (C^{17}), 61.3 (d, $^2J_{C\text{-}P}$ 7, C^{19}), 56.1 (9-N_3 ring), 55.9 (C^7), 46.3 (C^8), 16.8 (d, $^3J_{C\text{-}P}$ 6, C^{20}), 13.7 (d, $^1J_{C\text{-}P}$ 104, C^{18}), 12.3 (C^9); **^{31}P{^{1}H}-NMR** (162 MHz, $CDCl_3$) δ +40.1; **ESI-LRMS** (+) *m/z* 1325 $[M+H]^+$, 663 $[M+2H]^{2+}$, 443 $[M+3H]^{3+}$; **ESI-HRMS** (+) calcd for $[C_{72}H_{98}N_9O_9P_3]^{2+}$ 662.8350, found 662.8334.

7.7.1.2. Synthesis of ***[Ln.L$^{1-3}$]*** *(Ln = Eu, Gd)*

[Eu.L^{1}]

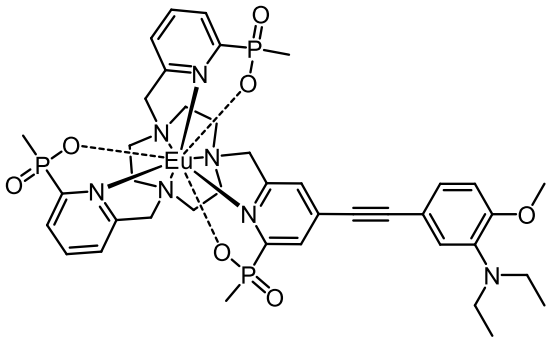

The ligand **L^{1}** (2 mg, 2 µmol) was dissolved in a mixture of CH_3OH/H_2O (1:1, 2 mL total) and the pH was adjusted to 12 using aqueous NaOH solution (1 M). The solution was heated at 60 °C for 14 h. After cooling and adjustment of the pH to 6 using dilute hydrochloric acid (0.1 M), $EuCl_3.6H_2O$ (3 mg, 8 µmol) was added and the reaction mixture was heated to 60 °C for 15 h. The reaction mixture was purified by RP-HPLC (10 to 100% CH_3CN in H_2O over 10 min, $\mathbf{t_R}$ = 8.5 min) to yield a yellow solid (2 mg, 93%); **ESI-LRMS** (+) *m/z* 986 $[M+H]^+$, 495 $[M+2H]^{2+}$; **ESI-HRMS** (+) calcd for $[C_{40}H_{52}N_7O_7P_3{}^{151}Eu]^+$ 986.2340, found 986.2327; $\boldsymbol{\tau_{H2O}}$ (ms) = 0.50 (pH 9), 0.53 (pH 8), 0.74 (pH 7), 1.06 (pH 6), 1.15 (pH 5), 1.16 (pH 4); $\boldsymbol{\varepsilon_{331\ nm}}$ = 11,450 M^{-1} cm^{-1}; $\boldsymbol{\Lambda_{pH\ 8}}$ = 0.5%, $\boldsymbol{\Lambda_{pH\ 4}}$ = 17.0% (λ_{exc} = 331 nm).

[Gd.L^{1}]

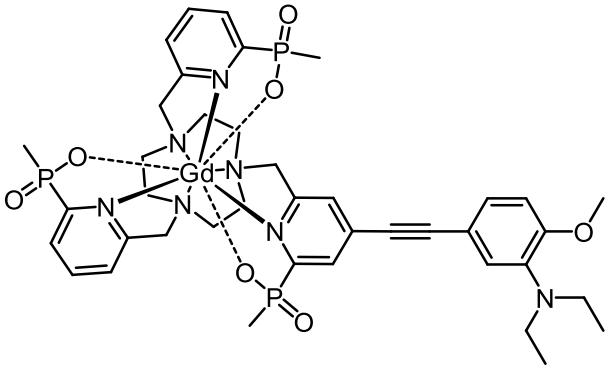

The ligand **L^{1}** (11.5 mg, 0.0102 mmol) was dissolved in a mixture of CH_3OH/H_2O (1:1, 4 mL total) and the pH was adjusted to 12 using aqueous NaOH solution (1 M). The solution was heated at 60 °C for 15 h. After cooling and adjustment of the pH to 6

using dilute hydrochloric acid (0.1 M), $GdCl_3.6H_2O$ (5 mg, 0.0135 mmol) was added and the reaction mixture was heated to 60 °C for 21 h. After this time, the solution was separated from the inorganic salts by centrifugation and purified by RP-HPLC (10 to 100% CH_3OH in H_2O over 10 min, $\mathbf{t_R}$ = 13.7 min) to yield a yellow solid (3.4 mg, 57%); **ESI-LRMS** (+) *m/z* 1194 $[M+H]^+$, 598 $[M+2H]^{2+}$, 399 $[M+3H]^{3+}$; **ESI-HRMS** (+) calcd for $[C_{53}H_{68}N_8O_8P_3{}^{158}Gd]^{2+}$ 597.6814, found 597.6762.

[Eu.L^2]

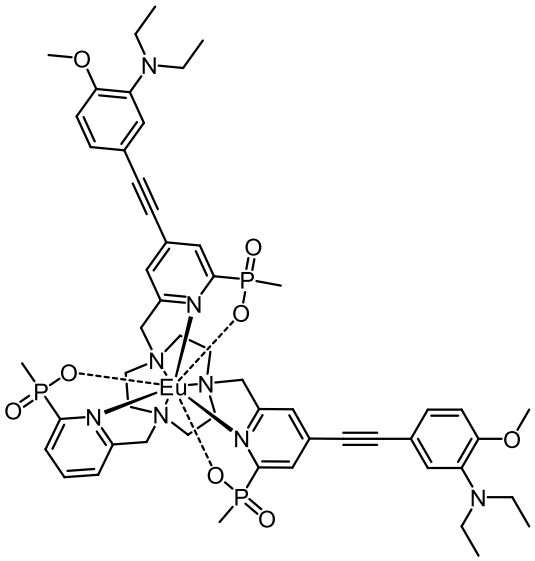

The ligand **L^2** (11.5 mg, 0.0102 mmol) was dissolved in a mixture of CH_3OH/H_2O (1:1, 4 mL total) and the pH was adjusted to 12 using aqueous NaOH solution (1 M). The solution was heated at 60 °C for 15 h. After cooling and adjustment of the pH to 6 using dilute hydrochloric acid (0.1 M), $EuCl_3.6H_2O$ (6 mg, 0.016 mmol) was added and the reaction mixture was heated to 60 °C for 17 h. After this time, the solution was separated from the inorganic salts by centrifugation and purified by RP-HPLC (10 to 100% CH_3OH in H_2O over 10 min, $\mathbf{t_R}$ = 13.6 min) to yield a yellow solid (7 mg, 58%); **ESI-LRMS** (+) *m/z* 1189 $[M+H]^+$, 595 $[M+2H]^{2+}$, 397 $[M+3H]^{3+}$; **ESI-HRMS** (+) calcd for $[C_{53}H_{68}N_8O_8P_3{}^{151}Eu]^{2+}$ 595.1796, found 595.1741; $\boldsymbol{\tau_{H2O}}$ (ms) = 0.34 (pH 9), 0.34 (pH 8), 0.47 (pH 7), 0.78 (pH 6), 0.96 (pH 5), 1.00 (pH 4); $\boldsymbol{\chi_{328\ nm}}$ = 35,000 M^{-1} cm^{-1}; $\boldsymbol{\Lambda_{pH\ 8}}$ = 0.2%, $\boldsymbol{\Lambda_{pH\ 4}}$ = 17.6% (λ_{exc} = 328 nm).

[Gd.L^2]

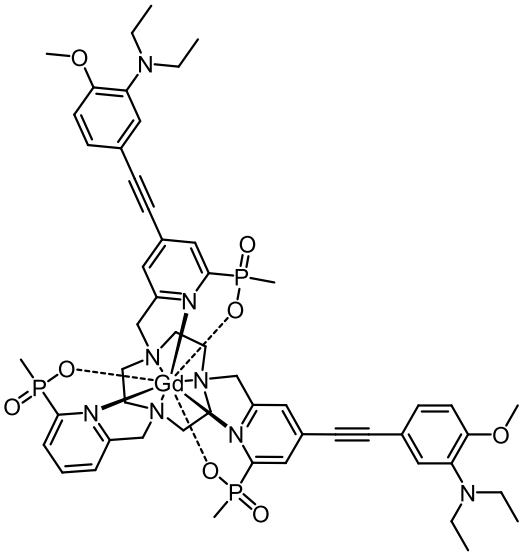

The ligand **L^2** (11.5 mg, 0.0102 mmol) was dissolved in a mixture of CH_3OH/H_2O (1:1, 4 mL total) and the pH was adjusted to 12 using aqueous NaOH solution (1 M). The solution was heated at 60 °C for 15 h. After cooling and adjustment of the pH to 6 using dilute hydrochloric acid (0.1 M), $GdCl_3.6H_2O$ (5 mg, 0.013 mmol) was added and the reaction mixture was heated to 60 °C for 21 h. After this time, the solution was separated from the inorganic salts by centrifugation and purified by RP-HPLC (10 to 100% CH_3OH in H_2O over 10 min, $\mathbf{t_R}$ = 13.7 min) to yield a yellow solid (7 mg, 57%); **ESI-LRMS** (+) *m/z* 1194 $[M+H]^+$, 598 $[M+2H]^{2+}$, 399 $[M+3H]^{3+}$; **ESI-HRMS** (+) calcd for $[C_{53}H_{68}N_8O_8P_3{}^{158}Gd]^{2+}$ 597.6814, found 597.6762.

[Eu.L^3]

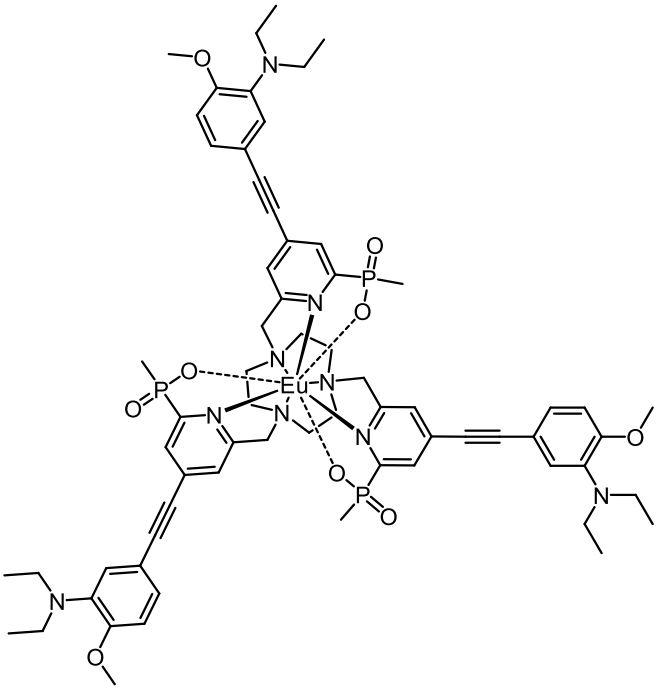

The ligand **L^3** (8 mg, 6 µmol) was dissolved in a mixture of CH_3OH/H_2O (1:1, 2 mL total) and the pH was adjusted to 12 using aqueous NaOH solution (1 M). The solution was heated at 60 °C for 4 h. After cooling and adjustment of the pH to 6 using hydrochloric acid (1 M), $EuCl_3.6H_2O$ (3 mg, 8 µmol) was added and the reaction mixture was heated to 60 °C for 19 h. The reaction mixture was purified by RP-HPLC (10 to 100% CH_3CN in H_2O over 10 min, $\mathbf{t_R}$ = 12.4 min) to yield a yellow solid (4 mg, 48%); **ESI-LRMS** (+) *m/z* 1390 $[M+H]^+$, 696 $[M+2H]^{2+}$, 464 $[M+3H]^{3+}$; **ESI-HRMS** (+) calcd for $[C_{66}H_{82}N_9O_9P_3{}^{151}Eu]^+$ 1390.467, found 1390.470; $\boldsymbol{\tau_{H2O}}$ (ms) = 0.24 (pH 9), 0.25 (pH 8), 0.32 (pH 7), 0.59 (pH 6), 0.83 (pH 5), 0.84 (pH 4); $\boldsymbol{\chi_{331\ nm}}$ = 45,000 (pH 8) – 60,000 (pH 4) $M^{-1}\ cm^{-1}$; $\boldsymbol{\Lambda_{pH\ 8}}$ = 0.1%, $\boldsymbol{\Lambda_{pH\ 4}}$ = 17.0% (λ_{exc} 331 nm).

[Gd.L^3]

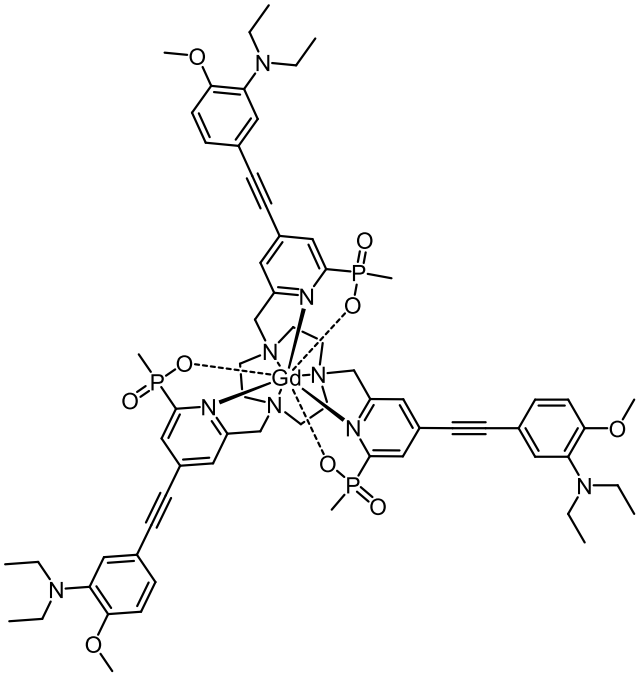

The ligand **L^3** (35 mg, 0.026 mmol) was dissolved in a mixture of CH_3OH/H_2O (1:1, 4 mL total) and the pH was adjusted to 12 using aqueous NaOH solution (1 M). The solution was heated at 60 °C for 15 h. After cooling and adjustment of the pH to 6 using dilute hydrochloric acid (0.1 M), $GdCl_3.6H_2O$ (15 mg, 0.040 mmol) was added and the reaction mixture was heated to 60 °C for 24 h. After this time, the solution was separated from the inorganic salts by centrifugation and purified by RP-HPLC (10 to 100% CH_3CN in 25 mM ammonium bicarbonate buffer over 10 min, $\mathbf{t_R}$ = 12.0 min) to yield a yellow solid (22 mg, 60%); **ESI-LRMS** (+) *m/z* 1395 $[M+H]^+$, 698 $[M+2H]^{2+}$, 466 $[M+3H]^{3+}$; **ESI-HRMS** (+) calcd for $[C_{66}H_{82}N_9O_9P_3{}^{158}Gd]^+$ 1395.471, found 1395.464.

7.7.2. Synthesis of the O-Substituted Sulfonated Complexes

7.7.2.1. Synthesis of pro-L[9a-b]

Ethyl 4-(4-bromo-2-nitrophenoxy)butanoate, 12

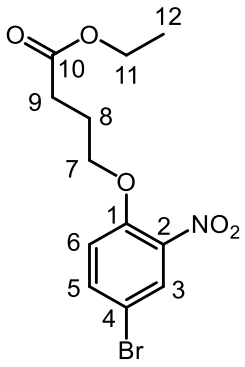

To a mixture of 4-bromo-2-nitrophenol (2.49 g, 11.4 mmol) and K_2CO_3 (2.31 g, 16.7 mmol) in anhydrous CH_3CN (40 mL) under argon was added ethyl 4-bromobutyrate (2.3 mL, 17.2 mmol). The mixture was heated at 70 °C for 64 h before removal of solvent under reduced pressure. DCM (50 mL) was added to the residue and the resulting suspension washed with H_2O (5 × 50 mL). The organic layer was dried over K_2CO_3 before removal of solvent under reduced pressure to yield a crude residue that was purified by column chromatography (SiO_2, 1:1 hexane/CH_2Cl_2 to 100% CH_2Cl_2) to afford a pale yellow oil (3.38 g, 98%); **^{1}H-NMR** (700 MHz, $CDCl_3$) δ 7.95 (1H, d, $^4J_{H\text{-}H}$ 2.5, H^3), 7.60 (1H, dd, $^3J_{H\text{-}H}$ 8.9, $^4J_{H\text{-}H}$ 2.5, H^5), 6.97 (1H, d, $^3J_{H\text{-}H}$ 8.9, H^6), 4.17–4.12 (4H, m, H^7 & H^{11}), 2.55 (2H, t, $^3J_{H\text{-}H}$ 7.0, H^9), 2.18–2.12 (2H, m, H^8), 1.25 (3H, t, $^3J_{H\text{-}H}$ 7.1, H^{12}); **^{13}C-NMR** (176 MHz, $CDCl_3$) δ 173.1 (C^{10}), 151.6 (C^2), 140.4 (C^1), 137.0 (C^5), 128.5 (C^3), 116.3 (C^6), 112.1 (C^4), 68.9 (C^7), 60.8 (C^{11}), 30.3 (C^9), 24.3 (C^8), 14.4 (C^{12}); **ESI-LRMS** (+) *m/z* 332 $[M+H]^+$; **ESI-HRMS** (+) calcd for $[C_{12}H_{15}NO_5Br]^+$ 332.0134, found 332.0146; $\mathbf{R_f}$ = 0.47 (SiO_2, 100% CH_2Cl_2).

Ethyl 4-(2-amino-4-bromophenoxy)butanoate, 13

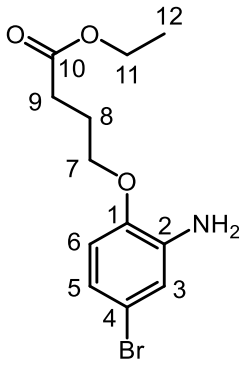

Compound **12** (4.30 g, 12.95 mmol), iron powder (3.60 g, 64.5 mmol) and glacial acetic acid (3.7 mL, 64.6 mmol) were combined in ethanol (20 mL) under argon and heated at 50 °C for 6 h. The mixture was allowed to cool before filtering and removal of solvent under reduced pressure. DCM (50 mL) was added to the resulting mixture and the resulting solution washed with saturated aqueous Na_4EDTA solution (3 × 40 mL) and H_2O (2 × 40 mL). The combined aqueous layers were extracted with CH_2Cl_2 (6 × 40 mL). The combined organic layers were dried over K_2CO_3 and the solvent was removed under reduced pressure to afford a pale golden oil (3.5 g, 90%); **^{1}H-NMR** (700 MHz, $CDCl_3$) δ 6.75 (1H, d, $^4J_{H\text{-}H}$ = 2.4, H^3), 6.70 (1H, dd, $^3J_{H\text{-}H}$ 8.4, $^4J_{H\text{-}H}$ 2.4, H^5), 6.55 (1H, d, $^3J_{H\text{-}H}$ 8.4, H^6), 4.11 (2H, q, $^3J_{H\text{-}H}$ 7.2, H^{11}), 3.93 (2H, t, $^3J_{H\text{-}H}$ 6.1, H^9), 3.89 (2H, br s, NH_2), 2.46 (1H, t, $^3J_{H\text{-}H}$ 7.1, H^7), 2.11–2.06 (2H, m, H^8), 1.22 (3H, t, $^3J_{H\text{-}H}$ 7.2, H^{12}); **^{13}C-NMR** (176 MHz, $CDCl_3$) δ 173.1 (C^{10}), 145.3 (C^2), 138.0 (C^1), 120.3 (C^5), 117.2 (C^3), 113.3 (C^4), 112.6 (C^6), 67.4 (C^9), 60.5 (C^{11}), 31.0 (C^7), 24.6 (C^8), 14.2 (C^{12}); **ESI-LRMS** (+) *m/z* 302 $[M+H]^+$; **ESI-HRMS** (+) calcd for $[C_{12}H_{17}NO_3Br]^+$ 302.0392, found 302.0402.

Ethyl 4-(2-*N*-aminoethyl-4-bromophenoxy)butanoate, 14

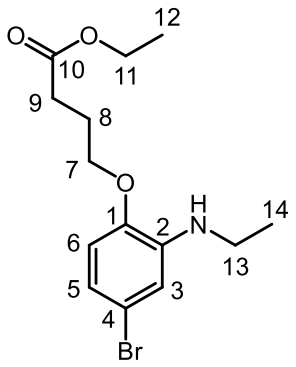

To compound **13** (3.50 g, 11.6 mmol) and K_2CO_3 (4.8 g, 34.5 mmol) in anhydrous CH_3CN under argon (3 mL) was added iodoethane (1.21 mL, 15.0 mmol). This mixture was heated at 55 °C for 70 h before filtration to remove the inorganic salts, followed by removal of the solvent under reduced pressure. The resulting oil was purified by column chromatography (SiO_2, 100% DCM) to afford a pale yellow oil (1.65 g, 43%); **^{1}H-NMR** (700 MHz, $CDCl_3$) δ 6.70 (1H, dd, $^3J_{H\text{-}H}$ 8.3, H^5), 6.67 (1H, s, H^3), 6.57 (1H, d, $^3J_{H\text{-}H}$ 8.3, H^6), 4.15 (2H, q, $^3J_{H\text{-}H}$ 7.1, H^{11}), 4.00 (2H, t, $^3J_{H\text{-}H}$ 6.1, H^9), 3.13 (2H, q, $^3J_{H\text{-}H}$ 7.2, H^{13}), 2.49 (2H, t, $^3J_{H\text{-}H}$ 7.1, H^7), 2.18–2.11 (2H, m, H^8), 1.29 (3H, t, $^3J_{H\text{-}H}$ 7.2, H^{14}), 1.25 (3H, t, $^3J_{H\text{-}H}$ 7.1, H^{12}); **^{13}C-NMR** (176 MHz, $CDCl_3$) δ 173.3 (C^{10}), 145.0 (C^2), 139.8 (C^1), 118.4 (C^5), 114.3 (C^4), 112.7 (C^3), 111.6 (C^6), 67.6 (C^9), 60.7 (C^{11}), 38.2 (C^{13}), 31.3 (C^7), 24.7 (C^8), 14.7 (C^{14}), 14.4 (C^{12}); **ESI-LRMS** (+) *m/z* 331 $[M+H]^+$; **ESI-HRMS** (+) calcd for $[C_{14}H_{21}NO_3Br]^+$ 330.0705, found 330.0714; **R_f** = 0.4 (SiO_2, neat DCM).

Ethyl 4-(4-bromo-2-*N*,*N*-(diethylamino)phenoxy)butanoate, 15a

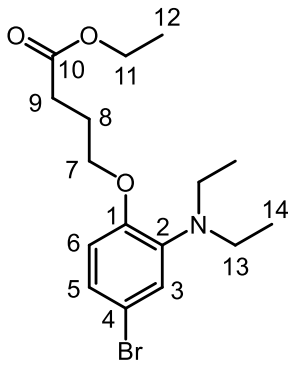

To compound **13** (3.19 g, 10.6 mmol) and K_2CO_3 (3.73 g, 27.0 mmol) in anhydrous CH_3CN (10 mL) under argon was added iodoethane (4 mL, 50 mmol). The mixture

was heated at 70 °C for 65 h before removal of solvent under reduced pressure. The resulting residue was dissolved in DCM (50 mL) and washed with H_2O (4 × 50 mL), before drying over K_2CO_3. Removal of solvent under reduced pressure yielded a crude residue that was purified by column chromatography (SiO_2, neat DCM to 1% CH_3OH in DCM) to afford a light red oil (2.51 g, 66%); **^{1}H-NMR** (700 MHz, $CDCl_3$) δ 6.99–6.96 (2H, m, H^5 & H^3), 6.69 (1H, d, $^3J_{H\text{-}H}$ 8.4, H^6), 4.13 (2H, q, $^3J_{H\text{-}H}$ 7.2, H^{11}), 3.99 (2H, t, $^3J_{H\text{-}H}$ 6.3, H^7), 3.13 (4H, q, $^3J_{H\text{-}H}$ 7.0, H^{13}), 2.51 (2H, t, $^3J_{H\text{-}H}$ 7.4, H^9), 2.15–2.10 (2H, m, H^8), 1.25 (3H, t, $^3J_{H\text{-}H}$ 7.0, H^{12}), 1.04 (6H, t, $^3J_{H\text{-}H}$ 7.0, H^{14}); **^{13}C-NMR** (176 MHz, $CDCl_3$) δ 173.2 (C^{10}), 151.8 (C^2), 141.8 (C^1), 124.4 (C^3), 124.1 (C^5), 114.8 (C^6), 113.4 (C^4), 67.8 (C^7), 60.6 (C^{11}), 45.7 (C^{13}), 31.0 (C^9), 24.9 (C^8), 14.4 (C^{12}), 12.5 (C^{14}); **ESI-LRMS** (+) *m/z* 358 $[M+H]^+$; **ESI-HRMS** (+) calcd for $[C_{16}H_{25}NO_3Br]^+$ 358.1018, found 358.1020; **R_f** = 0.04 (SiO_2, neat DCM), 0.3 (1% CH_3OH in DCM).

Ethyl 4-(4-bromo-2-*N*,*N*-(ethylmethylamino)phenoxy)butanoate, 15b

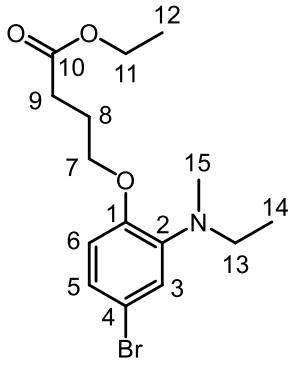

Compound **14** (939 mg, 2.84 mmol), paraformaldehyde (415 mg, 4.61 mmol) and a few drops of acetic acid were combined in anhydrous ethanol (25 mL). The mixture was stirred at room temperature under argon for 20 min, at which point $NaBH_3CN$ was added (640 mg, 10 mmol) and the reaction stirred for a further 48 h. Following the removal of solvent under reduced pressure, the resulting residue was dissolved in DCM (30 mL) and washed successively with $NaHCO_3$ solution (1 × 30 mL) and H_2O (3 × 30 mL). The organic layer was dried over K_2CO_3 and the solvent removed under reduced pressure to yield a pale yellow oil (833 mg, 85%); **^{1}H-NMR** (400 MHz, $CDCl_3$) δ 7.00 (1H, dd, $^3J_{H\text{-}H}$ 8.3, $^4J_{H\text{-}H}$ 2.3, H^5), 6.98 (1H, d, $^4J_{H\text{-}H}$ 2.3, H^3), 6.70 (1H, d, $^3J_{H\text{-}H}$ 8.3, H^6), 4.16 (2H, q, $^3J_{H\text{-}H}$ 7.1, H^{11}), 4.02 (2H, t, $^3J_{H\text{-}H}$ 6.3, H^7), 3.13 (2H, q, $^3J_{H\text{-}H}$ 7.2, H^{13}), 2.76 (2H, s, H^{15}), 2.54 (2H, t, $^3J_{H\text{-}H}$ 7.3, H^9), 2.17–2.10 (2H, m, H^8), 1.27 (3H, t,

$^{3}J_{H\text{-}H}$ 7.1, H^{12}), 1.12 (3H, t, $^{3}J_{H\text{-}H}$ 7.2, H^{14}); **^{13}C-NMR** (176 MHz, $CDCl_3$) δ 172.9 (C^{10}), 150.6 (C^{1}), 143.3 (C^{2}), 123.9 (C^{5}), 118.0 (C^{3}), 113.8 (C^{6}), 113.3 (C^{4}), 67.4 (C^{7}), 60.5 (C^{11}), 49.2 (C^{13}), 39.0 (C^{15}), 30.8 (C^{9}), 24.7 (C^{8}), 14.2 (C^{12}), 12.2 (C^{14}); **ESI-LRMS** (+) m/z 344 $[M+H]^+$; **ESI-HRMS** (+) calcd for $[C_{15}H_{23}NO_3Br]^+$ 344.0861, found 344.0872.

Ethyl 4-(2-*N*,*N*-(diethylamino)-4-((trimethylsilyl)ethynyl)phenoxy)butanoate, 16a

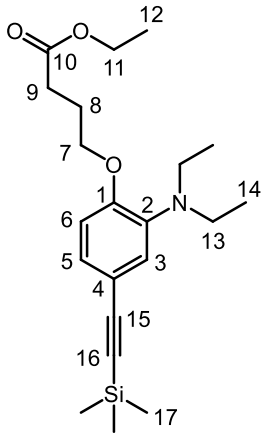

Compound **15a** (3.03 g, 8.46 mmol) and $Pd_2Cl_2(allyl)_2$ (310 mg, 0.85 mmol) were combined and the vessel was degassed then back-filled with argon in three cycles, followed by the addition of anhydrous CH_3CN (15 mL). To this mixture was added P(*t*-Bu)$_3$ (0.31 mL, 1.28 mmol), trimethylsilylacetylene (2.4 mL, 17.3 mmol) and piperidine (2.1 mL, 21.3 mmol) in that order. The reaction mixture was stirred at 35 °C for 30 h. The solvent was subsequently removed under reduced pressure and the residue dissolved in DCM (50 mL). The solution was washed with H_2O (4 × 50 mL) before drying over K_2CO_3. Removal of solvent under reduced pressure yielded a brown oil which was purified by column chromatography (SiO_2, 100% hexane to 6% EtOAc in hexane) to afford a yellow oil (2.29 mg, 75%); **^{1}H-NMR** (600 MHz, $CDCl_3$) δ 7.06 (1H, dd, $^{3}J_{H\text{-}H}$ 8.4, $^{4}J_{H\text{-}H}$ 2.0, H^{5}), 7.01 (1H, d, $^{4}J_{H\text{-}H}$ 2.0, H^{3}), 6.74 (1H, d, $^{3}J_{H\text{-}H}$ 8.4, H^{6}), 4.14 (2H, q, $^{3}J_{H\text{-}H}$ 7.1, H^{11}), 4.03 (2H, t, $^{3}J_{H\text{-}H}$ 6.1, H^{7}), 3.13 (4H, q, $^{3}J_{H\text{-}H}$ 7.2, H^{13}), 2.52 (2H, t, $^{3}J_{H\text{-}H}$ 7.3, H^{9}), 2.17–2.11 (2H, m, H^{8}), 1.27 (3H, t, $^{3}J_{H\text{-}H}$ 7.1, H^{12}), 1.03 (6H, t, $^{3}J_{H\text{-}H}$ 7.2, H^{14}), 0.24 (9H, s, H^{17}); **^{13}C-NMR** (151 MHz, $CDCl_3$) δ 173.1 (C^{10}), 153.3 (C^{2}), 139.7 (C^{1}), 126.6 (C^{5}), 125.0 (C^{3}), 115.2 (C^{4}), 112.6 (C^{6}), 105.8 (C^{15}) 91.7 (C^{16}), 67.3 (C^{7}), 60.4 (C^{11}), 45.6 (C^{13}), 30.9 (C^{9}), 24.6 (C^{8}), 14.2 (C^{12}), 12.3 (C^{14}), 0.10 (C^{17}); **^{29}Si NMR** (139 MHz, $CDCl_3$) δ -16.0; **ESI-LRMS** (+) *m/z* 376 $[M+H]^+$; **ESI-HRMS** (+) calcd for $[C_{21}H_{34}NO_3Si]^+$ 376.2308, found 376.2299; **R_f** = 0.30 (SiO_2, 10% EtOAc in hexane).

Ethyl 4-(2-*N*,*N*-(ethylmethylamino)-4-((trimethylsilyl)ethynyl)phenoxy)butanoate, 16b

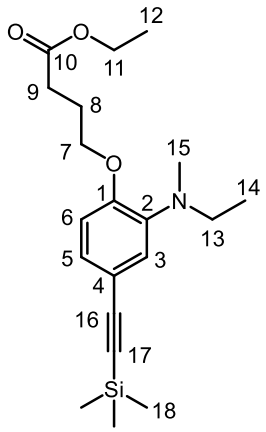

Compound **4b** (1.47 g, 4.27 mmol) and $Pd_2Cl_2(allyl)_2$ (160 mg, 0.44 mmol) were combined and the vessel was degassed then back-filled with argon in three cycles followed by the addition of anhydrous CH_3CN (8 mL). To this mixture was added P(*t*-Bu)$_3$ (0.16 mL, 0.66 mmol), trimethylsilylacetylene (1.2 mL, 8.66 mmol) and piperidine (1.0 mL, 10.1 mmol) in that order. The reaction mixture was stirred at 35 °C for 19 h. The solvent was subsequently removed under reduced pressure and the residue dissolved in DCM (50 mL). The solution was washed with H_2O (2 × 50 mL) before drying over K_2CO_3. Removal of solvent under reduced pressure yielded a brown oil which was purified by column chromatography (SiO_2, 100% hexane to 7% EtOAc in hexane) to afford a pale orange oil (1.19 g, 77%); **^{1}H-NMR** (600 MHz, $CDCl_3$) δ 7.05 (1H, d, $^3J_{H\text{-}H}$ 8.2, H^5), 7.00 (1H, s, H^3), 6.73 (1H, d, $^3J_{H\text{-}H}$ 8.2, H^6), 4.14 (2H, q, $^3J_{H\text{-}H}$ 7.1, H^{11}), 4.04 (2H, t, $^3J_{H\text{-}H}$ 6.2, H^7), 3.09 (2H, d, $^3J_{H\text{-}H}$ 7.0, H^{13}), 2.75 (3H, s, H^{15}), 2.53 (2H, t, $^3J_{H\text{-}H}$ 7.3, H^9), 2.20–2.13 (2H, m, H^8), 1.25 (3H, t, $^3J_{H\text{-}H}$ 7.1, H^{12}), 1.09 (3H, t, $^3J_{H\text{-}H}$ 7.0, H^{14}), 0.24 (9H, s, H^{18}); **^{13}C-NMR** (151 MHz, $CDCl_3$) δ 173.2 (C^{10}), 152.3 (C^1), 141.7 (C^2), 126.4 (C^5), 122.7 (C^3), 115.4 (C^4), 112.1 (C^6), 105.9 (C^{16}), 92.0 (C^{17}), 67.3 (C^7), 60.6 (C^{11}), 49.5 (C^{13}), 39.3 (C^{15}), 31.0 (C^9), 24.8 (C^8), 14.4 (C^{12}), 12.3 (C^{14}), 0.2 (C^{18}); **^{29}Si-NMR** (139 MHz, $CDCl_3$) δ -18.3; **ESI-LRMS** (+) *m/z* 362 $[M+H]^+$; **ESI-HRMS** (+) calcd for $[C_{20}H_{32}NO_3Si]^+$ 362.2151, found 362.2152; **R_f** = 0.20 (SiO_2, 10% EtOAc in hexane).

Ethyl 4-(2-*N*,*N*-(diethylamino)-4-ethynylphenoxy)butanoate, 17a

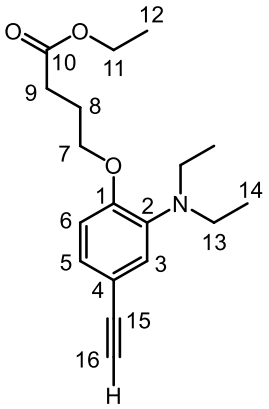

Triethylamine trihydrofluoride (6.25 mL, 38 mmol) was added to compound **16a** (960 mg, 2.56 mmol) in anhydrous THF (8 mL) under argon. The solution was stirred at 30 °C for 24 h before removal of solvent under reduced pressure. The residue was subsequently dissolved in DCM (30 mL) and washed with H_2O (6 × 30 mL). The combined aqueous layers were extracted with DCM (2 × 30 mL) before drying the combined organic layers over K_2CO_3 to yield a yellow oil (749 mg, 97%). The product was used in the next step without further purification; **^{1}H-NMR** (700 MHz, $CDCl_3$) δ 7.07 (1H, dd, $^3J_{H\text{-}H}$ 8.3, $^4J_{H\text{-}H}$ 2.0, H^5), 7.03 (1H, d, $^4J_{H\text{-}H}$ 2.0, H^3), 6.75 (1H, d, $^3J_{H\text{-}H}$ 8.3, H^6), 4.13 (2H, q, $^3J_{H\text{-}H}$ 7.2, H^{11}), 4.03 (2H, t, $^3J_{H\text{-}H}$ 6.3, H^7), 3.13 (4H, q, $^3J_{H\text{-}H}$ 7.2, H^{13}), 2.97 (1H, s, H^{16}), 2.52 (2H, t, $^3J_{H\text{-}H}$ 7.4, H^9), 2.17–2.12 (2H, m, H^8), 1.25 (3H, t, $^3J_{H\text{-}H}$ 7.2, H^{12}), 1.03 (6H, t, $^3J_{H\text{-}H}$ 7.1, H^{14}); **^{13}C-NMR** (176 MHz, $CDCl_3$) δ 173.1 (C^{10}), 153.4 (C^1), 139.8 (C^2), 126.4 (C^5), 125.0 (C^3), 114.0 (C^4), 112.7 (C^6), 84.3 (C^{15}), 75.2 (C^{16}), 67.3 (C^7), 60.4 (C^{11}), 45.6 (C^{13}), 30.9 (C^9), 24.6 (C^8), 14.2 (C^{12}), 12.3 (C^{14}); **ESI-LRMS** (+) *m/z* 304 $[M+H]^+$; **ESI-HRMS** (+) calcd for $[C_{18}H_{26}NO_3]^+$ 304.1913, found 304.1914.

Ethyl 4-(2-(*N*,*N*-ethylmethylamino)-4-ethynylphenoxy)butanoate, 17b

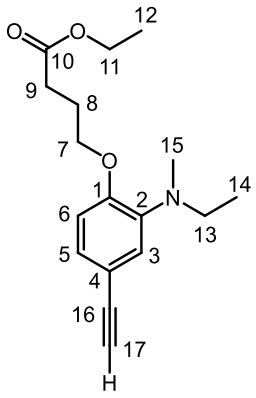

Triethylamine trihydrofluoride (3.6 mL, 22.0 mmol) was added to compound **16b** (530 mg, 1.47 mmol) in anhydrous THF (5 mL) under argon. The solution was stirred at 30 °C for 17 h before removal of solvent under reduced pressure. The residue was subsequently dissolved in DCM (30 mL) and washed with H_2O (3 × 30 mL). The combined aqueous layers were extracted with DCM (2 × 30 mL) and the combined organic layers dried over K_2CO_3 to yield a yellow oil (410 mg, 97%). The product was used in the next step without further purification; **^{1}H-NMR** (600 MHz, $CDCl_3$) δ 7.07 (1H, dd, $^3J_{H\text{-}H}$ 8.3, $^4J_{H\text{-}H}$ 2.0, H^5), 7.02 (1H, d, $^4J_{H\text{-}H}$ 2.0, H^3), 6.75 (1H, d, $^3J_{H\text{-}H}$ 8.3, H^6), 4.14 (2H, q, $^3J_{H\text{-}H}$ 7.1, H^{11}), 4.04 (2H, t, $^3J_{H\text{-}H}$ 6.3, H^7), 3.10 (2H, q, $^3J_{H\text{-}H}$ 7.2, H^{13}), 2.97 (1H, s, H^{17}), 2.75 (3H, s, H^{15}), 2.53 (2H, t, $^3J_{H\text{-}H}$ 7.3, H^9), 2.21–2.14 (2H, m, H^8), 1.25 (3H, t, $^3J_{H\text{-}H}$ 7.1, H^{12}), 1.10 (3H, t, $^3J_{H\text{-}H}$ 7.2, H^{14}); **^{13}C-NMR** (151 MHz, $CDCl_3$) δ 173.2 (C^{10}), 152.5 (C^1), 141.8 (C^2), 126.3 (C^5), 122.8 (C^3), 114.3 (C^4), 112.2 (C^6), 84.4 (C^{16}), 75.4 (C^{17}), 67.3 (C^7), 60.6 (C^{11}), 49.4 (C^{13}), 39.2 (C^{15}), 31.0 (C^9), 24.8 (C^8), 14.4 (C^{12}), 12.4 (C^{14}); **ESI-LRMS** (+) *m/z* 290 $[M+H]^+$; **ESI-HRMS** (+) calcd for $[C_{17}H_{24}NO_3]^+$ 290.1756, found 290.1752.

Ethyl 4-(2-*N*,*N*-(diethylamino)-4-((2-(ethoxy(methyl)phosphoryl)-6-(hydroxymethyl)pyridine-4-yl)ethynyl)phenoxy)butanoate, 18a

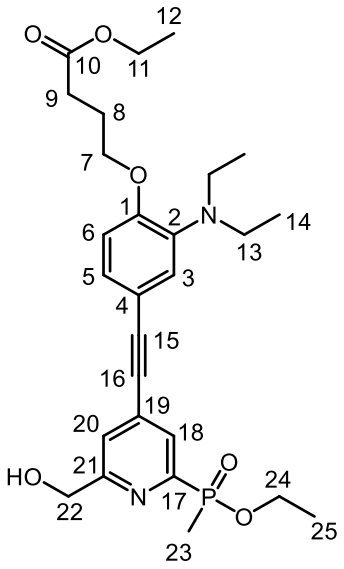

Compound **17a** (528 mg, 1.74 mmol) and compound **5** (486 mg, 1.65 mmol) were combined in anhydrous CH_3CN (10 mL) under argon. To this solution was added $Pd_2Cl_2(allyl)_2$ (70 mg, 0.191 mmol), $P(^tBu)_3$ (0.06 mL, 0.25 mmol) and piperidine (0.43 mL, 4.70 mmol) in that order. The resulting mixture was stirred at 40 °C under argon for 36 h before removal of the solvent under reduced pressure. The residue was dissolved in DCM (40 mL) and washed with H_2O (3 × 40 mL) before drying over K_2CO_3 followed by removal of solvent under reduced pressure. The crude product was purified by RP-HPLC (10 to 100% CH_3CN in H_2O over 10 min, $\mathbf{t_R}$ = 12.2 min) to yield a pale orange oil (359 mg, 40%); **^{1}H-NMR** (400 MHz, $CDCl_3$) δ 8.04 (1H, d, $^3J_{H\text{-}P}$ 6.0, H^{18}), 7.47 (1H, s, H^{20}), 7.13 (1H, d, $^3J_{H\text{-}H}$ 8.4, H^5), 7.07 (1H, s, H^3), 6.82 (1H, d, $^3J_{H\text{-}H}$ 8.4, H^6), 4.81 (2H, s, H^{22}), 4.22–3.78 (6H, m, H^7, H^{11} & H^{24}), 3.17 (4H, q, $^3J_{H\text{-}H}$ 6.9, H^{13}), 2.53 (2H, t, $^3J_{H\text{-}H}$ 7.2, H^9), 2.22–2.11 (2H, m, H^8), 1.78 (3H, d, $^2J_{H\text{-}P}$ 15, H^{23}), 1.31–1.22 (6H, m, H^{12} & H^{25}), 1.06 (6H, t, $^3J_{H\text{-}H}$ 6.9, H^{14}); **^{13}C-NMR** (101 MHz, $CDCl_3$) δ 173.0 (C^{10}), 160.4 (d, $^3J_{C\text{-}P}$ 19, C^{21}), 153.9 (C^1), 153.1 (d, $^1J_{C\text{-}P}$ 155, C^{17}), 140.0 (C^2), 133.2 (d, $^3J_{C\text{-}P}$ 11, C^{19}), 128.3 (d, $^2J_{C\text{-}P}$ 22, C^{18}), 126.5 (C^5), 124.8 (C^3), 124.0 (d, $^4J_{C\text{-}P}$ 3, C^{20}), 113.6 (C^4), 112.8 (C^6), 97.1 (C^{15}), 84.7 (C^{16}), 67.4 (C^7), 64.0 (C^{22}), 61.2 (d, $^2J_{C\text{-}P}$ 6.2, C^{24}), 60.5 (C^{11}), 45.6 (C^{13}), 30.8 (C^9), 24.6 (C^8), 16.5 (d, $^3J_{C\text{-}P}$ 6.0, C^{25}), 14.2 (C^{12}), 13.5 (d, $^1J_{C\text{-}P}$ 105, C^{23}), 12.3 (C^{14}); **^{31}P{^{1}H}-NMR** (162 MHz, $CDCl_3$) δ +39.4; **ESI-LRMS** (+) *m/z* 517 $[M+H]^+$; **ESI-HRMS** (+) calcd for $[C_{27}H_{38}N_2O_6P]^+$ 517.2468, found 517.2451.

Ethyl 4-(2-*N*,*N*-(ethylmethylamino)-4-((2-(ethoxy(methyl)phosphoryl)-6-(hydroxymethyl)pyridine-4-yl)ethynyl)phenoxy)butanoate, 18b

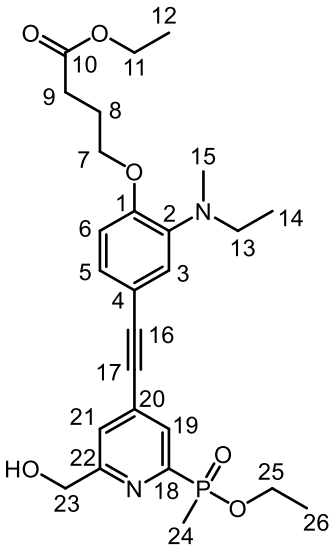

Compound **17b** (396 mg, 1.37 mmol) and compound **5** (362 mg, 1.23 mmol) were combined in anhydrous CH_3CN (10 mL) under argon. To this solution was added $Pd_2Cl_2(allyl)_2$ (50 mg, 0.137 mmol), $P(^tBu)_3$ (0.05 mL, 0.21 mmol) and piperidine (0.4 mL, 4.37 mmol) in that order. The resulting mixture was stirred at 40 °C under argon for 36 h before removal of the solvent under reduced pressure. The residue was dissolved in DCM (40 mL) and washed with H_2O (3 × 40 mL) before drying over K_2CO_3 and removal of the solvent under reduced pressure to give an orange oil that was purified by RP-HPLC (10 to 100% CH_3CN over 10 min, $\mathbf{t_R}$ = 13.2 min) to afford a pale orange oil (185 mg, 30%); **^{1}H-NMR** (600 MHz, $CDCl_3$) δ 8.02 (1H, d, $^3J_{H\text{-}P}$ 6.0, H^{19}), 7.47 (1H, s, H^{21}), 7.12 (1H, dd, $^3J_{H\text{-}H}$ 8.3, $^4J_{H\text{-}H}$ 2.0, H^5), 7.05 (1H, d, $^4J_{H\text{-}H}$ 2.0, H^3), 6.80 (1H, d, $^3J_{H\text{-}H}$ 8.3, H^6), 4.80 (2H, s, H^{23}), 4.14 (2H, q, $^3J_{H\text{-}H}$ 7.2, H^{11}), 4.12–4.08 & 3.90–3.83 (2H, m, H^{25}), 4.07 (2H, t, $^3J_{H\text{-}H}$ 6.4, H^7), 3.12 (2H, q, $^3J_{H\text{-}H}$ 7.0, H^{13}), 2.78 (3H, s, H^{15}), 2.53 (2H, t, $^3J_{H\text{-}H}$ 7.3, H^9), 2.21–2.15 (2H, m, H^8), 1.77 (3H, d, $^2J_{H\text{-}P}$ 15, H^{24}), 1.27 (3H, t, $^3J_{H\text{-}H}$ 7.0, H^{26}), 1.25 (3H, t, $^3J_{H\text{-}H}$ 7.2, H^{12}), 1.12 (3H, t, $^3J_{H\text{-}H}$ 7.0, H^{14}); **^{13}C-NMR** (151 MHz, $CDCl_3$) δ 173.1 (C^{10}), 160.7 (d, $^3J_{C\text{-}P}$ 19, C^{22}), 153.3 (d, $^1J_{C\text{-}P}$ 155, C^{18}), 153.1 (C^1), 142.1 (C^2), 133.3 (d, $^3J_{C\text{-}P}$ 11, C^{20}), 128.3 (d, $^2J_{C\text{-}P}$ 22, C^{19}), 126.4 (C^5), 124.1 (d, $^4J_{C\text{-}P}$ 3, C^{21}), 122.6 (C^3), 113.9 (C^4), 112.3 (C^6), 97.1 (C^{16}), 84.9 (C^{17}), 67.4 (C^7), 64.2 (C^{23}), 61.3 (d, $^2J_{C\text{-}P}$ 6, C^{25}), 60.6 (C^{11}), 49.4 (C^{13}), 39.2 (C^{15}), 31.0 (C^9), 24.7 (C^8), 16.6 (d, $^3J_{C\text{-}P}$ 6, C^{26}), 14.3 (C^{12}), 13.6 (d, $^1J_{C\text{-}P}$ 104, C^{24}), 12.4 (C^{14}); **^{31}P{^{1}H}-NMR** (162 MHz, $CDCl_3$) δ +39.5; **ESI-LRMS** (+) *m/z* 503 $[M+H]^+$; **ESI-HRMS** (+) calcd for $[C_{26}H_{36}N_2O_6P]^+$ 503.2311, found 503.2297.

Ethyl-4-(2-*N*,*N*-(diethylamino)-4-((2-(ethoxy(methyl)phosphoryl)-6-(((methylsulfonyl)oxy)methyl)pyridine-4-yl)ethynyl)phenoxy)butanoate, 19a

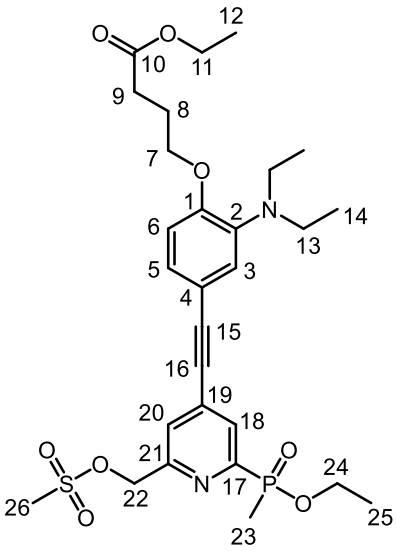

Compound **18a** (250 mg, 0.484 mmol), methanesulfonic anhydride (126 mg, 0.72 mmol) and DIEA (0.25 mL, 1.44 mmol) were combined in anhydrous THF (2 mL) under argon. The reaction mixture was stirred at room temperature for 1 h, monitoring the progress of the reaction by TLC. Following complete conversion, the solvent was removed under reduced pressure and the resulting crude residue dissolved in DCM (40 mL), washed with H_2O (3 × 40 mL) and the organic layer dried over K_2CO_3. Removal of solvent under reduced pressure afforded an orange oil (288 mg, quant.); **^{1}H-NMR** (400 MHz, $CDCl_3$) δ 8.10 (1H, d, $^3J_{H\text{-}P}$ 6.0, H^{18}), 7.64 (1H, s, H^{20}), 7.15 (1H, d, $^3J_{H\text{-}H}$ 8.4, H^5), 7.09 (1H, s, H^3), 6.83 (1H, d, $^3J_{H\text{-}H}$ 8.4, H^6), 5.37 (2H, s, H^{22}), 4.19–3.82 (6H, m, H^7, H^{11} & H^{24}), 3.18 (4H, q, $^3J_{H\text{-}H}$ 7.0, H^{13}), 3.14 (3H, s, H^{26}), 2.54 (2H, t, $^3J_{H\text{-}H}$ 7.2, H^9), 2.22–2.13 (2H, m, H^8), 1.78 (3H, d, $^2J_{H\text{-}P}$ 15, H^{23}), 1.32–1.24 (6H, m, H^{12} & H^{25}), 1.07 (6H, t, $^3J_{H\text{-}H}$ 6.9, H^{14}); **ESI-LRMS** (+) *m/z* 595 $[M+H]^+$; **ESI-HRMS** (+) calcd for $[C_{28}H_{40}N_2O_8SP]^+$ 595.2242, found 595.2236; $\mathbf{R_f}$ = 0.4 (SiO_2, 5% CH_3OH in CH_2Cl_2).

Ethyl-4-(2-*N*,*N*-(ethylmethylamino)-4-((2-(ethoxy(methyl)phosphoryl)-6-(((methylsulfonyl)oxy)methyl)pyridine-4-yl)ethynyl)phenoxy)butanoate, 19b

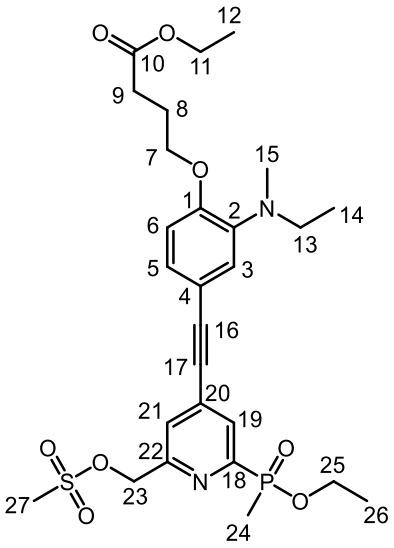

Compound **18b** (160 mg, 0.318 mmol), methanesulfonic anhydride (111 mg, 0.637 mmol) and DIEA (0.11 mL, 0.632 mmol) were combined in anhydrous THF (4 mL) under argon. The reaction mixture was stirred at room temperature for 1 h at which point the solvent was removed under reduced pressure. The resulting crude residue was dissolved in DCM (40 mL), washed with H_2O (3 × 40 mL) and the combined aqueous layers were extracted with DCM (3 × 40 mL). The combined organic layers were dried over K_2CO_3 and the solvent removed under reduced pressure to afford an orange oil (167 mg, 90%); **^{1}H-NMR** (400 MHz, $CDCl_3$) δ 8.10 (1H, d, $^3J_{H\text{-}P}$ 6.0, H^{18}), 7.64 (1H, s, H^{20}), 7.15 (1H, d, $^3J_{H\text{-}H}$ 8.4, H^5), 7.09 (1H, s, H^3), 6.83 (1H, d, $^3J_{H\text{-}H}$ 8.4, H^6), 5.37 (2H, s, H^{22}), 4.19–3.82 (6H, m, H^7, H^{11} & H^{24}), 3.18 (4H, q, $^3J_{H\text{-}H}$ 7.0, H^{13}), 3.14 (3H, s, H^{26}), 2.54 (2H, t, $^3J_{H\text{-}H}$ 7.2, H^9), 2.22–2.13 (2H, m, H^8), 1.78 (3H, d, $^2J_{H\text{-}P}$ 15, H^{23}), 1.32–1.24 (6H, m, H^{12} & H^{25}), 1.07 (6H, t, $^3J_{H\text{-}H}$ 6.9, H^{14}); **ESI-LRMS** (+) *m/z* 595 $[M+H]^+$; **ESI-HRMS** (+) calcd for $[C_{27}H_{38}N_2O_8SP]^+$ 581.2087, found 581.2099; **R_f** = 0.4 (SiO_2, 5% CH_3OH in DCM).

***Tert*-butyl-*E*-(3-(2-(ethoxy(methyl)phosphoryl)-6-(hydroxymethyl)pyridine-4-yl)allyl)carbamate, 20**

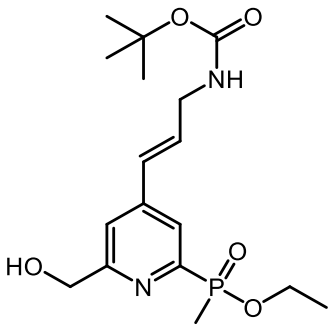

Compound **5** (74 mg, 0.25 mmol), *tert*-butyl N-allylcarbamate (155 mg, 0.99 mmol), palladium(II) acetate (11 mg, 0.05 mmol) and triphenylphosphine (20 mg, 0.08 mmol) were combined in toluene (2 mL) under an argon atmosphere. The reaction mixture was degassed by bubbling argon through the solution for 15 min. Triethylamine (0.3 mL, 2.2 mmol) was added and the mixture was heated to 80 °C under argon for 18 h. After cooling, the solvent was removed under reduced pressure and the resulting residue dissolved in DCM (30 mL), washed with H_2O (4 × 30 mL) and dried over $MgSO_4$. Removal of solvent under reduced pressure gave a crude product that was purified by RP-HPLC (10 to 100% CH_3CN in H_2O over 10 min, $\mathbf{t_R}$ = 9.1 min) to yield a yellow oil as an *E*/*Z* isomeric mixture (93 mg, 63%); **^{1}H-NMR** (400 MHz, $CDCl_3$) *δ* 8.03–7.91 (1H, 2 × d), 7.45–7.28 (1H, 2 × s), 6.61–6.44 (2H, m), 4.83–4.77 (2H, 2 × s), 4.14–4.03 & 3.89–3.77 (2H, m), 3.97–3.93 (2H, m), 1.80–1.74 (3H, 2 × d), 1.48–1.40 (3H, 2 × t); **^{31}P{^{1}H}-NMR** (298 K, 162 MHz, $CDCl_3$) *δ* +40.5, +40.4; **ESI-LRMS** (+) *m/z* 371 $[M+H]^+$; **ESI-HRMS** (+) calcd for $[C_{17}H_{28}N_2O_5P]^+$ 371.1736, found 371.1746.

***Tert*-butyl-(3-(2-(ethoxy(methyl)phosphoryl)-6-(hydroxymethyl)pyridine-4-yl)propyl)carbamate, 21**

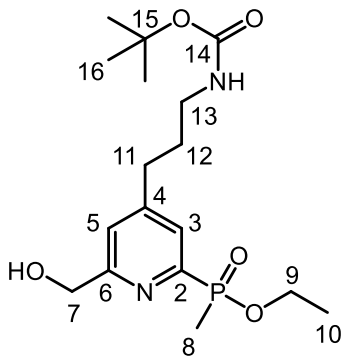

The *E/Z* isomeric mixture of compound **20** (210 mg, 0.57 mmol) was dissolved in ethanol (60 mL) to which palladium on carbon (Pd content 10%, 10 mg) was added. The vessel was then loaded onto a Parr hydrogenator (pressure 40 bar H_2) and the reaction mixture was agitated for 8 h. After this time, the catalyst was removed by filtration and the solvent removed under reduced pressure to yield a pale yellow oil (211 mg, quant.); **^{1}H-NMR** (600 MHz, $CDCl_3$) δ 7.82 (1H, d, $^{3}J_{H\text{-}P}$ 6.0, H^{3}), 7.24 (1H, s, H^{5}), 4.78 (2H, s, H^{7}), 4.66 (1H, br s, NH), 4.12–3.79 (2H, m, H^{9}), 3.18–3.11 (2H, m, H^{13}), 2.73–2.68 (2H, m, H^{11}), 1.87–1.81 (2H, m, H^{12}), 1.76 (3H, d, $^{2}J_{H\text{-}P}$ 15, H^{8}), 1.43 (9H, s, H^{16}), 1.26 (3H, t, $^{3}J_{H\text{-}H}$ 7.0, H^{10}); **^{13}C-NMR** (151 MHz, $CDCl_3$) δ 160.5 (d, $^{3}J_{C\text{-}P}$ 19, C^{6}), 156.1 (C^{14}), 153.0 (d, $^{1}J_{C\text{-}P}$ 156, C^{2}), 152.2 (d, $^{3}J_{C\text{-}P}$ 10, C^{4}), 127.0 (d, $^{2}J_{C\text{-}P}$ 21, C^{3}), 123.0 (C^{5}), 79.5 (C^{15}), 64.1 (C^{7}), 61.2 (d, $^{2}J_{C\text{-}P}$ 6, C^{9}), 40.0 (C^{13}), 32.6 (C^{11}), 30.8 (C^{12}), 28.5 (C^{16}), 16.6 (d, $^{3}J_{C\text{-}P}$ 6, C^{10}), 13.7 (d, $^{1}J_{C\text{-}P}$ 104, C^{8}); **^{31}P{^{1}H}-NMR** (243 MHz, $CDCl_3$) δ +39.9; **ESI-LRMS** (+) *m/z* 373 $[M+H]^+$; **ESI-HRMS** (+) calcd for $[C_{17}H_{30}N_2O_5P]^+$ 373.1892, found 373.1880; **R_f** = 0.40 (SiO_2, 5% CH_3OH in DCM).

(4-(3-((*Tert*-butoxycarbonyl)amino)propyl)-6-(ethoxy(methyl)phosphoryl)pyridine-2-yl)methyl methanesulfonate, 22

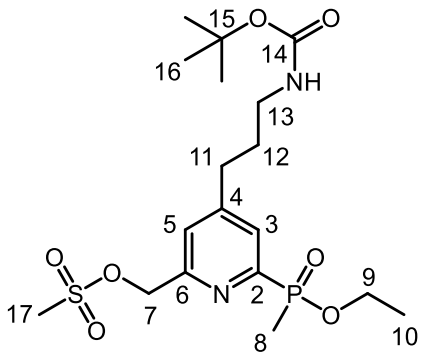

Compound **21** (25 mg, 0.067 mmol), methanesulfonic anhydride (20 mg, 0.115 mmol) and DIEA (0.03 mL, 0.172 mmol) were combined in anhydrous THF (0.5 mL) under argon. The reaction mixture was stirred at room temperature for 1 h, with monitoring by TLC. Following complete conversion, the solvent was removed under reduced pressure and the resulting crude residue dissolved in CH_2Cl_2 (40 mL), washed with water (3 × 40 mL) and the organic layer dried over K_2CO_3. Removal of solvent under reduced pressure afforded a clear oil (30 mg, quant.); **^{1}H-NMR** (400 MHz, $CDCl_3$) δ 7.86 (1H, d, $^3J_{H\text{-}P}$ 6.0, H^3), 7.41 (1H, s, H^5), 5.33 (2H, s, H^7), 4.66 (1H, br s, NH), 4.15–3.77 (2H, m, H^9), 3.19–3.09 (5H, m, H^{13} & H^{17}), 2.76–2.67 (2H, m, H^{11}), 1.89–1.79 (2H, m, H^{12}), 1.74 (3H, d, $^2J_{H\text{-}P}$ 15, H^8), 1.42 (9H, s, H^{16}), 1.25 (3H, t, $^3J_{H\text{-}H}$ 7.1, H^{10}); **ESI-LRMS** (+) *m/z* 373 $[M+H]^+$; **ESI-HRMS** (+) calcd for $[C_{18}H_{32}N_2O_7PS]^+$ 451.1668, found 451.1666; **R_f** = 0.50 (SiO_2, 5% CH_3OH in CH_2Cl_2).

Compound 23a

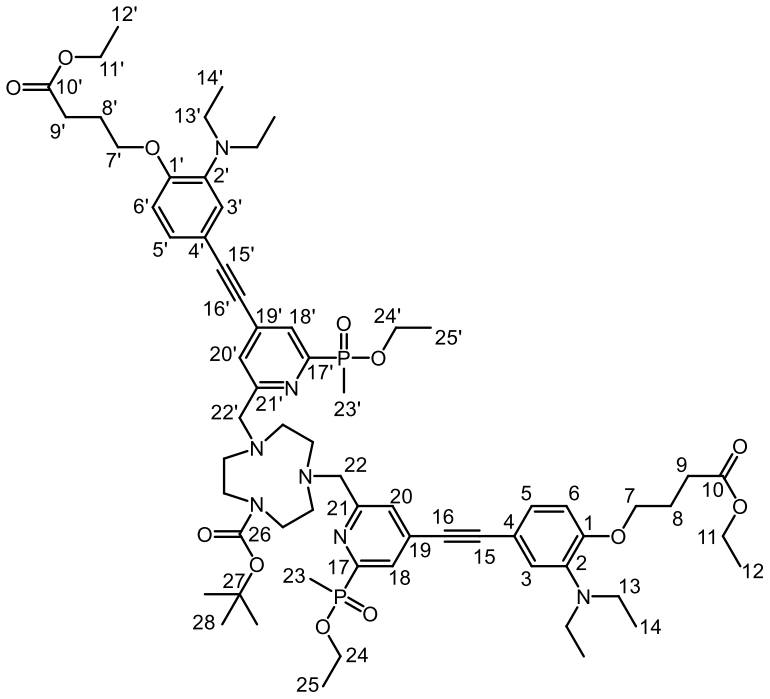

1-*Tert*-butoxycarbonyl-1,4,7-triazacyclononane dihydrochloride (66 mg, 0.218 mmol), the mesylate **19a** (288 mg, 0.484 mmol) and K_2CO_3 (122 mg, 0.833 mmol) were combined in anhydrous CH_3CN (2.5 mL) under argon. The resulting mixture was heated to 70 °C for 16 h before cooling to room temperature. Separation from the inorganic salts was achieved by filtration and removal of the solvent under reduced pressure yielded a crude product as a viscous residue that was purified by RP-HPLC (10 to 100% CH_3CN in H_2O over 10 min, $\mathbf{t_R}$ = 17.5 min) to afford an orange oil (160 mg, 59%); **^{1}H-NMR** (700 MHz, $CDCl_3$) δ 8.01–7.97 (2H, m, H^{18} & $H^{18'}$), 7.65 (1H, s, H^{20}), 7.56 (1H, s, $H^{20'}$), 7.11 (2H, d, H^5 & $H^{5'}$), 7.05 (2H, s, H^3 & $H^{3'}$), 6.80 (2H, d, H^6 & $H^{6'}$), 4.13 (4H, q, H^{11} & $H^{11'}$), 4.11–4.06 & 3.88–3.80 (4H, m, H^{24} & $H^{24'}$), 4.05 (4H, t, H^7 & $H^{7'}$), 3.94 (2H, s, H^{22}), 3.93 (2H, s, $H^{22'}$), 3.41–3.31 (4H, m, 9-N_3 ring), 3.15 (8H, q, H^{13} & $H^{13'}$), 3.12–3.04 (4H, m, 9-N_3 ring), 2.74–2.62 (4H, m, 9-N_3 ring), 2.51 (4H, t, H^9 & $H^{9'}$), 2.18–2.11 (4H, m, H^8 & $H^{8'}$), 1.76 (3H, d, $^2J_{H\text{-}P}$ 15, H^{23}), 1.75 (3H, d, $^2J_{H\text{-}P}$ 15, $H^{23'}$), 1.47 (9H, s, H^{28}), 1.26–1.22 (12H, m, H^{12}, $H^{12'}$, H^{25} & $H^{25'}$), 1.04 (12H, t, H^{14} & $H^{14'}$); **^{13}C-NMR** (176 MHz, $CDCl_3$) δ 173.1 (C^{10} & $C^{10'}$), 161.7 (d, $^3J_{C\text{-}P}$ 20, C^{21}), 161.4 (d, $^3J_{C\text{-}P}$ 20, $C^{21'}$), 155.7 (C^{26}), 154.1 (C^1 & $C^{1'}$), 153.9 (d, $^1J_{C\text{-}P}$ 157, $C^{17'}$), 153.6 (d, $^1J_{C\text{-}P}$ 157, C^{17}), 140.1 (C^2 & $C^{2'}$), 132.8 (app. t, $^3J_{C\text{-}P}$ 11, C^{19} & $C^{19'}$), 127.9 (app. t, $^2J_{C\text{-}P}$ 21, C^{18} & $C^{18'}$), 126.5 (C^5 & $C^{5'}$), 126.4 (d, $^4J_{C\text{-}P}$ 3, C^{20}), 126.2 (d, $^4J_{C\text{-}P}$ 3, $C^{20'}$), 124.8 (C^3 & $C^{3'}$), 114.0 ($C^{4'}$), 113.8 (C^4), 112.8 (C^6 & $C^{6'}$), 96.5 ($C^{15'}$), 96.3 (C^{15}), 85.2 ($C^{16'}$), 85.1

(C^{16}), 79.5 (C^{27}), 67.5 (C^{7} & $C^{7'}$), 62.9 ($C^{22'}$), 62.6 (C^{22}), 61.1 (d, $^{2}J_{C\text{-}P}$ 6.4, $C^{24'}$), 61.0 (d, $^{2}J_{C\text{-}P}$ 6.4, C^{24}), 60.6 (C^{11} & $C^{11'}$), 56.1 (9-N_3 ring), 55.0 (9-N_3 ring), 54.7 (9-N_3 ring), 54.0 (9-N_3 ring), 50.0 (9-N_3 ring), 49.7 (9-N_3 ring), 45.7 (C^{13} & $C^{13'}$), 30.9 (C^{9} & $C^{9'}$), 28.8 (C^{28}), 24.7 (C^{8} & $C^{8'}$), 16.6 (d, C^{25} & $C^{25'}$), 14.3 (C^{12} & $C^{12'}$), 13.4 (d, $^{1}J_{C\text{-}P}$ 104, C^{23}), 13.3 (d, $^{1}J_{C\text{-}P}$ 104, $C^{23'}$), 12.4 (C^{14} & $C^{14'}$); **$^{31}P\{^{1}H\}$-NMR** (283 MHz, $CDCl_3$) δ +40.1, +40.0; **ESI-LRMS** (+) *m/z* 1226 $[M+H]^+$; **ESI-HRMS** (+) calcd for $[C_{65}H_{94}N_7O_{12}P_2]^+$ 1226.644, found 1226.646.

Note: ^{1}H, ^{31}P and ^{13}C NMR analysis each indicate that the chromophore environments are non-equivalent, but are highly similar in several respects. As an illustration, C^{10} and $C^{10'}$ have different corresponding resonances in the ^{13}C spectrum (Δ = 0.01 ppm). It is not prudent to report these environments individually when reporting to an accuracy of 0.1 ppm for ^{13}C NMR. The chemical shift differences for the resonances of the chromophore were observed to decrease as a function of the distance from the macrocyclic ring. Due to the non-equivalent nature of their chemical environments, the *J*-coupling constant values for the resonances corresponding to these multiple environments are not given.

Compound 23b

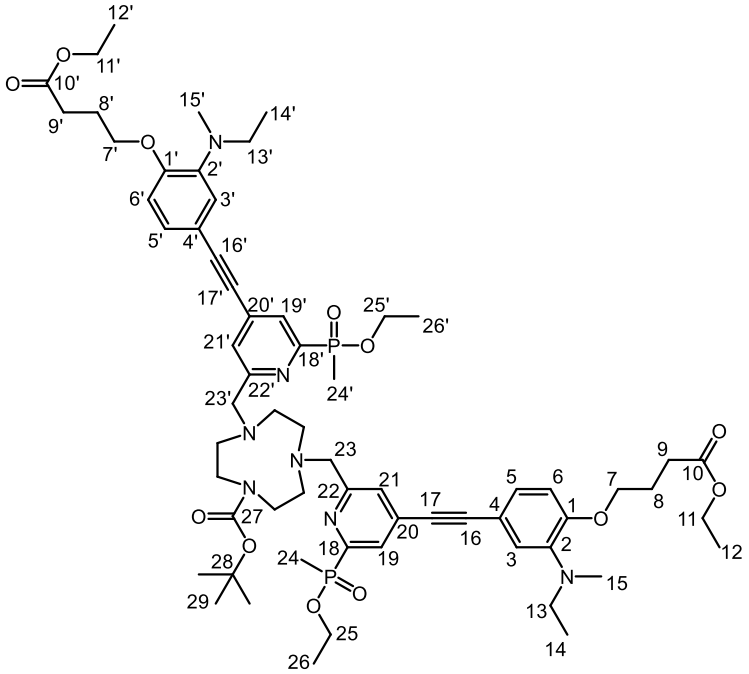

1-*Tert*-butoxycarbonyl-1,4,7-triazacyclononane dihydrochloride (38 mg, 0.126 mmol), the mesylate **8b** (167 mg, 0.288 mmol) and K_2CO_3 (104 mg, 0.753 mmol) were combined in anhydrous CH_3CN (4 mL) under argon. The resulting mixture was heated to 60 °C for 48 h before cooling to room temperature. Separation from the inorganic salts was achieved by filtration and removal of the solvent under reduced pressure yielded a crude product that was purified by RP-HPLC (10 to 100% CH_3CN in H_2O over 10 min, $\mathbf{t_R}$ = 12.2 min) to afford a pale orange oil (110 mg, 73%); **^{1}H-NMR** (400 MHz, $CDCl_3$) δ 8.00 (2H, d, H^{19} & $H^{19'}$), 7.65 (1H, s, H^{21}), 7.59 (1H, s, $H^{21'}$), 7.12 (2H, dd, H^5 & $H^{5'}$), 7.06 (2H, s, H^3 & $H^{3'}$), 6.80 (2H, d, H^6 & $H^{6'}$), 4.18–3.78 (16H, m, H^{11}, $H^{11'}$, H^7, $H^{7'}$, H^{23}, $H^{23'}$, H^{25} & $H^{25'}$), 3.47–3.32 (4H, m, 9-N_3 ring), 3.21–3.06 (8H, m, H^{13}, $H^{13'}$ & 9-N_3 ring), 2.83–2.72 (10H, m, H^{15}, $H^{15'}$ & 9-N_3 ring), 2.53 (4H, t, H^9 & $H^{9'}$), 2.23–2.14 (4H, m, H^8 & $H^{8'}$), 1.76 (6H, d, H^{24} & $H^{24'}$), 1.48 (9H, s, H^{29}), 1.28–1.22 (12H, m, H^{12}, $H^{12'}$, H^{26} & $H^{26'}$), 1.11 (6H, t, H^{14} & $H^{14'}$); **^{31}P{^{1}H}-NMR** (162 MHz, $CDCl_3$) δ +40.2, +40.1; **ESI-LRMS** (+) *m/z* 400 $[M+3H]^{3+}$, 600 $[M+2H]^{2+}$, 1198 $[M+H]^+$; **ESI-HRMS** (+) calcd for $[C_{63}H_{90}N_7O_{12}P_2]^+$ 1198.612, found 1198.607.

Compound 24a, trifluoroacetate salt

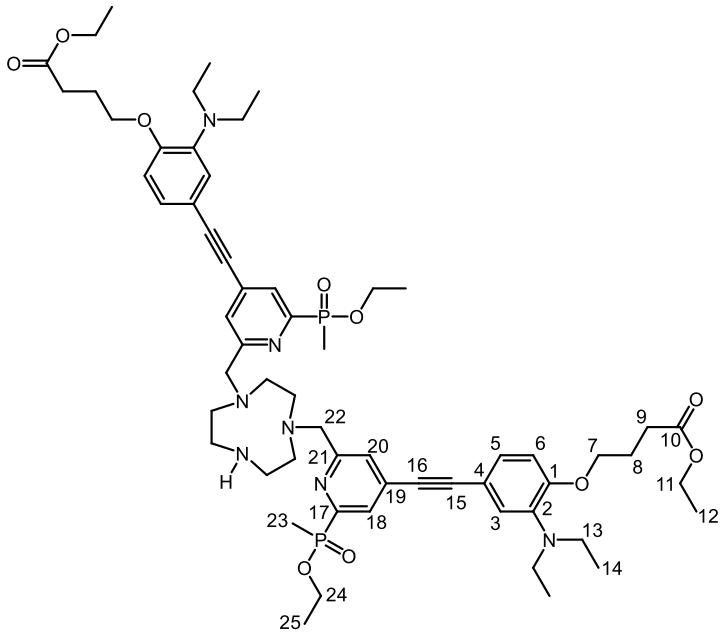

A solution of compound **23a** (19 mg, 0.016 mmol) in TFA and DCM was prepared (10% v/v, 3 mL total) and stirred under argon for 40 min. Immediately following this, the solvent was removed under reduced pressure. Additional DCM (~50 mL) was added and the solvent removed under reduced pressure. This procedure was repeated 3 times. The residue was dissolved in DCM (30 mL), washed with aqueous Na_2CO_3 solution (4%, pH = 11, 3 × 30 mL) and dried over K_2CO_3. Removal of the solvent under reduced pressure yielded an orange oil (17 mg, quant.); **^{1}H-NMR** (400 MHz, $CDCl_3$) δ 7.95 (2H, dd, $^{3}J_{H\text{-}P}$ 6.0, $^{4}J_{H\text{-}H}$ 1.3, H^{18}), 7.38 (2H, app. s, H^{20}), 7.12 (2H, dd, $^{3}J_{H\text{-}H}$ 8.4, $^{4}J_{H\text{-}H}$ 2.0, H^{5}), 7.06 (2H, d, $^{4}J_{H\text{-}H}$ 2.0, H^{3}), 6.81 (2H, d, $^{3}J_{H\text{-}H}$ 8.4, H^{6}), 4.23–4.10 & 3.96–3.86 (8H, m, H^{11} & H^{24}), 4.05 (4H, t, $^{3}J_{H\text{-}H}$ 6.4, H^{7}), 3.99 (4H, s, H^{22}), 3.31–3.24 (4H, m, 9-N_3 ring), 3.16 (8H, q, $^{3}J_{H\text{-}H}$ 7.1, H^{13}), 3.13–3.07 (4H, m, 9-N_3 ring), 2.73 (4H, br s, 9-N_3 ring), 2.52 (4H, t, $^{3}J_{H\text{-}H}$ 7.2, H^{9}), 2.20–2.11 (4H, m, H^{8}), 1.77 (6H, d, $^{2}J_{H\text{-}P}$ 15, H^{23}), 1.31–1.22 (12H, m, H^{12} & H^{25}), 1.05 (12H, t, $^{3}J_{H\text{-}H}$ 7.1, H^{14}); **^{13}C-NMR** (101 MHz, $CDCl_3$) δ 173.2 (C^{10}), 159.4 (d, $^{3}J_{C\text{-}P}$ 20, C^{21}), 154.6 (d, $^{1}J_{C\text{-}P}$ 157, C^{17}), 154.2 (C^{1}), 140.2 (C^{2}), 133.4 (d, $^{3}J_{C\text{-}P}$ 12, C^{19}), 127.9 (d, $^{2}J_{C\text{-}P}$ 22, C^{18}), 126.7 (C^{5}), 126.3 (C^{20}), 124.8 (C^{3}), 113.5 (C^{4}), 112.8 (C^{6}), 97.5 (C^{15}), 84.7 (C^{16}), 67.5 (C^{7}), 61.3 (d, $^{2}J_{C\text{-}P}$ 6, C^{21}), 60.7 (C^{11}), 60.0 (C^{22}), 53.9 (9-N_3 ring), 51.6 (9-N_3 ring), 50.1 (9-N_3 ring), 49.4 (9-N_3 ring), 49.2 (9-N_3 ring), 45.7 (C^{13}), 44.8 (9-N_3 ring), 31.0 (C^{9}), 24.7 (C^{8}), 16.7 (d, $^{3}J_{C\text{-}P}$ 6, C^{25}), 14.4 (C^{12}), 13.8 (d, $^{1}J_{C\text{-}P}$ 103, C^{23}), 12.5 (C^{14}); **^{31}P{^{1}H}-NMR** (162 MHz,

$CDCl_3$) δ +39.2; **ESI-LRMS** (+) *m/z* 1127 $[M+H]^+$; **ESI-HRMS** (+) calcd for $[C_{60}H_{86}N_7O_{10}P_2]^+$ 1126.592, found 1126.592.

Compound 24b, trifluoroacetate salt

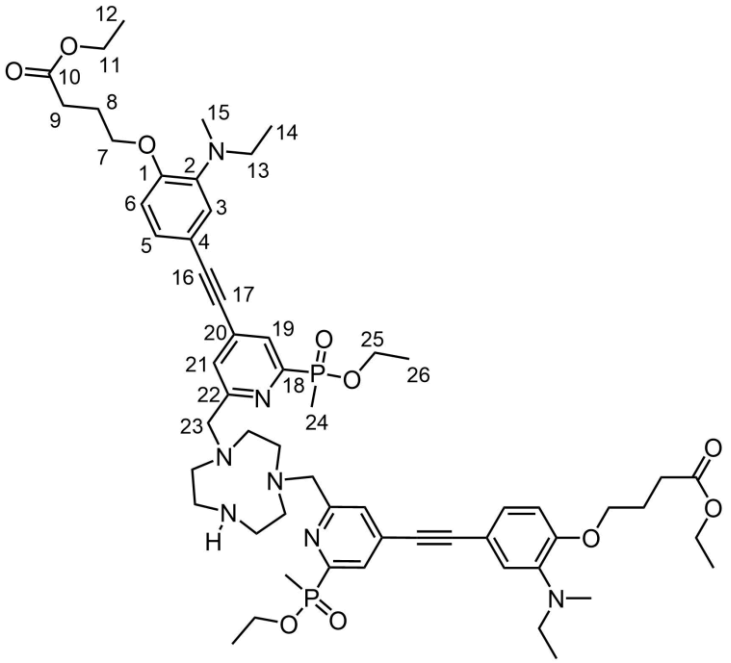

A solution of compound **23b** (110 mg, 0.092 mmol) in TFA and DCM was prepared (10% v/v, 3 mL total) and stirred under argon for 60 min. The solvent was removed under reduced pressure, additional DCM (~50 mL) was added and the solvent removed under reduced pressure. This process was repeated 4 times. The residue was dissolved in DCM (30 mL), washed with aqueous Na_2CO_3 solution (4%, pH = 11, 3 × 30 mL) and dried over K_2CO_3. Removal of the solvent under reduced pressure yielded an orange oil (111 mg, quant.); **^{1}H-NMR** (700 MHz, $CDCl_3$) δ 7.89 (2H, d, $^3J_{H\text{-}P}$ 6.0, H^{19}), 7.77 (2H, s, H^{21}), 7.64 (2H, dd, $^3J_{H\text{-}H}$ 8.5, $^4J_{H\text{-}H}$ 1.3, H^5), 7.57 (2H, s, H^3), 7.13 (2H, d, $^3J_{H\text{-}H}$ 8.5, H^6), 4.39 (4H, s, H^{23}), 4.22 (4H, t, $^3J_{H\text{-}H}$ 6.5, H^7), 4.15–4.07 & 3.97–3.90 (8H, m, H^{11} & H^{25}), 3.68 (4H, q, $^3J_{H\text{-}H}$ 7.2, H^{13}), 3.64–3.51 (8H, m, 9-N_3 ring), 3.43–3.35 (4H, m, 9-N_3 ring), 3.29 (6H, s, H^{15}), 2.51 (4H, t, $^3J_{H\text{-}H}$ 6.8, H^9), 2.21–2.16 (4H, m, H^8), 1.75 (6H, d, $^2J_{H\text{-}P}$ 15, H^{24}), 1.27 (6H, td, $^3J_{H\text{-}H}$ 7.1, $^4J_{H\text{-}P}$ 3.0, H^{26}), 1.23 (6H, t, $^3J_{H\text{-}P}$ 7.1, H^{12}), 1.18 (6H, t, $^3J_{H\text{-}H}$ 7.2, H^{14}); **^{13}C-NMR** (176 MHz, $CDCl_3$) δ 173.1 (C^{10}), 156.2 (d, $^3J_{C\text{-}P}$ 21, C^{22}), 153.3 (d, $^1J_{C\text{-}P}$ 160, C^{18}), 152.5 (C^1), 135.6 (C^5), 128.2 (C^3), 128.1 (d, $^2J_{C\text{-}P}$ 20, C^{19}), 127.7 (C^2), 127.1 (d, $^4J_{C\text{-}P}$ 4, C^{21}), 115.4 (C^4), 114.2 (C^6), 94.6 (C^{16}), 86.2 (d, $^4J_{C\text{-}P}$ 2.6, C^{17}), 69.1 (C^7), 62.6 (d, $^2J_{C\text{-}P}$ 7.0, C^{25}), 61.0 (C^{11}), 59.7 (C^{23}),

54.1 (C^{13}), 53.6 (9-N_3 ring), 51.5 (9-N_3 ring), 50.0 (9-N_3 ring), 44.2 (C^{15}), 30.5 (C^9), 24.0 (C^8), 16.3 (d, $^3J_{C\text{-}P}$ 6.2, C^{26}), 14.2 (C^{12}), 13.4 (d, $^1J_{C\text{-}P}$ 102, C^{24}), 10.3 (C^{14}); **^{31}P-NMR** (162 MHz, $CDCl_3$) δ +40.8; **ESI-LRMS** (+) *m/z* 1098 $[M+H]^+$; **ESI-HRMS** (+) calcd for $[C_{58}H_{82}N_7O_{10}P_2]^+$ 1098.556, found 1098.557.

pro-L^{9a}

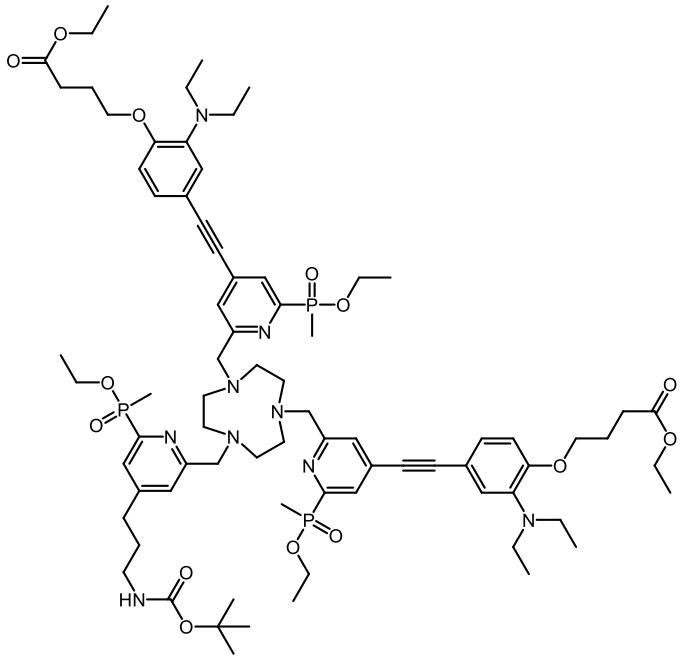

Compounds **24a** (43 mg, 0.038 mmol), **22** (45 mg, 0.10 mmol) and K_2CO_3 (30 mg, 0.22 mmol) were combined in anhydrous CH_3CN (2 mL) under argon and heated at 65 °C for 18 h. After this time, LC/MS analysis confirmed the complete transformation of **24a**. The reaction mixture was allowed to cool before separation from the inorganic salts by filtration. Removal of the solvent under reduced pressure afforded an orange solid (88 mg) that was used directly in the next step without further purification; **ESI-LRMS** (+) *m/z* 1481 $[M+H]^+$; **ESI-HRMS** (+) calcd for $[C_{77}H_{113}N_9O_{14}P_3]^+$ 1480.762, found 1480.760.

pro-L^{9b}

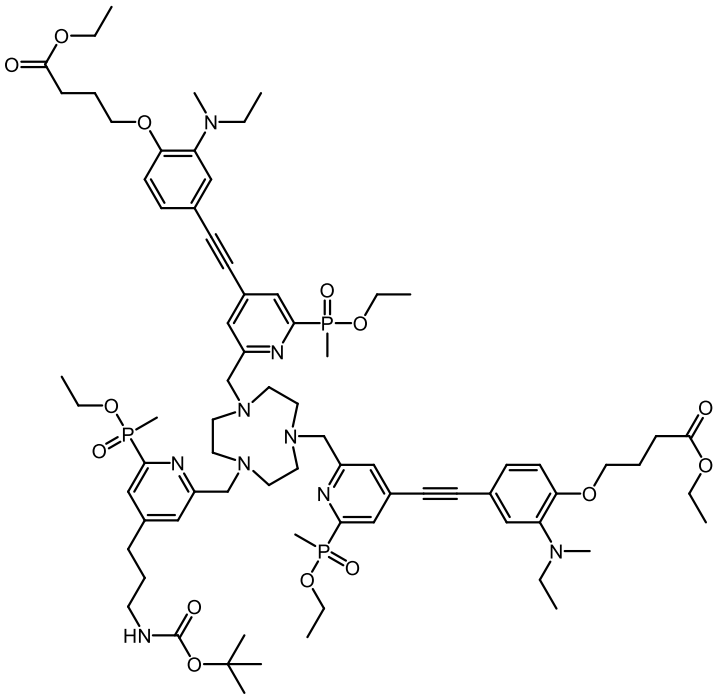

Compounds **24b** (111 mg, 0.0919 mmol), **22** (59 mg, 0.13 mmol) and K_2CO_3 (45 mg, 0.33 mmol) were combined in anhydrous CH_3CN (3 mL) under argon and heated at 65 °C for 16 h. After this time, LC/MS analysis confirmed the complete transformation of the macrocycle **24b**. The reaction mixture was allowed to cool before separation from the inorganic salts by filtration. Removal of the solvent under reduced pressure afforded an orange oil (165 mg) that was used directly in the next step without further purification; **ESI-LRMS** (+) *m/z* 1453 $[M+H]^+$; **ESI-HRMS** (+) calcd for $[C_{75}H_{109}N_9O_{14}P_3]^+$ 1452.731, found 1452.729.

7.7.2.2. Synthesis of ***[Eu.L^{9a}]***

[Eu.L^{9a}]

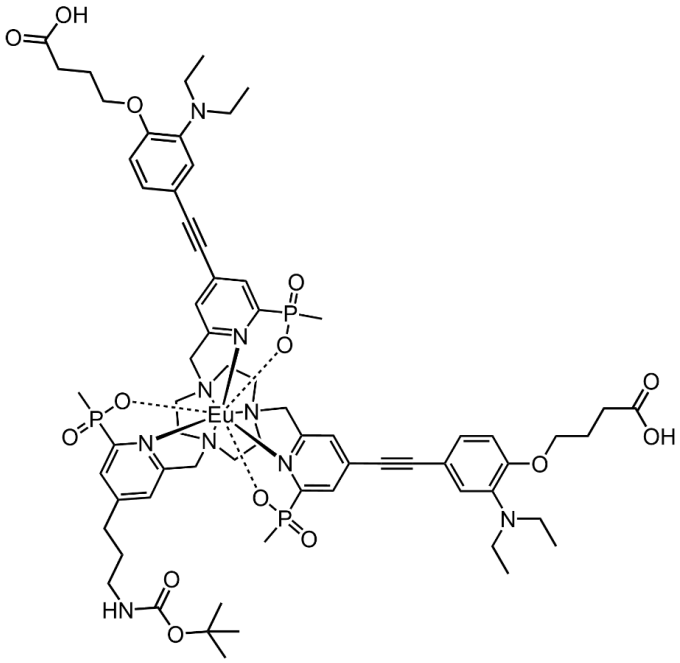

The crude ligand **pro-L^{9a}** (88 mg) from the previous step was dissolved in a mixture of CH_3OH/H_2O (4:1, 2.5 mL total) and the pH was adjusted to 12 using aqueous NaOH solution (1 M). The solution was heated at 60 °C for 1.5 h. After this time, LC/MS analysis confirmed complete hydrolysis of the phosphinate and carboxylic acid ester groups. After cooling and adjustment of the pH to 6 using hydrochloric acid (0.1 M), $EuCl_3.6H_2O$ (42 mg, 0.115 mmol) was added and the reaction mixture was heated to 60 °C for 18 h. The reaction mixture was purified by RP-HPLC (10 to 100% CH_3CN in H_2O over 10 min, $\mathbf{t_R}$ = 8.5 min) to yield a yellow solid (22 mg, 39% over three steps); **ESI-LRMS** (+) *m/z* 1490 $[M+H]^+$, 746 $[M+2H]^{2+}$; **ESI-HRMS** (+) calcd for $[C_{67}H_{91}{}^{151}EuN_9O_{14}P_3]^{2+}$ 745.7561, found 745.7562; $\boldsymbol{t_{H2O}}$ (ms) = 0.27 (pH = 8), 0.39 (pH = 7), 0.53 (pH = 6), 0.95 (pH = 5), 0.97 (pH = 4).

[Eu.L^{9b}]

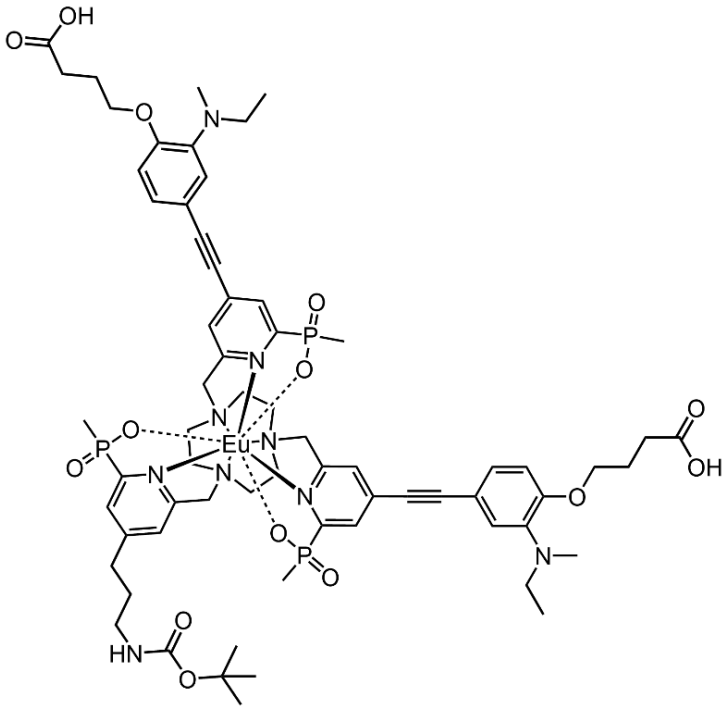

The crude ligand (165 mg) from the previous step was dissolved in a mixture of CH_3OH/H_2O (1:1, 2 mL total) and the pH was adjusted to 12 using aqueous NaOH solution (1 M). The solution was heated at 60 °C for 1.5 h. After this time, LC/MS analysis confirmed complete hydrolysis of the phosphinate and carboxylic acid ester groups. After cooling and adjustment of the pH to 6 using hydrochloric acid (0.1 M), $EuCl_3.6H_2O$ (34 mg, 0.093 mmol) was added and the reaction mixture was heated to 60 °C for 17 h. The reaction mixture was purified by RP-HPLC (10 to 100% CH_3CN in H_2O over 10 min, $\mathbf{t_R}$ = 8.7 min) to yield a yellow solid (50 mg, 37% over three steps); **ESI-LRMS** (+) *m/z* 1462 $[M+H]^+$, 732 $[M+2H]^{2+}$; **ESI-HRMS** (+) calcd for $[C_{65}H_{86}{}^{151}EuN_9O_{14}P_3]^+$ 1462.473, found 1462.468.

[Eu.L^{9a}]

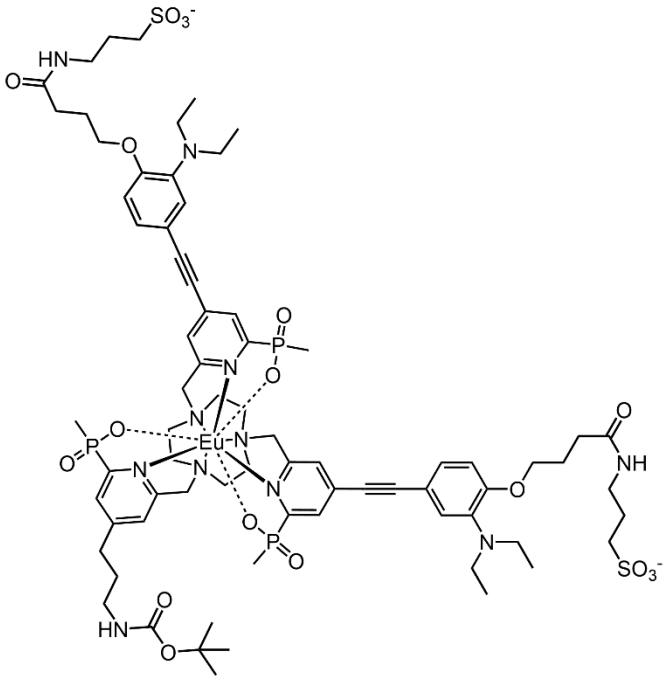

The complex **[Eu.L^{9a}]** (3.9 mg, 2.6 µmol) and DIEA (6 µL, 34 µmol) were combined in anhydrous DMSO (0.4 mL) under argon. To this solution was added HATU (5 mg, 13 µmol), homotaurine (2 mg, 14 µmol) and H_2O (40 µL). The mixture was stirred at room temperature for 19 h. Following dilution with H_2O, the reaction mixture was purified by RP-HPLC (10 to 100% CH_3OH in H_2O over 10 min, t_R = 11.6 min) yielding a yellow solid (4 mg, 89%); **ESI-LRMS** (-) *m/z* 1730 $[M-H]^-$, 865 $[M-2H]^{2-}$; **ESI-HRMS** (-) calcd for $[C_{73}H_{101}{}^{151}EuN_{11}O_{18}P_3S_2]^{2-}$ 864.7601, found 864.7610; t_{H2O} (ms) = 0.25 (pH 8), 0.34 (pH 7), 0.70 (pH 6), 0.98 (pH 5), 1.04 (pH 4); $\varepsilon_{332\ nm}$ = 39,000 M^{-1} cm^{-1}; $\Phi_{pH\ 8}$ = 0.3%, $\Phi_{pH\ 4}$ = 16% (λ_{exc} = 332 nm).

[Eu.L$^{9\ b}$]$^{\hat{o}}$

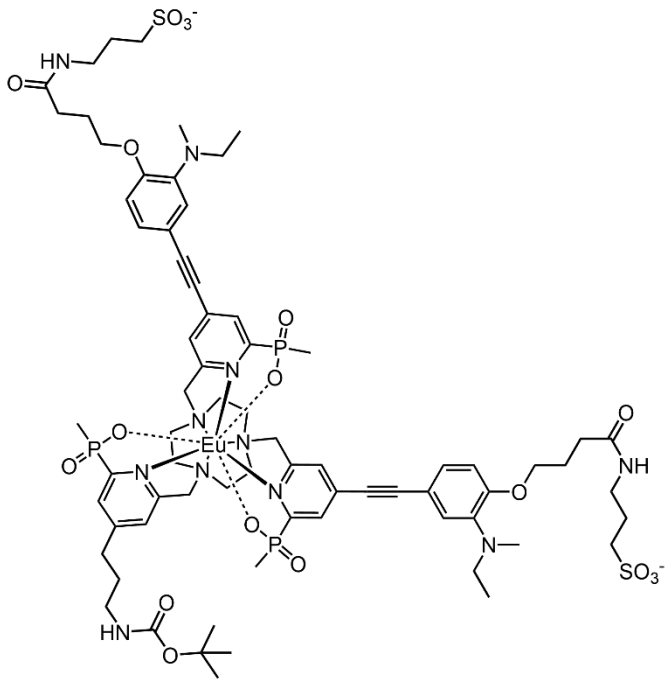

The complex **[Eu.L^{9b}]** (20 mg, 13.7 µmol) and DIEA (15 µL, 85 µmol) were combined in anhydrous DMSO (0.5 mL) under argon. To this solution was added HATU (12 mg, 31 µmol), homotaurine (4.5 mg, 31 µmol) and H_2O (50 µL), and the mixture was stirred at room temperature for 16 h. Following dilution with H_2O, the reaction mixture was purified by RP- HPLC (10 to 100% CH_3OH in H_2O over 10 min, $\mathbf{t_R}$ = 10.6 min) to yield a yellow solid (9 mg, 38%); **ESI-LRMS** (-) *m/z* 1701 $[M-H]^-$, 850 $[M-2H]^{2-}$; **ESI-HRMS** (+) calcd for $[C_{71}H_{99}{}^{151}EuN_{11}O_{18}P_3S_2]^{2+}$ 852.7530 found 852.7601; $\boldsymbol{\tau_{H2O}}$ (ms) = 0.30 (pH 8), 0.29 (pH 7), 0.42 (pH 6), 0.77 (pH 5), 1.05 (pH 4); $\boldsymbol{\chi_{332\ nm}}$ = 39,000 M^{-1} cm^{-1}; $\boldsymbol{\Lambda_{pH\ 8}}$ = 0.01%, $\boldsymbol{\Lambda_{pH\ 4}}$ = 14.5% (λ_{exc} = 332 nm).

7.7.3. Synthesis of the N-Substituted Sulfonated Complexes

7.7.3.1. Synthesis of pro-L$^{10a-b,11}$

Trifluoroethyl-3-bromopropylsulfonate, 25

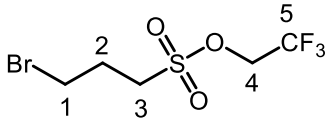

To a mixture of the sodium salt of 3-bromopropanesulfonic acid (1 g, 4.44 mmol), anhydrous acetonitrile (4 mL) and anhydrous DMF (0.1 mL) cooled to 0 °C under argon, oxalyl chloride (0.75 mL, 8.75 mmol) was added dropwise. The mixture was stirred at 0 °C for 2 h before removal of the solvent under reduced pressure (bath temperature <20 °C). The resulting residue was dried further under high vacuum. To this residue was added anhydrous CH_3CN (4 mL) and TFE (9 mL, 125 mmol) under argon. Triethylamine (3 mL, 21.5 mmol) was added dropwise with cooling to 0 °C. The mixture was stirred at 0 °C for 5 h before removal of the solvent under reduced pressure. Ethyl acetate (40 mL) and H_2O (40 mL) were added to the crude residue before washing the organic layer with H_2O (3 × 40 mL). The organic layer was dried over Na_2SO_4 and the solvent removed under reduced pressure to yield a pale orange oil (1.1 g, 87%); **^{1}H-NMR** (600 MHz, $CDCl_3$) δ 4.53 (2H, q, $^3J_{H\text{-}F}$ 8.0, H^4), 3.54 (2H, t, $^3J_{H\text{-}H}$ 6.2, H^1), 3.45–3.41 (2H, m, H^3), 2.47–2.42 (2H, m, H^2); **^{13}C-NMR** (151 MHz, $CDCl_3$) δ 122.0 (q, $^1J_{C\text{-}F}$ 280, C^5), 64.0 (q, $^2J_{C\text{-}F}$ 40, C^4), 49.9 (C^3), 30.1 (C^1), 26.7 (C^2); **^{19}F-NMR** (151 MHz, $CDCl_3$) δ -74.0.

2-*N*-(Trifluoroethyl-3-propyl-sulfonate)amino-4-iodo-methoxybenzene, 26

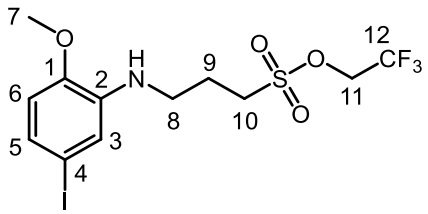

5-Iodo-o-anisidine (245 mg, 0.984 mmol), compound **25** (1.1 g, 3.86 mmol), K_2CO_3 (425 mg, 3.08 mmol) and sodium iodide (40 mg, 0.27 mmol) were combined in anhydrous CH_3CN (5 mL) under argon. The resulting mixture was heated to 78 °C for 3 d before removal of the solvent under reduced pressure. DCM (40 mL) and H_2O (40 mL) were added to the crude residue before washing the organic layer with H_2O (2 × 40 mL). The organic layer was dried over K_2CO_3 and the solvent removed under reduced pressure to give the crude product as a pale brown residue that was purified by column chromatography (SiO_2, 100% hexane to 20% EtOAc in hexane) to yield a pale yellow oil (283 mg, 63%); **^{1}H-NMR** (400 MHz, $CDCl_3$) δ 6.99 (1H, dd, $^3J_{H\text{-}H}$ 8.3, $^4J_{H\text{-}H}$ 2.0, H^5), 6.82 (1H, d, $^4J_{H\text{-}H}$ 2.0, H^3), 6.50 (1H, d, $^3J_{H\text{-}H}$ 8.3, H^6), 4.53 (2H, q, $^3J_{H\text{-}F}$

8.0, H^{11}), 3.86 (3H, s, H^7), 3.39–3.29 (4H, m, H^8 & H^{10}), 2.26–2.17 (2H, m, H^9); **^{13}C-NMR** (101 MHz, $CDCl_3$) δ 146.9 (C^1), 138.9 (C^2), 126.0 (C^5), 122.2 (q, $^1J_{C\text{-}F}$ 280, C^{12}), 118.3 (C^3), 111.5 (C^6), 84.1 (C^4), 63.9 (q, $^2J_{C\text{-}F}$ 40, C^{11}), 55.7 (C^7), 49.1 (C^8), 41.4 (C^{10}), 23.5 (C^9); **^{19}F-NMR** (376 MHz, $CDCl_3$) δ -73.9; **ESI-LRMS** (+) *m/z* 454 $[M+H]^+$; **ESI-HRMS** (+) calcd for $[C_{12}H_{16}NO_4SF_3I]^+$ 453.9797, found 453.9792; **R_f** (SiO_2, 20% EtOAc in hexane) = 0.3.

2-*N*,*N*-(Ethyl(trifluoroethyl-3-propyl-sulfonate))amino-4-iodo-methoxybenzene, 27a

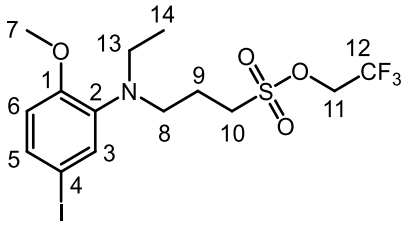

Compound **26** (310 mg, 0.684 mmol) and acetaldehyde (0.46 mL, 8.16 mmol) were combined in anhydrous ethanol (3 mL) under argon with two drops of glacial acetic acid. The resulting mixture was stirred at room temperature for 15 min before the addition of $NaBH_3CN$ (170 mg, 2.71 mmol). The mixture was once more stirred at room temperature under argon for 16 h, after which the solvent was removed under reduced pressure to give a yellow residue. DCM (40 mL) and H_2O (40 mL) were added to this residue and the organic layer washed with H_2O (3 × 40 mL). The combined aqueous layers were extracted with DCM (1 × 40 mL) and the combined organic layers dried over K_2CO_3. Removal of the solvent under reduced pressure yielded a pale yellow oil (247 mg, 75%); **^{1}H-NMR** (400 MHz, $CDCl_3$) δ 7.29 (1H, dd, $^3J_{H\text{-}H}$ 8.4, $^4J_{H\text{-}H}$ 2.1, H^5), 7.18 (1H, d, $^4J_{H\text{-}H}$ 2.1, H^3), 6.60 (1H, d, $^3J_{H\text{-}H}$ 8.4, H^6), 4.46 (2H, q, $^3J_{H\text{-}F}$ 8.0, H^{11}), 3.79 (3H, s, H^7), 3.37–3.30 (2H, m, H^{10}), 3.15 (2H, t, $^3J_{H\text{-}H}$ 6.6, H^8), 3.07 (2H, q, $^3J_{H\text{-}H}$ 7.1, H^{13}), 2.06–1.97 (2H, m, H^9), 1.00 (3H, t, $^3J_{H\text{-}H}$ 7.1, H^{14}); **^{13}C-NMR** (101 MHz, $CDCl_3$) δ 154.1 (C^1), 140.2 (C^2), 132.3 (C^5), 130.9 (C^3), 122.0 (q, $^1J_{C\text{-}F}$ 280, C^{12}), 113.7 (C^6), 82.9 (C^4), 63.7 (q, $^2J_{C\text{-}F}$ 40, C^{11}), 55.4 (C^7), 49.8 (C^8), 49.0 (C^{10}), 46.6 (C^{13}), 21.5 (C^9), 12.1 (C^{14}); **^{19}F-NMR** (376 MHz, $CDCl_3$) δ -74.0; **ESI-LRMS** (+) *m/z* 482 $[M+H]^+$; **ESI-HRMS** (+) calcd for $[C_{14}H_{20}NO_4SF_3I]^+$ 482.0110, found 482.0106.

2-*N*,*N*-(Methyl(trifluoroethyl-3-propyl-sulfonate))amino-4-iodo-methoxybenzene, 27b

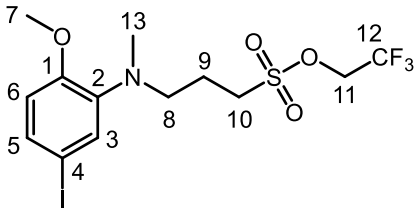

Compound **26** (269 mg, 0.594 mmol) and paraformaldehyde (800 mg, 8.89 mmol) were combined in anhydrous ethanol (8 mL) under argon with two drops of glacial acetic acid. The resulting mixture was stirred at room temperature for 15 min before the addition of $NaBH_3CN$ (300 mg, 4.77 mmol). The mixture was once more stirred at room temperature under argon for 18 h, after which the solvent was removed under reduced pressure to give a yellow residue. DCM (40 mL) and H_2O (40 mL) were added to this residue and the organic layer washed with H_2O (3 × 40 mL). The combined aqueous layers were extracted with DCM (2 × 40 mL) and the combined organic layers dried over K_2CO_3. Removal of the solvent under reduced pressure yielded a pale yellow oil (249 mg, 90%); **^{1}H-NMR** (400 MHz, $CDCl_3$) δ 7.27 (1H, dd, $^3J_{H\text{-}H}$ 8.3, $^4J_{H\text{-}H}$ 2.0, H^5), 7.17 (1H, d, $^4J_{H\text{-}H}$ 2.0, H^3), 6.59 (1H, d, $^3J_{H\text{-}H}$ 8.3, H^6), 4.50 (2H, q, $^3J_{H\text{-}F}$ 8.0, H^{11}), 3.81 (3H, s, H^7), 3.44–3.37 (2H, m, H^{10}), 3.11 (2H, t, $^3J_{H\text{-}H}$ 6.7, H^8), 2.72 (3H, s, H^{13}), 2.18–2.07 (2H, m, H^9); **^{13}C-NMR** (176 MHz, $CDCl_3$) δ 152.6 (C^1), 143.0 (C^2), 131.8 (C^5), 128.4 (C^3), 122.2 (q, $^1J_{C\text{-}F}$ 280, C^{12}), 113.5 (C^6), 83.4 (C^4), 63.8 (q, $^2J_{C\text{-}F}$ 40, C^{11}), 55.5 (C^7), 53.1 (C^8), 49.1 (C^{10}), 39.5 (C^{13}), 21.6 (C^9); **^{19}F-NMR** (376 MHz, $CDCl_3$) δ -73.9; **ESI-LRMS** (+) *m/z* 468 $[M+H]^+$; **ESI-HRMS** (+) calcd for $[C_{13}H_{18}NO_4SF_3I]^+$ 467.9953, found 467.9952.

2-*N*,*N*-(Ethyl(trifluoroethyl-3-propyl-sulfonate))amino-4-((trimethylsilyl)ethynyl)-methoxybenzene, 28a

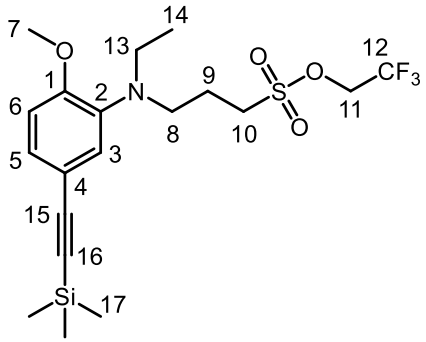

The sulfonate ester **27a** (176 mg, 0.366 mmol) and trimethylsilylacetylene (0.1 mL, 0.72 mmol) were combined in anhydrous CH_3CN (3 mL) under argon. To this solution was added $Pd_2Cl_2(allyl)_2$ (14 mg, 0.038 mmol), $P(^tBu)_3$ (0.015 mL, 0.062 mmol) and piperidine (0.09 mL, 0.91 mmol) in that order. The resulting mixture was stirred at 35 °C under argon for 20 h. Removal of the solvent under reduced pressure gave the crude product as a brown residue that was purified by column chromatography (SiO_2, 100% hexane to 20% EtOAc in hexane) to yield a pale orange oil (151 mg, 91%); **^{1}H-NMR** (400 MHz, $CDCl_3$) δ 7.16 (1H, dd, $^3J_{H\text{-}H}$ 8.4, $^4J_{H\text{-}H}$ 2.0, H^5), 7.06 (1H, d, $^4J_{H\text{-}H}$ 2.0, H^3), 6.77 (1H, d, $^3J_{H\text{-}H}$ 8.4, H^6), 4.45 (2H, q, $^3J_{H\text{-}F}$ 8.0, H^{11}), 3.83 (3H, s, H^7), 3.38–3.30 (2H, m, H^{10}), 3.16 (2H, t, $^3J_{H\text{-}H}$ 6.5, H^8), 3.08 (2H, q, $^3J_{H\text{-}H}$ 7.2, H^{13}), 2.06–1.94 (2H, m, H^9), 0.99 (3H, t, $^3J_{H\text{-}H}$ 7.2, H^{14}), 0.24 (9H, s, H^{17}); **^{13}C-NMR** (101 MHz, $CDCl_3$) δ 154.9 (C^1), 138.2 (C^2), 128.3 (C^5), 126.1 (C^3), 122.0 (q, $^1J_{C\text{-}F}$ 280, C^{12}), 115.3 (C^4), 111.5 (C^6), 105.3 (C^{15}), 92.4 (C^{16}), 63.8 (q, $^2J_{C\text{-}F}$ 40, C^{11}), 55.5 (C^7), 49.9 (C^8), 49.1 (C^{10}), 46.9 (C^{13}), 21.6 (C^9), 12.2 (C^{14}), 0.2 (C^{17}); **^{19}F-NMR** (376 MHz, $CDCl_3$) δ -74.0; **ESI-LRMS** (+) *m/z* 452 $[M+H]^+$; **ESI-HRMS** (+) calcd for $[C_{19}H_{29}NO_4F_3Ssi]^+$ 452.1539, found 452.1545; **R_f** (SiO_2, 20% EtOAc in hexane) = 0.3.

2-*N*,*N*-(Methyl(trifluoroethyl-3-propyl-sulfonate))amino-4-((trimethylsilyl)ethynyl)-methoxybenzene, 28b

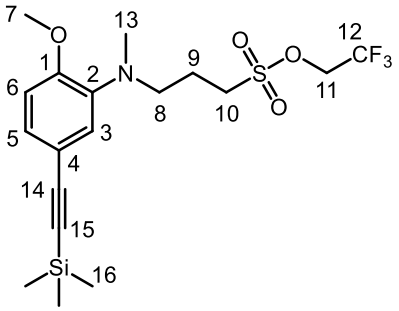

Compound **27b** (240 mg, 0.514 mmol) and trimethylsilylacetylene (0.14 mL, 1.01 mmol) were combined in anhydrous CH_3CN (2.5 mL) under argon. To this solution was added $Pd_2Cl_2(allyl)_2$ (20 mg, 0.055 mmol), $P(^tBu)_3$ (0.013 mL, 0.054 mmol) and piperidine (0.13 mL, 1.32 mmol) in that order. The resulting mixture was stirred at 35 °C under argon for 16 h before removal of the solvent under reduced pressure to give the crude product as a brown residue that was purified by column chromatography (SiO_2, 100% hexane to 20% EtOAc in hexane) to afford a pale orange oil (157 mg, 70%); **^{1}H-NMR** (700 MHz, $CDCl_3$) δ 7.13 (1H, dd, $^3J_{H\text{-}H}$ 8.3, $^4J_{H\text{-}H}$ 1.8, H^5), 7.05 (1H, d, $^4J_{H\text{-}H}$ 1.8, H^3), 6.76 (1H, d, $^3J_{H\text{-}H}$ 8.3, H^6), 4.49 (2H, q, $^3J_{H\text{-}F}$ 8.0, H^{11}), 3.84 (3H, s, H^7), 3.42–3.38 (2H, m, H^{10}), 3.10 (2H, t, $^3J_{H\text{-}H}$ 6.7, H^8), 2.73 (3H, s, H^{13}), 2.14–2.08 (2H, m, H^9), 0.24 (9H, s, H^{16}); **^{13}C-NMR** (151 MHz, $CDCl_3$) δ 153.2 (C^1), 141.0 (C^2), 127.5 (C^5), 123.3 (C^3), 122.2 (q, $^1J_{C\text{-}F}$ 280, C^{12}), 115.6 (C^4), 111.2 (C^6), 105.4 (C^{14}), 92.4 (C^{15}), 63.8 (q, $^2J_{C\text{-}F}$ 40, C^{11}), 55.5 (C^7), 53.1 (C^8), 49.1 (C^{10}), 39.6 (C^{13}), 21.5 (C^9), 0.2 (C^{16}); **^{19}F-NMR** (376 MHz, $CDCl_3$) δ -74.0; **ESI-LRMS** (+) *m/z* 438 $[M+H]^+$; **ESI-HRMS** (+) calcd for $[C_{18}H_{27}NO_4F_3Ssi]^+$ 438.1382, found 438.1377; **R_f** (SiO_2, 20% EtOAc in hexane) = 0.3.

2-*N*,*N*-(Ethyl(trifluoroethyl-3-propyl-sulfonate))amino-4-ethynyl-methoxybenzene, 29a

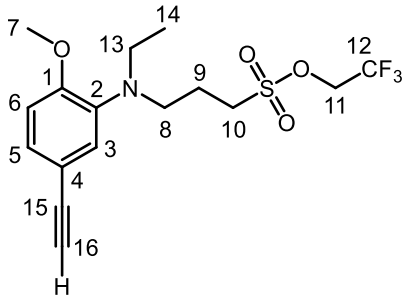

Triethylamine trihydrofluoride (3 mL, 6.75 mmol) was added to the silane **28a** (341 mg, 0.755 mmol) in anhydrous THF (5 mL) under argon. The solution was stirred at 30 °C for 3 d before removal of solvent under reduced pressure. The residue was subsequently dissolved in DCM (30 mL) and washed with H_2O (4 × 30 mL). The combined aqueous layers were extracted with DCM (1 × 30 mL) and the combined organic layers dried over K_2CO_3 to yield after solvent evaporation a pale brown oil (207 mg, 72%). This product was used in the next step without further purification; **^{1}H-NMR** (400 MHz, $CDCl_3$) δ 7.18 (1H, dd, $^{3}J_{H\text{-}H}$ 8.4, $^{4}J_{H\text{-}H}$ 2.0, H^{5}), 7.08 (1H, d, $^{4}J_{H\text{-}H}$ 2.0, H^{3}), 6.80 (1H, d, $^{3}J_{H\text{-}H}$ 8.4, H^{6}), 4.46 (2H, q, $^{3}J_{H\text{-}F}$ 8, H^{11}), 3.84 (3H, s, H^{7}), 3.38–3.31 (2H, m, H^{10}), 3.17 (2H, t, $^{3}J_{H\text{-}H}$ 6.6, H^{8}), 3.09 (2H, q, $^{3}J_{H\text{-}H}$ 7.1, H^{13}), 2.99 (1H, s, H^{16}), 2.05–1.95 (2H, m, H^{9}), 0.99 (3H, t, $^{3}J_{H\text{-}H}$ 7.1, H^{14}), **^{13}C-NMR** (101 MHz, $CDCl_3$) δ 155.0 (C^{1}), 138.3 (C^{2}), 128.2 (C^{5}), 126.1 (C^{3}), 122.2 (q, $^{1}J_{C\text{-}F}$ 280, C^{12}), 114.2 (C^{4}), 111.6 (C^{6}), 83.9 (C^{15}), 75.8 (C^{16}), 63.8 (q, $^{2}J_{C\text{-}F}$ 40, C^{11}), 55.5 (C^{7}), 49.9 (C^{8}), 49.1 (C^{10}), 46.7 (C^{13}), 21.6 (C^{9}), 12.2 (C^{14}); **^{19}F-NMR** (376 MHz, $CDCl_3$) δ -74.0; **ESI-LRMS** (+) *m/z* 380 $[M+H]^+$; **ESI-HRMS** (+) calcd for $[C_{16}H_{21}NO_4SF_3]^+$ 380.1143, found 380.1155.

2-*N*,*N*-(Methyl(trifluoroethyl-3-propyl-sulfonate))amino-4-ethynyl-methoxybenzene, 29b

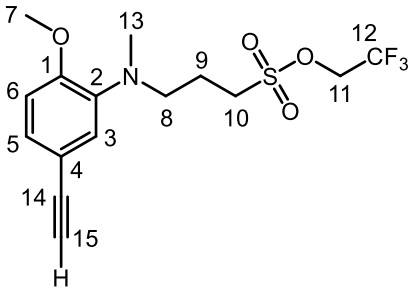

Triethylamine trihydrofluoride (1.1 mL, 6.75 mmol) was added to compound **28b** (195 mg, 0.446 mmol) in anhydrous THF (3 mL) under argon. The solution was stirred at 30 °C for 48 h before removal of solvent under reduced pressure. The residue was subsequently dissolved in DCM (30 mL) and washed with H_2O (3 × 30 mL). The combined aqueous layers were extracted with DCM (2 × 30 mL) and the combined organic layers dried over K_2CO_3 to give a pale brown oil (160 mg, 98%). This product was used in the next step without further purification; **^{1}H-NMR** (400 MHz, $CDCl_3$) δ 7.15 (1H, dd, $^{3}J_{H\text{-}H}$ 8.3, $^{4}J_{H\text{-}H}$ 1.9, H^{5}), 7.07 (1H, d, $^{4}J_{H\text{-}H}$ 1.9, H^{3}), 6.78 (1H, d, $^{3}J_{H\text{-}H}$ 8.3, H^{6}), 4.50 (2H, q, $^{3}J_{H\text{-}F}$ 8.0, H^{11}), 3.85 (3H, s, H^{7}), 3.43–3.37 (2H, m, H^{10}), 3.10 (2H, t, $^{3}J_{H\text{-}H}$ 6.6, H^{8}) 2.99 (1H, s, H^{15}), 2.73 (3H, s, H^{13}), 2.17–2.07 (2H, m, H^{9}); **^{13}C-NMR** (101 MHz, $CDCl_3$) δ 153.3 (C^{1}), 141.1 (C^{2}), 127.4 (C^{5}), 123.2 (C^{3}), 122.2 (q, $^{1}J_{C\text{-}F}$ 280, C^{12}), 114.4 (C^{4}), 111.2 (C^{6}), 83.9 (C^{14}), 75.8 (C^{15}), 63.8 (q, $^{2}J_{C\text{-}F}$ 40, C^{11}), 55.5 (C^{7}), 53.0 (C^{8}), 49.0 (C^{10}), 39.4 (C^{13}), 21.5 (C^{9}); **^{19}F-NMR** (376 MHz, $CDCl_3$) δ -74.0; **ESI-LRMS** (+) *m/z* 366 $[M+H]^+$; **ESI-HRMS** (+) calcd for $[C_{15}H_{19}NO_4SF_3]^+$ 366.0987, found 366.0986.

2-*N*,*N*-(Ethyl(trifluoroethyl-3-propyl-sulfonate))amino)-4-((2-(ethoxy(methyl)phosphoryl)-6-(hydroxymethyl)pyridine-4-yl)ethynyl)methoxybenzene, 30a

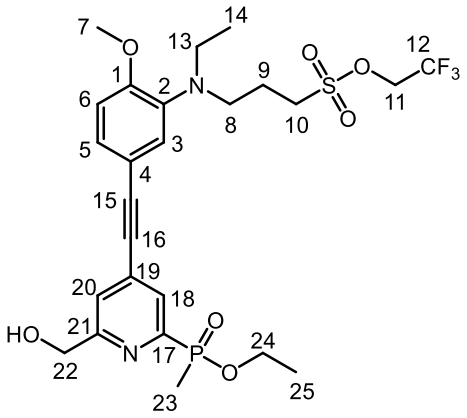

Compound **29a** (207 mg, 0.546 mmol) and compound **5** (152 mg, 0.517 mmol) were combined in anhydrous CH_3CN (5 mL) under argon. To this solution was added $Pd_2Cl_2(allyl)_2$ (20 mg, 0.055 mmol), $P(^tBu)_3$ (0.02 mL, 0.082 mmol) and piperidine (0.11 mL, 1.11 mmol) in that order. The resulting mixture was stirred at 35 °C under argon for 18 h before removal of the solvent under reduced pressure. The residue was dissolved in DCM (40 mL), washed with H_2O (3 × 40 mL) and the combined aqueous layers were extracted with DCM (2 × 40 mL). The combined organic layers were dried over K_2CO_3 and removal of the solvent under reduced pressure afforded an orange oil that was purified by RP-HPLC (10 to 100% CH_3CN over 10 min, $\mathbf{t_R}$ = 11.3 min) to yield a pale yellow oil (111 mg, 36%); **^{1}H-NMR** (400 MHz, $CDCl_3$) δ 8.02 (1H, d, $^3J_{H\text{-}P}$ 6.0, H^{18}), 7.51 (1H, s, H^{20}), 7.21 (1H, dd, $^3J_{H\text{-}H}$ 8.4, $^4J_{H\text{-}H}$ 2.0, H^5), 7.11 (1H, d, $^4J_{H\text{-}H}$ 2.0, H^3), 6.84 (1H, d, $^3J_{H\text{-}H}$ 8.4, H^6), 4.81 (2H, s, H^{22}), 4.46 (2H, q, $^3J_{H\text{-}F}$ 8, H^{11}), 4.16–4.05 & 3.91–3.79 (2H, m, H^{24}), 3.86 (3H, s, H^7), 3.38–3.31 (2H, m, H^{10}), 3.19 (2H, t, $^3J_{H\text{-}H}$ 6.6, H^8), 3.11 (2H, q, $^3J_{H\text{-}H}$ 7.1, H^{13}), 2.08–1.99 (2H, m, H^9), 1.77 (3H, d, $^2J_{H\text{-}P}$ 15, H^{23}), 1.31–1.14 (3H, t, $^3J_{H\text{-}H}$ 7.0, H^{25}), 1.01 (3H, t, $^3J_{H\text{-}H}$ 7.1, H^{14}); **^{13}C-NMR** (101 MHz, $CDCl_3$) δ 161.0 (d, $^3J_{C\text{-}P}$ 19, C^{21}), 155.6 (C^1), 153.2 (d, $^1J_{C\text{-}P}$ 155, C^{17}), 138.6 (C^2), 133.1 (d, $^3J_{C\text{-}P}$ 11, C^{19}), 128.2 (d, $^2J_{C\text{-}P}$ 22, C^{18}), 128.1 (C^5), 125.8 (C^3), 124.1 (d, $^4J_{C\text{-}P}$ 3, C^{20}), 122.1 (q, $^1J_{C\text{-}F}$ 280, C^{12}), 113.8 (C^4), 111.8 (C^6), 96.4 (C^{15}), 85.2 (d, $^4J_{C\text{-}P}$ 2, C^{16}), 64.2 (C^{22}), 63.7 (q, $^2J_{C\text{-}F}$ 40, C^{11}), 61.3 (d, $^2J_{C\text{-}P}$ 6, C^{24}), 55.6 (C^7), 49.8 (C^8), 49.1 (C^{10}), 46.7 (C^{13}), 21.6 (C^9), 16.5 (d, $^3J_{C\text{-}P}$ 6, C^{25}), 13.5 (d, $^1J_{C\text{-}P}$ 104, C^{23}) 12.2 (C^{14}); **^{19}F-NMR** (376 MHz, $CDCl_3$) δ -74.0; **^{31}P-NMR** (162 MHz, $CDCl_3$) δ +39.5; **ESI-LRMS** (+) *m/z* 593 $[M+H]^+$; **ESI-HRMS** (+) calcd for $[C_{25}H_{33}N_2O_7SF_3P]^+$ 593.1698, found 593.1709.

2-*N*,*N*-(Methyl(trifluoroethyl-3-propyl-sulfonate))amino)-4-((2-(ethoxy(methyl)phosphoryl)-6-(hydroxymethyl)pyridine-4-yl)ethynyl)methoxybenzene, 30b

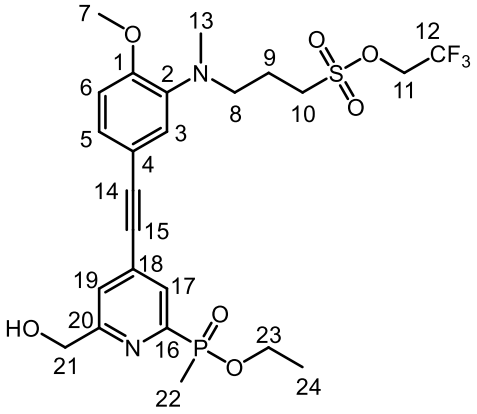

Compound **29b** (160 mg, 0.438 mmol) and compound **5** (116 mg, 0.395 mmol) were combined in anhydrous CH_3CN (3 mL) under argon. To this solution was added $Pd_2Cl_2(allyl)_2$ (16 mg, 0.044 mmol), $P(^tBu)_3$ (0.016 mL, 0.066 mmol) and piperidine (0.09 mL, 0.92 mmol) in that order. The resulting mixture was stirred at 35 °C under argon for 16 h before removal of the solvent under reduced pressure. The residue was dissolved in DCM (40 mL), washed with H_2O (3 × 40 mL) and the combined aqueous layers extracted with DCM (2 × 40 mL). The combined organic layers were dried over K_2CO_3 and removal of the solvent under reduced pressure afforded a brown oil that was purified by RP-HPLC (10 to 100% CH_3CN over 10 min, $\mathbf{t_R}$ = 10.8 min) to afford a pale yellow oil (119 mg, 52%); **^{1}H-NMR** (700 MHz, $CDCl_3$) δ 8.00 (1H, d, $^3J_{H\text{-}P}$ 6.0, H^{17}), 7.50 (1H, s, H^{19}), 7.18 (1H, dd, $^3J_{H\text{-}H}$ 8.4, $^4J_{H\text{-}H}$ 2.0, H^5), 7.09 (1H, d, $^4J_{H\text{-}H}$ 2.0, H^3), 6.82 (1H, d, $^3J_{H\text{-}H}$ 8.4, H^6), 4.80 (2H, s, H^{21}), 4.49 (2H, q, $^3J_{H\text{-}F}$ 8.0, H^{11}), 4.13–4.06 & 3.91–3.82 (2H, m, H^{23}), 3.86 (3H, s, H^7), 3.42–3.38 (2H, m, H^{10}), 3.12 (2H, t, $^3J_{H\text{-}H}$ 6.3, H^8), 2.75 (3H, s, H^{13}), 2.16–2.09 (2H, m, H^9), 1.76 (3H, d, $^2J_{H\text{-}P}$ 15, H^{22}), 1.26 (3H, t, $^3J_{H\text{-}H}$ 7.1, H^{24}); **^{13}C-NMR** (101 MHz, $CDCl_3$) δ 161.0 (d, $^3J_{C\text{-}P}$ 19, C^{20}), 153.9 (C^1), 153.3 (d, $^1J_{C\text{-}P}$ 155, C^{16}), 141.4 (C^2), 133.1 (d, $^3J_{C\text{-}P}$ 11, C^{18}), 128.2 (d, $^2J_{C\text{-}P}$ 22, C^{17}), 127.5 (C^5), 124.1 (d, $^4J_{C\text{-}P}$ 3, C^{19}), 123.0 (C^3), 122.2 (q, $^1J_{C\text{-}F}$ 280, C^{12}), 114.0 (C^4), 111.5 (C^6), 96.4 (C^{14}), 85.2 (d, $^4J_{C\text{-}P}$ 2, C^{15}), 64.2 (C^{21}), 63.8 (q, $^2J_{C\text{-}F}$ 40, C^{11}), 61.3 (d, $^2J_{C\text{-}P}$ 7, C^{23}), 55.5 (C^7), 53.0 (C^8), 49.0 (C^{10}), 39.4 (C^{13}), 21.5 (C^9), 16.5 (d, $^3J_{C\text{-}P}$ 6, C^{24}), 13.5 (d, $^1J_{C\text{-}P}$ 104, C^{22}); **^{19}F-NMR** (376 MHz, $CDCl_3$) δ -73.9; **^{31}P{^{1}H}-NMR** (162 MHz, $CDCl_3$) δ +39.6; **ESI-LRMS** (+) *m/z* 579 $[M+H]^+$; **ESI-HRMS** (+) calcd for $[C_{24}H_{31}N_2O_7SF_3P]^+$ 579.1542, found 579.1543.

2-*N*,*N*-(Ethyl(trifluoroethyl-3-propyl-sulfonate))amino)-4-((2-(ethoxy(methyl)phosphoryl)-6-((methylsulfonyl)oxy)methylpyridine-4-yl)ethynyl)methoxybenzene, 31a

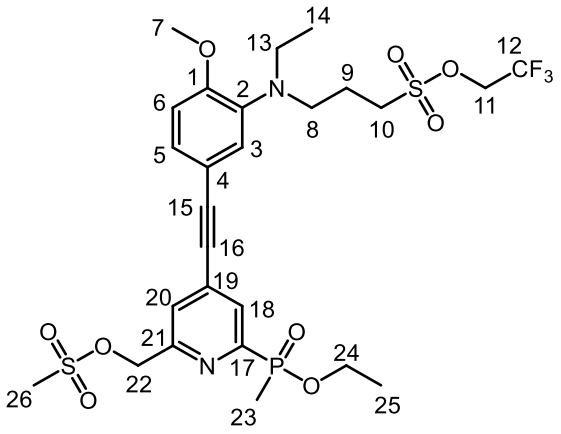

Compound **30a** (110 mg, 0.186 mmol), methanesulfonic anhydride (65 mg, 0.373 mmol) and DIEA (0.065 mL, 0.373 mmol) were combined in anhydrous THF (3 mL) under argon. The reaction mixture was stirred at room temperature for 2 h before removal of the solvent under reduced pressure. The resulting residue was dissolved in DCM (40 mL), washed with H_2O (3 × 40 mL) and the organic layer dried over K_2CO_3. Removal of solvent under reduced pressure afforded a yellow oil (125 mg, 100%); **^{1}H-NMR** (400 MHz, $CDCl_3$) δ 8.09 (1H, dd, $^3J_{H\text{-}P}$ 6.0, $^4J_{H\text{-}H}$ 1.3, H^{18}), 7.63 (1H, s, H^{20}), 7.24 (1H, dd, $^3J_{H\text{-}H}$ 8.4, $^4J_{H\text{-}H}$ 1.9, H^5), 7.13 (1H, d, $^4J_{H\text{-}H}$ 1.9, H^3), 6.86 (1H, d, $^3J_{H\text{-}H}$ 8.4, H^6), 5.36 (2H, s, H^{22}), 4.46 (2H, q, $^3J_{H\text{-}F}$ 8.0, H^{11}), 4.18–4.06 & 3.93–3.83 (2H, m, H^{24}), 3.87 (3H, s, H^7), 3.38–3.32 (2H, m, H^{10}), 3.20 (2H, t, $^3J_{H\text{-}H}$ 6.4, H^8), 3.15–3.09 (5H, m, H^{13} & H^{26}), 2.09–1.99 (2H, m, H^9), 1.77 (3H, d, $^2J_{H\text{-}P}$ 15, H^{23}), 1.27 (3H, t, $^3J_{H\text{-}H}$ 7.1, H^{25}), 1.02 (3H, t, $^3J_{H\text{-}H}$ 7.0, H^{14}); **ESI-LRMS** (+) *m/z* 671 $[M+H]^+$; **ESI-HRMS** (+) calcd for $[C_{26}H_{35}N_2O_9S_2F_3P]^+$ 671.1474, found 671.1473.

2-*N*,*N*-(Methyl(trifluoroethyl-3-propyl-sulfonate))amino)-4-((2-(ethoxy(methyl)phosphoryl)-6-((methylsulfonyl)oxy)methylpyridine-4-yl)ethynyl)methoxybenzene, 31b

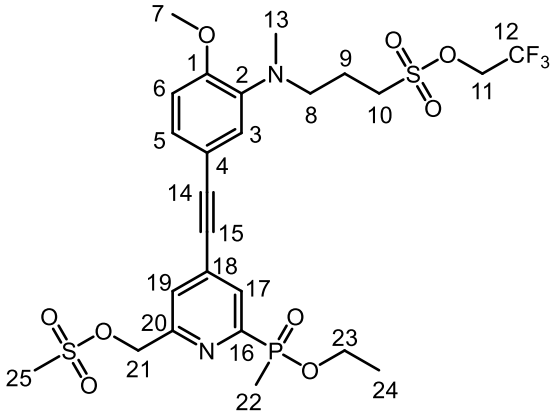

Compound **30b** (119 mg, 0.206 mmol), methanesulfonic anhydride (72 mg, 0.413 mmol) and DIEA (0.072 mL, 0.413 mmol) were combined in anhydrous THF (3 mL) under argon. The reaction mixture was stirred at room temperature for 2 h before removal of the solvent under reduced pressure. The resulting residue was dissolved in DCM (40 mL), washed with H_2O (3 × 40 mL) and the organic layer dried over K_2CO_3. Removal of solvent under reduced pressure afforded a clear colourless oil (88 mg, 65%); **^{1}H-NMR** (400 MHz, $CDCl_3$) δ 8.08 (1H, d, $^3J_{H\text{-}P}$ 6.0, H^{17}), 7.63 (1H, s, H^{19}), 7.21 (1H, dd, $^3J_{H\text{-}H}$ 8.3, $^4J_{H\text{-}H}$ 2.0, H^5), 7.11 (1H, d, $^4J_{H\text{-}H}$ 2.0, H^3), 6.84 (1H, d, $^3J_{H\text{-}H}$ 8.3, H^6), 5.36 (2H, s, H^{21}), 4.50 (2H, q, $^3J_{H\text{-}F}$ 8.0, H^{11}), 4.17–4.08 & 3.93–3.83 (2H, m, H^{23}), 3.87 (3H, s, H^7), 3.44–3.38 (2H, m, H^{10}), 3.17–3.11 (5H, m, H^8 & H^{25}), 2.77 (3H, s, H^{13}), 2.18–2.09 (2H, m, H^9), 1.76 (3H, d, $^2J_{H\text{-}P}$ 15, H^{22}), 1.27 (3H, t, $^3J_{H\text{-}H}$ 7.1, H^{24}).

Compound 32a

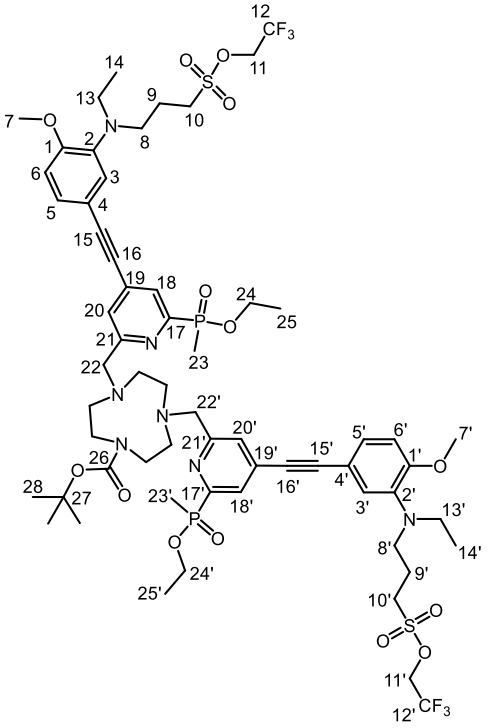

The dihydrochloride salt of 1-(*tert*-butoxycarbonyl)-1,4,7-triazacyclononane (24 mg, 0.0794 mmol), the mesylate **31a** (125 mg, 0.186 mmol) and K_2CO_3 (44 mg, 0.32 mmol) were combined in anhydrous CH_3CN (3 mL) under argon. The resulting mixture was heated to 65 °C for 16 h before separation of the crude solution from the inorganic salts and removal of solvent under reduced pressure to yield an orange oil that was purified by RP-HPLC (10 to 100% CH_3CN in H_2O with 0.1% formic acid over 10 min, $\mathbf{t_R}$ = 13.5 min) to afford a pale yellow oil (88 mg, 80%); **^{1}H-NMR** (700 MHz, $CDCl_3$) δ 8.01 (2H, s, H^{18} & $H^{18'}$), 7.66 (1H, s, H^{20}), 7.61 (1H, s, $H^{20'}$), 7.22 (2H, d, H^5 & $H^{5'}$), 7.12 (2H, s, H^3 & $H^{3'}$), 6.84 (2H, d, H^6 & $H^{6'}$), 4.46 (4H, q, H^{11} & $H^{11'}$), 4.17–3.77 (14H, m, H^7, $H^{7'}$, H^{22}, $H^{22'}$, H^{24} & $H^{24'}$), 3.46–3.31 (8H, m, H^{10}, $H^{10'}$ & 9-N_3 ring), 3.25–3.04 (12H, m, H^8, $H^{8'}$, H^{13}, $H^{13'}$ & 9-N_3 ring), 2.87–2.65 (4H, m, 9-N_3 ring), 2.11–1.98 (4H, m, H^9 & $H^{9'}$), 1.77 (6H, d, H^{23} & $H^{23'}$), 1.48 (9H, s, H^{28}), 1.25 (6H, t, H^{25} & $H^{25'}$), 1.01 (6H, t, H^{14} & $H^{14'}$); **^{13}C-NMR** (101 MHz, $CDCl_3$) δ 161.5 (d, C^{21} & $C^{21'}$), 155.6 (d, C^{17} & $C^{17'}$), 155.5 (C^1 & $C^{1'}$), 153.1 (C^{26}), 138.6 (C^2), 132.7 (d, C^{19} & $C^{19'}$), 128.1 (C^5 & $C^{5'}$), 127.9 (d, C^{20} & $C^{20'}$), 126.5 (d, C^{18} & $C^{18'}$), 125.8 (C^3 & $C^{3'}$), 122.1 (q, C^{12} & $C^{12'}$), 113.9 (d, C^4 & $C^{4'}$), 111.8 (C^6 & $C^{6'}$), 96.1 (C^{15} & $C^{15'}$), 85.4 (C^{16} & $C^{16'}$), 79.7 (C^{27}), 63.8 (q, C^{11} & $C^{11'}$), 62.5 (C^{22} & $C^{22'}$), 61.1 (d, C^{24} & $C^{24'}$), 55.7 (9-N_3 ring), 55.6 (C^7 & $C^{7'}$), 54.8 (9-N_3 ring), 54.4 (9-N_3 ring), 53.7 (9-N_3 ring), 49.8 (C^8 & $C^{8'}$), 49.4 (9-N_3 ring), 49.1 (C^{10}

& $C^{10'}$), 46.7 (C^{13} & $C^{13'}$), 46.0 (9-N_3 ring), 28.7 (C^{28}), 21.6 (C^{9} & $C^{9'}$), 16.6 (d, C^{25} & $C^{25'}$), 13.4 (2 × d, C^{23} & $C^{23'}$), 12.2 (C^{14} & $C^{14'}$); **^{19}F-NMR** (376 MHz, $CDCl_3$) δ -74.0; **^{31}P-NMR** (162 MHz, $CDCl_3$) δ +40.1 (s); **ESI-LRMS** (+) *m/z* 1379 $[M+H]^+$; **ESI-HRMS** (+) calcd for $[C_{61}H_{84}F_6N_7O_{14}P_2S_2]^+$ 1378.490, found 1378.489.

Compound 32b

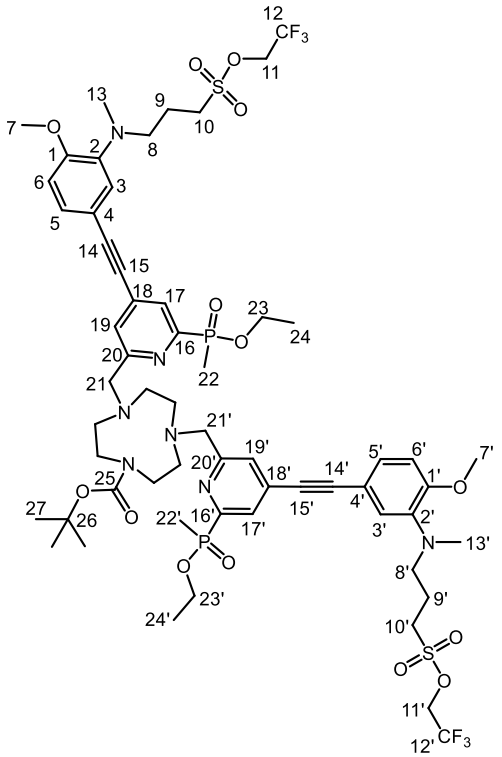

The dihydrochloride salt of 1-(*tert*-butoxycarbonyl)-1,4,7-triazacyclononane (18 mg, 0.06 mmol), the mesylate **31b** (88 mg, 0.134 mmol) and K_2CO_3 (35 mg, 0.25 mmol) were combined in anhydrous CH_3CN (3 mL) under argon. The resulting mixture was heated to 65 °C for 18 h before separation of the crude solution from the inorganic salts and removal of solvent under reduced pressure to yield an orange oil that was purified by RP-HPLC (10 to 100% CH_3CN in H_2O over 10 min, $\mathbf{t_R}$ = 14.2 min) to afford a pale yellow oil (58 mg, 72%); **^{1}H-NMR** (700 MHz, $CDCl_3$) δ 8.02–7.98 (2H, m, H^{17} & $H^{17'}$), 7.65 (1H, s, H^{19}), 7.58 (1H, s, $H^{19'}$), 7.20 (2H, d, H^5 & $H^{5'}$), 7.11 (2H, s, H^3 & $H^{3'}$), 6.83 (2H, d, H^6 & $H^{6'}$), 4.50 (4H, q, H^{11} & $H^{11'}$), 4.15–4.06 & 3.89–3.81 (10H, m, H^7, H^{23} & $H^{23'}$), 3.95 (4H, 2 × s, H^{21}), 3.44–3.32 (8H, m, H^{10}, $H^{10'}$ & 9-N_3 ring), 3.16–3.05 (8H, m, H^8, $H^{8'}$ & 9-N_3 ring), 2.76 (6H, s, H^{13} & $H^{13'}$), 2.73–2.65 (4H, m, 9-N_3 ring),

2.17–2.10 (4H, m, H^{9} & $H^{9'}$), 1.76 (6H, 2 × d, H^{22} & $H^{22'}$), 1.48 (9H, s, H^{27}), 1.28–1.22 (6H, m, H^{24} & $H^{24'}$); **^{19}F-NMR** (376 MHz, $CDCl_3$) δ -73.9; **^{31}P-NMR** (162 MHz, $CDCl_3$) δ +40.1 (s); **ESI-LRMS** (+) *m/z* 1350 $[M+H]^+$; **ESI-HRMS** (+) calcd for $[C_{59}H_{80}F_6N_7O_{14}P_2S_2]^+$ 1350.458, found 1350.455.

Compound 33a, trifluoroacetate salt

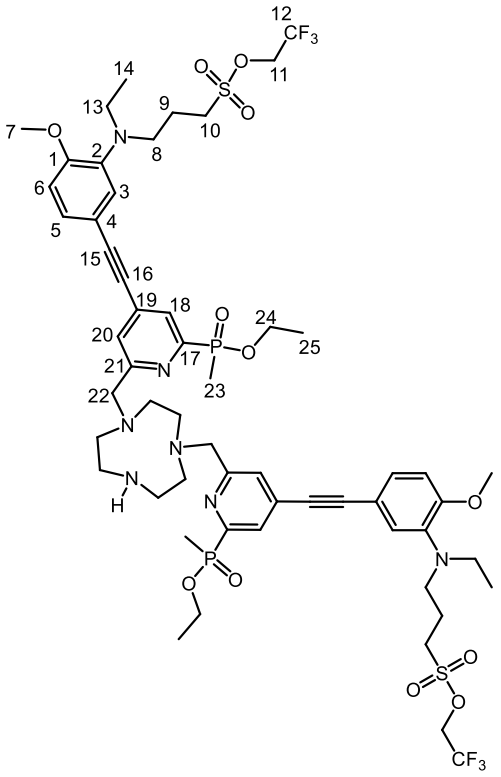

A solution of the carbamate **32a** (88 mg, 0.064 mmol) in TFA and DCM was prepared (10% v/v, 3 mL total) and stirred under argon for 60 min. The solvent was removed under reduced pressure and additional DCM (~50 mL) was added and the solvent removed under reduced pressure. This procedure was repeated 3 times. Drying under high vacuum for several hours yielded the trifluoroacetate salt as an orange oil (88 mg, quant.); **^{1}H-NMR** (400 MHz, CD_3OD) δ 8.00 (2H, d, $^{4}J_{H\text{-}H}$ 1.9, H^{3}), 7.98 (2H, dd, $^{3}J_{H\text{-}P}$ 6.0, $^{4}J_{H\text{-}H}$ 1.1, H^{18}), 7.82 (2H, dd, $^{3}J_{H\text{-}H}$ 8.8, $^{4}J_{H\text{-}H}$ 1.9, H^{5}), 7.75–7.74 (2H, m, H^{20}), 7.42 (2H, d, $^{3}J_{H\text{-}H}$ 8.8, H^{6}), 5.20–5.08 (12H, m, 9-N_3 ring), 4.70 (4H, q, $^{3}J_{H\text{-}F}$ 8.3, H^{11}), 4.43 (4H, s, H^{22}), 4.16–3.90 (10H, m, H^{7} & H^{24}), 3.88–3.80 (4H, m, H^{8}), 3.75 (4H, q, $^{3}J_{H\text{-}H}$ 7.1, H^{13}), 3.49 (4H, t, $^{3}J_{H\text{-}H}$ 7.2, H^{10}), 2.04–1.94 (4H, m, H^{9}), 1.80 (6H, d, $^{2}J_{H\text{-}P}$ 15, H^{23}), 1.30 (6H, t, $^{3}J_{H\text{-}H}$ 7.0, H^{25}), 1.13 (6H, t, $^{3}J_{H\text{-}H}$ 7.1, H^{14}); **^{13}C-NMR** (101 MHz,

CD_3OD) δ 161.3 (d, $^3J_{C\text{-}P}$ 20, C^{21}), 155.5 (C^1), 155.1 (d, $^1J_{C\text{-}P}$ 157, C^{17}), 137.0 (C^2), 134.2 (d, $^3J_{C\text{-}P}$ 12, C^{19}), 128.9 (d, $^4J_{C\text{-}P}$ 2.5, C^{20}), 128.8 (d, $^2J_{C\text{-}P}$ 22, C^{18}), 127.8 (C^5), 126.1 (C^3), 123.8 (q, $^1J_{C\text{-}F}$ 280, C^{12}), 116.8 (C^4), 115.0 (C^6), 94.9 (C^{15}), 87.2 (d, $^4J_{C\text{-}P}$ 2.2, C^{16}), 65.7 (q, $^2J_{C\text{-}F}$ 38, C^{11}), 63.1 (d, $^2J_{C\text{-}P}$ 6.5, C^{24}), 60.6 (9-N_3 ring), 57.7 (C^{22}), 56.6 (9-N_3 ring), 55.3 (9-N_3 ring), 52.4 (9-N_3 ring), 51.0 (9-N_3 ring), 48.0 (C^7), 45.5 (9-N_3 ring), 32.7 (C^8), 26.7 (C^3), 23.7 (C^{10}), 20.8 (C^9), 16.8 (d, $^3J_{C\text{-}P}$ 6.2, C^{25}), 13.7 (d, $^1J_{C\text{-}P}$ 103, C^{23}), 10.4 (C^{14}); **^{19}F-NMR** (376 MHz, CD_3OD) δ -73.5 (-$SO_2CH_2C\underline{F}_3$), -74.9 (trifluoroacetate anion); **^{31}P-NMR** (162 MHz, CD_3OD) δ +40.8; **ESI-LRMS** (+) *m/z* 1279 $[M+H]^+$; **ESI-HRMS** (+) calcd for $[C_{56}H_{76}F_6N_7O_{12}P_2S_2]^+$ 1278.437, found 1278.440.

Compound 33b, trifluoroacetate salt

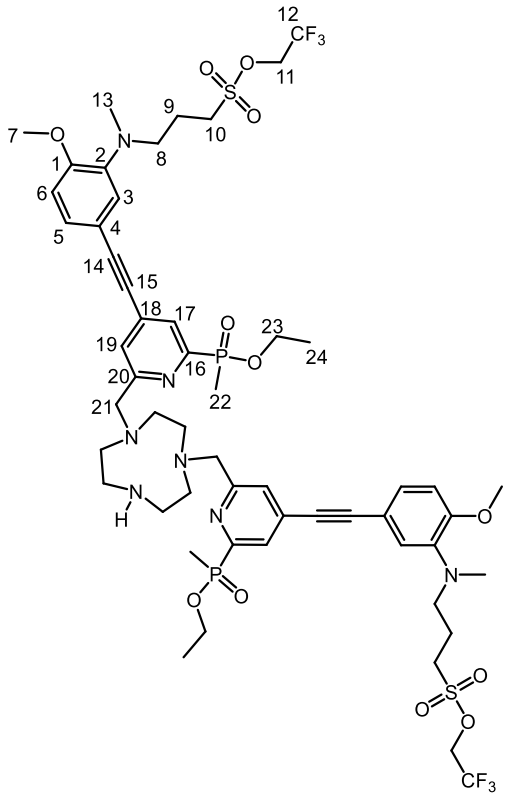

A solution of compound **32b** (29 mg, 0.021 mmol) in TFA and DCM was prepared (10% v/v, 3 mL total) and stirred under argon for 60 min. The solvent was removed under reduced pressure and additional DCM (~50 mL) added and the solvent removed under reduced pressure. This procedure was repeated 3 times. Drying under high vacuum for several hours yielded the trifluoroacetate salt as an orange oil (29 mg, quant.); **^{1}H-NMR** (400 MHz, $CDCl_3$) δ 7.87 (2H, d, $^3J_{H\text{-}P}$ 6.0, H^{17}), 7.57–7.43 (6H, m,

H^3, H^5 & H^{19}), 7.00 (2H, d, $^3J_{H\text{-}H}$ 8.5, H^6), 4.51 (4H, q, $^3J_{H\text{-}F}$ 7.9, H^{11}), 4.27–4.09 & 4.03–3.87 (14H, m, H^7, H^{21}, H^{23}), 3.67–3.53 (6H, m, H^{10} & 9-N_3 ring), 3.47–3.26 (12H, m, H^8 & 9-N_3 ring), 3.13–3.03 (8H, m, H^{13} & 9-N_3 ring), 2.14–2.05 (4H, m, H^9), 1.77 (6H, d, $^2J_{H\text{-}P}$ 15, H^{22}), 1.31 (6H, t, $^3J_{H\text{-}H}$ 7.4, H^{24}); **^{19}F-NMR** (376 MHz, $CDCl_3$) δ -74.6 (-$SO_2CH_2C\underline{F}_3$), -76.3 (trifluoroacetate salt); **^{31}P-NMR** (162 MHz, $CDCl_3$) δ +40.3; **ESI-LRMS** (+) *m/z* 1250 $[M+H]^+$; **ESI-HRMS** (+) calcd for $[C_{54}H_{72}N_7F_6O_{12}P_2S_2]^+$ 1250.406, found 1250.408.

pro-L^{10a}

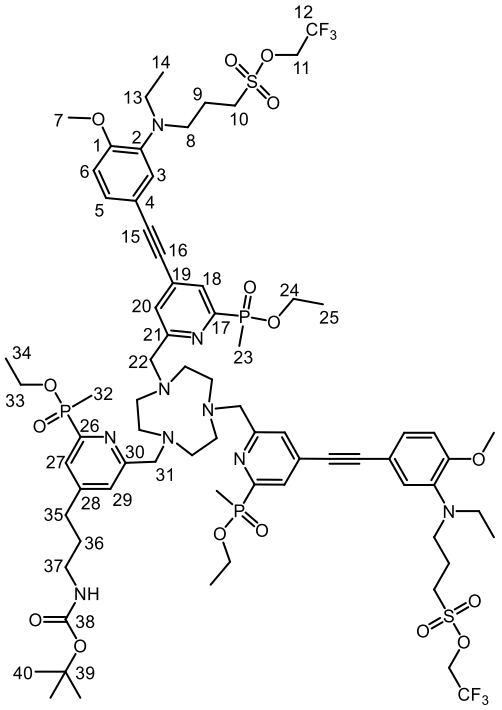

Compound **33a** (44 mg, 0.032 mmol), compound **22** (30 mg, 0.067 mmol) and K_2CO_3 (30 mg, 0.22 mmol) were combined in anhydrous CH_3CN (2 mL) under argon and heated at 60 °C for 15 h. After this time, LC/MS analysis confirmed the complete transformation of the macrocycle **33a**. The reaction mixture was allowed to cool before separation of the inorganic salts by filtration. Removal of the solvent under reduced pressure afforded a yellow oil (70 mg) that was used directly in the next step without further purification; **^{1}H-NMR** (400 MHz, $CDCl_3$) δ 7.96 (1H, d, $^3J_{H\text{-}P}$ 6.2, H^{27}), 7.78 (2H, d, $^3J_{H\text{-}P}$ 6.2, H^{18}), 7.42 (1H, s, H^{29}), 7.24 (2H, s, H^{20}), 7.19 (2H, dd, $^3J_{H\text{-}H}$ 8.4, $^4J_{H\text{-}H}$ 2.0, H^5), 7.09 (2H, d, $^4J_{H\text{-}H}$ 2.0, H^3), 6.82 (2H, d, $^3J_{H\text{-}H}$ 8.4, H^6), 4.76 (6H, s, H^{22} & H^{31}) 4.68

(1H, br s, NH), 4.45 (4H, q, $^{3}J_{H\text{-}F}$ 8.0, H^{11}), 4.12–3.76 (16H, m, H^{7}, H^{24}, H^{33} & 9-N_3 ring), 3.37–3.30 (4H, m, H^{10}), 3.20–3.05 (10H, m, H^{8}, H^{13} & H^{37}), 2.94–2.82 (8H, m, 9-N_3 ring), 2.72–2.64 (2H, m, H^{35}), 1.83–1.79 (4H, m, H^{9} & H^{36}), 1.73 (9H, d, $^{2}J_{H\text{-}P}$ 15, H^{23} & H^{32}), 1.41 (9H, s, H^{40}), 1.26–1.20 (9H, m, H^{25} & H^{34}), 0.99 (6H, t, $^{3}J_{H\text{-}H}$ 7.1, H^{14}); **^{19}F-NMR** (376 MHz, $CDCl_3$) δ -74.0; **^{31}P-NMR** (162 MHz, $CDCl_3$) δ +40.0; **ESI-LRMS** (+) *m/z* 1633 $[M+H]^+$, 817 $[M+2H]^{2+}$; **ESI-HRMS** (+) calcd for $[C_{73}H_{104}F_6N_9O_{16}P_3S_2]^{2+}$ 816.8080, found 816.8085.

pro-L^{10b}

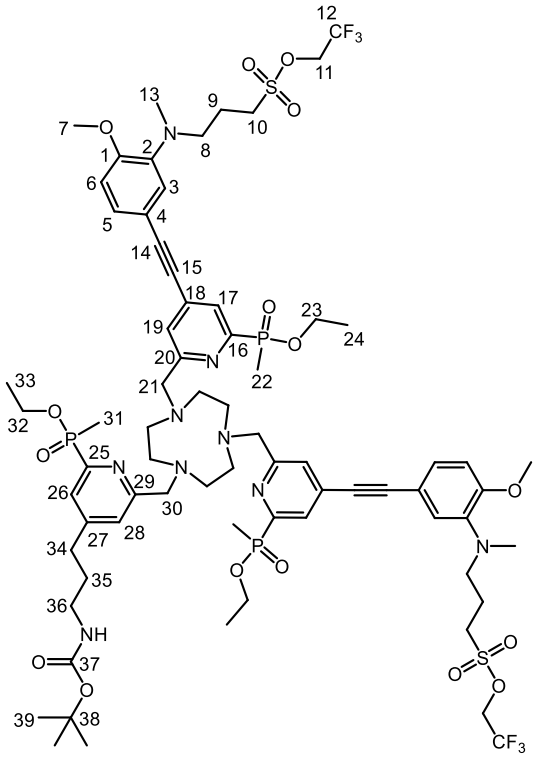

Compounds **33b** (29 mg, 0.021 mmol), **22** (19 mg, 0.042 mmol) and K_2CO_3 (20 mg, 0.15 mmol) were combined in anhydrous CH_3CN (2 mL) under argon and heated at 60 °C for 15 h. After this time, LC/MS analysis confirmed the complete transformation of the macrocycle **33b**. The reaction mixture was allowed to cool before separation from the inorganic salts by filtration. Removal of the solvent under reduced pressure afforded a yellow oil (47 mg) that was used directly in the next step without further purification; **^{1}H-NMR** (400 MHz, $CDCl_3$) δ 7.99 (1H, d, $^{3}J_{H\text{-}P}$ 6.0, H^{26}), 7.80 (2H, dd, $^{3}J_{H\text{-}P}$ 6.0, $^{4}J_{H\text{-}H}$ 1.4, H^{17}), 7.44–7.42 (1H, m, H^{28}), 7.25–7.22 (2H, m, H^{19}), 7.22–7.16 (2H, m, H^{5}), 7.09 (2H, d, $^{4}J_{H\text{-}H}$ 1.8, H^{3}), 6.83 (2H, d, $^{3}J_{H\text{-}H}$ 8.4, H^{6}), 4.77 (6H, s, H^{21} & H^{30}),

4.50 (4H, q, $^{3}J_{H\text{-}F}$ 8.0, H^{11}), 4.13–3.76 (16H, m, H^{7}, H^{23}, H^{32} & 9-N_3 ring), 3.43–3.38 (2H, m, H^{10}), 3.17–3.09 (14H, m, H^{8}, H^{36} & 9-N^3 ring), 2.75 (6H, s, H^{13}), 2.71–2.66 (2H, m, H^{34}), 1.85–1.80 (4H, m, H^{9} & H^{35}), 1.74 (9H, d, $^{2}J_{H\text{-}P}$ 15, H^{22} & H^{31}), 1.42 (9H, s, H^{39}), 1.25 (9H, t, $^{3}J_{H\text{-}H}$ 7.1, H^{24} & H^{33}); **^{19}F-NMR** (376 MHz, $CDCl_3$) *δ* -73.9; **^{31}P-NMR** (162 MHz, $CDCl_3$) *δ* +40.0; **ESI-LRMS** (+) *m/z* 1605 $[M+H]^+$; **ESI-HRMS** (+) calcd for $[C_{71}H_{99}F_6N_9O_{16}P_3S_2]^+$ 1604.577, found 1604.577.

2-*N,N*-(Diethylamino)-4-(ethynyl)-*tert*-butoxy-carbamoyl-propoxy-benzene 35

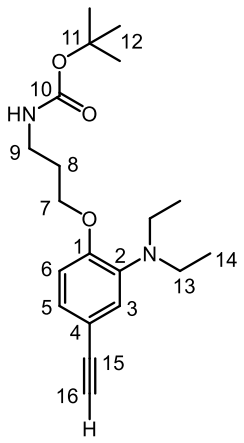

Triethylamine trihydrofluoride (1.1 mL, 6.75 mmol) was added to compound **34** (185 mg, 0.442 mmol) in anhydrous THF (5 mL) under argon. The solution was stirred at 30 °C for 38 h before removal of solvent under reduced pressure. The residue was subsequently dissolved in DCM (30 mL) and washed with H_2O (3 × 30 mL). The combined aqueous layers were extracted with DCM (2 × 30 mL) and the combined organic layers dried over K_2CO_3 to yield a pale yellow oil (74 mg, 48%). The product was used in the next step without further purification; **^{1}H-NMR** (600 MHz, $CDCl_3$) *δ* 7.13 (1H, d, $^{3}J_{H\text{-}H}$ 8.2, H^{5}), 7.10 (1H, s, H^{3}), 6.76 (1H, d, $^{3}J_{H\text{-}H}$ 8.2, H^{6}), 4.06 (2H, t, $^{3}J_{H\text{-}H}$ 5.7, H^{7}), 3.40–3.31 (2H, m, H^{9}), 3.12 (4H, q, $^{3}J_{H\text{-}H}$ 7.0, H^{13}), 2.98 (1H, s, H^{16}), 2.02–1.95 (2H, m, H^{8}), 1.45 (9H, s, H^{12}), 0.99 (6H, t, $^{3}J_{H\text{-}H}$ 7.0, H^{14}); **^{13}C-NMR** (151 MHz, $CDCl_3$) *δ* 156.4 (C^{10}), 154.5 (C^{1}), 139.6 (C^{2}), 127.5 (C^{5}), 125.9 (C^{3}), 114.4 (C^{4}), 112.7 (C^{6}), 84.3 (C^{15}), 79.0 (C^{11}), 75.5 (C^{16}), 68.4 (C^{7}), 46.3 (C^{13}), 39.3 (C^{9}), 29.7 (C^{8}), 28.6 (C^{12}), 12.0 (C^{14}); **ESI-LRMS** (+) *m/z* 347 $[M+H]^+$; **ESI-HRMS** (+) calcd for $[C_{20}H_{31}N_2O_3]^+$ 347.2353, found 347.2350.

2-*N,N*-(Diethylamino)-4-(((2-(ethoxy(methyl)phosphoryl))-6-(hydroxymethyl)pyridine-4-yl)-(ethynyl)-*tert*-butoxy-carbamoyl-propoxy-benzene, 36

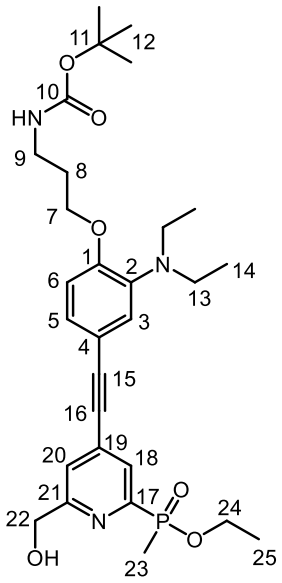

Compound **35** (172 mg, 0.496 mmol) and compound **5** (139 mg, 0.473 mmol) were combined in anhydrous CH_3CN (3 mL) under argon. To this solution was added $Pd_2Cl_2(allyl)_2$ (20 mg, 0.055 mmol), $P(^tBu)_3$ (0.02 mL, 0.082 mmol) and piperidine (0.12 mL, 1.22 mmol) in that order. The resulting mixture was stirred at 35 °C under argon for 24 h before removal of the solvent under reduced pressure. The residue was dissolved in DCM (40 mL) and washed with H_2O (3 × 40 mL) before drying over K_2CO_3. Removal of the solvent under reduced pressure afforded a brown oil that was purified by RP-HPLC (10 to 100% CH_3CN over 10 min, $\mathbf{t_R}$ = 11.7 min) to give a pale yellow oil (64 mg, 24%); **^{1}H-NMR** (700 MHz, $CDCl_3$) δ 8.03 (1H, d, $^3J_{H\text{-}P}$ 6.0, H^{18}), 7.50 (1H, s, H^{20}), 7.17 (1H, d, $^3J_{H\text{-}H}$ 8.2, H^5), 7.12 (1H, s, H^3), 6.81 (1H, d, $^3J_{H\text{-}H}$ 8.2, H^6), 5.83 (1H, br s, NH), 4.80 (2H, s, H^{22}), 4.14–4.06 & 3.89–3.82 (2H, m, H^{24}), 4.08 (2H, t, $^3J_{H\text{-}H}$ 5.8, H^7), 3.38–3.32 (2H, m, H^9), 3.15 (4H, q, $^3J_{H\text{-}H}$ 7.0, H^{13}), 2.03–1.97 (2H, m, H^8), 1.77 (3H, d, $^2J_{H\text{-}P}$ 15, H^{23}), 1.44 (9H, s, H^{12}), 1.26 (3H, t, $^3J_{H\text{-}H}$ 7.1, H^{25}), 1.01 (6H, t, $^3J_{H\text{-}H}$ 7.0, H^{14}); **^{13}C-NMR** (176 MHz, $CDCl_3$) δ 160.8 (d, $^3J_{C\text{-}P}$ 19, C^{21}), 156.4 (C^{10}), 155.0 (C^1), 153.3 (d, $^1J_{C\text{-}P}$ 155, C^{17}), 139.8 (C^2), 133.2 (d, $^3J_{C\text{-}P}$ 11, C^{19}), 128.3 (d, $^2J_{C\text{-}P}$ 22, C^{18}), 127.5 (C^5), 125.7 (C^3), 124.1 (d, $^4J_{C\text{-}P}$ 3, C^{20}), 113.9 (C^4), 112.8 (C^6), 96.9 (C^{15}), 85.0 (d, $^4J_{C\text{-}P}$ 2, C^{16}), 79.1 (C^{11}), 68.4 (C^7), 64.2 (C^{22}), 61.3 (d, $^2J_{C\text{-}P}$ 7, C^{24}), 46.2 (C^{13}), 39.2 (C^9), 29.6 (C^8), 28.6 (C^{12}), 16.5 (d, $^3J_{C\text{-}P}$ 6, C^{25}), 13.5 (d, $^1J_{C\text{-}P}$ 105, C^{23}), 12.1

(C^{14}); **^{31}P{^{1}H}-NMR** (162 MHz, $CDCl_3$) δ +39.5; **ESI-LRMS** (+) *m/z* 560 $[M+H]^+$; **ESI-HRMS** (+) calcd for $[C_{29}H_{43}N_3O_6P]^+$ 560.2889, found 560.2879.

2-*N,N*-(Diethylamino)-4-(((2-(ethoxy(methyl)phosphoryl))-6-(((methylsulfonyl)oxy)methyl)pyridine-4-yl)-(ethynyl)-*tert*-butoxy-carbamoyl-propoxy-benzene, 37

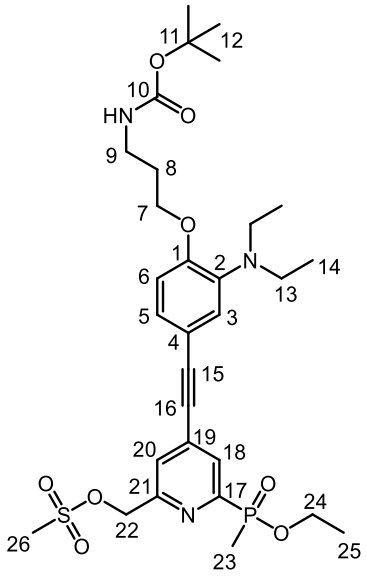

The alcohol **36** (40 mg, 0.072 mmol), methanesulfonic anhydride (25 mg, 0.143 mmol) and DIEA (0.025 mL, 0.025 mmol) were combined in anhydrous THF (2 mL) under argon. The reaction mixture was stirred at room temperature for 90 min before removal of the solvent under reduced pressure. The resulting residue was dissolved in DCM (40 mL), washed with H_2O (3 × 40 mL) before extraction of the combined aqueous layers with DCM (2 × 40 mL). The combined organic layers were dried over K_2CO_3 and the solvent removed under reduced pressure to afford a yellow oil (45 mg, 100%); **^{1}H-NMR** (400 MHz, $CDCl_3$) δ 8.09 (1H, dd, $^{3}J_{H\text{-}P}$ 6.0, $^{4}J_{H\text{-}H}$ 1.4, H^{18}), 7.63 (1H, s, H^{20}), 7.19 (1H, dd, $^{3}J_{H\text{-}H}$ 8.2, $^{4}J_{H\text{-}H}$ 1.6, H^{5}), 7.14 (1H, d, $^{4}J_{H\text{-}H}$ 1.6, H^{3}), 6.82 (1H, d, $^{3}J_{H\text{-}P}$ 8.2, H^{6}), 5.86 (1H, br s, NH), 5.36 (2H, s, H^{22}), 4.18–4.02 & 3.94–3.80 (4H, m, H^{7} & H^{24}), 3.40–3.31 (2H, m, H^{9}), 3.19–3.12 (7H, m, H^{13} & H^{26}), 2.03–1.99 (2H, m, H^{8}), 1.77 (3H, d, $^{2}J_{H\text{-}P}$ 15, H^{23}), 1.44 (9H, s, H^{12}), 1.27 (3H, t, $^{3}J_{H\text{-}H}$ 7.1, H^{25}), 1.04–1.00 (6H, m, H^{14}); **ESI-LRMS** (+) *m/z* 638 $[M+H]^+$; **ESI-HRMS** (+) calcd for $[C_{30}H_{45}N_3O_8SP]^+$ 638.2665, found 638.2676.

pro-L[11]

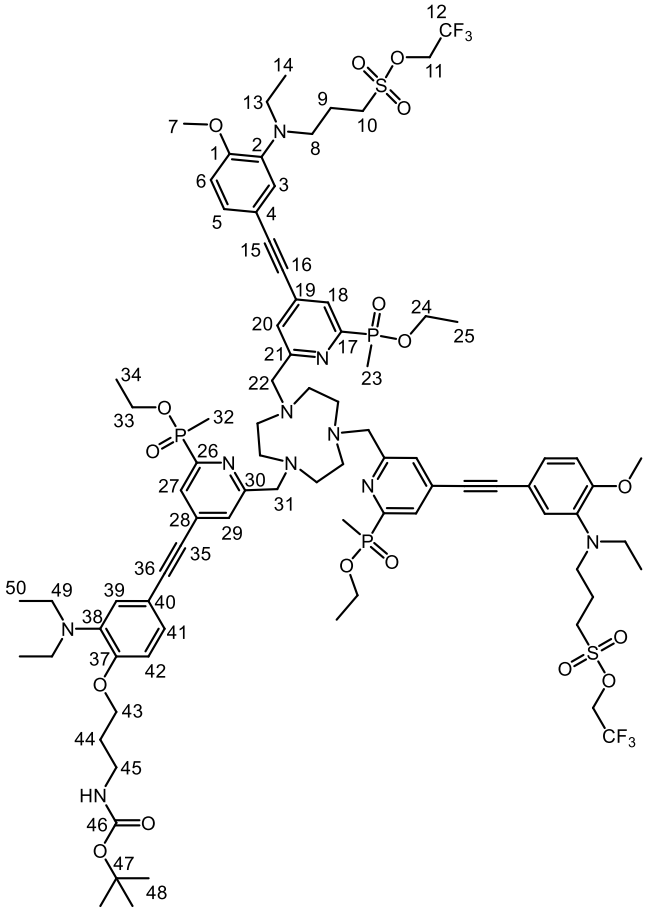

Compound **33a** (44 mg, 0.032 mmol), compound **37** (31 mg, 0.049 mmol) and K_2CO_3 (30 mg, 0.22 mmol) were combined in anhydrous CH_3CN (2 mL) under argon and heated at 60 °C for 14 h. After this time, LC/MS analysis confirmed the complete transformation of the macrocycle **33a**. The reaction mixture was allowed to cool before separation of the inorganic salts by filtration. Removal of the solvent under reduced pressure afforded a yellow oil (47 mg) that was used directly in the next step without further purification; **^{1}H-NMR** (400 MHz, CD_3OD) δ 7.91–7.82 (5H, m, H^3, H^{18} & H^{27}), 7.30–7.16 (7H, m, H^5, H^{20}, H^{29}, H^{39} & H^{41}), 6.99–6.93 (3H, m, H^6 & H^{42}), 4.84 (6H, s, H^{22} & H^{31}), 4.64 (4H, q, $^3J_{H\text{-}F}$ 8.1, H^{11}), 4.14–3.84 (22H, m, H^7, H^8, H^{24}, H^{33}, H^{43} & 9-N_3 ring), 3.43–3.37 (2H, m, H^{10}), 3.30–3.24 (2H, m, H^{45}), 3.19–3.07 (8H, m, H^{13} & H^{49}), 2.91–2.83 (8H, m, 9-N_3 ring), 2.02–1.89 (6H, m, H^9 & H^{44}), 1.77 (9H, d, $^2J_{H\text{-}P}$ 15, H^{23} & H^{32}), 1.44 (9H, s, H^{48}), 1.26–1.21 (9H, m, H^{25} & H^{34}), 1.03–0.98 (12H, m, H^{14} & H^{50}); **^{19}F-NMR** (376 MHz, CD_3OD) δ -76.8; **^{31}P-NMR** (162 MHz, CD_3OD) δ + 41.8; **ESI-LRMS** (+) *m/z* 1821 $[M+H]^+$, 911 $[M+2H]^{2+}$; **ESI-HRMS** (+) calcd for $[C_{85}H_{117}F_6N_{10}O_{17}P_3S_2]^{2+}$ 910.8594, found 910.8554.

*7.7.3.2. Synthesis of complexes **[Eu.L$^{10a-b,11}$]***

[Eu.L^{10a}]

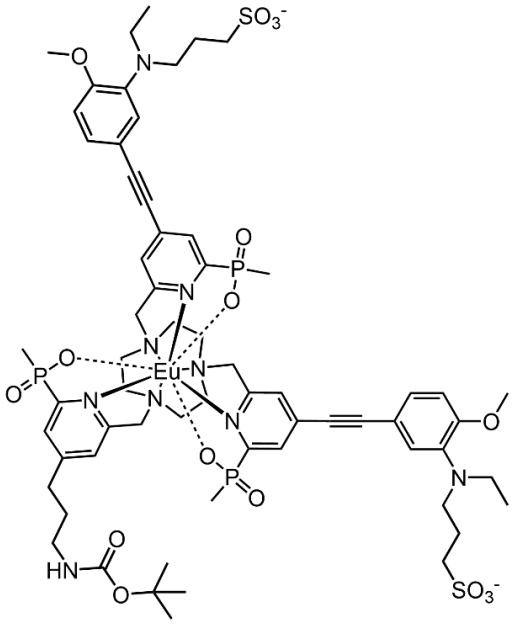

The crude ligand **pro-L^{10a}** (57 mg) was dissolved in a mixture of CD_3OD/aqueous NaOD solution (0.1 M, 3:1, 2 mL total). The solution was heated at 70 °C for 24 h. After this time, LC/MS analysis confirmed complete hydrolysis of the phosphinate and sulfonate ester groups. After cooling and adjustment of the pH to 6 using dilute hydrochloric acid (0.1 M), $EuCl_3.6H_2O$ (14 mg, 0.038 mmol) was added and the reaction mixture was heated to 75 °C for 24 h. The reaction mixture was purified by RP-HPLC (10 to 100% CH_3CN in H_2O over 10 min, $\mathbf{t_R}$ = 7.9 min) to yield a pale yellow solid (13 mg, 27% over two steps); $\boldsymbol{\tau_{H2O}}$ (ms) = 0.31 (pH 9), 0.31 (pH 8), 0.29 (pH 7), 0.41 (pH 6), 0.76 (pH 5), 1.07 (pH 4); $\boldsymbol{\chi_{332\ nm}}$ = 35,000 M^{-1} cm^{-1}; $\boldsymbol{\Lambda_{pH\ 8}}$ = 0.06%, $\boldsymbol{\Lambda_{pH\ 4}}$ = 13.4% (λ_{exc} 332 nm).

[Eu.L^{10b}]

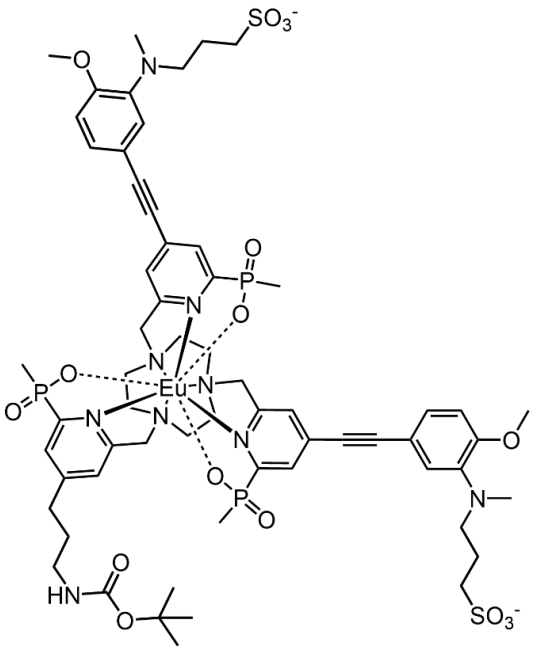

The crude ligand **pro-L^{10b}** (23 mg) was dissolved in a mixture of CD_3OD/aqueous NaOD solution (0.1 M, 3:1, 2 mL total). The solution was heated at 70 °C for 48 h. After this time, LC/MS analysis confirmed complete hydrolysis of the phosphinate and sulfonate ester groups. After cooling and adjustment of the pH to 6 using hydrochloric acid (0.1 M), $EuCl_3.6H_2O$ (8 mg, 0.022 mmol) was added and the reaction mixture was heated to 75 °C for 24 h. The reaction mixture was purified by RP-HPLC (10 to 100% CH_3CN in H_2O over 10 min, $\mathbf{t_R}$ = 7.9 min) to yield a dark yellow solid (1.8 mg, 11% over two steps); τ_{H2O} (ms) = 0.30 (pH 6.5), 0.31 (pH 6), 0.40 (pH 5), 0.83 (pH 4), 1.01 (pH 3); $\varepsilon_{336\ nm}$ = 35,000 M^{-1} cm^{-1}; $\Phi_{pH\ 7}$ = 0.06%, $\Phi_{pH\ 3}$ = 13% (λ_{exc} 336 nm).

[Eu.L^{11}]

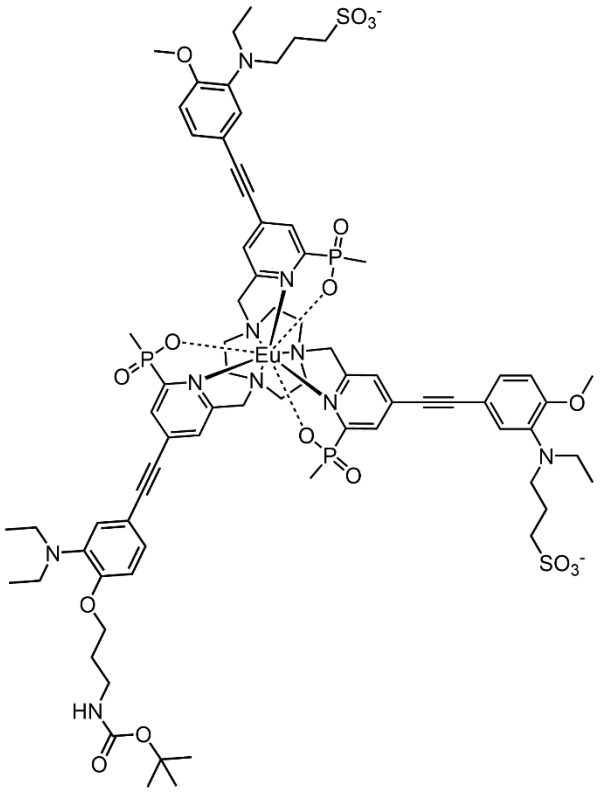

The crude ligand **pro-L^{11}** (38 mg) was dissolved in a mixture of CD_3OD/aqueous NaOD solution (0.1M, 3:1, 2 mL total). The solution was heated at 70 °C for 24 h. After this time, LC/MS analysis confirmed complete hydrolysis of the phosphinate and sulfonate ester groups. After cooling and adjustment of the pH to 6 using hydrochloric acid (0.1 M), $EuCl_3.6H_2O$ (14 mg, 0.038 mmol) was added and the reaction mixture was heated to 75 °C for 24 h. The reaction mixture was purified by RP-HPLC (10 to 100% CH_3CN in H_2O over 10 min, $\mathbf{t_R}$ = 8.8 min) to yield a pale yellow solid (11 mg, 25% over two steps); $\boldsymbol{\tau_{H2O}}$ (ms) = 0.20 (pH 9), 0.21 (pH 8), 0.22 (pH 7), 0.35 (pH 6), 0.69 (pH 5), 0.98 (pH 4), 0.98 (pH 4), 1.01 (pH 3.5); $\boldsymbol{\varepsilon_{332\ nm}}$ = 75,000 M^{-1} cm^{-1}; $\boldsymbol{\Phi_{pH\ 8}}$ = 0.01%, $\boldsymbol{\Phi_{pH\ 4}}$ = 15.9% (λ_{exc} 332 nm).

7.7.4. Synthesis of the BG derivatives

[Eu.L^{9} a]-NH$_2$

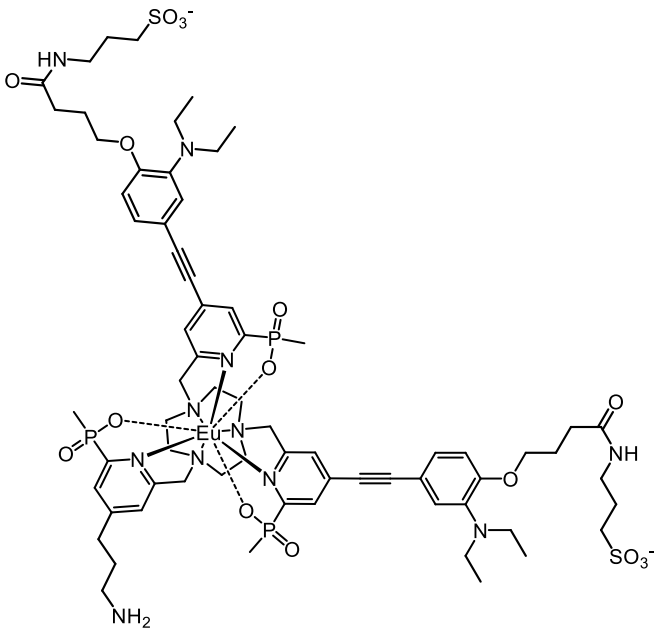

To the complex **[Eu.L^{9} a]** (6.93 mg, 4 µmol) was added TFA (200 µL). The mixture was stirred at room temperature for 1 h and then purified by preparative HPLC (2 to 40% CH_3CN in 25 mM TEAAc (pH 7) over 18 min) to afford a yellow solid (3.5 µmol, 87%); **ESI-LRMS** (-) *m/z* 814.7 $[M]^{2-}$.

[Eu.L^{9} ^{h}]$^{\hat{o}}$NH$_2$

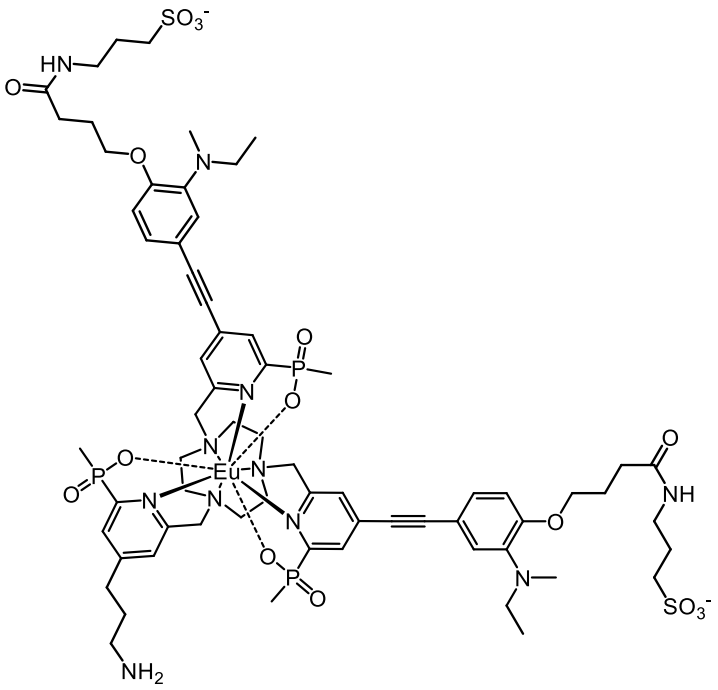

To the complex **[Eu.L^{9} ^{h}]$^{\hat{o}}$**(9 mg, 5283 nmol) was added TFA (1 mL). The mixture was stirred at room temperature for 1 h and then purified by preparative HPLC (2 to 40% CH_3CN in 25 mM TEAAc (pH 7) over 18 min) to give a yellow solid (4256 nmol, 81%); **ESI-LRMS** (-) *m/z* 800.8 $[M]^{2-}$.

[Eu.L^{12a}]

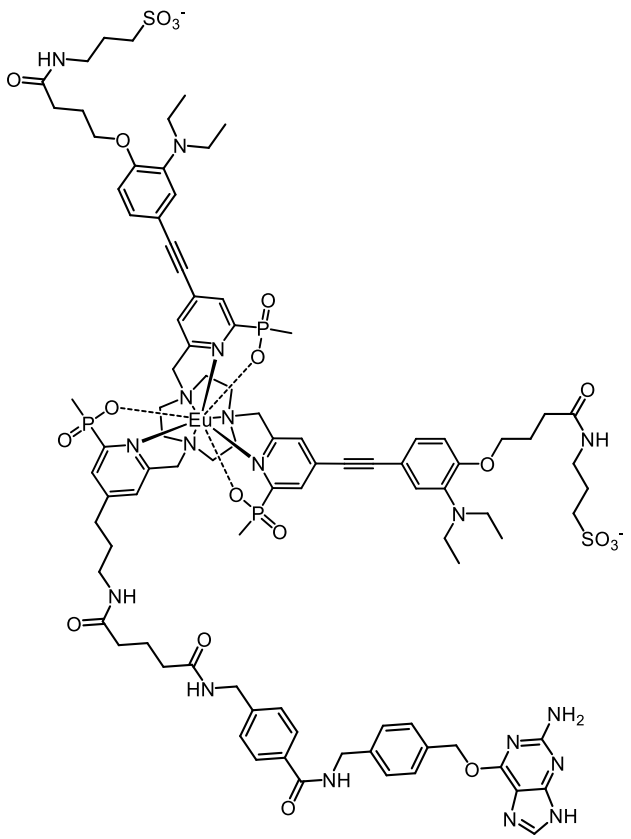

A solution of **BG-MB-NHS** (0.615 mg, 1 µmol) in anhydrous DMSO (100 µL) was added to **[Eu.L^{9a}]-NH$_2$** (1.403 mg, 860 nmol). To the resulting solution was added DIEA (0.5 µL, 2862 nmol) and the mixture was stirred at room temperature for 1 h and purified by preparative HPLC (2 to 40% CH_3CN in 25 mM TEAAc (pH 7) over 18 min) to give a white powder (370 nmol, 43%); **ESI-LRMS** (-) *m/z* 1064.9 $[M]^{2-}$.

[Eu.L^{12b}]

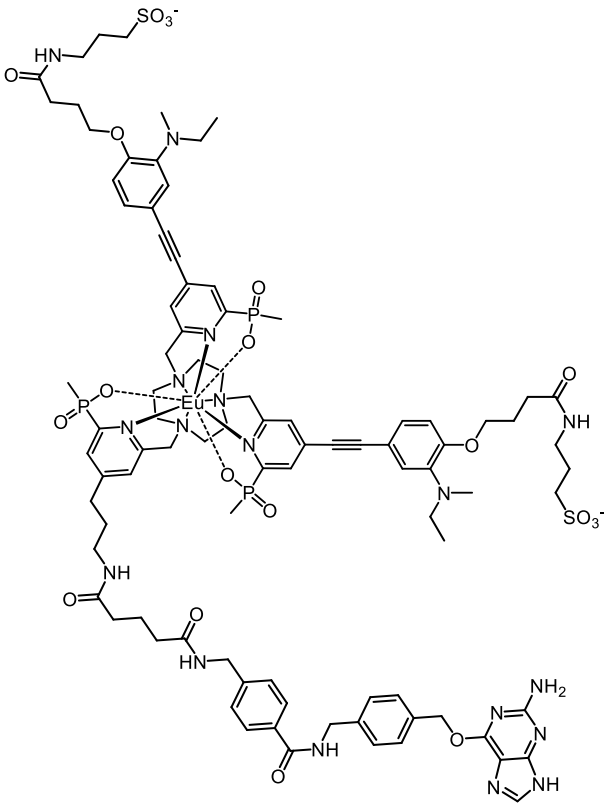

A solution of **BG-MB-NHS** (0.738 mg, 1.20 µmol) in anhydrous DMSO (430 µL) was added to **[Eu.L$^{9\ b}$]-NH$_2$** (1.924 mg, 1.2 µmol). To the resulting solution was added DIEA (0.5 µL, 2862 nmol) and the mixture was stirred at room temperature for 1 h and purified by preparative HPLC (2 to 40% CH_3CN in 25 mM TEAAc (pH 7) over 18 min) to give a white powder (0,728 µmol, 60% yield); **ESI-LRMS** (-) *m/z* 1051.1 $[M]^{2-}$.

7.8. References

[1] K. Nakamaru, *Bull. Chem. Soc. Jpn.,* 1982, **55**, 2697–2705.

[2] M. Starck, J. D. Fradgley, S. Di Vita, J. A. Mosely, R. Pal and D. Parker, *Bioconjugate Chem*., 2020, **31**, 229–240.

[3] R. Pal, *Faraday Discuss*., 2015, **177**, 507–515.

[4] J. W. Walton, R. Carr, N. H. Evans, A. M. Funk, A. M. Kenwright, D. Parker, D. S. Yufit, M. Botta, S. De Pinto and K.-L. Wong, *Inorg. Chem.*, 2012, **51**, 8042–8056.

[5] L. Lamarque, M. Delbianco, S. J. Butler and D. Parker, Nouveaux agents complexants hydrosolubles et complexes de lanthanide correspondants, WO201411166.

[6] J. M. Zwier, H. Bazin, L. Lamarque and G. Mathis, *Inorg. Chem.,* 2014, **53**, 1854–1866.

Appendices

Publications and intellectual property during period of study

1. *Targeted Luminescent Europium Peptide Conjugates: Comparative Analysis Using Maleimide and para-Nitropyridyl Linkages for Organelle Staining*, M. Starck, **J. D. Fradgley**, S. Di Vita, J. A. Mosely, R. Pal and D. Parker, *Bioconjugate Chem.*, 2020, **31**, 229–240.

2. *Europium(III) Complexes as pH Sensors,* **J. D. Fradgley**, M. Starck, L. Lamarque and D. Parker, European Patent Application Number 20206296.3, October 28 2020 priority date.

3. *Synthesis and Evaluation of Europium Complexes that Switch on Luminescence in Lysosomes of Living Cells*, M. Starck, **J. D. Fradgley**, R. Pal, J. M. Zwier, L. Lamarque and D. Parker, *Chem. Eur. J.*, 2021, **27**, 766–777.

Future publications

1. *Synthesis and Evaluation of pH Switched Europium Complexes to Monitor Receptor Internalisation*, **J. D. Fradgley**, M. Starck, M. Laget, E. Bourrier, E. Dupuis, L. Lamarque, J. M. Zwier and D. Parker, *Chem. Commun*., *submitted*.

2. *Striking Solvent Dependence of Total Emission and Circularly Polarised Luminescence in Coordinatively Saturated Chiral Europium Complexes: the Solvent Significantly Perturbs the Ligand Field*, **J. D. Fradgley**, A. T. Frawley and D. Parker, *Phys. Chem. Chem. Phys., submitted*.

3. *How to Design Responsive Luminescent Lanthanide Systems*, D. Parker, **J. D. Fradgley** and K.-L. Wong, *Chem. Soc. Rev., submitted.*

4. *Lanthanide Excited State Lifetime Quenching by Energy and Electron Transfer*, **J. D. Fradgley**, M. Delbianco, J. W. Walton, J. M. Zwier and D. Parker, *manuscript in preparation.*